INTEGRATED ANALYSES IN PLASTICS FORMING

WANG, BO

A thesis submitted in partial fulfilment of the requirement of
Sheffield Hallam University for the Degree of
Doctor of Philosophy

School of Engineering
Sheffield Hallam University

March 1996

Sheffield Hallam University

ABSTRACT

This is the thesis which explains the progress made in the analysis, simulation and testing of plastics forming. This progress can be applied to injection and compression mould design. Three activities of plastics forming have been investigated, namely filling analysis, cooling analysis and ejecting analysis. The filling section of plastics forming has been analysed and calculated by using MOLDFLOW® and FILLCALC V®. software. A comparing of high speed compression moulding and injection moulding has been made. The cooling section of plastics forming has been analysed by using MOLDFLOW® software and a finite difference computer program. The latter program can be used as a sample program to calculate the feasibility of cooling different materials to required target temperatures under controlled cooling conditions. The application of thermal imaging has been also introduced to determine the actual process temperatures. Thermal imaging can be used as a powerful tool to analyse mould surface temperatures and to verify the mathematical model. A buckling problem for ejecting section has been modelled and calculated by PATRAN®/ABAQUS® finite element analysis software and tested. These calculations and analysis are applied to the special case but can be use as an example for general analysis and calculation in the ejection section of plastics forming.

ACKNOWLEDGEMENT

The author wish to sincerely thank his supervisors Dr David W. Clegg and Mr Ian Tranter for their continued support and guidance throughout the course of this work. Thanks are also due to Mr. David Croft for his assistance.

The author also wish to thank Mr. Mick Muldownie for his help, expertise and advice with the Polymer Laboratory work.

A special thank to the staff of school of engineering for their co-operation, patience and assistance.

A thank also to MCG Closures Ltd, specially to Mr. Nigel Thompson, for their sponsorship.

A particular thank you is given to my dear parents for their great support over the years.

Finally, all my love to my wife, Xiaoqi, with her infinite love and support making the dream come true.

CONTENT

LIST OF TABLES

LIST OF FIGURES

LIST OF SYMBOLS

CHAPTER 2.1.2

$\dot{\gamma}$ ----- Shear rate

η ----- Shear viscosity

ν ----- Velocity

τ_{ij} ----- Shear stress

P ----- Pressure

T ----- Temperature

x,y ---- coordinates

CHAPTER 2.1.3

ε ----- emissivity

α ----- radiant absorptance

ρ ----- radiant reflection

τ ----- radiant transmittance

Cp ---- specific heat of coolant;

D ----- hydraulic diameter;

d ------ a characteristic dimension;

h ------ heat convection coefficient;

k ----- thermal conductivity of coolant;

M ---- viscosity of coolant;

N ---- radiation from real body

N_b ---- radiation from black body

Nr -----Nusselt number

Pr -----Prandtl number

R_b ---- radiation which would be produced by a black body at temperature t

Re ---- Reynolds number

R_o ---- background radiation corresponding to room temperature

R_t ---- radiation from the surface at temperature t

t ------ temperature

V ----- flow velocity.

CHAPTER 2.2.1

$\dot{\varepsilon}$ ---- strain rate

λ ----- a scalar.

β ----- in a strut with unequal end-couple

σ ----- stress

η ----- tensile viscosity

ε ------ strain

ν------ Poisson's ratio

γ_{xy} ---- shear strain

[K] --- stiffness matrix

{P} --- applied nodal loads

$\{P\}_{cr}$ -- critical level of the applied load distribution,

$\{P\}_{ref}$ -- an arbitrary level of the same load distribution (reference load),

{U} -- vectors of displacement

A ----- maximum buckling deflection

D ----- diameter

E ----- Young's modulus of elasticity

l ----- effective length

l ----- the length of the cylinder

m ---- the number of half-waves in x direction

r ----- radius of the shell

t ----- thickness of the shell

U ---- strain energy

W ---- radial displacement

x,y ---- coordinates

CHAPTER 3.2

T_p---- Compression time

T_c----- Cooling time

T_o ---- Clamp open time

CHAPTER 3.3

ρ ------ density (kg/m^3)

μ ----- dynamic viscosity

σ ------ the Stefan-Boltzmann constant = 5.67×10^{-8} W/m^2K^4

ΔT ---- temperature increase

Δt ----- time increase

ΔX --- coordinate increase

A ---- Characteristic dimension

Bi ----- Biot number

Cp --- specific heat

d ----- diameter of the tube

f ----- friction factor

Fo ---- Fourier number

h ----- heat transfer coefficient

k ----- Thermal conductivity of fluid

m ------ the mass of the substance (kg)

Nu ---- Nussselt number

Pr ---- Prandtl number

Q ----- heat flow

Re --- Reynolds number

T_f ---- temperature of fluid

T_s ---- temperature of solid

U_m -- weighted mean velocity

V ------ the volume of the substance (m^3)

CHAPTER 3.4

$\overline{S}$ ----- the mean peak value

σ ----- the population standard deviation

$\dot{\gamma}$ ----- shear rate

Q ----- the volumetric flow rate

R ----- the die radius

V ----- the ram speed

D ----- barrel diameter

Q ----- deflection Force (N)

f ----- hoop undercut (mm)

d1 ---- diameter at the joint (mm)

X ----- geometry factor, taking into account the geometric rigidity.

Es ---- elasticity modulus (N/mm^2)

F ----- ejection Force

ρ ----- angle of the friction cone

μ ----- friction coefficient $\mu = \tan \rho$

a ------ angle of inclination

d_a ----- external diameter of the hub (mm)

d ------ diameter at the joint (mm)

ν ------ Poisson's ratio

A ----- area of the cross-section of closure (mm^2)

σ_p----- ejecting compression stress (N/mm^2)

CHAPTER 3.5

$K_{(Q)}^{NM}$ -- an initial stress and load stiffness matrix

$K_{(b)}^{NM}$ -- elastic stiffness matrix

ϕ_i^M ---- buckling mode shapes (eigenvectors)

ν ------ Poisson's ratio for the material

σ_{cr} --- critical buckling stress (N/mm^2)

λ_j ----- load multipliers (eigenvalues)

λ ------ eigenvalue

σ_m ---- mean ejection stress (N)

A ----- cross-section area (mm^2)

A_{top} --- area of top surface (mm^2)

E ----- Young's modulus for the material (N/mm^2)

F_{ee} ---- equivalent ejection force (N)

F_m ---- mean ejection force (N)

P ------ initial load (pressure) (N/mm^2)

Q ----- critical buckling load (N/mm^2)

Q^M --- vector

R ----- rotation of the element

r ------ mean radius of cylinder (mm)

S_{yy} ---- YY stress at top surface (N/mm^2)

T ----- translation of the element

t ------ thickness of the wall (mm)

1. INTRODUCTION

Plastics forming is an expanding industry, using plastics that can be readily formed into complex shapes with excellent mechanical, chemical and electrical properties. These components may be difficult if not impossible to manufacture from other materials.

The plastics industry is also becoming increasingly more competitive, with the market place demanding better quality and more cost effective plastic products.

The industry is recognising that the traditional " trial and error" approach to plastics design and production is inefficient, time consuming, and can lead to inconsistent product quality and high reject rates.

To meet the challenges of competition and market demand the plastics forming, industry needs to improve production efficiency, reduce time to market, and optimise product quality.

This thesis summarises the new advanced techniques of plastics forming, and with the aid of a study on the special production technique used to manufacture bottle closures, several plastics forming problems are thoroughly investigated.

With the development of computer techniques, it is possible for engineers to analyse and simulate plastics forming and, therefore, to get the optimum design in order to achieve the highest quality and highest possible production rates.

Computer-based analysis and simulation in plastics product design and forming are becoming widely used. They may be divided into several major design problem areas as follows [1]:

1. MATERIAL SELECTION: to select a material for a particular application from a material database;
2. MOULDABLE SELECTION: to determine the size of a mould, location and sizes of leader pins and ejector pins, etc.;
3. RUNNER-GATE-CAVITY SYSTEM DESIGN: to determine the location and size of runners and gates for the whole process;
4. COOLING SYSTEM DESIGN: to determine an optimum layout of cooling channels and cooling conditions for the cooling stage of the process.

Injection moulding is the main high speed plastics moulding process in use. With suitable machine design, compression moulding can match the speed and quality of injection moulding. High speed compression moulding is the subject of this study.

In this study, the key aim is to investigate high speed compression moulding in relation to cooling of the part in the mould tool and the relationship to the thermo-mechanical properties of the moulded part. There are at least two important concepts

to keep in mind concerning cooling system analysis and design: (a) minimising cycle time and (b) achieving the required temperature distribution.

The cooling performance is related to heat transfer; the size, location and arrangement of the cooling channels; the temperature, flow rate and thermal properties of the coolant; mould and plastics material properties. The finite difference method (FDM) and the finite element method (FEM) are used to predict the cooling process and the thermal imaging (infrared imaging) technique is used to experimentally test and verify the mathematical model. Information is generated on how the heat will transfer from the plastics to the mould and how the cooling system will extract heat from the mould. Using these guidelines, an optimum cooling system can be designed to achieve the required heat extraction and, where necessary, uniform cooling, ensuring rapid product manufacture at high speed and with acceptable quality.

Ejection is another important step in plastics forming. To obtain a high quality product, a correct ejection time, ejection temperature and ejection force must be achieved to ensure that the final shape of the product is perfect. In this project, the closure ejection is investigated by several different methods. There are direct measurement from production machine, simulation ejection in the laboratory and ejection modelling using a finite element method (FEM) simulation. Associated with the ejection problem, an analysis of buckling involved the computer models and the applications of finite element method (FEM).

1.1 PROJECT STATEMENT

The research is based on a plastics closure, the main product of MCG Closures Limited shown in Figure 1.1[@] . This is a complex product which is, in this case, produced by high speed compression moulding using thermoplastic material. It is of necessity manufactured in large quantities at high production rates.

The structure of the closure can be divided into three regions, shown in Figure 1.2.

Certain guidelines for improvement of the cooling of the closure have been proposed for the case of an optimum temperature profile at ejection, as follows:

1. a cool rim to avoid buckling during ejection.
2. a warmer thread region to provide minimum resistance to ejection, whilst maintaining integrity of the thread profile.
3. a homogeneously cool base.

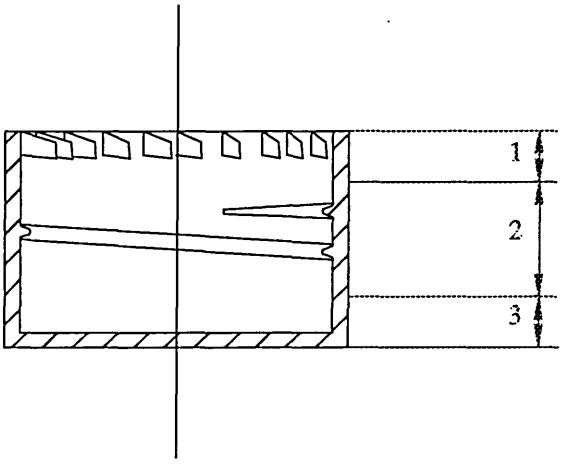

1. Rim region
2. Thread region
3. Base region

Figure 1.2 Structure regions of the closure

[@] *means that the Figure or Table is located in the attached pages.*

4. cool wings to ensure integrity during ejection.

5. a minimum cooling time while satisfying the above conditions.

To achieve these goals, a series of analyses, tests, measurements and re-design of the cooling system of the closure mould are involved. The flow diagram of the work programme is shown in Figure 1.3.

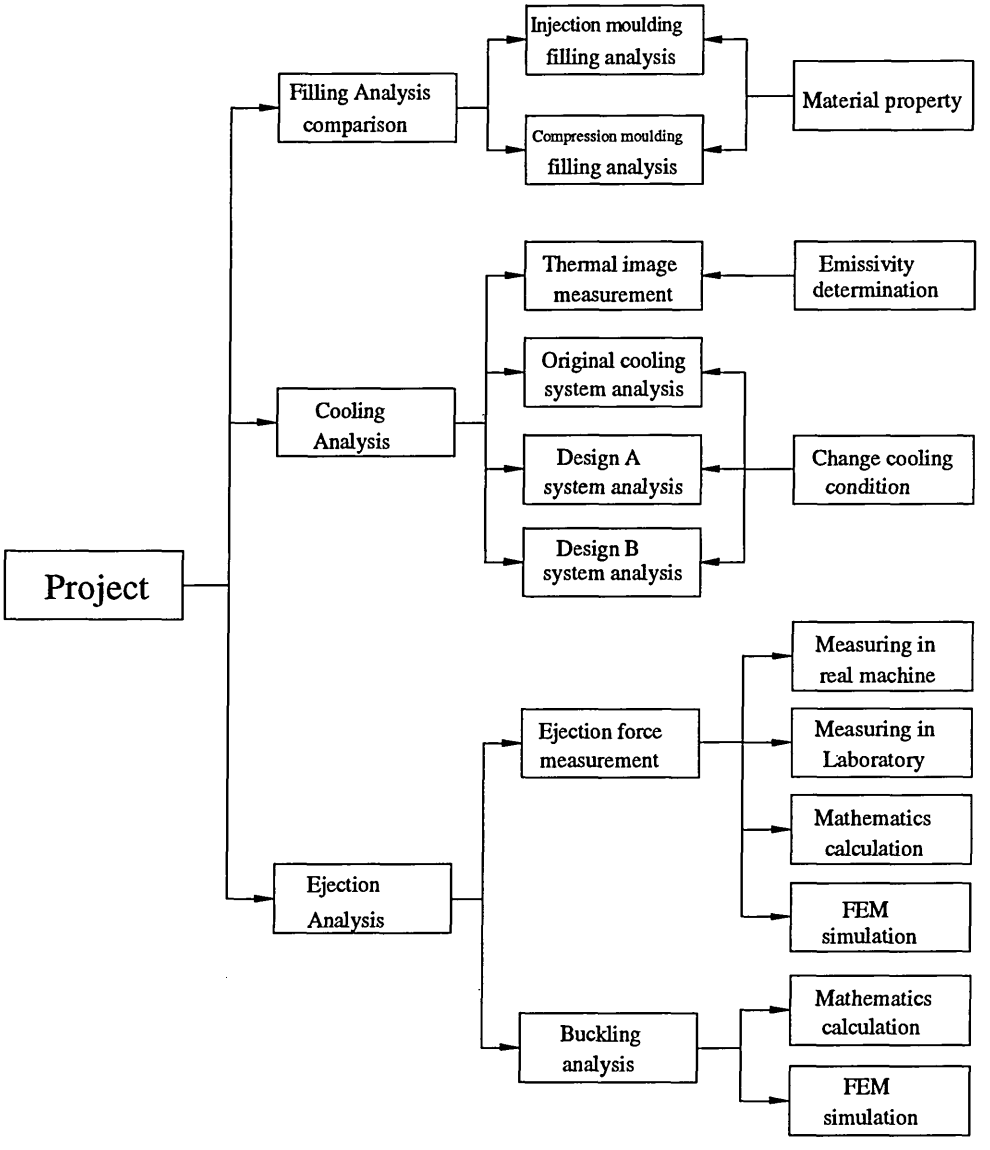

Figure 1.3. Flow diagram of the PhD research programme

2. LITERATURE SURVEY

2.1 COMPUTER AIDED ENGINEERING FOR PLASTICS FORMING

Whenever a new project involving plastics moulding is begun, a design engineer starts with a conceptual design of the part, decides which plastics material will be used and chooses a machine basing his ideas on simple calculations. This is followed by the selection of the dimensions and material of the mould base, design of the runner system, estimation of cycle time and coolant requirements. Then comes runner balancing. With this, a preliminary process design is complete [2]. However, while moulding, many problems may be encountered such as short shots, unbalanced runners, weld lines in undesirable locations, inadequate cooling, large shrinkage and warpage, inconsistent part quality or process performance. In order to overcome these problems, the designer would have to either change the process and/or modify or rebuild the mould. This approach is therefore very expensive and time consuming.

Nowadays, these moulding trials can be performed by computer before the mould is built. It is called computer aided engineering (CAE) [3] [4] [5] [6]. CAE for plastics moulding may be divided into four major problem areas [1] [5][7] [8] [9], shown in Figure 2.1.1 or a three-layer approach [2], shown in Figure 2.1.2.

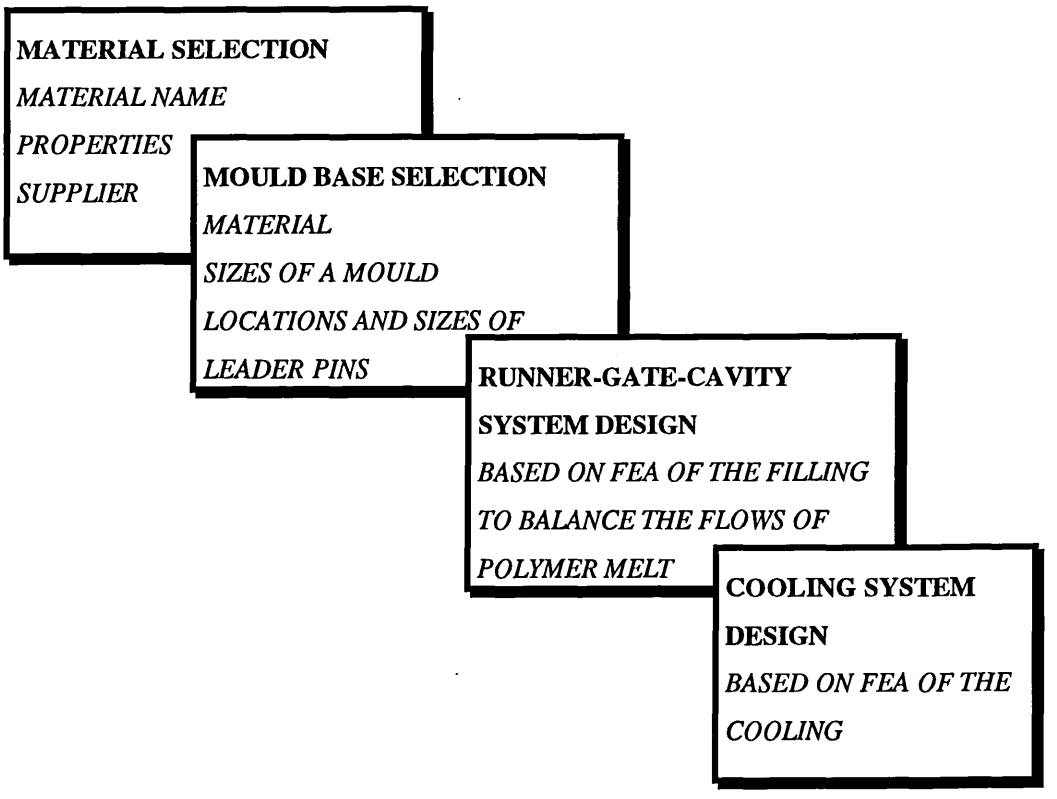

Figure 2.1.1. Functionalities in different design stages

With the development of computer techniques, computer aided design and analysis of plastics forming reaches into almost every detail of the design, such as:

- Geometry generation
- Flow analysis including runner balancing
- Cooling analysis including the generation of the cooling systems
- Shrinkage analysis
- Warpage analysis
- Stress analysis

2.1.1 MATERIAL DATABASE

The material databases may be split into two types for different purposes: plastics material databases, including rubber, and mould material databases.

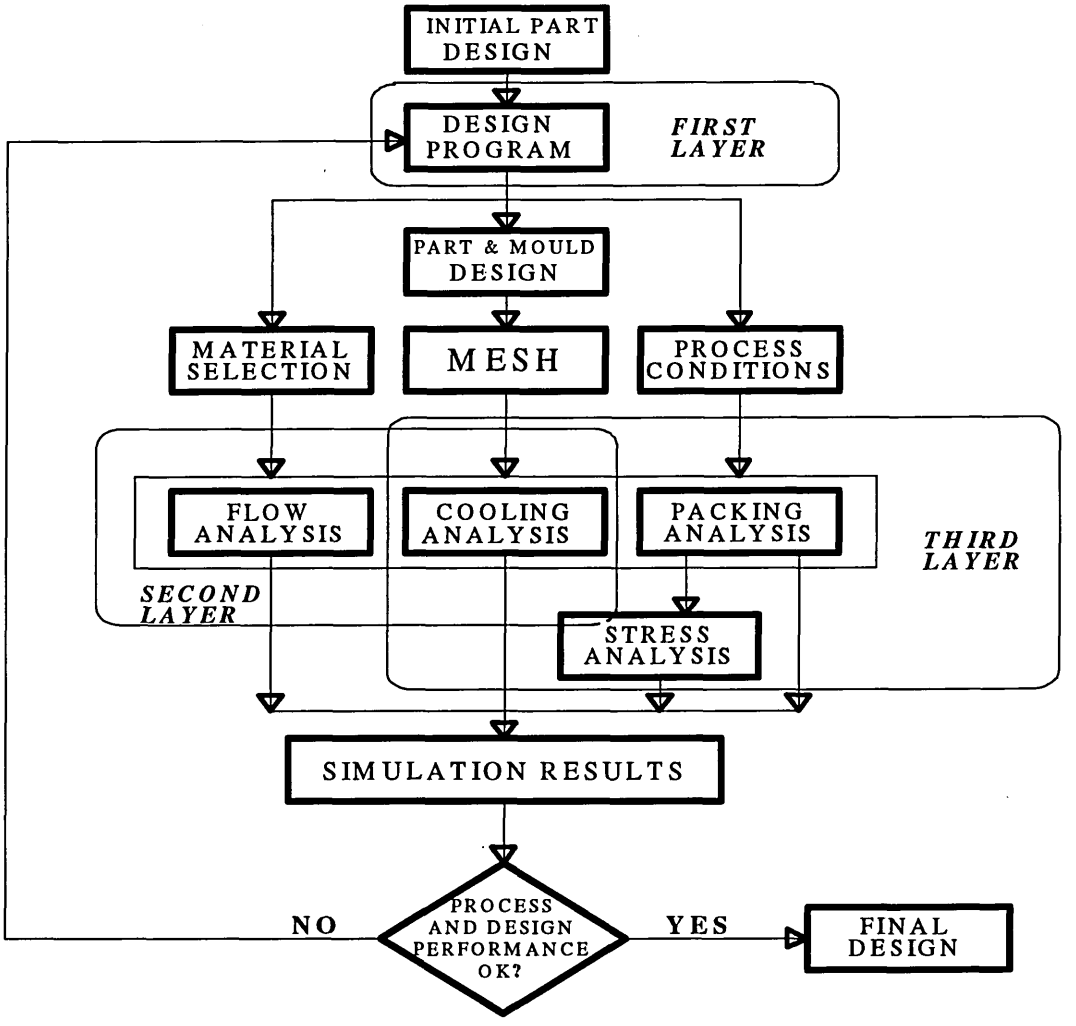

Figure 2.2.2. Over structure of the three-layer CAE approach

2.1.1.1 PLASTICS MATERIAL DATABASE

CAE for materials selection helps the user to select one or more plastics to meet the design requirements and also helps the user to find the physical properties of the material he chooses [9] [10] [11]. The user can choose the plastics directly by supplying the generic name, manufacturer's name and a specific commercial grade out of almost 7000 different plastics (resins) in the database; or he can input some physical criteria concerning the desired material and ask the expert system to make the

selection by comparing the input criteria with more than eighty different material properties, such as in CAMPUS. The material selection module also provides some utilities for the user to compare properties between different plastics materials to aid in decision-making.

There are a number of independent material databases for plastics available on the market [12] [13] [14], such as MATDB[@] of Moldflow of Australia, PLASCAM[@] of Rapra of the UK and CAMPUS[@] of CWFG of Germany. There are also lot of computer aided design and analysis software which carry a material database with them, such as PATRAN[@], MOLDFLOW[@] and FILLCALC V[@].

Normally, there is an editor for the material database, such as MADRAS for MATDB. The editor allows you to search and inspect the standard material database and to edit your own Personal database which you can create and update yourself [12]. The standard material database is regularly updated and the Personal database is created and updated by yourself.

The material database allows you to make an initial selection from the wide range of plastics for your specific application. You can obtain meaningful and comparable data on the properties of material if the material database meets the following requirement [14]:

- Computer database with uniform user interface and structure for different plastics manufacturers.
- Comparable data as a result of uniform selection of properties specimen preparation and test conditions.

- Constant update of the families, extension of the test methods and adaptation to development in standards.

The properties included in the database are varied with different software packages. Normally the material database contains uniform information on the preparation of specimens and the following properties:

- mechanical
- thermal
- electrical
- processing
- optical
- other properties
- behaviour towards external influences

Besides the independent plastics material databases, many computer based design and analysis software packages contain their own material database, such as MOLDFLOW® and FILLCALC V®, which can be used directly, modified and transferred automatically to the design and analysis program.

The material databases are moving more and more towards an industry standard, such as MATDB of Moldflow in injection moulding of plastics, which is accepted by many software companies as the standard material database for their computer aided design packages.

2.1.1.2 MOULD-BASE

For the mould-base selection, a library for mould design is developing [7] [8] [15]. A mould design system will need three major classes of capability. The first one is layering. Similar to placing multiple overlays on an overhead projector, layering in CAD allows the breaking of a drawing of an assembly into its component parts. With all layers shown, one may view the complete mould assembly. With one or two layers active, one can view a specific part of that assembly. A system that can offer one hundred or more layers is quite adequate for mould design. The second one is symbolism. This is the ability to create a drawing, store it, then place it at will into another drawing. Usual parameters for placing symbols include: angle of rotation, scale factor, and mirror image. The third one is more general: editing capabilities. These can supply the modify abilities such as trim, extend, layer, etc.

2.1.2 MOULD FILLING

Mould filling is based on the flow analysis of the material inside the mould. The first consideration to be taken into account is the flow behaviours of the plastics material.

2.1.2.1 FLOW BEHAVIOUR OF THE PLASTICS MATERIAL

The flow behaviours of plastics melts are , to say the least, complex [16]. The flow behaviours, also called rheological properties, are of practical interest to all those sections of the plastics industry in which materials are processed in the molten state.

A fundamental rheological property of a molten polymer is its shear viscosity. This is defined as the ratio of the shear stress to the shear rate in a simple shear flow:

$$\eta \equiv \frac{\tau_{21}}{\dot{\gamma}}$$

For single phase fluids containing only low molecular mass compounds, the viscosity is independent of the shear rate and dependant only on the temperature and pressure:

$$\eta = \eta(T,P)$$

The general relationship between stress and velocity gradients for such materials, shown in Figure 2.1.2.1, is given by:

$$\tau_{ij} = \eta\left(\frac{\partial v_i}{\partial x_j} + \frac{\partial v_j}{\partial x_i}\right)$$

which is called Newton's equation and a fluid which obeys this particular constitutive equation is called a Newtonian fluid. It can be assumed that single phase, low molecular mass fluids are Newtonian fluids [17].

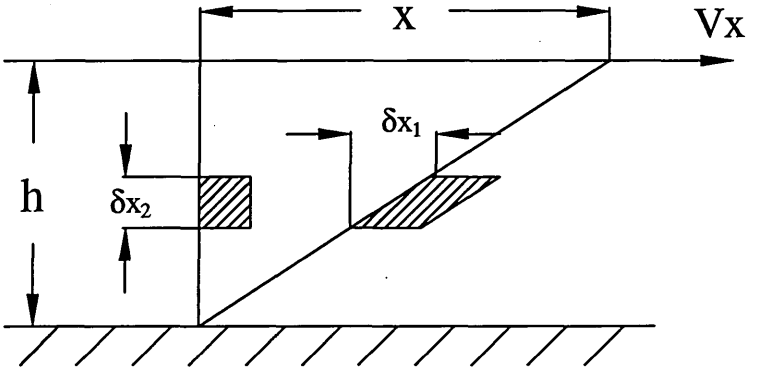

Figure 2.1.2.1 Shearing between parallel plates

Fluids, in which the viscous dissipation of energy is due to collisions between large molecules, a dispersed second phase or colloidal system, do not obey Newton's equation, which are called non-Newtonian fluids. Three main classes of non-Newtonian fluid flow behaviour are recognised and are summarised below [18]:

- Time-independent fluids: fluids in which the shear viscosity is a single valued function of the shear stress.
- Time-dependant fluids: fluids in which the shear viscosity depends on the shear stress and the duration of shear.
- Elastic-viscous fluids: fluids that are predominately viscous but possess elasticity like solids.

2.1.2.2 CAE IN MOULD FILLING ANALYSIS

Runner-gate-cavity system design is quite complex. CAE on this level is based on flow analysis [19] [20]. The basic theories of flow analysis are the finite difference approach, branching flow approach and finite element approach. More commonly now, the three-dimensional mould filling program uses a hybrid finite element/finite difference approach to solve for the generalised Hele-Shaw flow of an incompressible viscous fluid under non-isothermal conditions [3] [21] [22]. The shear viscosity of the polymer melt is represented by a modified-cross model with temperature and pressure dependence. A control volume scheme is employed to handle automatic melt-front advancement during the cavity-filling stage. Other capabilities of the filling analysis program include moulding with valve-gate control and co-injection moulding simulation. In addition, using artificial intelligence, the mould filling analysis software automatically interprets the formation of weld lines and air traps and predicts their position, even in a mould of complex geometry. By performing this cavity filling analysis, one can accurately determine clamp force requirements, balance the runner system, profile injection speed, predict weld line and vent locations, determine

optimum gate location, refine the thickness selection and check for short shot problems [2].

The plastics forming design and analysis software, the special purpose computer aided design and analysis packages [23] [24], are always including the following:

- Geometry generator
- Material database
- Finite element mesh generator
- Boundary conditions and moulding conditions editor
- Pre and post graphic interface

For the flow analysis, or so-called filling analysis, the software packages provide two kind of analyses: fast and slow analyses. These depend on what kind of viscosity model is to be used. As mentioned in the last section, the polymer melt is classed into Newtonian flow and Non-Newtonian flow which includes first order and second order flow.

The fast analysis is based on the Newtonian flow viscosity model, where viscosity is independent of shear rate. It is intended to be used for rapid calculations in order to balance the runner system, to find weld lines and hence the location of the gate before applying one of the more comprehensive analysis models to calculate the finer details. This type of analysis is carried out isothermally.

The slow analysis, or called laminate analysis, is based on the non-Newtonian flow viscosity mode, first order or second order, where the calculations are considerably

slower than the Newtonian model in that the pressure calculations ignored in the Newtonian model are carried out. They also allow the detection of such behaviour as gate freeze-off or thermoset gelling.

For the fast algorithm, viscosity is an "equivalent value" determined across the cavity thickness. Whilst for the laminate algorithm, a finite difference algorithm, viscosity is calculated for each laminate in the material, and from these individual "laminate viscosities" an overall equivalent viscosity is determined. The viscosity as calculated from the laminate viscosities is more accurate than the equivalent value determined from the fast algorithm because the viscosity profile across the cavity has been more accurately approximated.

2.1.3 MOULD COOLING

Cooling system design in plastics moulding industries is of great importance because it significantly affects productivity and the quality of the final part [1] [25] [26] [27] [28] [29] [30] [31]. The basic character of the injection moulding cycle is made up of three segments: (i) melt injection; (ii) cooling; and (iii) parts ejection. In a typical moulding cycle, the moulding cycle consists of 5% injection time, 15% ejection time and 80% cooling time [23] [32] [33]. Therefore, reducing the duration of the cooling segment of the moulding cycle can effect a significant reduction of total cycle time. For economic reasons, in recent years, increased attention has been paid to the design of a cooling system. In order to systematically improve the performance of a cooling system in terms of rapid, uniform, and even cooling, computer simulations have been developed for mould heat transfer during the cooling stage of a moulding process.

On the one hand, people are trying to use mathematical methods to simulate the cooling process, and on the other hand, people also use dynamic mechanical measurements to verify the cooling analysis [34] [35] [36]. The key point of the cooling is heat transfer, and temperature distribution is the manifestation of the heat transfer. We can use a mathematical heat transfer model to calculate temperature distribution in the mould and measure temperature distribution to verify the results of the computer calculation.

2.1.3.1 HEAT TRANSFER

The cooling analysis is based on the modelling of heat transfer in mould and heat transfer calculations from plastics to mould and from mould to coolant. The potential for improving the consistency of the quality of finished parts also is a function of heat transfer from the mould. When heat flow from the mould is not balanced, the result can be differential shrinkage, residual stress and/or warping of the mould part.

In heat transfer, the determination of detailed heat flow conditions involves complex mathematical calculations based upon three heat transfer dimensionless numbers. These are:

1. Reynolds number: index of the flow characteristics (laminar, transitional or turbulent) of fluid flowing in a passage.
2. Prandtl number: the ratio of fluid viscosity of thermal diffusivity.
3. Nusselt number, which relates heat loss by conduction to the temperature difference and takes into account the configuration of each channel passage along with the thermal conductivity of the fluid.

The following equations [37] [38] show the formulae for these three dimensionless numbers as well as other quantitative factors that must be taken into account in computing the heat load of individual cooling channels for the purpose of circuiting.

Reynolds number $$Re=\frac{DV}{M}$$

Prandtl number $$\mathrm{Pr}=\frac{C_p M}{k}$$

Nusselt number $$Nr=\frac{hd}{k}$$

here, M -- viscosity of coolant;

Cp -- specific heat of coolant;

h -- heat convection coefficient;

D -- hydraulic diameter;

k -- thermal conductivity of coolant;

d -- a characteristic dimension;

V -- flow velocity.

One of the most important factors in cooling, mentioned in many papers, is the coolant flow rate. It is almost always necessary to have turbulent flow in the coolant channels in the mould in order to satisfy the cooling requirement for minimum cycle time.

At a Reynolds number of less than 2100-2300, the flow is laminar and the heat transfer is primarily by molecular motion in the fluid. As the Reynolds number is increased over 2300, turbulent cells start to form and cause the laminar fluid to be

intermixed. At Reynolds number of 3500 and above, the flow can be considered turbulent, where complete turbulence occurs at a Reynolds number of 10,000. In practice, a Reynolds number of at least 4000 should be achieved in injection moulds for efficient heat removal.

In a cooling system, its contribution to heat transfer from the mould is contingent upon the operating characteristics of a coolant: specifically, coolant temperature, pressure and flow characteristics.

In the case of coolant temperature, there is a widely held misconception that, other factors being equal, lowering of the coolant temperature will accelerate heat removal from the mould. Actually, the contrary is often the case for the reason illustrated in Figure 2.1.3.1. Commercially available water chillers by convention are rated for operation at 50 °F (10 °C) leaving water temperature. For each degree (°F) by which water temperature is reduced below 50 °F, the chiller loses about 2% of its capacity. At a coolant temperature of 10 °F, capacity of a 100 t (28.4 kW) chiller is reduced to about 28 t. Therefore, from the standpoint of cost effectiveness, it is counterproductive to operate chillers at lower than their rated temperature.

With respect to coolant flow, other things being equal, the greater the velocity of the coolant flow, the greater is the heat transfer from the mould to the coolant. However, after a certain value of turbulence is reached, increasing coolant velocity does not appreciably improve heat transfer from the mould. The point at which this occurs varies for each mould. Here again, adding pumping power to increase flow rate after optimum level of turbulence had been reached would be counterproductive from a

cost standpoint and also because increased pumping power would add heat to the system.

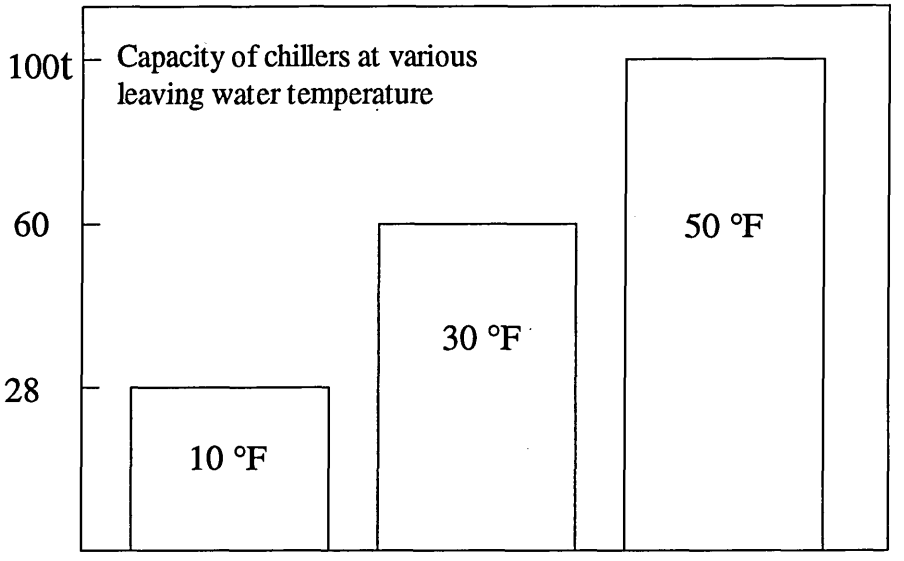

Figure 2.1.3.1 Chiller capacity versus coolant temperature

2.1.3.2 MOULD TEMPERATURE MEASUREMENT

Cooling system design, together with coolant flow rate and temperature, melt temperature and mould temperature are all important since they affect the final quality of the moulded part, as well as heat removal, which directly influences cycle time and possibly microstructure and properties. Thus, it is desirable to have a detailed understanding of the mould temperature variation in both time and space. The key point for verification of the mould temperature is how to actually measure the temperature distribution.

In general, thermocouples are effective and widely used for this purpose [39] [40] [41] [42] [43] [44]. The critical considerations in using thermocouples to measure the

mould surface temperature are mounting the thermocouple as close as the mould surface and using a fast response thermocouple.

As a non-contact determination of temperature, the use of infrared radiation techniques (IR), such as infrared pyrometry and infrared sensing, has been reported for many years [45][46]. With the development of digital recording and computer techniques, thermal imaging has been developed as a useful method to measure the surface temperature distribution directly [47-60]. Although certainly not a new technology, it has evolved from one, classified by some as a scientific curiosity suitable only for laboratory applications, to a highly useful and cost-effective method for verifying designs, and assuring that products conform to specification and for fault identification.

Thermal imaging systems are well known in various applications such as medical diagnostics, pollution monitoring, satellite reconnaissance and weather forecasting. Extensive notes and papers have been written describing these applications. With the development of the technology, thermal imaging has found more and more applications in manufacturing, such as die casting, polyethylene film production, paper processing, timber curing, and plastic moulding, and as a result enhances manufacturing operations [54]. It is worth bearing in mind the appropriate uses for thermal imaging, how thermal imaging views applications and how these images can be used to improve production processes.

The technology provides non-contact, line-of -sight temperature measurements of the surface of virtually any object [52]. Thermal imaging is well-suited to situations in

which traditional contact measurement techniques, such as thermocouples or probes, could alter the operating performance of the device being tested or create safety hazards. Thermal imaging also provides a comprehensive map of temperature data across the surface that would be difficult, if not impossible, to obtain through single-point measurements.

As with most types of test equipment, there are many different thermograph system designs and configurations, and each manufacturer produces equipment with varying levels of performance capability. However, to meet the need of modern testing, it is essential that these systems meet certain basic criteria. They include producing high resolution thermal images, having the ability to analyse the image data and being able to convert these data into information suitable for both human and machine decision making.

Thermal images are devices that detect and measure energy in the infrared range of the electromagnetic spectrum and convert that radiated energy into temperature information. Thermal radiation incident upon a surface is partially absorbed, partially reflected, and partially transmitted. It can be explained as follows:

$$\alpha + \rho + \tau = 1$$

in which α is the radiant absorptance, ρ the radiant reflectance, and τ the radiant transmittance of the material object subjected to the radiation. An object which absorbs all incident radiation is called a black body.

Experiments have shown that the same radiance N from a real body is always smaller than that from a black body at the same temperature. It depends on the chemical

composition of the material, the angle of emission, and the surface condition. These parameters in turn are dependent on the wavelength of the emitted radiation and the temperature of the object. The ratio of the radiation N from a real body to the radiation N_b from a black body at the same temperature is called the emissivity ε [47]:

$$\varepsilon = N / N_b$$

The radiation that is emitted by a surface at some temperature t °C is given by [57]:

$$R_t = \varepsilon R_b + R_o(1-\varepsilon) \qquad (1)$$

$$\varepsilon = (R_t - R_o)/(R_b - R_o) \qquad (2)$$

where R_t is the radiation from the surface at temperature t, R_b is the radiation which would be produced by a black body at temperature t, ε is the surface emissivity, which we assume to be constant and R_o is the background radiation corresponding to room temperature. If room temperature and t are known, the emissivity of the surface may be calculated using equation (2). Alternatively, if the emissivity is known, the temperature t may be found by equation (1). Since different surfaces and materials radiate different levels of infrared energy at the same temperature, it is necessary to take the emissivity into account when converting infrared energy data into absolute temperature data. An accurate temperature measurement with thermal images can only be made when the emissivity of the measured target is known.

The choice of operating waveband for thermal images is further constrained by the attenuation characteristics of the atmosphere. There are two "windows" or regions of minimum attenuation, at 3 - 5 μm and at 8 - 13 μm. To the physicist, both these bands fall in the mid, or intermediate IR region; but by common usage, the thermal imaging community refer to 3 - 5 μm as the mid-IR band (or short wave band) and 8 - 13 μm

as the far-IR band (or long wave band) [52] [60]. For specific applications, one or the other has specific advantage in terms of sensitivity. Generally speaking, for temperatures of 20 °C and below, the long wave band has higher sensitivity as most of the radiated energy lies in the long wave area at those temperatures. Sensitivity evens out as one approaches 30 °C, after which the short wave band is more sensitive.

The greatest boost to thermal image processing for measurement and evaluation has been the marriage of the computer microprocessor and the scanner, via software, to solve complicated analyses. For example, accurate non-contact measurement is highly dependent on a knowledge of the emissivity of the object. Software now exists to correct for emissivity and to determine the true surface temperatures for multicomponent objects with varying radiation properties, such as PC boards, hybrid circuits and transistors as small as 1 mm × 1 mm. The software differs from normal image-processing programs because it is strongly geared toward temperature measurement and display in various ways.

Image acquisition is a key feature, where live/freeze frame events are captured by automatic sequential recording at various speeds. Examples are: recording once a second for a minute to study the heating of PC boards or objects under thermal or mechanical stress; or at full speed, 25 images a second for dynamic thermal events, such as the laser-beam impact on an object where heating occurs very quickly.

Image enhancement is different than the corresponding function for normal images. It focuses on the distribution of temperature. Edge detection, Laplace transforms, spatial

filtering and similar software function are available, but usually do not play a major role in the enhancement of thermal images.

When considering the major characteristics of a thermal image system, it can be conveniently divided into four primary subsystems: Optical Image Data Generation, Image Processing, System Control and Image Output. More details about thermal image systems can be found in [47] [48] [50] [51].

2.1.3.3 CAE IN MOULD COOLING ANALYSIS

Mould cooling analysis performs an integrated simulation of cooling channel network flow, transient three dimensional mould heat transfer and transient non- linear polymer cooling [1] [25] [61] [62]. First of all, coolant flow in a complicated cooling channel network with several loops and branches is solved using the Newton-raphson iterative method to obtain the flow rate and pressure drop in each cooling channel. Further, the cooling analysis uses a modified three dimensional finite element or boundary element method for mould analysis and an implicit finite difference method with variable mesh for the polymer analysis [26] [30]. These two analyses are iteratively coupled to match the temperature and heat flux at the mould-polymer interface. From this mould cooling analysis, users determine cycle time, hot spot locations, coolant pumping requirements, cooling line effectiveness and differential (asymmetric) cooling problems. A quality conscious designer will proceed to a more sophisticated analysis to predict part quality in terms of shrinkage, warpage and occurrence of sink-marks by performing filling/postfilling/residual stress analyses concurrently with a mould cooling analysis.

These simulations are based on different methods for different purposes. Each method may have its own advantage. In the present study, SFA (Shape Factor Approach), FDM (Finite Difference Method), FEM (Finite Element Method) and BEM (Boundary Element Method) are applied in the mould cooling simulations through several proposed cooling systems.

There are many methods for analysis of surface temperature. One dimensional heat transfer analysis can be used to calculate the feasibility of cooling materials to required target temperatures under controlled cooling conditions, but has limited value in achieving a uniform temperature profile across the wall surface.

Two dimensional heat transfer analysis can be very valuable where the moulding has a relatively constant cross-section. Two dimensional cases can be handled quite adequately by a finite element approach. The finite element technology involved breaking the surface down into small elements and the heat load across each element is calculated as a set of equations. By solving the simultaneous equations for all the elements, the temperature profiles are solved. The mould cross-section can be easily meshed in 2D. The heat load at the nodes on the surface is determined by the thickness and temperature of the plastic. The temperature of the nodes near the cooling channel is determined from the coolant temperature. This gives sufficient information for a heat transfer analysis to predict the isotherms throughout the metal.

While this two dimensional approach has some practical value, real problems in plastics moulding occur as a result of the complex three dimensional geometry inherent in plastics moulding.

In three dimensions, the finite element approach becomes less practical since it is necessary to form a solid element mesh, which can result in modelling and computational problems. In recent years, the boundary element technique has been introduced in cooling analysis as an alternative approach [1] [26-30] [61] [63].

SHAPE FACTOR APPROACH

In the preliminary cooling system design stage, the shape factor technique provides an efficient method for the calculation of the heat balance between the plastic melt and the coolant. For a given plastics material and mould material with known values of melt temperature, ejection temperature, average part thickness, part surface area, pitch and depth of cooling channels, geometrical information, coolant temperature and coolant flow rate, the corresponding cooling time, pressure drop and heat flow rate across each cooling circuit can be calculated as function of coolant flow rate. In the present study, pitch and depth of each channel are automatically analysed through the finite element shell mesh implemented on the part surface. The shape factor is calculated based on the corresponding pitch, depth and type of each cooling line. The plastic melt profiles are also computed by one dimensional transient heat conduction analysis in combined with shape factor. The effects of cooling channel geometry and operating conditions of the coolant are therefore incorporated into the plastic melt temperature, mould surface temperature and cooling time evaluation.

FINITE DIFFERENCE METHOD

Two dimensional finite difference grids are implemented on the plastic part and mould. Fine grids are used in the plastic melt region, while the mould region is covered by large grids and some incomplete rectangular grids located at cooling

channel surface. Control volume formulation with grid points specified at the volume centre is adopted in order to handle the melt-mould interface and mould-channel surface. Two dimensional transient cooling analysis is performed using the alternating direction implicit (A.D.I.) scheme. It is a tedious work for such analysis. However, the transient temperature distribution in the whole mould can be evaluated in more detail.

FINITE ELEMENT METHOD

For comparative purposes, two dimensional heat transfer analysis is also carried out based on the Galerkin finite element method. Triangular elements are implemented on the mould, whereas triangular and/or quadrilateral elements are used in the melt region. Although the analysis is a time consuming process, the whole mould including the plastic melt region can be analysed simultaneously. The transient temperature distribution of the part, cavity surface and mould can be investigated in detail.

BOUNDARY ELEMENT METHOD

In the present boundary element method simulation, a cycle-averaged heat flux is imposed on the melt-mould interface as the boundary condition. The average heat flux along mould-melt interfaces can be calculated either by one dimensional transient heat conduction across the gapwise direction of the plastic melt or by average melt-mould heat transfer coefficient [1] [27] [28] [62]. The steady state conduction equation of Laplace type then can be discretized into linear algebraic equations via standard boundary element methods using the fundamental solution approach. After introducing the boundary conditions, the temperature distribution along the mould cavity surface can be computed. Through several iterative calculations, the cycle-

average mould wall temperature can be obtained. Both two or three dimensional cases have been worked out.

Several CAE software package have been developed based on the approaches discussed above to simulate the problem of mould cooling [30][64][65]. The following are some of them:

- MCAP (also known as POLYCOOL) is a General Electric Company computer program developed at Research and Development Centre, Schenectady, New York.
- SIMUCOOL is owned by Graphics Technology Corp., Boulder, Colorado.
- MOLDCOOL is a software developed by Application Engineering Corp., Elk Grove Village, Illinois
- DIEPAK is developed by Scientific Process and Research Inc., Somerset, New Jersey.
- MF\COOL is developed by MOLDFLOW Pty. Ltd.

2.2 MECHANICAL DEFORMATION

2.2.1 BEHAVIOUR OF THE SOLID PLASTICS MATERIAL

Ejection is one of the major processes in plastics forming. When the ejection process is to be studied, first of all, the solid behaviour and mechanical properties of the plastic material must be investigated.

Plastic materials are unusual in that the vast majority of them simultaneously exhibit the properties of both elastic solids and viscous liquids, under a wide range of conditions. They are thus said to be viscoelastic in nature. As a result their response to stress is time dependent and their mechanical properties depend on the temperature, the rate of deformation, and material structure (in particular its molecular mass and density). For example, with polypropylene a shift in temperature from 20 °C to 60 °C would typically cause a 50% reduction in allowable design stress. In addition, for each kg/m^3 change in the density of this material there is a corresponding 4% change in design stress [66].

All of the additional factors which influence the behaviour of plastics mean that, as far as design is concerned it is useless to have properties (such as modulus) quoted as a single value because they will only apply for the conditions at which they are measured. Therefore since standard test procedures such as BS 2782 recommend quite specific tests conditions, they are only useful as a means of quality control. This point is highlighted by the fact that , for exactly the same sample of plastics, the Americium standard (D 638) would give a different modulus value from BS 2782 simply because each standard specifies different test conditions. As a result of factors it is not reasonable to quote properties such as modulus, yield strength, etc. as a single value without qualifying these with details of the test method.

In a perfectly elastic, Hookean, material the stress σ is directly proportional to the strain ε and the relationship may be written, for uniaxial stress and strain, as

$$\sigma = E\varepsilon$$

where, σ - stress

ε - strain

E - Hook constant, referred to as Young's modulus

In a perfectly viscous, Newtonian, fluid the shear stress τ is directly proportional to the rate of strain $\dot{\varepsilon}$ and the relationship may be written as

$$\sigma = \eta\dot{\varepsilon}$$

where, τ - shear stress

η - tensile viscosity

$\dot{\varepsilon}$ - strain rate

Plastic materials exhibit mechanical properties which come somewhere between these two ideal cases and hence they are termed ***Viscoelastic***.

The most characteristic features of viscoelastic materials are that they exhibit a time dependent strain response to a constant stress, called ***creep***, and a time dependent stress response to a constant strain, called ***relaxation***. In additional when the applied stress is removed the material has the ability to recover slowly over a period of time, called ***recovery***. These effects may also be observed in metals but the difference is that in plastics they occur at room temperature whereas in metals they generally occur at much higher temperatures.

Creep is very important in stressed engineering components such as beams and cables as excessive deflections and failure can occur. Stress relaxation is important in gaskets

and seals of all types because as the stress in the sealing material decays the effectiveness of the seal is reduced.

These manifestations of viscoelastic behaviour can be described by phenomenological model made up of Hookean springs and Newtonian dashpots. They are shown in Figure 2.2.1.1

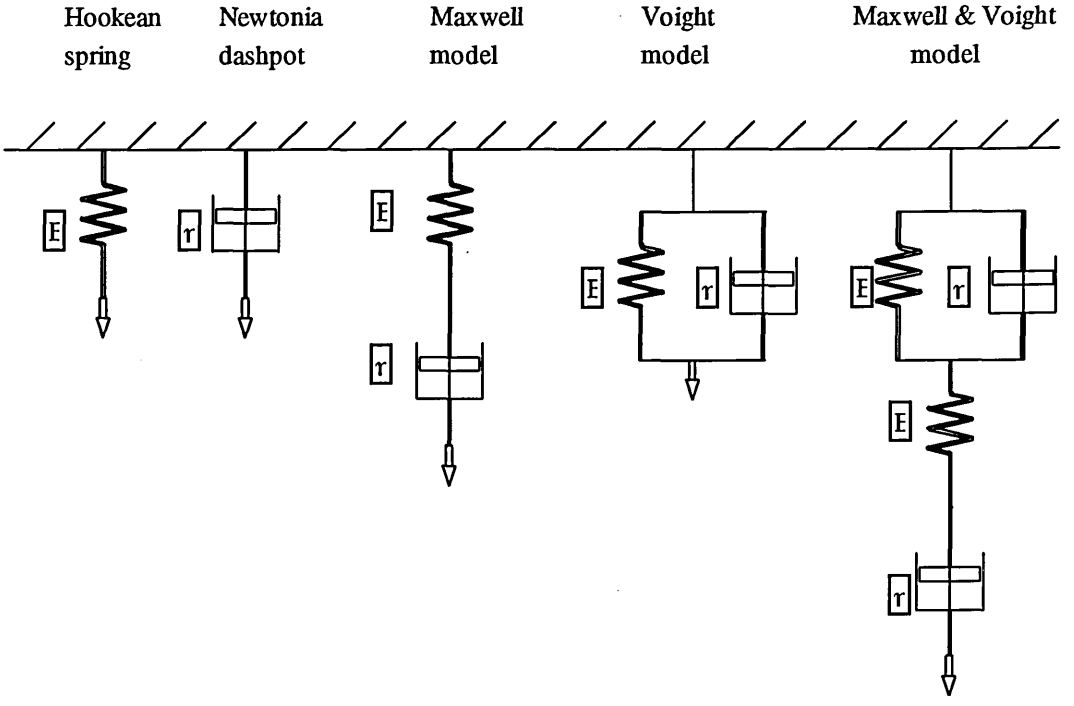

Figure 2.2.1.1 Mechanical models representing various viscoelastic behaviours

It can be seen that although the exponential responses predicted by these models are not true representations of the complex viscoelastic response of plastic materials, the overall picture is, for many purposes, an acceptable approximation to the actual behaviour. As more and more elements are added to the model then the simulation becomes better but the mathematics become complex.

The major solid behaviours can be classed into viscoelastic, creep, and stress relaxation. The last two become more important over relatively long times. In the investigating the ejection process in plastics forming creep and stress relaxation normally are negligible because the ejection process occurs in a very short time.

2.2.2 THE BUCKLING PROBLEM

A review of the relevant literature has revealed that although a significant body of work has been carried out on warpage resulting from the generation of internal stress during cooling [23] [24] little if any work has been carried out on buckling and distortion resulting from the application of ejector mechanisms forces.

In general, the phenomenon of buckling occurs when a critical load is reached, that is, the stress in the part reaches a critical value at which buckling occurs. Buckling renders the part faulty.

A component may buckle if sufficiently high levels of membrane stress develop. These stresses act in the plane of elements (that is, at a tangent to the part mid-surface). Buckling occurs when a part converts membrane strain energy into strain energy of bending.

Injection moulded parts are frequently thin walled and exhibit membrane stiffness orders of magnitude greater than their bending stiffness. As an analogy, consider a piece of wire. It may be quite stiff in tension (high membrane stiffness) but offers little resistance to bending (low bending stiffness). Parts with high membrane stiffness can

store large amounts of strain energy for relatively small in-plane deformation. Consequently, if the bending stiffness is low, buckling usually produces large lateral deflections.

For example, when a part is ejected from the mould, buckling may occur when the stress in the part caused by ejection load reaches the critical value. Differential shrinkage and orientation effects create membrane stresses which also can produce buckling.

The basic equation of linear static stress analysis is:

$$[K]\{U\}=\{P\}$$

where [K] is the stiffness matrix and {U} and {P} are, respectively, the vectors of displacement and applied nodal loads.

GENERALISED BUCKLING ANALYSIS

In buckling analysis, the aim is to determine the critical buckling load for some known distribution {P} of applied loading. By definition then, it can be written:

$$\{P\}_{cr} = \lambda\{P\}_{ref}$$

where: $\{P\}_{cr}$ is the critical level of the applied load distribution,

$\{P\}_{ref}$ is an arbitrary level of the same load distribution (reference load),

λ is a scalar.

With these definitions, buckling occurs when the load multiplier λ reaches a critical value λ_{cr}. The starting point in buckling analysis is the assumption that each coefficient of the stiffness matrix $[K_t]$ varies linearly with the applied load. As described above, the applied load can be thought of as some parameter (say λ)

multiplied by a constant vector of forces $\{P\}_{ref}$. Given two known states of the structure, ($[K_t]_{\lambda 1}$, λ_1 and $[K_t]_{\lambda 2}$, λ_2), and the assumption of linearity, the stiffness matrix at any given equilibrium configuration, $[K_t]_\lambda$ is given by:

$$[K_t]_\lambda = [K_t]_{\lambda 1} + \frac{\lambda - \lambda_1}{\lambda_2 - \lambda_1}([K_t]_{\lambda 2} - [K_t]_{\lambda 1})$$

If we define the fraction term as μ , and the change in stiffness from λ_1 to λ_2 as $[\Delta K_t]$, then:

$$[K_t]_\lambda = [K_t]_{\lambda 1} + \mu\,[\Delta K_t] \qquad (2\text{-}2\text{-}2\text{-}1)$$

At a buckling point, these are two equilibrium configurations, {U} and {U+δU}, both at the same load level. This is illustrated in Figure 2.2.2.1a and b, which shows the equilibrium configurations for the two basic types of buckling.

Using the basic equation of linear analysis, it can therefore be written:

$$[K_t]\{U\} = \{P\}_{ref}$$

$$[K_t]\{U+\delta U\} = \{P\}_{ref}$$

where{U} are the displacements corresponding to load {P}, and {δU} denotes the (infinitesimal) displacements between the two equilibrium configurations. Subtracting the first equation from the second gives:

$$[K_t]\{\delta U\} = 0$$

where $[K_t]$ is a function of λ. From linear algebra, it is known that solving the above equation is equivalent to solving:

$$\det[K_t] = 0$$

Hence, buckling occurs when the determinant of $[K_t]$ is zero. The equation to be solved for the generalised buckling problem is therefore (from the Equation (2-2-2-1):

$$\det([K_t]_{\lambda 1} + \mu\,[\Delta K_t]) = 0 \qquad (2\text{-}2\text{-}2\text{-}2)$$

This is an eigenproblem, in which μ is an unknown to be found. Equation (2-2-2-2) can be solved by standard methods (for example subspace iterations).

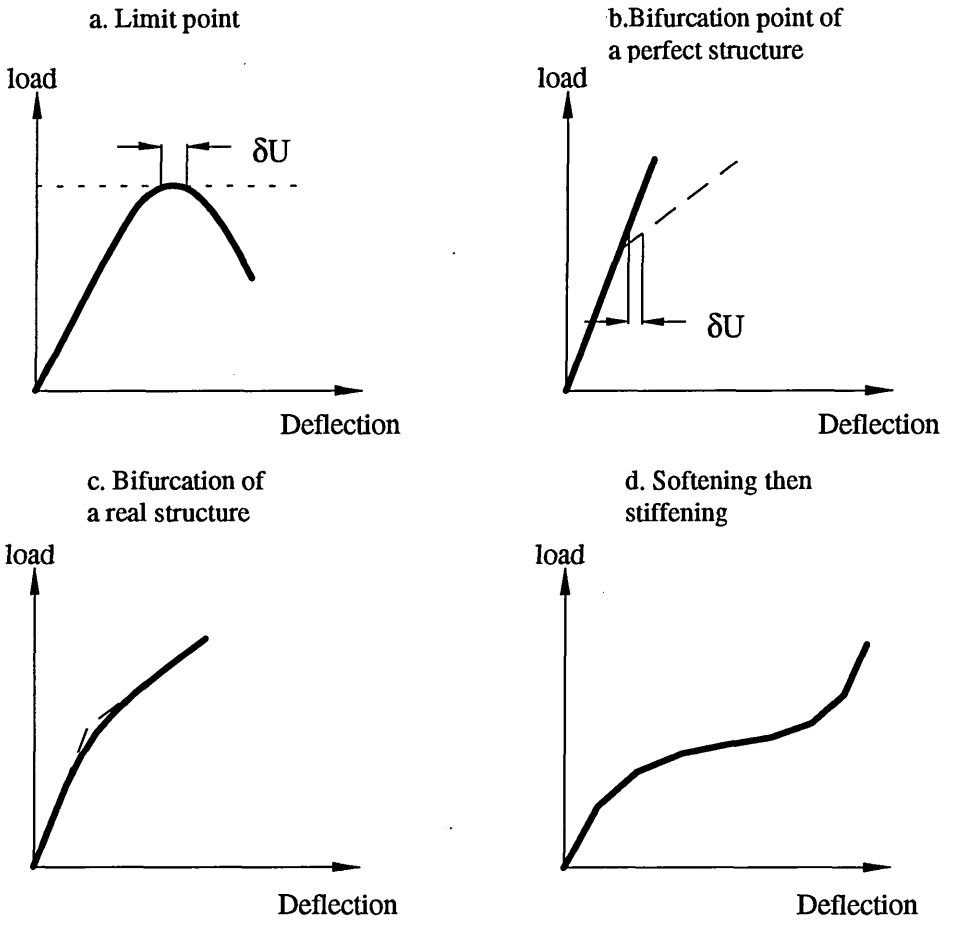

Figure 2.2.2.1 Equilibrium configuration at a buckling point

By rearranging the definition of μ , it is found that:

$$\lambda = \lambda_1 + \mu\,(\lambda_2 + \lambda_1) \qquad (2\text{-}2\text{-}2\text{-}3)$$

This tells the load multiplier required to cause buckling. The analysis could use two simplifications of this general method, which are called Linear (Classical) Buckling Analysis and Linearized Buckling Analysis [23]. Some FEA software is equipped with both algorithms e.g. MF/WARP of MOLDFLOW®, and some just uses the classical algorithm, e.g. ABAQUS®.

LINEAR (CLASSICAL BUCKLING) ANALYSIS

In this method, it is chosen $\lambda_1 = 0$ and $\lambda_2 = 1$, that is zero and full applied load are taken as the reference state. In this case, μ reduces to λ (from Equation (2-2-2-3)) and Equation (2-2-2-2) becomes:

$$\det([K_t]_0 + \lambda ([K_t]_1 - [K_t]_0)) = 0$$

Updated Lagrangian theory allows $[K_t]$ to be split into two components:

$$[K_t] = [K_L] + [K_G]$$

Where $[K_L]$ is a first order stiffness matrix and $[K_G]$ is a higher order stiffness matrix (also called stress or geometric matrix). $[K_G]$ is a linear function of material stresses.

If the part is initially unstressed, then $\lambda_1 = 0$ means that $[K_G]_0 = 0$. Thus:

$$\det ([K_L]_0 + \lambda ([K_L]_1 + [K_G]_1 - [K_L]_0)) = 0 \quad (2\text{-}2\text{-}2\text{-}4)$$

The key assumption made in the classical method is that the response up to $\lambda_2 = 1$ is purely linear, that is stresses and $[K_G]_1$ will be evaluated using original coordinates. Another assumption made in the classical method is that the first order part of the stiffness does not change with load, that is $[K_L]_0 = [K_L]_1$. In total Lagrangian terminology, this is equivalent to neglecting the so-called "displacement-matrix" effect. So Equation (2-2-2-4) reduces to:

$$\det ([K_L]_0 + \lambda [K_G]_1) = 0 \qquad (2\text{-}2\text{-}2\text{-}5)$$

LINEARIZED BUCKLING ANALYSIS

In this method, it is chosen that $\lambda_1 = 0$ and λ_2 very close to λ_1, that is zero and a very small fraction of the load are taken as the reference states. Since only a very small step

is taken, equilibrium iterations are not required and the step using strategy Equation (2-2-2-5).

It is also assumed that $[K_L]_{\lambda 1} = [K_G]_{\lambda 2}$. Note that in this method the stresses are evaluated using updated coordinates. Equation (2-2-2-2) now becomes:

$$\det ([K_t]_{\lambda 1} + \mu ([K_G]_{\lambda 2} - [K_G]_{\lambda 1})) = 0 \qquad (2\text{-}2\text{-}2\text{-}6)$$

The simplest and fastest way to analyse pre-stressed components is to take $\lambda_1 = 0$ and $\lambda_2 = 0.001$. Thus only one step need be taken, and because no equilibrium iterations are carried out, the cost of solution is only slightly greater than the cost of the classical method.

There are two basic types of buckling, both satisfying the equation *det* $([K_t]) = 0$:

- Limit point
- Bifurcation

A *limit point,* loosely speaking, is a state where the component can accept no more load without a major change of shape, see Figure 2.2.2.1 a. This typically occurs in dome-shape component, where a central load may cause the dome to "snap-through". More generally, it is expected that buckling is of the limit point type when there is significant geometric nonlinearity before the buckling point. In the dome example, the component needs to become fairly flat before the stiffness matrix determinant becomes zero. After the "snap-through" (which may be gentle or severe), the component can accept more load, but generally components must be designed so that expected loads do not reach the limit point.

A *bifurcation* is a "branching" point where two possible equilibrium states lie close together. If you think of a perfectly symmetric flat plate, then the response of the plate to an in-plane compressive load is simple linear. However, once the load exceeds a critical value the equilibrium becomes unstable. So a real flat plate will buckle at that critical load level. Thus there are two possible equilibrium paths, and their intersection is called a "bifurcation point", see Figure 2.2.2.1 b.

Both these types of buckling can also appear in warpage or thermal loading problems, although bifurcation is more common. In the flat plate example, imperfection in the plate causes a blurring of the sharp change of stiffness at the Bifurcation point, as shown in Figure 2.2.2.1c. Another common response is "softening followed by stiffening", as shown in Figure 2.2.2.1d. In this case, the determinant of $[K_t]$ falls to some small value, but not zero.

Buckling analysis of cases, like Figure 2.2.2.1b and c, usually give a good indication of where the bifurcation is. Analysis of cases, like Figure 2.2.2.1a, tend to overpredict the limit point. In a problem, like Figure 2.2.2.1d, there is no clear-cut buckling load, however the buckling analysis will often indicate where the nonlinearity starts to become severe.

Shell buckling has become one of the major areas of interest in structural mechanics in recent years [67] [68]. A great number of experiments and analyses have been performed to investigate buckling problems of cylindrical shells subject to axial forces and external pressure and much of that data can be used in vessel design. As is well known, the buckling phenomena of shell structures are affected by various

parameters, for example, geometrical imperfections, boundary conditions and combined loading modes.

A perfect cylindrical shell in uniform axial compression may exhibit three kinds of buckling. Initial buckling in the small deflection range can occur in two possible modes. In the first of these the radial displacements are in the form of waves along the length of the shell with the displacements constant around the perimeter of any transverse section. This is known as symmetrical or 'ring' buckling. The other modes take the form of waves in both the longitudinal and transverse directions, giving a pattern of rectangular depressions and bulges all over the surface of the cylinder. This is known as 'chessboard' buckling. In the post-buckling range the deflections can no longer be regarded as infinitesimally small, and having reached the initial buckling load the cylinder snaps through into another state of equilibrium associated with a smaller axial load and a different pattern of buckles. The two pre-buckling configurations are illustrated diagrammatically in Figure 2.2.2.2.

INITIAL RING BUCKLING

It is assumed, see Figure 2.2.2.2, that the radial displacement w at buckling can be represented by [67]:

$$W = -A \sin \frac{m\pi x}{l} \qquad (2\text{-}2\text{-}2\text{-}7)$$

where l is the length of the cylinder, m is the number of half-waves in x direction, and A the maximum buckle deflection. It is not possible for a deformation of this nature to occur without extension of the middle surface in the circumferential direction around

the bulges, and contraction around the depressions. So strain energy due to bending

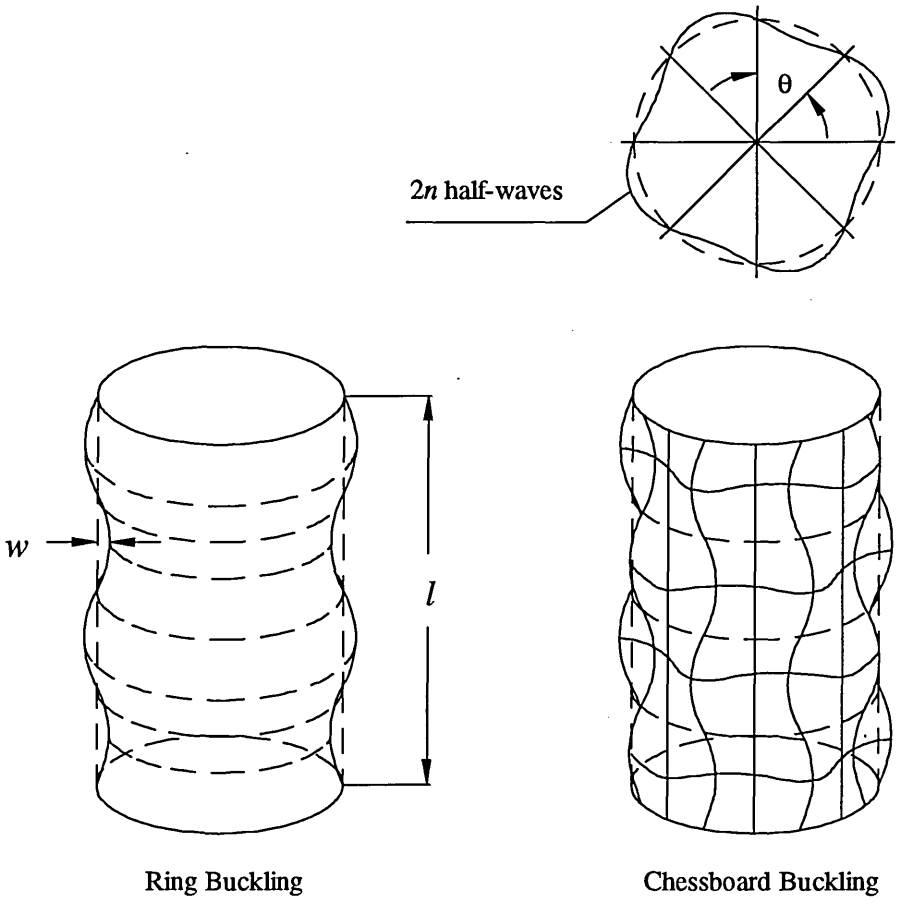

Figure 2.2.2.2 Cylindrical shell buckling configurations

and stretching is mobilised. The strain ε_1 and ε_2 in the axial and circumferential direction are found by assuming that the axial compressive force remains constant during buckling. The axial strain of the unbuckled cylinder (ε_0) at the critical stress σ_{cr} is given by:

$$\varepsilon_0 = -\frac{\sigma_{cr}}{E} \qquad (2\text{-}2\text{-}2\text{-}8)$$

and the axial strain after buckling is:

$$\varepsilon_0(1-\nu^2) = \varepsilon_1 + \nu\varepsilon_2 \qquad (2\text{-}2\text{-}2\text{-}9)$$

change of curvature in the y direction and no twist of an element of the shell wall. Thus,

$$\gamma_{xy}=\beta_y=\beta_{xy}=0. \tag{2-2-2-12}$$

Also, the change in x direction curvature is given by

$$\beta_x=\frac{\partial^2 w}{\partial x^2}=A\frac{m^2\pi^2}{l^2}\sin\frac{m\pi x}{l}, \tag{2-2-2-13}$$

and from energy theory, it is found that

$$\begin{aligned} U_b &= \frac{1}{2}\cdot\frac{Et^3}{12(1-\nu^2)}\int_0^l A^2\frac{m^4\pi^4}{l^4}\sin^2\frac{m\pi r}{l}\cdot 2\pi r dx \\ &= \frac{Et^3}{12(1-\nu^2)}\cdot\pi r l\frac{\pi^4 m^4}{2l^4} \end{aligned} \tag{2-2-2-14}$$

Further more,

$$\begin{aligned} U_s &= \frac{Et}{2(1-\nu^2)}[\int_0^l 2\pi r\varepsilon_0^2(1-\nu^2)dx-\int_0^l 2\nu(1-\nu^2)\varepsilon_0\frac{A}{r}\sin\frac{m\pi x}{l}dx \\ &\qquad +\int_0^l(1-\nu^2)\frac{A^2}{r^2}\sin^2\frac{m\pi x}{l}dx], \\ &= \pi rlEt\varepsilon_0^2-2\pi Et\nu\varepsilon_0\int_0^l A\sin\frac{m\pi x}{l}dx+\frac{Et\pi lA^2}{2r}. \end{aligned} \tag{2-2-2-15}$$

Now the strain energy in the cylinder before buckling is

$$\begin{aligned} &= \iint\frac{1}{2}N_x\varepsilon_0 dA \\ &= \pi rlEt\varepsilon_0^2, \end{aligned} \tag{2-2-2-16}$$

so that the change in strain energy during the buckling process (ΔU)

$$=U_b+U_s-\pi rlEt\varepsilon_0^2. \tag{2-2-2-17}$$

By substitution from Equation (2-2-2-14)and (2-2-2-15),

$$\Delta U=\frac{\pi EtlA^2}{2r}+\frac{\pi rlEt^3}{12(1-\nu^2)}\cdot\frac{\pi^4 m^4 A^4}{2l^4}-2\pi Et\nu\varepsilon_0\int_0^l A\sin\frac{m\pi x}{l}dx. \tag{2-2-2-18}$$

The work done by the external compressive force during buckling is equal to the end-load on the cylinder multiplied by the shortening of the axial length due to bending, and to the change ε_1-ε_0 in axial strain. Denoting this work as ΔT it may be deduced that

$$\Delta T = \sigma_{cr} t \cdot 2\pi r[\frac{A^2}{4} \cdot \frac{m^2\pi^2}{l} + \frac{\nu}{r}\int_0^l A \sin\frac{m\pi x}{l} dx], \qquad (2\text{-}2\text{-}2\text{-}19)$$

and equating ΔT and ΔU gives

$$\sigma_{cr} = \frac{Et^3}{12(1-\nu^2)}(\frac{m^2\pi^2}{tl^2}) + \frac{El^2}{r^2m^2\pi^2} . \qquad (2\text{-}2\text{-}2\text{-}20)$$

If σ_{cr} is taken as a continuous function of $m\pi/l$ this expression can be minimised to find the lowest value of σ_{cr}, designed $(\sigma_{cr})_{min}$. Then,

$$(\sigma_{cr})_{min} = \frac{E}{\sqrt{3(1-\nu^2)}} \cdot \frac{t}{r} , \qquad (2\text{-}2\text{-}2\text{-}21)$$

and for a long tube buckling into many longitudinal waves, the minimum buckling stress occurs when

$$\frac{m\pi}{l} = (\frac{Et}{r^2D})^{1/4} . \qquad (2\text{-}2\text{-}2\text{-}22)$$

In the above analysis it was assumed that the edges of the cylinder were free to move rapidly at the end point of the application of the end-load. If lateral expansion is prevented at the ends, often the case in compression tests between parallel platens, then the axial load applies a bending stress as well as pure compression and this must be accounted for in the theory.

INITIAL CHESSBOARD BUCKLING

To take account of the circumferential as well as longitudinal waving, the radial displacements are now represented by

$$w=-A\sin\frac{m\pi x}{l}\cdot\sin n\theta, \qquad (2\text{-}2\text{-}2\text{-}23)$$

where the circumference divides into 2n half-waves, shown in Figure 2.2.2.2.

Proceeding as before, it can be shown that, when m is large, and $(m\pi r/l)^2$ is a large number,

$$\sigma_{cr}=\frac{Et^2}{12(1-\nu^2)}\left[\frac{(n^2+(m\pi r/l)^2)^2}{r^2(m\pi r/l)^2}\right]+\frac{E(m\pi r/l)^2}{(n^2+(m\pi r/l)^2)^2}\ , \qquad (2\text{-}2\text{-}2\text{-}24)$$

and for $n = 0$ (i.e. no circumferential waves), the expression coincides with Equation (14).

Minimising to find the lowest value of σ_{cr} gives:

$$(\sigma_{cr})_{\min}=\frac{E}{\sqrt{3(1-\nu^2)}}\cdot\frac{t}{r}\ , \qquad (2\text{-}2\text{-}2\text{-}25)$$

occurring when

$$\frac{n^2l^2+(m\pi r)^2}{m\pi rl}=\left(\frac{Et}{r^2D}\right)^{1/4}\ . \qquad (2\text{-}2\text{-}2\text{-}26)$$

Thus the value of $(\sigma_{cr})_{\min}$ is the same as for ring buckling when m^2 is a large number, and is independent of the length or the number of circumferential lobes n. For short cylinders, however, account must be taken of the number of circumferential lobes, particularly when there are only one or two longitudinal half-waves formed at buckling.

3 THE RESEARCH WORK

3.1 MATERIAL PROPERTIES

The material, which is used to produce the closure and discussed in this project, is Polypropylene, NESTE PP VB19 85KNA.

Polypropylene (PP) is a semi-crystalline thermoplastic. Polypropylene was first produced in 1954 by Natta of Milan following on the work of K Ziegler in Germany. The expiry of the basic patents led to a surge in production capacity in 1970s which so exceeded demand that the material became available at abnormally low prices which, in turn, stimulated more growth in usage.

3.1.1 GENERAL PROPERTIES OF THE MATERIAL

In general, the most important properties of Polypropylene compared with Polyethylene are as following:

- It has a lower density (0.9 g/cm^2).
- It has a higher softening point and hence a higher maximum service temperature. Articles can withstand boiling water and may be subject to many steam sterilising operations.
- It appears to be free from environmental stress cracking problems. The only exception seems to be with concentrated sulphuric and chromic acids and with aqua regia.
- It has a higher brittle point.

- It is more susceptible to oxidation.

The mechanical and thermal properties of Polypropylene are dependent on the degree of isotacticity, the molecular mass and on other structural aspects. The properties of five commercial materials (all made by same manufacturer and subjected to the same test method) which are of approximately the same isotactic content, but which differ in melt flow index (molecular mass) and are either homopolymers or block copolymers are compared [16], in Table 3.1.1.

Table 3.1.1 The effect of melt flow index (molecular mass) on material properties

Property	Test details	Homopolymers			Copolymers	
Melt flow index	2.16kg at 230 °C	3.0	0.7	0.2	3.0	0.2
Teasel strength (MPa)	45mm/min	34	30	29	29	25
Elongation at break (%)	45 mm/min	350	115	175	40	240
Flexural modulus (MPa)		1310	1170	1100	1290	1030
Impact strength (J)	20 °C	13.5	34	46	46	57.5

The figures in Table 3.1.1 show quite clearly how a decrease in melt flow index (an increase in molecular mass) cause a reduction in tensile strength and stiffness but an increase in impact strength.

In the case of thermal properties, the specific heat of polypropylene is lower than that of polyethylene but higher than that of polystyrene. Therefore, the plasticising

capacity of an injection moulding machine using polypropylene is slower than when polystyrene is used but generally higher than a high density polyethylene.

In the case of melt flow properties, polypropylene is more non-Newtonian than polyethylene in that the apparent viscosity declines more rapidly with increase in shear rate. The melt viscosity is also more sensitive to temperature.

In the case of moulding shrinkage, polypropylene is less than experienced with polyethylene but is dependent on such processing factors as mould temperature, melt temperature and plunger dwell time. In general, conditions which tend to reduce the growth of crystalline structure will tend to reduce shrinkage. For example, low mould temperature will encourage quenching of the melt. It is also found that low shrinkage values are obtained with high melt temperatures. This is probably due to the fact that high melt temperatures lead to a highly disordered melt whereas some molecular order may be present in melts which have not been heated much above the crystalline melting point. Such regions of order would provide sites for crystal nucleation and hence crystallisation would be more rapid when cooling was carried out [16].

The general mechanical properties of the material are listed in Table 3.1.2, which are from the material date base of CAMPUS. Some other useful properties are listed in Table 3.1.3, which were obtained from NESTE CHEMICALS.

NESTE PP VB19 85KNA is suitable for injection moulding, extrusion, thermoforming and pellets. Other special characteristics are transparency, anti-static properties and heat stability.

Table 3.1.2 Properties of NESTE PP VB19 85KNA

PROPERTY	UNIT	VALUE
Density	g/ml	0.9
Stress at yield (50 mm/min)	MPa	36
Strain at yield (50 mm/min)	%	8.7
Young's modulus (1 mm/min)	MPa	1700
Heat defl.temp. HDT/A at 1.8 MPA	°C	60
Heat defl.temp. HDT/B at 0.45 MPa	°C	103
Vicat softening point at 10N	°C	155
Melt volume rate MVR (1st value)	ml/10min	2.6
Melt temperature	°C	225
Mould temperature	°C	60
Flow front velocity	mm/s	100

Table 3.1.3 Other Properties of NESTE VB19 85KNA

PROPERTY	UNIT	VALUE	TEST METHOD
Melt flow rate (230 °C/21.6 N)	g/10 min	1.9	ASTM D 1238
Flexural modulus (1% secant)	MPa	700	ASTM D 790
Izod impact strength (Notched at 23 °C)	J/m	60	ASTM D 256
Heat distortion temperature	°C	103	ASTM D 648

3.1.2 THE TEMPERATURE DEPENDENT BEHAVIOUR OF THE MATERIAL

The mechanical properties of plastics are very dependent on temperature and the shear rate. The general effect of temperature and strain rate on the stress-strain behaviour of a plastics is shown in Figure 3.1.1 and Figure 3.1.2. The higher the temperature, the softer and more flexible the material. The higher the shear rate, the harder and more rigid the material.

The property values of the plastics are highly dependent upon the equipment, specimen preparation and testing techniques used. The temperature dependent properties of the materials, listed in Table 3.1.3, are supplied by NESTE CHEMICALS, which are used in the analyses in this project. The illustration of the temperature dependent properties of the material is shown in Figure 3.1.3@.

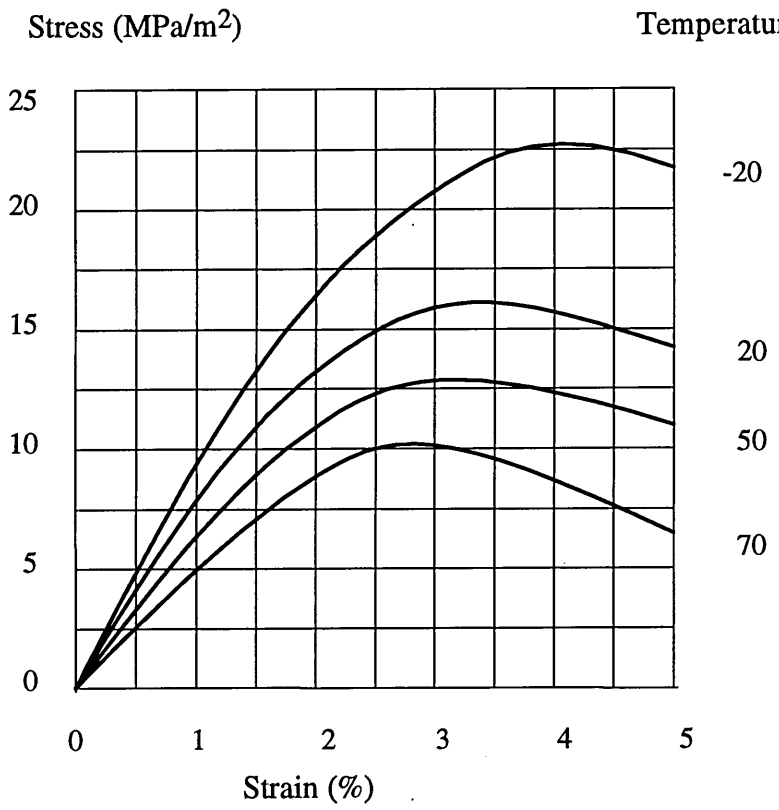

Figure 3.1.1 Effect of material temperature on stress-strain behaviour of plastics

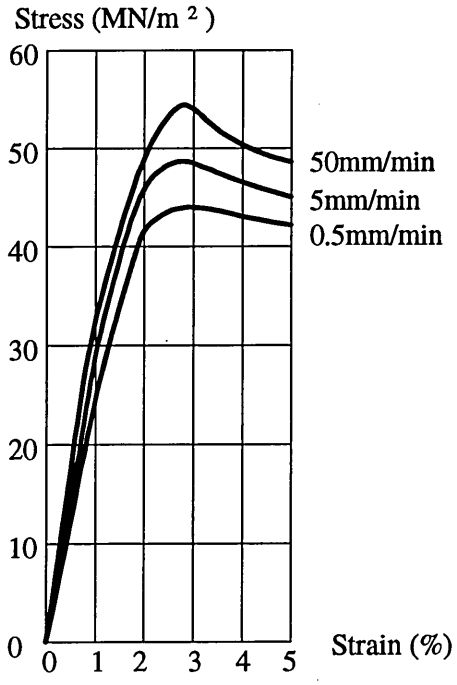

Figure 3.1.2 Effect of strain rate on stress-strain behaviour of plastics

Table 3.1.4 The effect of temperature on the material modulus

Temperature °C	Tensile Modulus (MPa/m^2)	Bending Modulus (MPa/m^2)
-40	3162.278	2154.438
-20	2993.574	2154.438
0	2154.438	1467.777
20	1930.696	898.628
40	1550.515	719.684
60	1056.355	577.968
80	719.684	415.967
100	464.152	299.999
120	268.271	
140	79.998	
150	41.596	

3.2 MOULD FILLING ANALYSIS

There are many ways of forming plastics. Injection moulding and compression moulding are two important possibilities. In the present case of closure processing, a high speed compression moulding is used.

The filling analysis may include many different requirements, such as temperature distribution, pressure distribution, filling time, runner balance and so on. The aim of filling analysis as discussed in this project is to obtain the temperature distribution in the part after mould filling has finished. The results of the filling analysis will be used as the initial boundary conditions of the cooling analysis, which is discussed in the next chapter.

Unlike normal compression moulding, the closure compression moulding utilises very high compressing speeds and uses thermoplastic material. It is a possibility to use an injection moulding to simulate this moulding process. To assess the difference between injection moulding and compression moulding for closure forming, two computer software, namely MOLDFLOW® and FILLCALC V® , were investigated to simulate and analyse closure filling. MOLDFLOW® is designed for injection moulding and the FILLCALC V® is suitable for compression moulding. A comparison of the analysis results of these two software packages was made in terms of the different temperature distributions achieved.

3.2.1. CLOSURE PROCESSING CONDITION

The manufacturing machine for closure forming is shown in Figure 3.2.1[@]. The processing conditions are as follows:

Number of the moulds in circle:	54 pieces around the machine periphery
Running speed:	515 closure per minutes
Working positions:	1 position for material injection
	1 position for compression
	46 positions for cooling
	4 positions for ejection
	2 positions for waiting
Compression time T_p:	$T_p = 60 / 512 = 0.117$ sec
Cooling time T_c:	$T_c = T_p * 46 = 5.39$ sec
Clamp open time T_o:	$T_o = T_p * 4 = 0.469$ sec
Coolant:	Water
Coolant inlet temperature:	16 °C

The processing cycle is as follows:

1. melt material injected into the cavity;
2. the mould compression (T_p);
3. cooling begins (T_c);
4. cavity open to eject closure (T_o);
5. waiting for next cycle.

3.2.2 INJECTION MOULDING ANALYSIS

The closure forming was simulated using MF/FLOW, MOLDFLOW® filling analysis software package, since the further cooling analysis could be based on the results of this simulation. Although MF/FLOW is designed primarily for injection moulding, it is found that is could be successfully adapts for compression moulding as is shown in the following sections.

3.2.2.1 THE MODEL FOR MF/FLOW ANALYSIS

A three dimension model and finite element mesh for the closure were generated using MF/VIEW, MOLDFLOW® pre/post processor package, shown in Figure 3.2.2@. Instead of the three dimension solid model, a three dimension shell surface model was built for the closure filling analysis because of the limitations of the geometrical modelling ability of the MF/VIEW software package. A triangular element mesh is used for MF/FLOW filling analysis.

The MF/FLOW, MOLDFLOW® filling analysis package, using the three dimension finite element mesh and actual processing conditions, give results which can be graphically displayed using MF/VIEW. There are many special functions available in MF/VIEW. The temperature distribution was of greatest interest in this project. There are two algorithms for temperature distribution calculation in MF/VIEW, fast analysis and multi-laminate analysis.

In a fast analysis, the criterion is that the temperature at the end of flow is approximately equal to the injection melt temperature. This implies, but does not guarantee, that the part will be able to be adequately packed. The degree of packing cannot be determined from a simple fill-only analysis.

In contrast, the multi-laminate analysis uses a finite difference algorithm that is much more computationally intensive, but provides more accurate results with additional information about the injection process.

Figure 3.2.3 shows the difference between the algorithms in terms of the temperature values in the output result files and, in principle, the effect of different injection speeds on the temperature profiles.

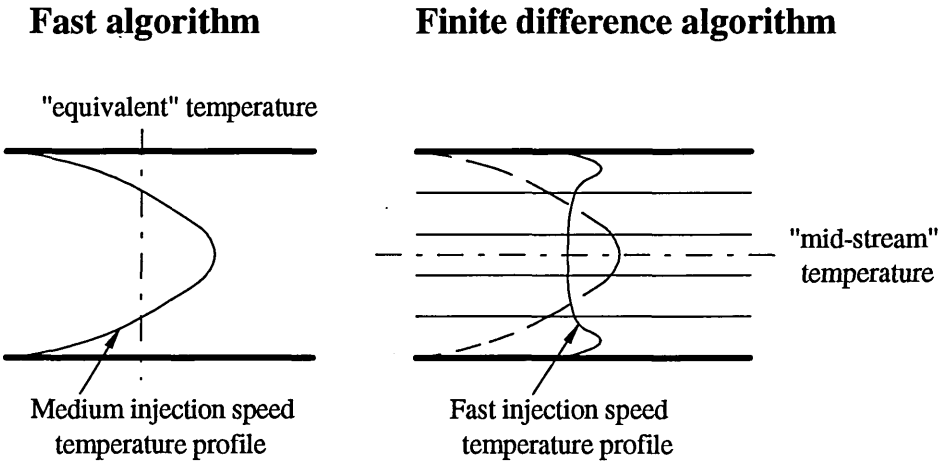

Figure 3.2.3 Temperature profiles using the different algorithms

FAST ALGORITHM:

The temperature from this algorithm is an "equivalent value" across the cavity thickness. The value is determined as the temperature that would give the same overall resistance to flow as obtained from using the actual temperature profile.

The fast algorithm assumes an approximately parabolic temperature profile. This is valid when the injection speed is such that the end of fill temperature is approximately equal to the injection melt temperature. That is, frozen layer thickness is not great, since shear heating is balanced by heat lost through conduction. The profile changes with faster and slower injection speeds but still remains basically parabolic over the range of suitable conditions.

If the temperature at the end of fill cannot be made to approximate the melt injection temperature due to a slow injection speed causing excessive thickness of the frozen layer, the multi-laminate type of analysis should be used.

MULTI-LAMINATE ALGORITHM:

Multi-laminate algorithm uses a finite difference algorithm. The temperature from this algorithm is the actual value at mid-stream position. This is based on the temperature at the grid point each laminate. The profile is similar to that of the fast algorithm only when injection speed is such that the end of fill temperature is approximately equal to the injection melt temperature. That is, frozen layer thickness is not great, since shear heating is balanced by heat lost through conduction.

At much faster and slower injection speeds, the change in frozen layer thickness results in a significant change in temperature profile. For example, at faster speeds, higher frictional heating results in a relatively thin frozen layer and, therefore, a temperature at the cavity wall which is greater than the mid-stream temperature.

The processing conditions used for the MF/FLOW analysis were as follows:

Material:	NESTE PP VB19 85KNA
Melt temperature:	200 °C
Mould temperature:	50 °C
Injection time:	0.117 sec
Total volume:	3.55 cu.cm
Flow rate:	32.27 cu.cm/s

3.2.2.2 FILLING ANALYSIS RESULTS

The summary of the filling analysis is listed at Appendix A1 and the temperature distribution of the closure at the end of the filling processing is shown in Figure 3.2.4@.

3.2.3 COMPRESSION MOULDING ANALYSIS

The compression moulding analysis for closure forming was simulated using FILLCALC V® computer software package. The aim of the analysis is to verify the MF/FLOW of MOLDFLOW® for the simulation of the closure filling process so that cooling analysis could be carried out using the MOLDFLOW® software.

3.2.3.1 THE MODEL FOR THE FILLCALC V® FILLING ANALYSIS

In the same way as for MF/FLOW of MOLDFLOW®, a three dimension surface model and a triangular finite element mesh of the moulding is generated for the FILLCALC V® filling analyses, as shown in Figure 3.2.5@.

In FILLCALC V®, the temperature distribution calculation is solved at the centroids /centres of the element using the finite difference technique proposed by S V Patankar [69], that employs a control volume formulation. Same as for MF/FLOW of MOLDFLOW®, the analysis is also based on the multi-laminate algorithm.

The processing conditions for FILLCALC V® analysis are as follows:

Material: PP NESTE VB19 85KNA

Melt temperature: 200 °C

Mould temperature: 50 °C

Compression time: 0.118 sec

Total volume: 3.55 cu.cm

3.2.3.2 FILLING ANALYSIS RESULTS

The summary of the filling analysis is listed in Appendix A2 and the temperature distribution of the closure at the end of the filling processing is shown in Figure 3.2.6@. There are two temperature distributions given by FILLCALC V®, namely the maximum temperature in the cross-section shown on Figure 3.2.6@ a, and the surface temperature, shown on Figure 3.2.6@ b.

3.2.4 COMPARISON OF THE FILLING ANALYSIS RESULTS OF INJECTION MOULDING AND COMPRESSION MOULDING

The results given by the MF/FLOW analysis, shown in Figure 3.2.4@, were the mid-steam temperatures located in centre of the cross-section, and the results given by FILLCALC V®, shown in Figure 3.2.6@ a, were maximum temperatures in the cross-section.

There are differences for these two software to plot out the temperature distributions. When the assumed injection (or compression) speed is moderate, these two analyses both present the temperature in the middle of the cross-section. When the assumed injection (or compression) speed is very fast, MF/FLOW analysis results still gives out the temperature located in middle of the cross-section of the part wall while the friction heating caused by the high flow speed makes the laminates near the surface have a high temperature, shown in Figure 3.2.3, FILLCALC V® analysis results will give a higher surface temperature than the middle of the cross-section.

Comparing the results given by these two different filling analyses, both results show a similar temperature distribution. But in some regions of the surface, the temperature distribution given by MF/FLOW is slightly lower than that given by FILLCALC V®. The maximum difference of the temperature between these two results is about 1.5 deg.C. In the closure moulding process, the compression time is very fast, at about

0.118 seconds. In the moulding, some parts of the closure will have a higher surface temperature than the centre of the cross-section, which is caused by the high speed melt flow. So the temperature difference between these two results is because of the different ways the temperature is plotted out by these two software. The temperature distributions generated by these two software are very close.

This means that in the case of this particular moulding, MF/FLOW and FILLCALC V ® both give very similar results for the filling temperature distribution.

The MF/FLOW filling analysis result provides a basis of the temperature boundary conditions for MF/COOL, MOLDFLOW® cooling analysis package, so that a further cooling analysis in closure moulding can be performed.

3.3 COOLING

3.3.1 FUNDAMENTALS OF COOLING TECHNOLOGY

For design engineers, there are at least two main concepts to keep in mind when considering the design of cooling systems:

1. Obtaining the minimum cooling cycle time;
2. Achieving the required temperature distribution.

The first concept is concerned mainly with economic benefits and the second concept is concerned with the final quality of the parts.

3.3.1.1 HEAT EXTRACTION

The mould is essentially a heat exchanger which must be capable of extracting heat at the required rate. The cooling analysis calculates a minimum cooling time based on the conductivity and specific heat of the material, and the mould and melt temperature. The cooling time represents the time the plastic takes to cool to its freeze temperature given these mould conditions. This usually represents 80% of the total processing cycle time.

Two major factors affecting the cooling time are melt temperature and mould temperature. Both may need to be varied in order to obtain a high quality part. Increasing either the melt or mould temperature increases the cooling time. Since the

part is usually ejected when the freeze temperature is reached, this will inevitably result in increased cycle times.

Running at lower mould temperatures results in shorter cycle times with subsequent benefits in improved economic performance. This is the outcome that an optimised cooling system should achieve.

3.3.1.2 HEAT EXCHANGE

Consider the mould as a heat exchanger. Heat passes into the mould and transfers out. The primary source of energy input is hot plastic injected into the cavity. There are two other possible sources of energy: cooling circuits and hot runners.

During mould filling, heat will be lost by three mechanisms:

1. coolant flow in the cooling circuits;
2. heat lost by conduction to the moulding machine platens;
3. heat lost to the atmosphere by convection and radiation.

Most of the heat will be extracted by coolant flow. When the mould is running at a higher temperature, the heat loss from platens and to the atmosphere may be significantly greater. The process of heat exchange is illustrated in Figure 3.3.1.1.

In an energy balance, the amount of heat passing into the system must be equivalent to the amount of heat being taken out.

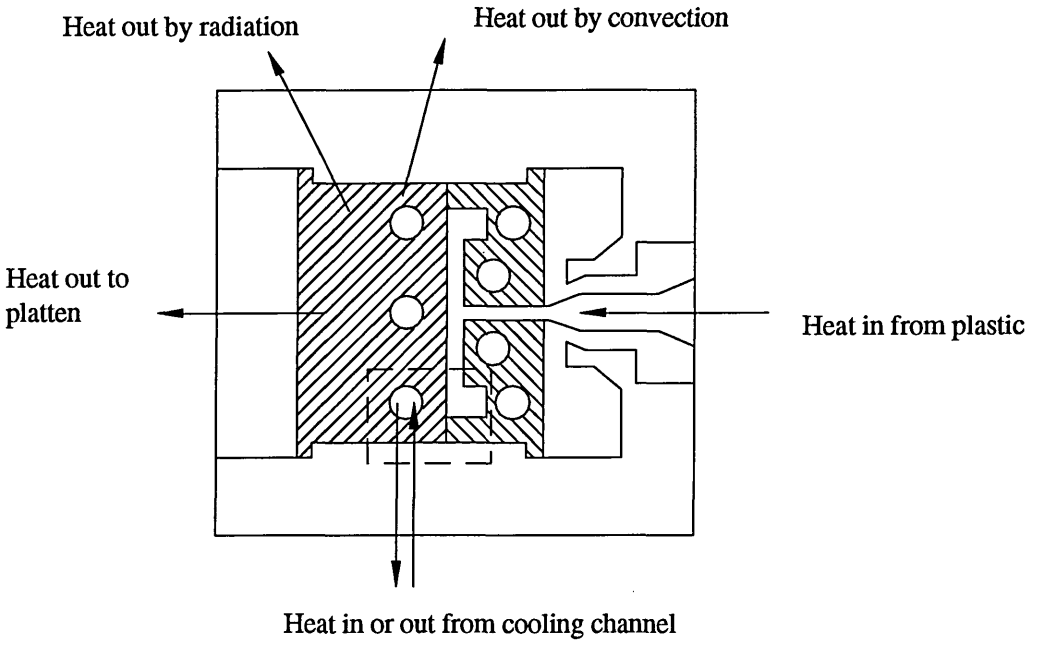

Figure 3.3.1.1 Heat exchange in mould

3.3.1.3 HEAT TRANSFER IN THE MOULD

The efficiency of heat extraction relates to heat transfer from the metal to the coolant.

The temperature gradient from the cavity to the cooling channel has two components, as shown in Figure 3.3.1.2:

1. the temperature gradient across the plastic/metal interface, which depends on the conductivity of the metal;

2. the temperature gradient across the coolant/metal interface, which depends on the coolant heat transfer coefficient which varies with the coolant flow type.

Consider a cooling channel in which the coolant flow is gradually increased. At very low speed the flow is laminar, the heat has to be conducted through various layers of

coolant to the centre of the cooling channel. Since the coolant is normally a poor heat conductor, heat transfer is very inefficient, see Figure 3.3.1.3a.

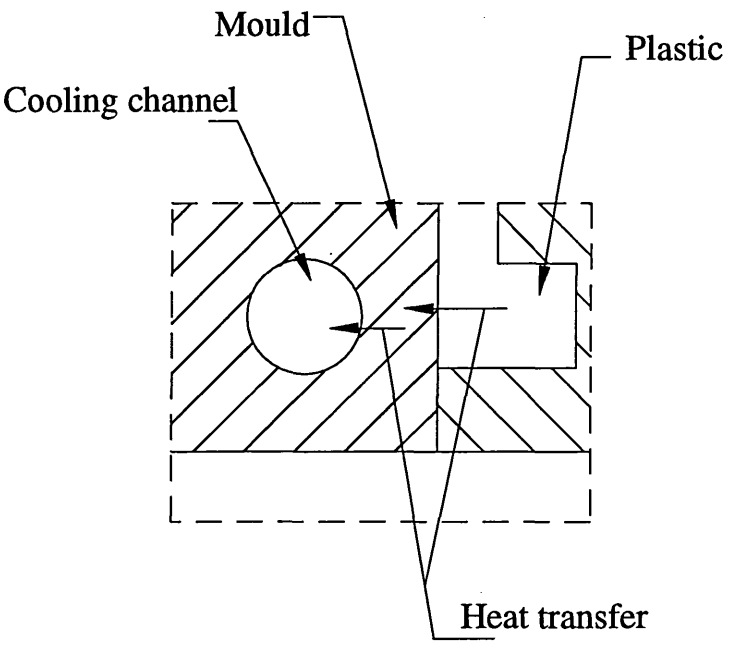

Figure 3.3.1.2 The heat flow path from plastic to cooling channel

As coolant flow increases, heat transfer increases at a marginal rate until the coolant flow become turbulent. There is now a component of coolant velocity perpendicular to the channel which causes a dramatic improvement in heat transfer, see Figure 3.3.1.3b.

The coolant heat transfer coefficient h can be calculated as:

$$\mathrm{Nu} = \frac{h \times A}{k} = Const \bullet (\mathrm{Re})^n \bullet (\mathrm{Pr})^m \qquad (3\text{-}3\text{-}1\text{-}1)^{[*]}$$

where:

A -- Characteristic dimension

k -- Thermal conductivity of fluid

Re -- Reynolds number

Pr -- Prandtl number

where:

$$Re_d = \frac{\rho U_m d}{\mu}$$ (Reynolds number in a tube) (3-3-1-2)[**]

$$Pr = \frac{C_p \mu}{k}$$ (3-3-1-3)[**]

where:

ρ -- density

Um -- weighted mean velocity

d -- diameter of the tube

μ -- dynamic viscosity

Cp -- specific heat

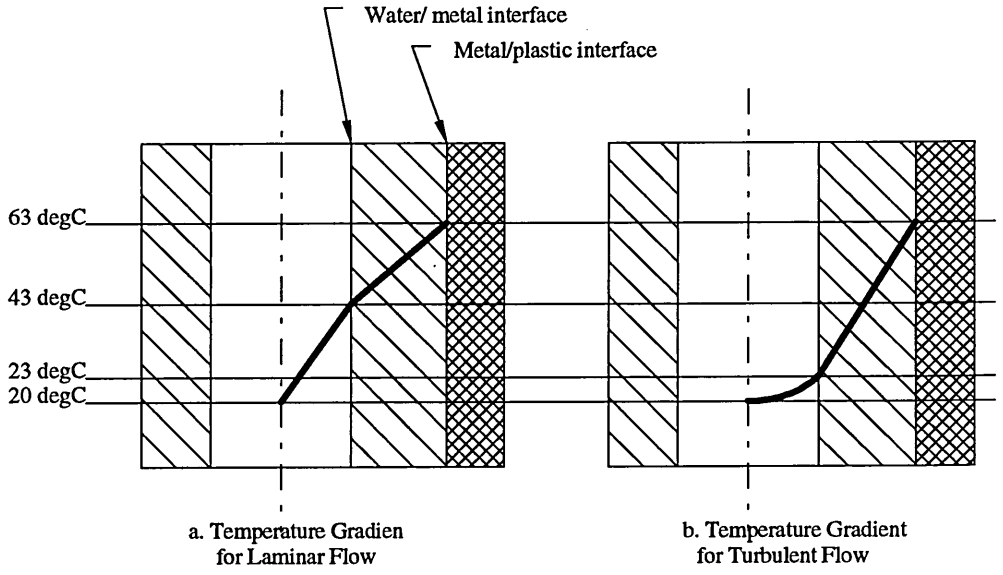

Figure 3.3.1.3 Temperature gradient for laminar and turbulent flow

3.3.1.4 LAMINAR AND TURBULENT FLOW

The relationship between heat transfer and coolant flow can be expressed as a power factor.

Cooling flow is either laminar, turbulent or in transition between laminar and turbulent. For the tube, the Reynolds number can be calculated as:

$$\mathrm{Re}_d = \frac{\rho U_m d}{\mu} \qquad (3\text{-}3\text{-}1\text{-}4)^{[**]}$$

It is calculated on the basis of the tube diameter d and the weighted mean velocity U_m. The weighted mean velocity at any cross-section is defined by the equation:

$$\int \rho U dA = \rho U_m A$$

where $\rho U_m A$ is the total rate of mass flow through A. If the Reynolds number exceeds the critical value for flow through tubes ($\approx$ 2300), the flow becomes turbulent in the approach length.

For convection heat transfer, the heat transfer can be calculated as:

$$Q = h \bullet A \bullet (T_s - T_f) \qquad (3\text{-}3\text{-}1\text{-}5)^{[*]}$$

h -- heat transfer coefficient

For laminar flow, in the case of forced flow convection in laminar flow past a flat plate, the heat transfer coefficient can be calculated as:

---

[*] *Heat Transfer Calculation Using Finite Different Equations,* David R. Croft & David G. Lilley

$$Nu_x = \frac{h_x \bullet x}{k} = 0.332 \bullet \mathrm{Pr}^{1/3} \bullet \mathrm{Re}_x^{1/2} \qquad (3\text{-}3\text{-}1\text{-}6)^{[**]}$$

The heat transfer coefficient increases as the square root of the flow rate. This means that doubling the coolant flow increases the heat transfer by about 40 percent.

For fully turbulent flow, in the case of forced flow convection in laminar flow past a flat plate, heat transfer coefficient can be calculated as:

$$Nu_x = \frac{h_x \bullet x}{k} = \frac{f_x}{2} \bullet \mathrm{Pr} \bullet \mathrm{Re}_x \qquad (3\text{-}3\text{-}1\text{-}7)^{[**]}$$

The heat transfer coefficient increases linearly with the flow rate. Therefore, in the turbulent zone, doubling the coolant flow increases heat transfer by 100 percent.

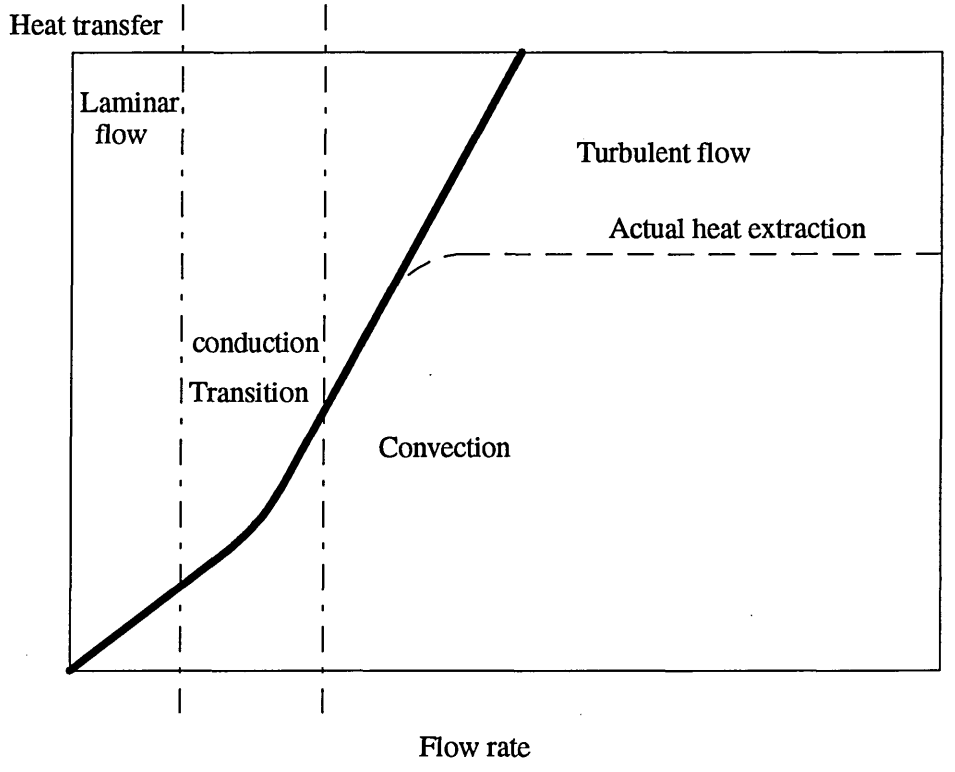

Figure. 3.3.1.4 The vary of the heat transfer with the coolant flow rate

---

[**] *Engineering Thermodynamics Work and Heat Transfer,* G F C Rogers & Y R Mayhew

Further increases in flow rate once turbulent flow is fully developed will continuously increase the moulds capacity to extract heat. However, the amount of heat that can be extracted is limited by the amount of heat passing into the mould. Thus the actual heat extracted from the system may not increase with further increase in flow rate. These relations are shown in Figure 3.3.1.4.

Obviously the most effective condition for heat transfer is to ensure that the coolant flow has entered the turbulent region, but that the capacity to extract heat does not greatly exceed the amount of heat available for extraction.

3.3.2 FINITE DIFFERENCE (FD) MATERIAL HEAT TRANSFER CALCULATIONS

The thermal properties of the plastic materials are very important factors in heat transfer. If its thermal conductivity is too low or its specific heat is too high, the material will not be easily cooled to the target temperature under limited cooling conditions. Therefore, a computer program was established in order to calculate the material cooling potential.

3.3.2.1 THE HEAT TRANSFER MODEL FOR THE MATERIAL COOLING POTENTIAL

An analysis of the feasibility of cooling the material to the required target temperature under limited cooling conditions has been made. A mathematical cooling model has been established using the finite difference method (FDM). The heat transfer model profile and subdivisions are showed in Figure 3.3.2.1.

The heat transfer calculation begins at the end of the moulding. At the end of the moulding, the temperature of the plastic is 215 °C, the mould is at 25 °C and the coolant is at 16 °C. The boundary temperature between mould and plastic is (25+215)/2 = 120 °C. The half thickness of the cooling channel is 0.5 mm, the mould wall thickness is 2.5 mm, and the half thickness of the plastic is 0.5 mm.

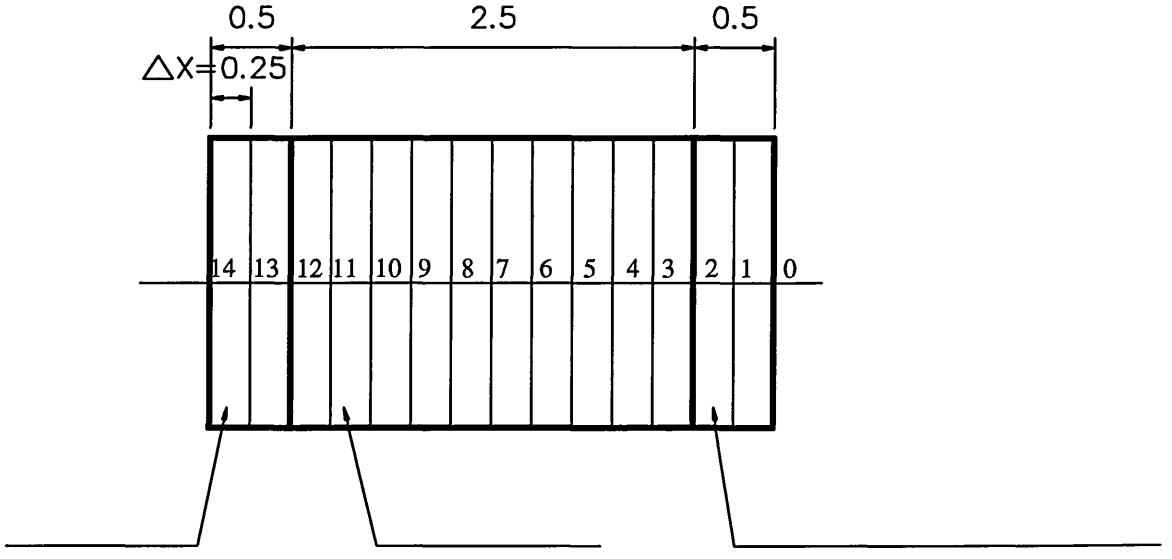

Figure 3.3.2.1 The heat transfer Model

The thermal properties of the materials used in the heat transfer calculations are as follows:

1. the plastics material is NESTE PP VB19 85KNA.

Thermal Conductivity K = 0.118 W/m°C

Specific heat Cp = 2930 J/Kg°C

Density $\rho = 907\ Kg/m^3$

2. the mould material is a Cr-Ni steel (P20).

Thermal Conductivity K = 16 W/m°C

Specific heat Cp = 460 J/Kg°C

Density $\rho = 7865\ Kg/m^3$

3. the coolant is water.

Thermal Conductivity K = 0.6 W/m°C

Specific heat Cp = 4200 J/Kg°C

Density $\rho = 1000\ Kg/m^3$

3.3.2.2 THE ESTABLISHMENT OF THE FD CALCULATION

The basic equations of heat transfer[*] are:

Conduction $Q_x = -kA\frac{\partial T}{\partial X}$ (W) (3-3-2-1)

Convection $Q = hA(T_s - T_f)$ (W) (3-3-2-2)

---

[*] *'Heat transfer calculation using finite difference equations'*, David R. Croft & David G. Lilley

Radiation $Q = \varepsilon\sigma T^4$ (W/m^2) (3-3-2-3)

For transient conditions, the temperature of the substances at a given point will be changing with time: the magnitude of the variation will be a function of the specific heat Cp of the material. In mathematical terms:

$$Q = mCp\frac{\partial T}{\partial t}$$

$$m = \rho V$$

so $$Q = \rho VCp\frac{\partial T}{\partial t} \quad (W) \quad (3\text{-}3\text{-}2\text{-}4)$$

Using the energy balance technique, the finite difference equations (FDEs) for every node can be built as follow:

For point 1 $$\rho v_1 C_p\frac{\Delta T_1}{\Delta t} = \frac{K}{\Delta X}(T_2 - T_1) + h(T_0 - T_1)$$

point i $$\rho v_i C_p\frac{\Delta T_i}{\Delta t} = \frac{K}{\Delta X}(T_{i+1} + T_{i-1} - 2T_i) \quad (i=2 \text{ to } 10)$$

point 11 $$\rho v_{11} C_p\frac{\Delta T_{11}}{\Delta t} = \frac{K}{\Delta X}(T_{11} - T_{12}) + \frac{K'}{\Delta X}(T_{13} - T_{12})$$

point 12 $$\rho v_{12} C_p \frac{\Delta T_{12}}{\Delta t} = \frac{K}{\Delta X}(T_{13} + T_{11} - 2T_{12})$$

point 13 $$\rho v_{13} C_p \frac{\Delta T_{13}}{\Delta t} = \frac{2K'}{\Delta X}(T_{12} - T_{13})$$

The Gauss-Seidel iteration method is used to calculate the temperature profile. That is, when sequentially with the update equations new update value is used as soon as it is available. So the nodes explicit equations are:

For point 1: $$T_1' = 2 \times Fo_1 \times [T_2 + B_i \times T_0 + (\frac{1}{2 \times Fo_1} - B_i - 1) \times T_1]$$

point i: $$T_i' = Fo_1 \times [T_{i-1} + T_{i+1} + (\frac{1}{Fo_{11}} - 2) \times T_i] \qquad \text{(i=2 to 10)}$$

point 11: $$T_{11}' = Fo_1 \times (T_{10} - T_{11}) + Fo_2 \times (T_{12} - T_{11}) + T_{11}$$

point 12: $$T_{12}' = Fo_2 \times [T_{11} + T_{13} + (\frac{1}{Fo_2} - 2) \times T_{12}]$$

point 13: $$T_{13}' = Fo_2 \times [2 \times T_{12} + (\frac{1}{Fo_2} - 2) \times T_{13}]$$

Where, the Fourier number Fo and Biot number Bi given by:

$$Fo = \frac{K\Delta t}{\rho Cp \Delta X} \qquad \text{(3-3-2-4)}$$

$$Bi = \frac{h\Delta X}{K} \qquad \text{(3-3-2-5)}$$

Between two compression processes, there is a short time no plastics material in the mould. During this time, the mould will be cooled continuously. The FDEs in this period for nodes are:

For point 1: $$T_1' = 2 \times Fo_1 \times [T_2 + B_i \times T_0 + (\frac{1}{2 \times Fo_1} - B_i - 1) \times T_1]$$

point i: $T_i' = Fo_1 \times [T_{i-1} + T_{i+1} + (\frac{1}{Fo_{11}} - 2) \times T_i]$ (i=2 to 10)

point 11: $T_{11}' = Fo_1 \times (T_{10} - T_{11}) + T_{11}$

For one dimension connective boundary nodes, the Fourier number is :

$$Fo \leq \frac{1}{2(1+Bi)} \qquad (3\text{-}3\text{-}2\text{-}6)$$

Here, the Biot number is evaluated as:

$$Bi = \frac{\Delta X}{K} \times h = \frac{0.25 \times 10^{-3}}{19} \times h = 1.3 \times 10^{-5} \times h \qquad (3\text{-}3\text{-}2\text{-}7)$$

Hence the stability criterion is,

$$Fo \leq \frac{1}{2(1+Bi)} = \frac{1}{2(1+1.3 \times 10^{-5} \times h)} \qquad (3\text{-}3\text{-}2\text{-}8)$$

So the time-step can be evaluated as:

$$\Delta t = \frac{Fo(\Delta X)^2 \rho Cp}{K} = \frac{5.95 \times 10^{-3}}{1+1.3158 \times 10^{-5} \times h} \qquad (3\text{-}3\text{-}2\text{-}9)$$

Since the conventional heat transfer coefficient h is a difficult parameter to determine, it may be chosen as a variable in the region from 250 to 1500 (the normal region for a water-metal interface). In order to accurately calculate the temperature distribution, the steady temperature state after several cycles is considered as the initial temperature of the mould.

A computer program, written in Turbo C++ language, has been written to calculate the process of heat transfer between plastic and metal and also between metal and coolant (see Appendix A3).

The flow diagram of the heat transfer calculation program is showed in Figure 3.3.2.2.

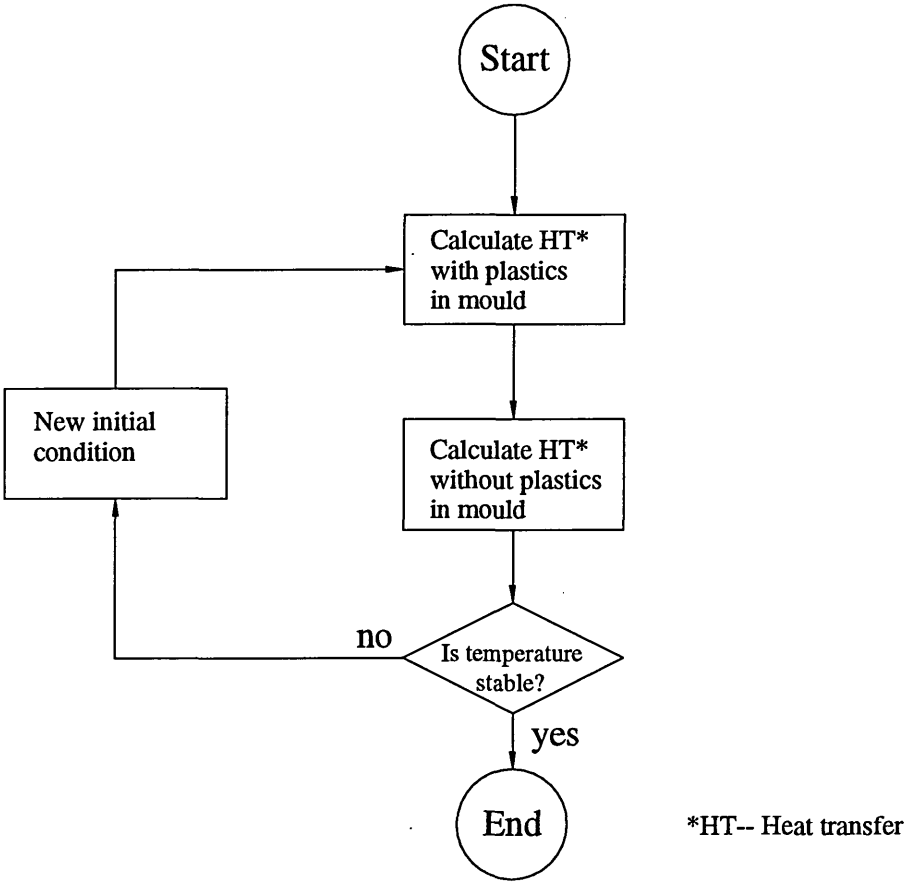

Figure 3.3.2.2 The flow diagram of the heat transfer calculation

The heat transfer calculation results are listed in Table 3.3.2.1 and illustrated in Figure 3.3.2.3.

In the Table 3.3.2.1, three points of temperature cross the profile are listed. These are:

1. temperature between coolant and mould (c&m).
2. temperature between mould and plastic (m&p).
3. temperature in the centre of the plastic (cop).

Table 3.3.2.1 The results of heat transfer calculation

Cycle	H = 200			H = 500			H = 1000			H = 1500		
No.	c&m	m&p	cop	c&m	m&p	cop	c&m	m&p	cop	c&m	m&p	cop
1	62.5	63.7	78.3	53.9	55.7	73.9	42.2	44.6	67.2	34.9	37.6	62.7
2	85.5	87.1	102.3	67.8	70.1	90.1	47.6	50.5	75.2	37.2	40.2	66.9
3	98.0	99.8	115.3	73.5	76.1	96.8	48.9	51.9	77.1	37.6	40.6	67.5
4	104.7	106.7	122.3	75.9	78.5	99.5	49.2	52.2	77.6	37.6	40.6	67.6
5	108.4	110.4	126.1	76.8	79.5	100.6	49.3	52.3	77.7	37.6	40.6	67.6
6	110.3	112.4	128.2	77.2	79.9	101.1	49.3	52.3	77.7	37.6	40.6	67.6
7	111.4	113.5	129.3	77.4	80.1	101.3	49.3	52.3	77.7	37.6	40.6	67.6
8	112.0	114.1	129.9	77.4	80.1	101.4	49.3	52.3	77.7	37.6	40.6	67.6
9	112.3	114.4	130.2	77.5	80.2	101.4	49.3	52.3	77.7	37.6	40.6	67.6
10	112.5	114.6	130.4	77.5	80.2	101.4	49.3	52.3	77.7	37.6	40.6	67.6

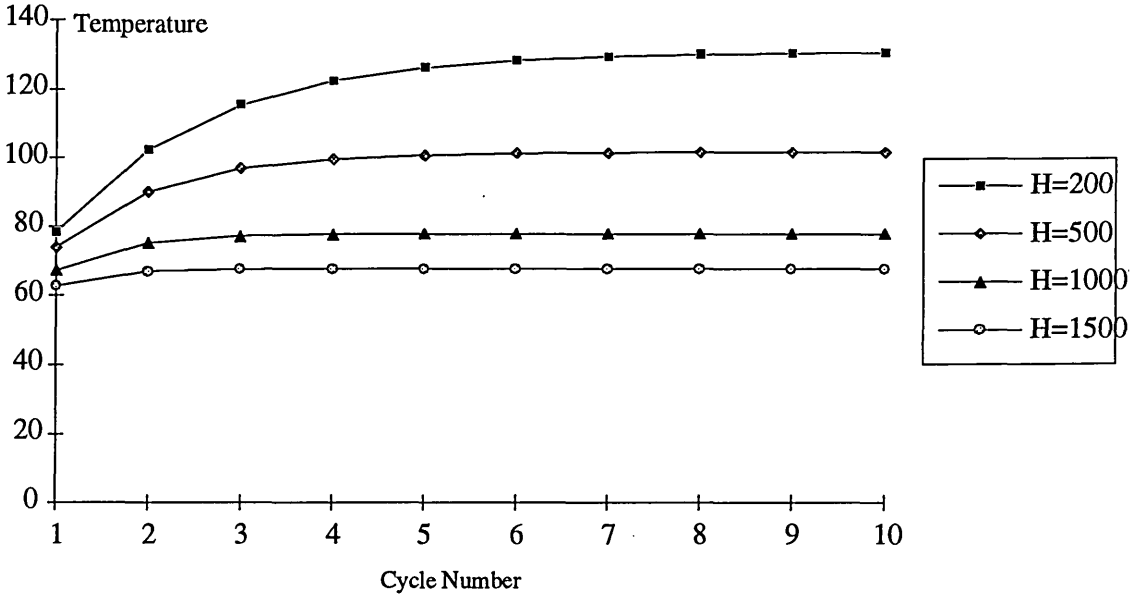

Figure 3.3.2.3 The relationship between the temperature in the centre of the plastics, cycle number and the conventional heat transfer coefficient

3.3.2.3 DISCUSSION OF THE HEAT TRANSFER CALCULATIONS

From the results of the heat transfer calculations, the following problems are clear:

1. Steady state heat transfer exists. During processing, some part of the heat coming from the heat source will remain in the mould since the cooling system cannot react quickly enough to remove all the heat from the mould. But it will tend to a balance between the heat remaining in the mould and heat transfer to the cooling system after about seven processing cycles, except for the case of a very low convection heat transfer coefficient.

2. The higher the heat transfer coefficient, the lower the steady mould temperature. So, the efficiency of the cooling system can be improved by increasing the convection heat transfer coefficient.

3. The thermal properties of the specified plastic material are suitable, so enabling it to be cooled to the target temperature under the limited cooling conditions in operation.

3.3.3 THE APPLICATION OF THERMAL IMAGING TO THE MEASUREMENT OF MOULDING TEMPERATURES

3.3.3.1 APPLICATION OF THERMAL IMAGING

A lot of work has been done in recent years to analyse the heat transfer and temperature distributions within moulds in order to improve the quality of products. However most work has been limited in terms of mathematics and by the simple test methods employed using thermocouples to analyse temperature distributions. Rarely has the mould surface temperature been measured directly to verify mathematical calculations. To achieve this, a thermal imaging system was employed to measure the mould surface temperature. The method of thermal imaging is arguably the best way to measure the surface temperature of an object directly.

A thermal imaging system is a device for converting the radiated energy from a scene into a corresponding visible light picture that the operator can view. The energy is radiated by each point in the scene by virtue of its own temperature rather than by illumination. Ideally, the thermal imaging system allows the operator to see the temperature pattern of the scene. The basic principle of a thermal imaging system is that it uses a lens to focus energy onto a detector. The detector converts infrared energy into an electrical voltage, this is amplified and processed electronically. The data may be stored in some form of memory and eventually converted into visible light by some display device, e.g. a TV monitor.

Unfortunately, like most other methods of measurement, thermal imaging systems are also easily affected by various factors. The major factors are:

(i) The actual target temperature and its emissivity which controls how much energy is radiated.

(ii) Atmospheric transmission which reduces the amount of energy reaching the system.

(iii) The aperture size of the image system which limits how much energy is collected.

(iv) The optics and scanner transmission which reduces the amount of energy reaching the detector.

(v) The detector which converts some of the collected energy into a useful signal but adds unwanted noise in the process.

(vi) Signal processing which converts some of the detector information into a unable form.

(vii) The display which converts the electrical signal into visible light.

The factors (iii) to (vii) are dependent on the accuracy of the equipment used.

In this work, the basic specifications of the equipment used are as follows:

(1) Temperature range:	-20 to 1500°C based on blackbody temperature	
(2) Focusing range:	0.5m to infinity	
(3) Frame frequency:	25 Hz	
(4) Spectral response:	"L" range	3.5 to 5 μm
	"M" or "H" range	3.9μm
(5) Resolution:	"L" range	1°C
	"M" range	2°C
	"H" range	5°C
(6) Accuracy:	"L" range	±1% temperature (absolute)
	"M" range	±1.5% temperature (absolute)
	"L" range	±3.5% temperature (absolute)

(7) Emissivity setting range: 0.10 to 1.00 in 0.01 intervals

3.3.3.2 EMISSIVITY CALCULATIONS

When temperature measurement is required it is necessary to understand how the target and atmosphere change the energy level detected by the equipment. The first factor to be considered, which affects the target temperature be measured, is emissivity. As stated earlier emissivity is defined as the ratio of the energy emitted by a given surface to the energy emitted by a blackbody at the same temperature, at the same wavelength and from the same area. For the same material, a different surface roughness will give a different emissivity.

A test to analyse the relationship between the surface condition of the closure, emissivity and temperature has been carried out, in order to prepare for the recording of the actual processing temperatures.

The closure has a rough surface on outside bottom with stick veins around outside wall and a smooth inside surface, see Figure 1.1[@].

The method of testing was:

1. The closures was kept in a controllable constant temperature water bath for an hour bringing them to a constant temperature (the temperature of the water bath was considered as the temperature of the closures).
2. The thermal imaging system was used to record the variation of emissivity with temperature.

The emissivity measurement at 90 °C is shown in Figure 3.3.3.2@. The results of the relation between the different surface conditions (bottom and wall) together with emissivity and temperature are shown in Table 3.3.3.1.

Table 3.3.3.1 The relation between the different surface conditions, emissivity and temperature

Ambient temperature 21.7°C

Water Bath Temperature °C	Emissivity	Average Temperature °C		Maximum Temperature °C	
		Bottom	Wall	Bottom	Wall
51	0.90	50.6	52.0	51.3	52.0
	0.93	49.8	51.0	50.5	51.0
	0.95	49.3	51.0	50.1	51.0
	0.96	49.2	50.0	49.9	50.0
	0.98	48.8	50.0	49.4	50.0
60	0.90	59.8	61.0	60.3	61.0
	0.93	59.0	60.0	59.5	60.0
	0.95	58.6	60.0	58.9	59.0
	0.96	58.3	59.0	58.8	60.0
	0.98	57.8	59.0	58.3	59.0
	1.00	57.3	58.0	57.9	59.0
70	0.90	69.5	70.0	69.8	70.0
	0.93	68.6	69.0	68.8	69.0
	0.95	68.0	69.0	68.2	69.0
	0.96	67.7	68.0	67.9	68.0
	0.98	67.1	68.0	67.3	68.0
	1.00	66.6	67.0	66.8	67.0
90	0.90	90.5	91.0	90.6	91.0
	0.93	89.3	90.0	89.4	90.0
	0.95	88.5	89.0	88.7	89.0
	0.96	88.2	89.0	88.3	89.0
	0.98	87.5	88.0	87.6	88.0
	1.00	86.7	88.0	86.9	88.0

From Table 3.3.3.1, it is clear that, for this material , the reflection for 3.5 to 5 μm infrared is very low since the difference in the temperature between the bottom and the wall is only 0.1 to 0.4 °C. So the effect of the surface roughness is very limited. The emissivity of the material was also measured and found to be approximately 0.94.

The results of these tests in conjunction with the results of thermal imaging were used to verify the mathematical model (using finite element methods) and finally to help to establish the customised theoretical model.

3.3.2.3 TEMPERATURE MEASUREMENT BY THERMAL IMAGING

The work reported in previous section established that, for the material NESTE PP VB19 85KNA used in the closure, the infrared radiation (wave length 3.5 to 5.0 μm as used by the thermal imaging camera) passes through the material easily. Thus, reflections from the material are minimal and the effects of surface roughness are very limited. Therefore, the measurements provide the maximum temperatures through any section of the closure. The emissivity of the material is approximately 0.94.

The manufacture machine for closure processing is shown in Figure 3.2.1[@]. The method of thermal imaging temperature measurement was as follows:

1. the machine was set to the standard processing conditions;
2. the thermal imaging camera was used to record the closure ejection process;

3. the thermal imaging analysis software was used to analyse the results recorded.

The thermal imaging analysis software provide many functions to analyse the measurement of the temperature. the basic functions are:

1. freezing and storing the 'live' process to images for analysis;
2. giving single point temperature measurement through out the image;
3. giving the temperature profiles (vertical, horizontal of both).

3.3.3.4 THE RESULTS OF THE THERMAL IMAGING MEASUREMENTS AND DISCUSSION

The results of thermal image measurement are shown in four different profiles. These are:

1. The temperature profiles in the bottom, shown in Fig. 3.3.3.3@.
2. The temperature measurement by points in the bottom, shown in Figure 3.3.3.4@.
3. The temperature profiles in the continuous thread region, shown in Figure 3.3.3.5@.
4. The temperature profile in the interrupted thread region, shown in Figure 3.3.3.6@.
5. The cooling system in the mould, shown in Figure 3.3.3.7@.

3.3.3.5 DISCUSSION OF THERMAL IMAGING RESULTS

1. THE BOTTOM OF THE CLOSURE

The temperature distribution is saddle-shaped, see Fig. 3.3.3.3@ and Fig. 3.3.3.4@. The temperature is lower in the centre part of the bottom of the cap moulding than at the edge region. The difference in temperature between the centre and the edge region is about 22 °C, see Figure 3.3.3.4@. This is expected because from Figure 3.3.3.7@, it can be seen that the cooling system is more powerful in the region of the centre than near the edge .

Another reason why the temperature at the edge of the bottom of the moulding is higher than the centre is that the edge of the moulding is thicker than the centre. It is thus more difficult to cool .

2. THE CLOSURE WALL

Since infrared waves pass through the material easily, the inside temperature of the structure of the closure can be seen very clearly.

From Figure 3.3.3.5@, the continuous thread region, it can be seen that the temperature of the thread is higher than the other parts of the wall, since it is thicker and stores more heat. The difference in temperature between the thread and the adjacent region is about 8°C.

From Figure 3.3.3.6@, showing the temperature in interrupted thread region, the interruptions are clearly visible, since the thickness varies considerably between the interruptions. The difference in temperature between the interruptions and threads is about 18°C.

Further investigations into the relationship between the thermal imaging results and the actual temperatures in the moulding are reported in the following sections.

3.3.4 FD/FEA COOLING ANALYSIS

The FD/FEA cooling analysis is based on the MOLDFLOW® software filling analysis results discussed in the section 3.2. They provide the temperature distributions through out the part just after the filling phase has finished.

3.3.4.1 MOLDFLOW SOFTWARE FOR MOULD COOLING ANALYSIS

MF/COOL, MOLDFLOW® cooling analysis software, is a software package for evaluating the cooling system of a mould. It is designed for use with the MF/FLOW, MOLDFLOW® 3D flow analysis programs.

Optimised values for mould temperature, melt temperature and injection time are obtained from the flow analysis. The mould temperature used in the cooling analysis is the target temperature for the design of the cooling system. A good cooling system

will maintain the mould temperature to within a few degrees of the target temperature. Any proposed or existing cooling system can be analysed with MF/COOL to ensure they meet this requirement.

There are two thermal analysis programs in MF/COOL: FCLP and TCL. The former is a 3D transient thermal analysis generally used for every cooling analysis and the latter is a 2D steady state thermal analysis for the thermal distribution through a cross section of the mould. FCLP is the program package selected to perform the cooling analyses in this project.

FCLP performs a detailed analysis of an existing or proposed cooling system. It can either specify certain cooling system parameters such as inlet temperature or coolant flow rates, or allow the program to optimise these for the current design. FCLP reads in the structure and cooling system models and then performs a 3D heat transfer analysis. The main output from the program is the mould temperature on each side of the plastics elements, at the end of the cycle time. Using the MOLDFLOW® Pre-post processor MF/VIEW, The mould temperature on each side of the elements can be displayed. The analysis also computes the time for each element to reach its freeze temperature (freeze time) and the maximum temperature in each element at the end of cycle time. The last element to freeze determines the overall cooling time of the structure.

3.3.4.2 THE SIMULATION OF THE MOULD COOLING SYSTEM AND COOLING ANALYSIS

Before the cooling analysis can be progressed, the computer simulation model of the cooling system must be built. The cooling channels are simulated using MF/VIEW, MOLDFLOW® pre and pro process package.

The cooling system contains two parts, the pin part and cavity part. The structures of these two sections, drawn using AutoCAD® software, are shown in:

1. Figure 3.3.4.1@, shows the cooling channels in the cavity of the mould. There are three annular channels in the bottom side and one annular channel in the wall. The coolant enters the channels from one groove and comes out from the other groove.

2. Figure 3.3.4.2@, shows the cooling channels in the pin of the mould. There is a cylindrical channel in the centre of the pin tool and a three-step annular cylindrical channel along the wall. The coolant goes into channels from the top of the centre channel and comes out from the top of the wall channels.

For use in the MOLDFLOW® simulation, the modelling ability of the MFW package is limited. The modelling is limited to 3D surface modelling and so the cooling channels in the mould were simplified, which are shown in:

1. Figure 3.3.4.3@, shows the cooling channel simulation in the cavity of the mould. There are six half-annular channels in the bottom and two half-annular

channels in the wall. The coolant enters from the channels from one end of channels and comes out from the other end.

2. Figure 3.3.4.4@, shows the cooling channel simulation in the pin of the mould. There are six three-step rectangular cooling channels in the wall of pin. The coolant enters from the bottom end of the channels and comes out from the top end of the channels.

3.3.4.3 COOLING CONDITIONS AND COOLING ANALYSIS

The cooling conditions used in the project were obtained from MCG Closures Ltd. They are based on conditions used on their high speed compression machine.

PROCESSING CONDITIONS

Number of the moulds:	54 pieces around the machine periphery
Processing speed:	515 caps/min
Working position:	1 mould in compression cycle
(per-circle)	46 moulds in cooling circle cycle
	4 moulds in ejection cycle
	2 moulds in waiting cycle
	1 mould in injecting material cycle

MELT TEMPERATURE OF THE MATERIAL

From Figure 3.2.1@, it can be seen that the material is melted in the pump, inside the orange box at lower right hand side, and through the yellow pipe is injected into the mould.

The melt temperature of the material at the pump is 221.6 to 227.7 °C (431 to 422 ° F). However the melt temperature at the nozzle in the end of yellow pipe is about 199 to 215 °C. Here 200 °C is chosen in the analysis as the melt temperature for the input of MF/FLOW, MOLDFLOW® filling analysis package.

COOLING TIME

Compression time:	$60/515 \approx 0.1165$ sec
Cooling time:	$0.1165 \times 46 \approx 5.36$ sec
Clamp open time:	$0.1165 \times 4 \approx 0.47$ sec

The total cooling time is 5.36 sec. Unlike in normal injection moulding, the clamp opening time is not calculated as part of cooling time since in the present case when the clamp opens, the cap is being ejected simultaneously.

COOLANT CONDITION

Coolant:	water
Inlet temperature:	16 °C
Standard flow rate:	1.26 l/min (0.333 US gal/min) in both pin and cavity

Maximum possible flow rate: increased by 25% in pin and 40% in cavity, that is 1.57 l/min in pin and 1.74 l/min in cavity.

The cooling analysis is based on the results of the filling analysis, shown in Figure 3.2.4@.

THE AIM OF THE COOLING ANALYSIS

The cooling analysis aims to:

1. Find out the cooling potential of the original cooling system for the MOLDFLOW@ suggesting cooling conditions, which are based on the minimum Reynolds number in cooling channels to be 10,000.

2. Find out the cooling ability of the original cooling system under the present cooling conditions.

3. Find out the cooling potential of the original cooling system under the maximum cooling conditions achievable on the moulding machine.

RESULTS USING DIFFERENT COOLING ANALYSIS METHOD

The following results show predicted temperature profiles obtained using different cooling conditions.

1. The MOLDFLOW flow rate (based on the minimum Reynolds number of 10000 in each channel) at 5.36 sec cooling time and 16°C inlet temperature, shown in Figure 3.3.4.5@.

2. The standard machine flow rate (1.26 l/min) at 5.36 sec cooling time and 16°C inlet temperature, shown in Figure 3.3.4.6@.

3. The machine maximum flow rate (increased 25% in pin and 40% in cavity than the standard machine flow rate) at 5.36 sec cooling time and 16°C inlet temperature, shown in Figure 3.3.4.7@.

4. Reducing inlet temperature to 10°C at standard machine flow rate and 5.36 sec cooling time, shown in Figure 3.3.4.8@.

5. Reducing inlet temperature to 10°C at the machine maximum flow rate and 5.36 sec cooling time, shown in Figure 3.3.4.9@.

6. Reducing cooling time to 4.5 sec at standard machine flow rate and at 16°C inlet temperature, shown in Figure 3.3.4.10@.

7. Reducing cooling time to 4.5 sec at the machine maximum flow rate and at 10°C inlet temperature, shown in Figure 3.3.4.11@.

A summary chart for the cooling analysis results is shown in Table 3.3.4.1@ and illustrated in Figure 3.3.4.12@.

3.3.4.4 DISCUSSION OF THE COOLING ANALYSES RESULTS

From the results of the MOLDFLOW® cooling analyses, several key points emerge as follows:

1. COOLANT FLOW RATE IS VERY IMPORTANT FOR COOLING EFFICIENCY.

Comparing the temperature distribution of the results of the MOLDFLOW® suggested flow rates, shown in Figure 3.3.4.5@, with the results of the standard machine flow rate, shown in Figure 3.3.4.6@, all the temperatures of the closure at the pin surface, cavity surface or the cross-section maximum are lower in the former than in the latter. It is obvious that increasing the coolant flow rate to ensure that the coolant flow is turbulent will much improve the cooling efficiency.

Considering the Reynolds Number, which MOLDFLOW® assumed as shown in Figure 3.3.4.13[@], the average can be seen to be 10000. In some parts like the entrance to the channels, the Reynolds Numbers are as high as 46000. The Reynolds Number in the analysis results for the standard cooling condition is just about 1000 in most of the part, shown in Figure 3.3.4.14[@]. Normally, when the Reynolds Number is higher than 2300, the flow is considered to be turbulent.

It is known that the convection heat transfer rate is directly related to the Reynolds Number,

$$Q = h \bullet A \bullet (T_s - T_f) \qquad (3\text{-}3\text{-}4\text{-}1)[*]$$

$$\frac{h \times A}{k} = Const \bullet (\mathrm{Re})^n \bullet (\mathrm{Pr})^m \qquad (3\text{-}3\text{-}4\text{-}2)[*]$$

The higher the Reynolds Number the higher the heat transfer efficiency. This can be seen by the metal surface temperature of the cooling channels, shown in Figure 3.3.4.13[@] and Figure 3.3.4.14[@]. The higher the Reynolds Number the lower the metal surface temperature. In the pin part, the difference of the temperature between the MOLDFLOW® assumed flow rate results and standard condition results can be as much as 30 °C.

Comparing the results of the standard machine flow rate, shown in Figure 3.3.4.6[@], with the results of the machine maximum flow rate, shown in Figure 3.3.4.7[@], the cooling efficiency of the latter is better than the former. But this is still inefficient compared with the results from the MOLDFLOW® assumed flow rate since in the main cooling areas, e.g. the pin area and the ring area, the Reynolds Number is still lower the 2300, as shown in Figure 3.3.4.15[@]. This means that the flow in most of the

channels is still in the laminar condition. Yet it is still worthwhile to change the coolant flow rate within the stated range even if the flow remains in a laminar condition.

2. REDUCING THE COOLANT INLET TEMPERATURE WILL MUCH IMPROVE THE COOLING EFFICIENCY.

Comparing the results of the standard machine flow rate, shown in Figure 3.3.4.6[@] with the results using reduced inlet temperature, shown in Figure 3.3.4.8[@], it is clear that it is worthwhile to reduce the inlet temperature.

Comparing the results of the machine maximum flow rate, shown in Figure 3.3.4.7[@] with the reduced inlet temperature, shown in Figure 3.3.4.8[@], it is more efficient to reduce the inlet temperature to 10 °C than to increase the coolant flow rate from the standard machine flow rate to the machine maximum flow rate (25% increased in pin and 40% increased in cavity).

3. THE POTENTIAL OF THE ORIGINAL COOLING SYSTEM.

Comparing the results of the standard condition, as shown in Figure 3.3.4.6[@] with the case of reduced cooling time (to 4.5 sec.) but increased the flow rate to the maximum machine flow rate and reduced the inlet temperature to (10 °C), as shown in Figure 3.3.4.11[@], for the highest temperature in the cross section, the latter is higher; but the high temperature range is located at the bottom. The cooling of the latter in the thread region and wing region is better than the former case. This means that the higher cross-section temperature in the bottom will not effect the ejection process. Compared with the standard 5.36 second cooling time, the results of the maximum

condition show that without change the cooling system design, the cooling time can still be reduced about 16 percent by using available maximum machine conditions.

Summarising, it is clear that changing the cooling conditions can improve the cooling efficiency and reduce the cooling time to get similar cooling results under the standard cooling conditions.

3.3.4.5 THE IMPROVEMENT OF THE MOULD COOLING SYSTEM

For the purpose of increasing productivity, two new cooling systems were designed. The major aims for the new designs are:

1. Increasing the cooling ability in the pin part to ensure that the thread region cooled quickly to a reasonable temperature and to obtain stiff threads during ejection.

2. Keeping the thread section in the cavity part in a warmer state to obtain an elastic deformation during ejection.

According to above design aims, the cooling system in the pin part was redesigned but there was no change in the cavity part. The detailed structures of the cooling system designs for the original design, new design A and new design B are illustrated on Figure 3.3.4.16[@].

For these two new designs, the cooling analyses based on the same types of analysis and cooling conditions, as the original cooling system analysis listed in the above

section, have been completed. The results of these three different cooling system are listed in Table 3.3.4.2@ and illustrated in Figure 3.3.4.17@ to Figure 3.3.4.19@. The summaries of these three cooling analyses in the standard cooling conditions are shown in Appendix A3 to A5.

RESULTS AND DISCUSSION

Comparing the analyses of the three cooling systems, the following conclusions can be determined:

(1) Since there are no changes in the cavity cooling channel structure in both new designs, there are no obvious changes in the temperature distribution on the outside surface of the closure.

(2) Under the same cooling conditions, both of the new design cooling systems improve the efficiency of the cooling in the pin part. The maximum surface temperature in the pin part drops by more than 10 °C.

(3) The change of the highest maximum temperature in the cross section of the part is less obvious, i.e. about 2 to 3 °C difference. This highest temperature being located in the part which has a thicker cross section. Since plastic is a poor heat conductor, the heat transfer within the part is not fast enough within the limited cooling time.

(4) The change of the lowest maximum temperature in the cross section is obvious, i.e. a reduction of about 20 °C in design A and 18 °C in design B.

(5) Comparing the design of the two new cooling systems, the cooling efficiency of design A is better than design B. From Figure 3.3.4.16@, it may be noted that the cooling channel geometry of design A changes more than design B. Comparing with Appendix A4 and A5, one may see that:

a. The Reynolds Numbers in the pin cooling channels (channel 11 to 18) in design A are 507 to 3069 and in design B are at a constant 599;

b. The metal surface temperature of the channels is 18.0 to 26.4 °C in design A and 23.0 to 27.5 °C in design B;

c. The pressure drops are 74.1 KPa in design A channels and 49.8 KPa in design B channels.

These can be explained as follows:

a. The Reynolds Number varies directly with the cooling channel dimension. For the Reynolds number in a tube:

$$\mathrm{Re}_d = \frac{\rho U_m d}{\mu} \qquad (3\text{-}3\text{-}4\text{-}3)[**]$$

Design A has a varied cooling channel geometry and the dimension of the channels are smaller than in design B. So design A has a higher Reynolds Number than design B.

b. The convection heat transfer rate varies directly with the Reynolds Number,

$$Q = h \bullet A \bullet (T_s - T_f) \qquad (3\text{-}3\text{-}4\text{-}4)[*]$$

$$\frac{h \times A}{k} = Const \bullet (\mathrm{Re})^n \bullet (\mathrm{Pr})^m \qquad (3\text{-}3\text{-}4\text{-}5)[*]$$

The higher the Reynolds Number the higher the heat transfer efficiency. So the metal surface temperature of the cooling channels is lower in design A than design B.

c. Dimension changes cause loss of the energy of the coolant flow. So there is more pressure drop in the channels of design A than of design B. This means that the design A cooling system needs more pump power than design B.

3.3.4.6 ANALYSIS OF THE ADVANTAGES OF THE NEW COOLING SYSTEMS

This section investigates the advantages of the new cooling system designs in reducing the cooling time while achieving the target temperature distribution using the standard cooling time and cooling conditions.

1. COOLING CONDITION

COOLING TIME AND MELT TEMPERATURE

This analysis is based on the standard processing speed of the machine at 540 closures/min. Therefore:

Compression time:	60 / 540	= 0.11 sec
Cooling time:	0.11×46	= 5.11 sec
Clamp open time:	0.11×4	= 0.44 sec
Melt temperature:	200 °C	

COOLANT FLOW RATE

The standard coolant flow rate is 1.26 l/min (0.333 US gal.). Therefore:

i. In the original cooling system computer model, there are 6 channels in the pin and 8 channels in the cavity. So the coolant flow rate is 0.21 l/channel/min in the pin and 0.16 l/channel/min in the cavity.

ii. In the new design cooling system computer models, there are 8 channels in the pin and 10 channels in the cavity. So the coolant flow rate is 0.16 l/channel/min in pin and 0.13 l/channel/min in cavity.

In the processing machine, the coolant flow rate can be increased by 25% in the pin and by 40% in the cavity. The maximum flow rate is 1.57 l/min in the pin and 1.74 l/min in the cavity. So:

i. In original cooling computer model, the coolant flow rate is 0.26 l/channel/min in the pin and 0.22 l/channel/min in the cavity.

ii. In the new design cooling system computer models, the coolant flow rate is 0.20 l/channel/min in the pin and 0.18 l/channel/min in the cavity.

2. TYPES OF ANALYSES

(1) A filling analysis based on the processing speed of 540 closure/min. The temperature distribution of the filling analysis is shown in Figure 3.3.4.20@ (cap2-1d).

(2) A cooling analysis based on the processing speed of 540 caps/min and the standard coolant flow rate:

i. Original cooling system -- cap1c231

ii. Design A cooling system -- cap3-210

iii. Design B cooling system -- cap3-110

(3) A cooling analysis based on the processing speed of 540 caps/min and the maximum machine coolant flow rate:

i. Original cooling channels -- cap1c232

ii. Design A cooling system -- cap3-211

iii. Design B cooling system -- cap3-111

3. THE METHOD OF THE ANALYSIS

(1). A reference target temperature distribution is established. The reference target temperature is the result of the cooling analysis of the original cooling system at the standard processing conditions. The standard processing conditions are based on the real product manufacturing process. The reference target temperatures based on these processing conditions are considered as the correct temperature distribution which the new design of the cooling systems should achieve.

(2). The cooling analyses for the two new design cooling systems were run at two coolant flow rates; the standard flow rate and the maximum machine flow rate. The cooling time was continuously reduced in each analysis cycle until the temperature distributions reached the reference target temperature.

The key point temperatures of the analysis results of the new design cooling systems are shown in Table 3.3.4.3@ to Table 3.3.4.6@, which are:

a. The minimum temperature in the cross-section, C-min.

b. The maximum temperature in the cross-section, C-max.

c. The maximum temperature in the thread cross-section, C-thread.

d. The surface temperature in the thread section, S-thread.

e. The maximum surface temperature in the pin, T-max.

f. The minimum surface temperature in the pin, T-min.

g. The average surface temperature in the pin, T-av.

h The maximum surface temperature in the cavity, B-max.

i. The minimum surface temperature in the cavity, B-min.

j. The average surface temperature in the cavity, B-av.

Figures 3.3.3.21[@] to 3.3.3.24[@] illustrate the contents of Tables 3.3.4.3[@] to 3.3.4.6[@].

3.3.4.7 COMPARISON OF THE EFFICIENCY OF THE ORIGINAL COOLING SYSTEM AND THE NEW COOLING SYSTEM

A comparison of the efficiency of the original cooling system and the new design cooling systems is as follows (the temperature distribution of the original cooling system was used as the reference target distribution):

1. The change in the maximum and thread temperature of the cross-section is limited. The process speed is about 560 caps/min when these two temperatures at new design cooling system achieve the reference temperature which original cooling system achieved at 540 caps/min. The increase is about 3.7%. Clearly the heat transfer efficiency within the material is limited. So with reduced cooling time, the shorter the cooling time the higher the centre temperature of the cross-section.

2. The change in the surface temperature of the closure on the cavity side was also limited. The increase is about 3.7%, at 560 caps/min process speed, since there was no change in the new cooling system in cavity side.

3. The change of the surface temperature of the closure in the pin side was very obvious since the new design cooling system improved cooling efficiency in the pin. The process speed could increase by more than 20% (about 650 caps/min) when the thread surface achieved the reference temperature and by more than 15% (about 620 caps/min) when the average surface temperature in the pin side achieved the reference temperature.

4. Comparing design A with B, it is obvious that the cooling of the pin in design A is better than in design B. It can be explained from the MOLDFLOW®'s FCLP summary of analysis files, list in Appendix A4 and A5, where the Reynolds Numbers in design B are at a constant of 599 but in design A vary from 507 to 3069. The higher the Reynolds Number, the higher the heat transfer efficiency.

5. From the above analysis, it is clear that the new designs improve the cooling efficiency whilst keeping the temperature in the thread and wing sections the same as the reference temperature to ensure that the closure has enough stiffness for ejection whereas the other part of the closure has a higher temperature in order to increase its elasticity. It is therefore proven that comparing the reference processing speed (540 closure/min), the new designs can increase the processing speed by from 15% to 20% to get the same cooling results. It should be borne in mind that when increasing the processing speed, other factors such as shrinkage and warpage must be considered to ensure a higher quality of product.

3.3.5 COMPARISON OF THE THERMAL IMAGE TEMPERATURE MEASUREMENTS AND THE FD/FEA COOLING ANALYSIS

The mathematical method of FD/FEA to calculate the temperature distribution and to analyses the cooling system efficiency is rapid, cost effective and flexible. It can give the optimum conditions for the engineer to design the mould. The analytical method needs to be verified.

The direct measurement of temperature by thermal imaging has been employed to provide the verification. The thermal image measurement is direct and quick. It allows the operator to "see" the temperature distribution. With the aid of the computer, both the general and detailed temperature measurements can be obtained. In this project, the cap temperature distribution was measured when just being ejected from the mould. The measurement results are shown in Figure 3.3.3.3[@] to Figure 3.3.3.6[@]. The results can be used to verify the FD/FEA modelling work.

It becomes essential to discuss these two different methods in order to determine the temperature distribution.

1. THE BOTTOM SIDE OF THE CAP

From the thermal imaging picture, Figure 3.2.2.3[@], the temperature distribution in bottom is saddle-shaped. The more detailed temperature measurement is shown in

Figure 3.3.2.4[@]. The maximum temperature is about 90 °C. The difference in temperatures between centre and edge is about 22 °C.

From the FD results, Figure 3.3.4.6[@] (cap1c216), the temperature distribution in bottom is saddle-shaped, the same as the thermal imaging picture. The maximum temperature is about 106 °C. The difference in temperatures between centre and edge is about 16 °C.

Both methods show the same profile of the temperature distribution. Since the time of the thermal imaging measurement is later than the FD calculation taken at a time when the cooling process has just finished, then the maximum temperature in thermal image measurement which is lower than FED calculation is understandable. Considering that the thickness in the centre of the closure is thinner than in the edge, the heat loss would be quicker at the centre than at the edge. The difference in temperature between centre and edge higher in thermal imaging than FD calculation is reasonable.

2. THE WALL SIDE OF THE CAP

Since the material (NESTE PP VB19 85KNA) is transparent for the wave length of infrared wave (3.5 to 5.0 μm), the thermal imaging picture shows the maximum temperature cross the thickness of the closure wall. It clearly shows the thread structure, see Figure 3.3.3.5[@] and Figure 3.3.3.6[@].

The FD analysis show the similar results as the thermal imaging, see Figure 3.3.4.6[@] (cap1c216) MAX TEMP. The FD analysis, however, gives more detail on the surface temperature on both sides of the closure and the position of the maximum

temperature located. These details help the designer to know if the cooling on the sides of the pin and the cavity is balanced and which side of the cooling is more efficient.

From the above discussion, it can be said that:

1. Both methods show similar results of the temperature distribution.

2. Thermal imaging gives a direct temperature distribution, it is a powerful tool for research work to discover the temperature distribution of the plastics part.

3. Thermal imaging verifies the validity of FD/FEA analysis.

4. FD/FEA cooling analysis results show more information about the cooling efficiency, thereby giving a powerful tool for the optimisation design.

3.4 EJECTION

Ejection is one of the important steps in plastics forming. For obtaining a high quality product, a correct ejection time, ejection temperature and ejection force must be achieved to ensure the final perfect shape of the product. In this chapter, the processing of the closure ejection was investigated.

3.4.1 THE FUNDAMENTAL OF CLOSURE EJECTION

The fundamental of closure ejection processing is shown in Figure 3.4.1.1. That is:

1. Tools moving alone the horizontal direction;
2. Pin tool raised with the roller which is guided by a machine guide;
3. Closure ejected when pin tool raised.

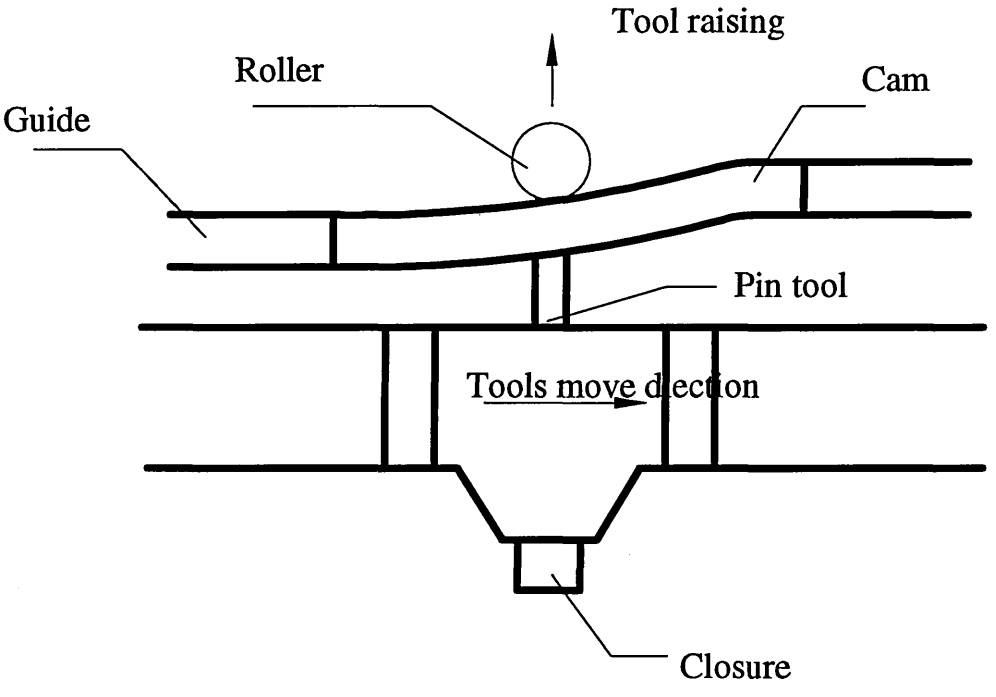

Figure 3.4.1.1 The fundamental of closure ejection

3.4.2 THE EJECTION FORCE MEASUREMENT IN PRODUCTION MACHINE

3.4.2.1 CAM CALIBRATION

The measurement of the mechanical responses of the cam is to determine the relationship between the load acting on the cam, the strain caused by the load and the position of the load acting on the cam.

The means of calibration is as follows: A strain gauge is mounted on the bottom of the cam. When the cam bends as the load acts on it, the geometry of the strain gauge will be changed with the bending of the cam. The change of the strain gauge geometry will cause a change of the resistance of the gauge. Measuring the change of the resistance with the load acting on the cam, at prescribed position along its length the relationship between the strain, the load and the position can be obtained. The geometry of the cams and measurement points are shown in Figure 3.4.2.1.

The method of the cam calibration is:

1. Mounting a strain gauge (gauge factor = 2.14) on the bottom side of the cam, shown in Figure 3.4.2.2@.

2. A known variable load acting on the top surface of the cam is supplied by a compression testing machine, shown in Figure 3.4.2.3@. The range of the loads was 0 to 9 kN.

3. The load is imposed on the different points of the top surface of the cam, shown on Figure 3.4.2.1.

4. The changes in the strain of the cam is indicated by a P-350 portable strain indicator.

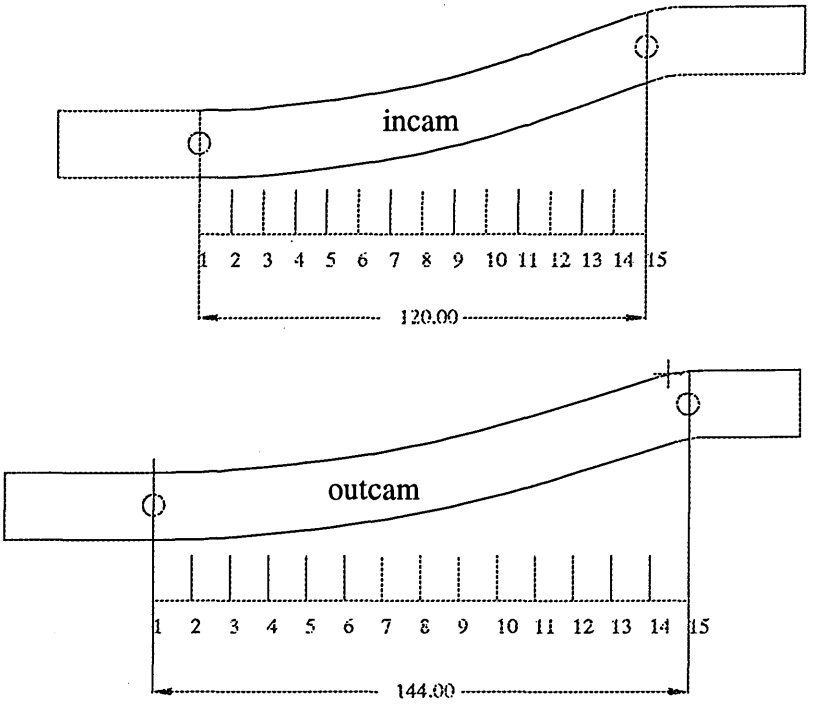

Figure 3.4.2.1 The geometry of the cams and measurement points

The results of the measurements are shown in Figure. 3.4.2.4@ and Figure. 3.4.2.5@. The 3-D Figures shown in Figure. 3.4.2.6@ and Figure. 3.4.2.7@ are based on the same results as shown in Figure. 3.4.2.4@ and Figure. 3.4.2.5@. These Figures give a clear relationship between the load, strain and position.

3.4.2.2 THE METHOD OF THE MEASUREMENT IN THE PRODUCTION MACHINE

The method of the measurement in production machine is as follows:

1. Fixing the cams mounted with the strain gauge in the machine guide;

2. Running machine on normal processing conditions;

3. Using the strain indicator to show the change of the strain.

4. Gould 1600 digital storage oscilloscope is used to record the variation of the strain against the time when the machine is running.

The measurement in production machine is to measure the relationship of strain of the cams and time. The results of the measurement are shown in Figure 3.4.2.8@ and Figure 3.4.2.9@.

From the geometry of the cams, shown in Figure 3.4.2.1, the distance between the support points of the cam is 120 mm for the inside cam and 144 mm for the outside cam. The distance between two nearby tools is 72 mm. Since there are always two tools on the cam at the same time, the results of the recording shown in the Figure. 3.4.2.8@ are the results of the double action of two tools.

In order to extract the effects of a single tool on the cam, the double action should be separated. The effects of superposition of two tools influence lines on the peak load measured can then be judged. For this reason, a sample tool is set up. One tool on both the left and right side of the sample tool is removed, see Figure 3.4.2.9@ . This is to make sure that only one tool, the sample tool, traverses the cam at any one time. The Figure. 3.4.2.9@ is the recording of the sample tools when passing the cams.

The result in Figure 3.4.2.8@ is recorded at 10.0 mv/unit and 500 ms/unit, 43 peak values are recorded.

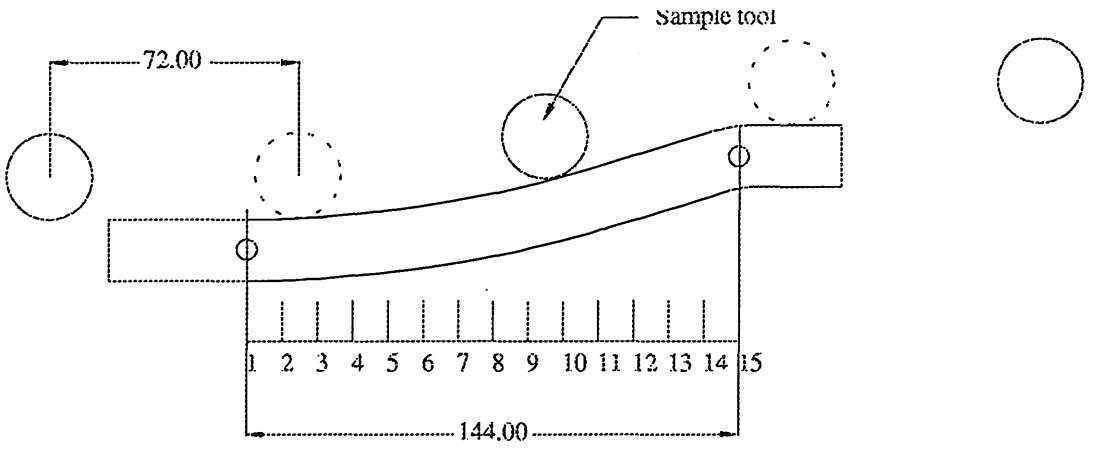

Figure 3.4.2.10 The sample tool in the measurement in production machine

For outside cam,

the mean peak value	$\bar{S}_{out} = 24.75$ mv
the population standard deviation	$\sigma_{nout} = 2.603$

For inside cam,

the mean peak value	$\bar{S}_{in} = 17.40$ mv
the population standard deviation	$\sigma_{nin} = 2.634$

For the sample tool, shown in Figure 3.4.2.9@, the peak values are:

$S_{out} = 26.00$ mv

$S_{in} = 18.00$ mv

Comparing the Figure. 3.4.2.9@ with Figure. 3.4.2.8@, the sample peak value (not effected by double action) is very close to the mean peak value (effected by double action). It is within the range of the deviation. So the results of the double action of

the two tools do not effect the accuracy of the measurement of the peak value. The peak values are used to calculate the maximum bending strain.

3.4.2.3 THE ANALYSIS OF THE EJECTION FORCE MEASUREMENT

From the calibration of the cams, the property of the cam is obtained, that is the relationship of the load, strain and position of the load acting, shown in Figure 3.4.2.4@ for outside cam and Figure 3.4.2.5@ for inside cam.

From the measurements on the production machine, results shown in Figure. 3.4.2.8@ and Figure 3.4.2.9@, the relationships of the strain against the time are obtained. Since the movement of the tools along the horizontal direction is considered to be at a constant speed V_H, the relationship of the strain against the time can be transferred to the strain against the position of tool action. Taking one cycle of the measurements of the sample tool, the zero value of the strain is considered the tool is right on support point of the cam and provides a positional datum for the time plot (the negative value of the strain is occurred by negative bending when sample tool acting outside of the support point of the cam). The measurement results of the sample tool, the strain versus time shown in Figure 3.4.2.9@, can be overlayed, with their x-axis transformed from time into position as derived above, on the cam calibration graphics, shown in Figure 3.4.2.4@ and Figure 3.4.2.5@. The overlay results are shown in Figure 3.4.2.11@ and Figure 3.4.2.12@.

From the results of the overlay, shown in Figure. 3.4.2.11@ and 3.4.2.12@, the following feature can be seen:

1. The imbalance of the ejection force between the outside cam and the inside cam. The ejection force acting on the outer cam is higher than on the inner cam.

2. The position of the maximum ejection force. The maximum ejection forces acting on inner and outer cams are at approximately the same position.

3. The range of the ejection force.

For the sample tool, shown in Figure 3.4.2.9@, the ejection forces were deduced (using Figures 3.4.2.11@ and 3.4.2.12@) for the inner and outer cams in Table 3.4.2.1:

Table 3.4.2.1 Ejection force measurement in sample tool

	Peak voltage/mv	Peak forces/N	Calibration factor/ N/mv
Outer	26.00	1700	65.4
Inner	18.00	1000	55.6

For the average tools, data taken from Figure 3.4.2.8@, the ejection force can be deduced for the inner and outer cams in Table 3.4.2.2:

Table 3.4.2.2 Ejection force measurement in average tools

	Average peak voltage/ mv	Average peak force/N
Outer	24.75 ±2.61	1619 ±171
Inner	17.40 ±2.63	967 ± 146

So, the sum of the ejection force measuring from the production machine is:

2586 ± 317 (N)

3.4.3 EJECTION FORCE MEASUREMENT IN THE LABORATORY MOULDING

As a comparison, a simulation of closure moulding is set up. Based on this laboratory moulding, the ejection force is measured directly in the testing machine.

3.4.3.1 THE METHOD OF THE LABORATORY MOULDING AND EJECTION FORCE MEASUREMENT

In order to study the ejection processing further, a compression moulding has been designed to simulate the production processing and following which, an ejection force measurement has been carried out.

1. THE MATERIAL PREPARATION PROCESS.

A Davenport Extrusion Rheometer is used as the material melt temperature control and injected shear rate control, see Figure 3.4.3.1@ (photo). According to the material properties of NESTE VB18 85KNA, the material melt temperature is controlled at 240 deg.C and the injected shear rate is at 2370 1/s.

The shear rate calculation is as follows[***],

$\gamma_{wa} = \frac{4Q}{\pi R^3}$ apparent shear rate at the wall of the die

$Q = \frac{\pi V D^2}{4}$ the volumetric flow rate

R=1.5 mm the die radius

V=20 mm/s the ram speed

D=20 mm barrel diameter

So the shear rate (1/s) can be obtained as :

$$\gamma = \frac{VD^2}{R^3}$$

E.g. $\gamma = \frac{20 \times 20^2}{1.5^3} = 2370$ (1/s).

2. THE COMPRESSION MOULDING PROCESS.

A compression machine is used as compression moulding. The compressing speed is 30 mm/s. See Figure 3.4.3.2@ (photo). A compression mould has been designed for the simulation. The structure of the compression mould is showed in Figure 3.4.3.3.

*** 'THE KAYENESS PRACTICAL RHEOLOGY HANDBOOK', *Tony Whelan & John Brydson,* Kayeness Inc. 1991

3. THE EJECTION PROCESS.

A JJ test machine is used for the processing of the closure ejection, shown in Figure 3.4.3.4@ (photo). and a thermal image system is used for determining the temperature while ejection on processing.

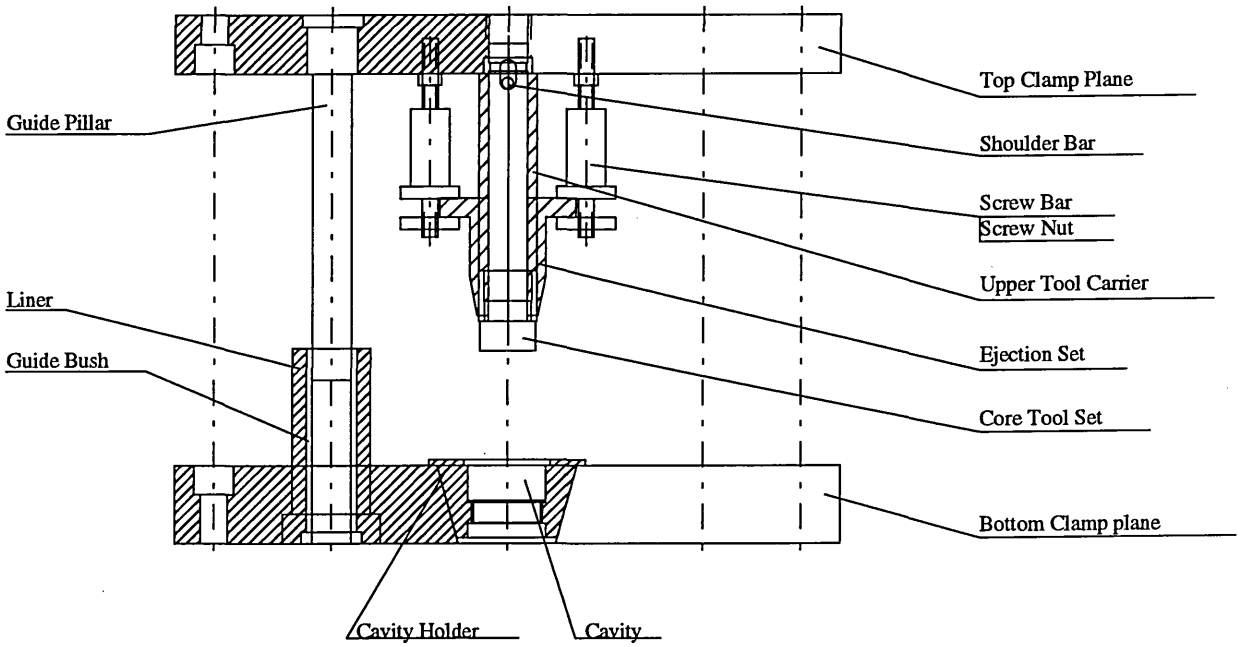

Figure 3.4.3.3 testing compression mould

The testing conditions of the JJ machine and X-Y plot are:

Ejection Speed	75 mm/min
Ejection Temperature	42 - 55 deg.C
Load Cell:	20 KN
Magnification	0.4
Full Range Lord	20*0.4 = 8 KN
Recording Range	250 mm
Force per unit	8/250 = 0.032 KN = 32 N

4. THE STEPS OF THE LABORATORY MOULDING AND EJECTION FORCE MEASUREMENT

The steps to follow for testing are as follows:

(1) melt the material in rheometer and inject into the cavity of the mould;

(2) moulding the closure in the compression mould;

(3) quickly moving the core tool with closure on it to the JJ test machine;

(4) ejecting the closure in JJ machine. In the same time, the progress is recorded by X-Y plotter and ejection temperature is determined by thermal image system.

3.4.3.2 THE ANALYSIS OF THE MEASUREMENT RESULTS

The ejection force measurement results are listed in Table 3.4.3.1. One set (set No. 2) of the measuring results plotted by X-Y plotter is shown in Figure. 3.4.3.5@.

Table 3.4.3.1 The results of ejection measurement (in measuring unit)

	Test No.	1	2	3	4	5	6	7	8
Sets No.									
1		44	41	44	43	42.5	42	43	45
2		46	36	46	44	45	44	46	
3		35.5	35.5	42	41	40	37		
4		41	37	37	38	37	38	36	39
5		39	38	39	39	43	44	40	
6		39	38	41	41	40	42	43	

1. CALCULATION IN MEASURING UNIT:

The number of the measurement	n=43
The class average mean	X=40.73
The population standard deviation (n weighted)	2.47
The sample standard deviation (n-1 weighted)	2.78

2. TRANSFER TO REAL EJECTION FORCE:

The class average mean	X = 40.73*32 = 1303 N
The population standard deviation (n weighted)	87.68
The sample standard deviation (n-1 weighted)	88.96

So, under the measurement conditions of temperature at 42 to 55 deg.C and ejection speed at 75 mm/min, the ejection is at 1300±90 N.

3.4.4 THE ANALYTICAL MODEL OF THE CLOSURE FOR EJECTION

In accordance with the structure of the closure, an analytical model of the closure can be established shown as Figure 3.4.4.1. Analysing the model, the stress, strain, deflection force and ejection force can be calculated. Because of the complexity of the geometry of the closure, the calculation is idealisation but the results of the calculation are useful for comparison with the direct measurement results and FEA results (discussed in next chapter).

The closure ejection process is similar to the separation of an annular snap joint with a rigid shaft (tool) and an elastic hub (closure)[****].

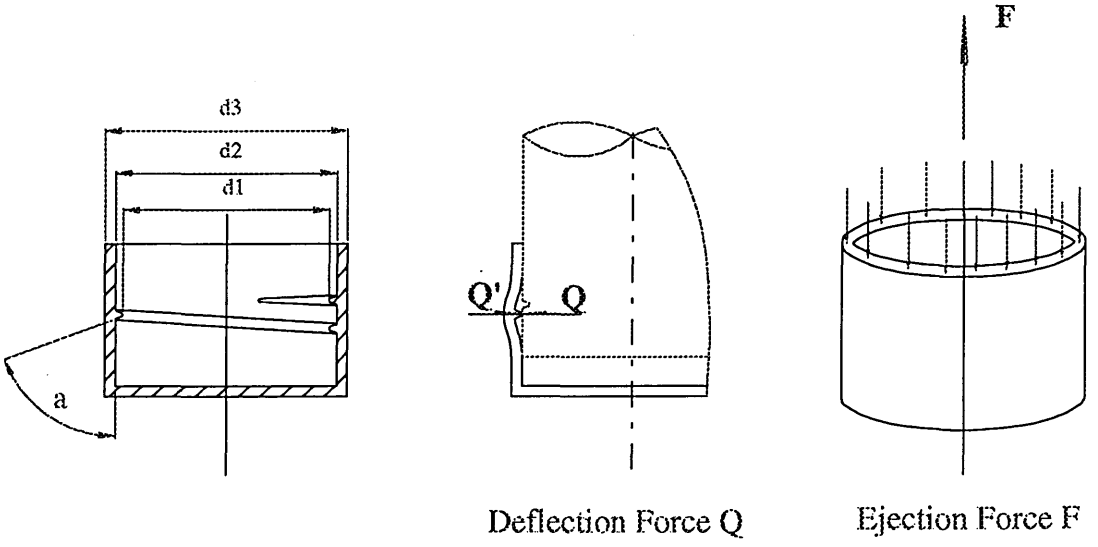

Figure 3.4.4.1 The mechanical model of the closure for ejection

The determination of the ejection force F is somewhat more complicated because the thickness of the thread on the tool is comparable to the thickness of the closure. Accordingly, the stress is also distributed over a large area of the material surrounding the thread.

Experimentally proven solutions to this problem are described in literature [69]. Such solutions are based on the theory of a beam of infinite length resting on a resilient foundation.

A somewhat simplified version of the theory discussed in [69] may be expressed as follows for closure ejection:

**** *According to ⟨⟨ Snap Joints in Plastics, Design and Dimensioning, Bayer ⟩⟩.*

$$Q = f \times d_1 \times E_S \times X \qquad (3\text{-}4\text{-}1)$$

Q -- Deflection Force (N)

f -- hoop undercut (mm)

d1 -- diameter at the joint (mm)

X -- geometry factor, taking into account the geometric rigidity.

Es -- elasticity modulus (N/mm^2)

During the ejection operation, the friction conditions and separation angle must also be taken into consideration. This means that the deflection force Q and friction force R have to be overcome , see Figure 3.4.4.1a. The ejection force is given by

$$F = Q \times \tan(\alpha+\rho) = Q \times \frac{\mu+\tan\alpha}{1-\mu\times\tan\alpha} \qquad (3\text{-}4\text{-}2)$$

here, ρ -- angle of the friction cone

μ -- friction coefficient $\mu = \tan\rho$

a -- angle of inclination , $a = 62°$

The geometric factor according to [69], assuming that the shaft (tool) is rigid and hub (closure) elastic, is as follows:

$$X = 0.62 \times \frac{\sqrt{(d_a/d-1)/(d_a/d+1)}}{[(d_a/d)^2+1]/[(d_a/d)^2-1]+\nu}$$

here, d_a -- external diameter of the hub (mm)

d -- diameter at the joint (mm)

ν -- Poisson's ratio

In here, $X \approx 0.012$

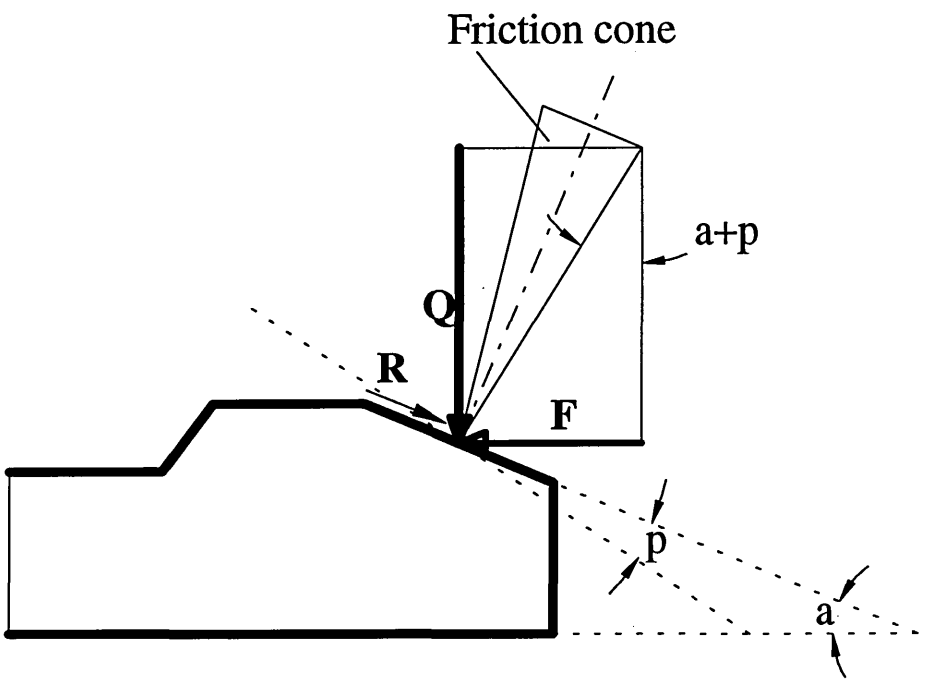

Figure 3.4.4.1a Model of the force relationship

The geometry given:

d1 = 25.60 mm

d2 = 27.60 mm

d3 = 30.00 mm

a = 65°

$f = d_2 - d_1 = 27.60 - 25.60 = 2.00$ mm

μ = 0.25, the friction coefficient for PP and steel

From equation (3-4-1),

$$Q = f \times d_1 \times E_S \times X$$

So,

$$Q = 2.00 \times 27.60 \times 0.012 \times E_S$$

$$= 0.6624 \times E_S \qquad (3\text{-}4\text{-}3)$$

The deflection force is the function of the secant elasticity modulus Es.

From the equation (3-4-2), the ejection force can be calculated as follows:

$$F=Q\times\frac{\mu+\tan\alpha}{1-\mu\times\tan\alpha}$$

So,

$$F=\frac{0.6624\times E_S(0.28+\tan 63^\circ)}{1-0.28\times\tan 63^\circ}$$

$$\approx 3.298E_S \qquad (3\text{-}4\text{-}4)$$

The stresses caused by ejection force can be calculated as follow:

$$\sigma_P=\frac{F}{A},$$

here, σ_P-- Ejecting compression stress (N/mm^2)

A -- Area of the cross-section of closure (mm^2):

$$A=\frac{\pi\times(d_3-d_2)}{4}$$

$$A=\frac{3.1416\times(30.0-27.31)}{4}\approx 121mm$$

So,

$$\sigma_P=\frac{F}{A}=\frac{5.74E_s}{121}=0.047E_s \qquad (3\text{-}4\text{-}5)$$

Since the elasticity modulus Es is the function of the temperature, the vary of the deflection force and ejection force with the temperature can be calculated. The results of the calculations are listed in Table 3.4.4.1.

Table 3.4.4.1 Values of Es, Q, F and σ_P

Temperature (°C)	20	40	60	80	100	120
Elesticity modulus E_s (N/mm^2)	1930	1550	1056	720	464	268
Deflection force Q (N)	1280	1030	700	480	310	180
Ejection force F (N)	6365	5112	3483	2375	1530	884
Ejection stress σ_P (N/mm^2)	52.6	42.2	28.8	19.6	12.6	7.3

3.4.5 THE SUMMARY OF THE EJECTION ANALYSES OF THE CLOSURE

There are three different methods used to determine the ejection force in this project. These are:

1. The measurement in production machine;
2. The measurement in the laboratory moulding;
3. The calculation on the mechanical model.

For the measurement in production machine, the results are listed in Table 3.4.2.2. The ejection temperature was measured by thermal image system, shown in Figure 3.3.3.4@. The temperature range in ejection time is: 70 to 89 deg.C and average temperature is about 80 deg.C. The sum of the ejection force measuring from the production machine is: 2586 ± 317 (N).

For the measurement in the laboratory moulding, the results are listed in Table 3.4.3.1. Under the measurement conditions, temperature at 42 to 55 deg.C and ejection speed at 75 mm/min, the ejection is at 1300±90 N.

For the calculation on the analytical model, the results are listed in Table 3.4.4.1. At temperature range 80 deg.C, the ejection force is at 2375 (N).

Comparing the results measured in these three different ways, the measurement in production machine and the calculation results are very similar. The former is slightly higher than the latter in the same temperature range. Considering the effect of the acceleration of gravity of the tool mass acting on the cams, the ejection force of the direct measurement should be higher than the production ejection force. So for normal industry product design, the mechanical model of ejection force calculation is acceptable.

The mechanical model of ejection force calculation also gives the variation of the ejection force with temperature. This is a very useful tool for selecting the suitable temperature range for the closure ejection.

The ejection force measured in the laboratory moulding seems much lower than the other two results. This is because the moulding conditions are very difficult to be simulated in the limited laboratory conditions. But this measurement does show the effect of the thread structure to the ejection processing when the two other measurement methods do not show. In the structure of the closure shown in Figure 3.4.4.1, there are two rings of thread. At first, when ejected, two rings of thread need

to be pushed out from the grooves of the tool, this is the first peak value of ejection force; Secondly, as the closure moved, the second ring of the thread goes in the first groove of the tool, to push it out is the second peak value of the ejection force. Looking at the load curve shown in Figure 3.4.3.5@, the measurements do show these two peak values. The measurement results also show that the second peak value is much smaller than the first one. So for the multi-thread structure, the first ejection force is the maximum ejection force.

3.5 BUCKLING AND FEM FOR EJECTION

In order to improve the mould cooling system to get a higher productivity in a reasonable quality of the product, there are two problems which is discussed in this chapter. These are the analytical model of the closure ejection and the possibility of the buckling in ejection.

The material mechanical properties vary with the temperature. The higher the temperature, the lower the strength of the material. For the cooling system, the higher the target temperature, the shorter the cooling time needed and the lower the ejection force, but the more possibility of buckling when the closure is ejected.

The aim of these studies is to establish the suitable target temperature for closure ejection.

3.5.1 THE POSSIBILITY OF BUCKLING INSTABILITY IN RIM SECTION

Similar to a cylindrical shell, the thickness is small compared with the diameter, the rim section of the closure may "crinkle" or form into folds under compression load when it be ejected. Related to the cooling this problem is the possibility of buckling.

The phenomenon of buckling occurs when a critical ejection load is reached, that is, the stress in the part reaches a critical value at which buckling occurs. Buckling renders the part faulty.

In this project, the buckling belongs to the type of cylindrical shell in uniform axial compression which exhibits three kinds of buckling. Initial buckling in the small deflection range can occur in two possible modes. In the first of these the radial displacements are in the form of waves along the length of the shell with the displacements constant around the perimeter of any transverse section. This is known as symmetrical or 'ring' buckling. The other modes take the form of waves in both the longitudinal and transverse directions, giving a pattern of rectangular depressions and bulges all over the surface of the cylinder. This is known as 'chessboard' buckling. In the post-buckling range the deflections can no longer be regarded as infinitesimally small, and having reached the initial buckling load the cylinder snaps through into another state of equilibrium associated with a smaller axial load and a different pattern of buckles.

The mechanical model of the closure ejection is shown in Figure 3.5.1.1.

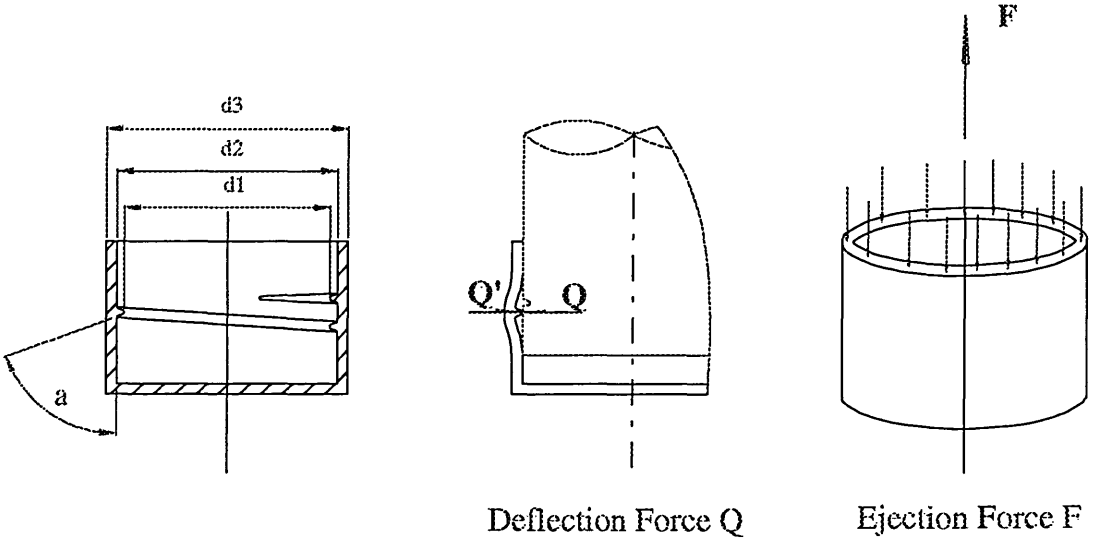

Figure 3.5.1.1 Mechanical model of closure ejection

The critical stress which cause the cylindrical shell buckling can be calculated by the equation[*] :

$$\sigma_{cr} = E \times \frac{t}{r} \times \sqrt{\frac{1}{3 \times (1-\upsilon^2)}} \qquad (3\text{-}5\text{-}1)$$

where, σ_{cr} = critical buckling stress (N/mm^2)

t = thickness of the wall (mm)

r = mean radius of cylinder (mm),

r = (d3+d2)/4 = 14.33 mm

E = Young's modulus for the material (N/mm^2)

ν = Poisson's ratio for the material.

For plastics ν = 0.35

Since the Young's modulus E is the function of temperature, the critical buckling stress σ_{cr} varies with the temperature. The critical buckling stress σ_{cr} calculated by the equation (3-5-1) is listed in Table 3.5.1.1. Also the ejecting compression stress σ_p calculated by equation (3-4-5) are listed in Table 3.5.1.1 as the comparison.

Table 3.5.1.1 The values of E, σ_{cr} and σ_p

Temperature (°C)	20	40	60	80	100	120
Young's modulus E (N/mm^2)	1930	1550	1056	720	464	268
Critical buckling stress σ_{cr} (N/mm^2)	112	90	61	42	27	16
ejecting stress σ_p (N/mm^2)	52.6	42.2	28.8	19.6	12.6	7.3

* *[Formula (7.25), "BACKGROUND TO BUCKLING"*, H G Allen & P S Bulson

The variation of the ejection stress and critical buckling stress with temperature are illustrated in Figure 3.5.1.2@.

Comparing the calculation results of mathematical model for ejection and for buckling, it is clear that:

- From the equations (3-4-3), (3-4-4) and (3-5-1), the ejection stress and critical buckling stress are linear with Young's modulus at different temperature.
- The critical buckling stress is about two times higher than the ejection stress.
- From the results of directly measurement on real machine, the ejection force F_m is around 2600±300 N. The ejection stress σ_m can be calculated as:

$$\sigma_m = \frac{F_m}{A} = 21.5 \pm 2.5 \text{ N/mm}^2$$

This means that the ejection stress at 60 to 80 °C of temperature range is lower than the critical buckling stress at the same temperature range.

So the possibility of buckling for this particular case is very small.

3.5.2 FINITE ELEMENT METHOD ON CLOSURE EJECTION ANALYSIS

Finite element method is a widely used tool for structure analysis. Using it, the structure can be modelled and the environment condition can be simulated, from which more design details can be obtained before the design is manufactured.

3.5.2.1 THE MODEL FOR CLOSURE EJECTION ANALYSIS

The model established for the closure ejection analysis is shown in Figure 3.5.2.1. The model is a two dimension axisymmetric solid model. The model is meshed in Quad4 , a four nodes element type.

The boundary conditions for the analysis are:

1. The top edge of the closure is fixed on three translation directions and free on three rotation direction while at the bottom side two translation directions (x and z direction) are fixed. The bottom only can move upward (y direction). And three rotation directions are free, that is:

Top edge: <T1 T2 T3> = <0,0,0> and <R1 R2 R3> = < , , >

Bottom edge <T1 T2 T3> = <0, ,0> and <R1 R2 R3> = < , , >

2. A uniform axisymmetric pressure is applied to the area of thread bottom side shown in Figure 3.5.2.1, which models the movement of the tool.

3. The material for the model is NESTE VB19 85KN. The material is considered as a perfect elastic body as the ejection processing is at a high speed. The properties of the material used on this analysis are:

- Young's Modulus
- Poisson rate
- Elastic limit

4. A non-linear state analysis is involved till the deformation of the thread section on radial direction equal to the height of the thread, in which the closure be considered ejected off from the tool.

5. The analyses are carried on in different temperature.

3.5.2.2 THE RESULTS OF THE STRUCTURE ANALYSIS AND DISCUSSION

The FEA results of the deformation and ejection stress distribution of the closure ejection under different temperature and pressure are shown in Figure 3.5.2.2@ to 3.5.2.7@.

The FEA results of ejection show that:

- how the deformation distributed and where the maximum deformation located when the closure is ejected.

- how the stress distributed and where the maximum stress located when the closure is ejected.

Figure 3.5.2.2 to Figure 3.5.2.6 show the minimum ejection load at different temperature. Figure 3.5.3.7 to Figure 3.5.3.9 show the variation of the deformation under different loads at same temperature.

The key points of FEA results for closure ejection are listed in Table 3.5.2.1. The tendency of the variance of the key point are shown in Figure 3.5.2.10.

Table 3.5.2.1 FEA results for closure ejection

Temperature (°C)	20	40	60	80	100
Young's modular E (N/mm^2)	1930	1550	1056	720	464
Minimum load for ejecting (N/mm^2)	45	35	25	17	11
Maximum deformation (x-axis, mm)	0.993	0.950	1.014	1.010	1.016
YY stress at top surface (N/mm^2)	60.33	46.77	33.12	22.82	14.77
Equivalent ejection force F_{ee} (N)	7300	5659	4008	2761	1787

The equivalent ejection force can be calculated as:

$$F_{ee} = S_{yy} \bullet A_{top}$$

here, F_{ee} -- equivalent ejection force (N)

S_{yy} -- YY stress at top surface (N/mm^2)

A_{top} -- area of top surface (mm^2)

$$A_{top} \approx 121 \text{ mm}^2$$

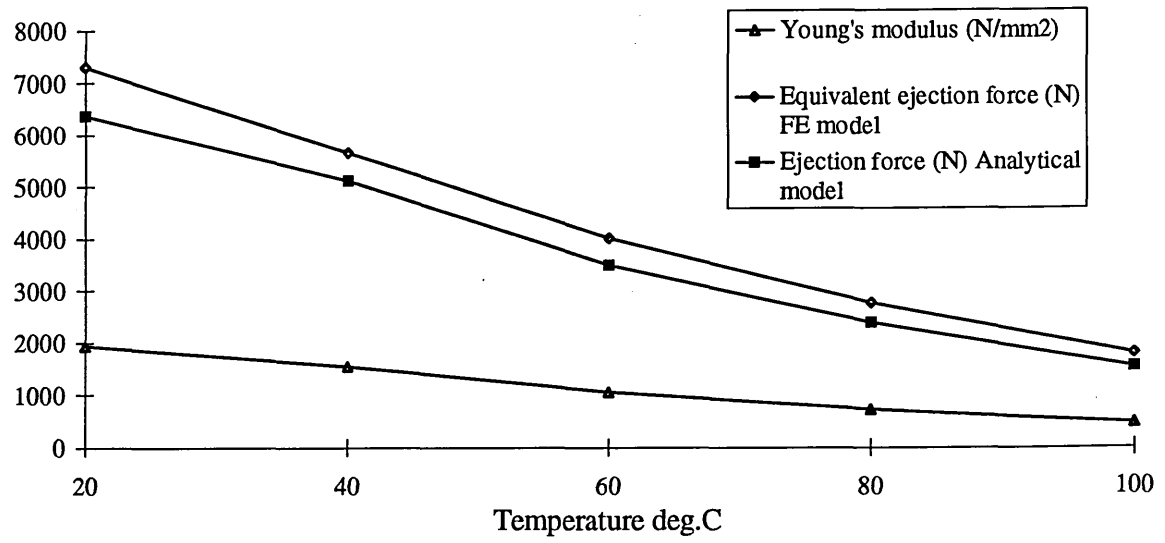

Figure 3.5.2.10 The tendency of the variance of the key points

From the FEA results for ejection force calculation, the following points are clear:

1. Ejection force is temperature dependent.
2. The maximum von-mises stress is located at the root of the first thread.
3. If temperature lower than 60 °C, the YY stress will exceed the elastic limit of the material (36 N/mm^2).
4. The equivalent ejection forces have the same dependence on temperature as the calculation results from the analytical model discussed in chapter 3.4.4, which can be seen in Figure 3.5.2.10
    - The equivalence ejection forces based on the results of finite element analysis are in good agreement with the calculation results of the mathematics model. The slightly higher value yielded by the finite element analysis is due to the use of uniform pressure loading on the thread, leading to a small overestimation of the force needed.

There is another important facet to closure ejection which must be considered. This is the possibility of buckling, which is discussed in next section.

3.5.3 CLASSICAL EIGENVALUE BUCKLING

The consideration of buckling for closure ejection processing is that the buckling may occur by a much lower stress which makes the ejection processing fail. Here, a eigenvalue buckling analysis is involved.

Classical eigenvalue buckling analysis is often used to estimate the critical buckling load of "stiff" structures. "Stiff" structures are those that carry their design loads primarily by axial or membrane action, rather than by bending action. Their response usually involves very little deformation prior to buckling. In finite element context, the classical eigenvalue buckling problem may be stated as follows. Given a structure with an elastic stiffness matrix, $K_{(b)}^{NM}$, a loading pattern defined by the vector Q^M, and an initial stress and load stiffness matrix, $K_{(Q)}^{NM}$, find load multipliers (eigenvalues), λ_i , and buckling mode shapes (eigenvectors), ϕ_i^M , which satisfy:

$$[K_{(b)}^{NM} + \lambda_i K_{(Q)}^{NM}]\phi_i^M = 0$$

The critical buckling loads are then given by , $\lambda_i Q^M$. Usually only the smallest load multiplier and its associated mode shape are of interest. (In the above, the superscripts

N and M refer to degrees of freedom N and M of the whole model. The subscript *i* refers to the *i*th mode.)

Eigenvalue buckling analysis is performed with ABAQUS by first storing the stiffness matrix at the state corresponding to the "base state" loading on the structure, then applying a small perturbation of "live" load. The initial stress matrix due to the live load is calculated and then an eigenvalue calculation is performed to determine a multiplier to the "live" load at which the structure reaches instability.

3.5.3.1 THE MODEL FOR THE EIGENVALUE BUCKLING ANALYSIS

The model for eigenvalue buckling analysis is two dimension axisymmetric solid model, the same as for ejection analysis, which is shown in Figure 3.5.2.1[@].

The boundary conditions for eigenvalue buckling analysis are:

- The top edge of the closure is fixed on three translation directions and free on three rotation direction while at the bottom side two translation directions (x and z direction) are fixed. The bottom only can move upward (y direction). And three rotation directions are free, that is:

  Top edge: <T1 T2 T3> = <0,0,0> and <R1 R2 R3> = < , , >

  Bottom edge <T1 T2 T3> = <0, ,0> and <R1 R2 R3> = < , , >

- A uniform initial axisymmetric pressure is applied to the area of thread bottom side shown in Figure 3.5.2.1, which give the model an initial loading pattern.
- An eigenvalue buckling analysis is involved till the critical eigenvalue buckling condition is achieved.

3.5.3.2 THE RESULTS OF THE EIGENVALUE BUCKLING ANALYSIS AND DISCUSSION

The finite element analysis results for buckling are as follows:

- The buckling deformation pattern under critical buckling stress at 80 °C is shown in Figure 3.5.3.1[@].
- The buckling von-mises stress distribution at 80 °C is shown in Figure 3.5.3.2[@].
- The buckling YY-COMP stress distribution at 80 °C is shown in Figure 3.5.3.3[@].
- The variation of the critical buckling load with temperature is listed in Table 3.5.3.1.
- The variation of the critical buckling load with initial load is listed in Table 3.5.3.2.

Table 3.5.3.1 The variation of the critical buckling load with temperature

Temperature (°C)	20	40	60	80	100
Young's modulus E (N/mm^2)	1930	1550	1056	720	464
Initial load (pressure) P (N/mm^2)	45	35	25	17	11
Eigenvalue λ	2.035	2.101	2.004	2.009	2.001
Critical buckling load Q (N/mm^2)	91.58	73.54	50.10	34.15	22.01

According to the theory of classical eigenvalue buckling, the critical buckling load can be calculated as follows:

$$Q=\lambda \times Q = \lambda * P$$

here, Q -- Critical buckling load (N/mm^2)

λ -- Eigenvalue

P -- initial load (pressure) (N/mm^2)

Table 3.5.3.2 The variation of the critical buckling load with Initial load

Temperature (°C)	80		
Initial load (pressure) P (N/mm^2)	15	17	20
Eigenvalue λ	2.2772	2.0093	1.7079
Critical buckling load Q (N/mm^2)	34.158	34.158	34.158

The FEA results for buckling calculation show that the eigenvalue of the closure structure exists. The critical buckling load has its characters as follows:

- The critical buckling load does change its value with the variation of the temperature, see Table 3.5.3.1.
- The critical buckling load does not change its value with the variation of the initial force applied on the structure, see Table 3.5.3.2.
- The buckling deformation shape patterns under critical buckling load are the same in different temperature ranges, shown in Figure 3.5.3.1.

This implies that the eigenvalue of the structure is only interrelated with the properties of the structure itself, such as the material and shape of the structure and is not interrelated with the force applied on the structure. The buckling deformation shape patterns are entirely determined by the geometry of the structure.

Comparing the results of finite element analysis for buckling against ejection force discussed in the last section, the relationships between critical buckling load and ejection load, listed in Table 3.5.3.3, are as follows:

Table 3.5.3.3 The compression of critical bucking load and minimum ejection load

Temperature (°C)	20	40	60	80	100
Minimum load for ejecting (N/mm^2)	45	35	25	17	11
Critical buckling load Q (N/mm^2)	91.58	73.54	50.10	34.15	22.01

- Critical bucking load and ejection load are all temperature dependent.
- Critical bucking load is about two times higher than ejection load. It is the same ratio as the ejection stress and critical buckling stress calculated by analytical model.

Analytical and numerical methods have been used for closure ejection analysis. From the results of these analyses, it is shown that the possibility of buckling for this particular case is very small.

4. CONCLUSIONS

The wide range of methods and technology have been successfully integrated to provide a route to modelling and predicting the behaviour during manufacture of high speed moulded products. The interrelation of the stages of analysis, from initial mould filling modelling through cooling to ejection have been demonstrated and the key data needed at each stage have been identified. Numerical models and analytical approaches have been developed and validated by laboratory experiments and production machine trials, showing good consistency.

1. A review of the application of computer aided engineering (CAE) in plastics forming has been made which including material databases, mould filling, mould cooling and buckling problems have been discussed. CAE is a very rapidly developing area. With the development of computer techniques, CAE has become a powerful tool for engineers to select materials, design moulds and parts, and simulate and analyses the plastics forming process. With the application of CAE, engineers can improve the quality of plastics products, increase productivity, reduce the reject rate, and finally increase the economic performance of the process.

2. The investigation of the application of thermal imaging in plastics forming has been proved to be highly valuable. Thermal imaging measurement gave the same temperature distribution on the closure as finite element analysis. The maximum temperature is 90°C where FEA is 106°C. The difference between these two may be caused by the fact that thermal imaging measurement is later than the time when FEA is taking place. Thermal imaging is a useful non-contact method for temperature

measurement, which has many advantages that normal contact temperature measurement methods do not provide. The application of thermal imaging allows both the measurement of temperature and also a means of obtaining the temperature distribution. Thermal imaging, by highlighting 'hot or cool' spots in a product at ejection, offers pointers to defect in the product or tooling design and therefore product quality may be improved.

3. Taking a particular example of an industrial product, a compression moulded bottle closure which embodies many generic problem common to moulded products, two different computer software packages, MOLDFLOW$^{@}$ for injection moulding and FILLCALC V$^{@}$ for compression moulding, have been compared in the mould filling phase. The capabilities of these two computer software packages have been investigated. In the special case of the closure moulding, the comparison shows that injection moulding and compression moulding have some similar characteristics, such as the very similar temperature distribution. These two software packages are used in different areas of plastics forming but have similar abilities to analyse the moulding process.

4. For the particular product under investigation, mould cooling as well as heat transfer in the mould have been investigated in more detail. A computer program was written using Turbo C^{++} for the calculation of the cooling potential of the material. Based on the cooling analysis of the original cooling system, the cooling conditions have been investigated and improved. With the improved cooling conditions, without changing the mould design, it has been shown that the cooling time can be reduced by up to 5%, which has been verified in the production process. Two new cooling

systems have been designed, analysed and compared with the original cooling system. Both new cooling systems could improve the efficiency of the mould cooling, which can increase the processing speed by 15% to 20% to get the same cooling results.

5. The closure ejection process has been studied. With the aim of finding out a suitable ejection temperature, four different methods have been developed to obtain the ejecting force. These are direct measurement on a production machine, measurement in a laboratory moulding process, general mathematical calculation, and finite element analysis of ejection. The different methods have their own advantages. The temperature dependent behaviours are considered in the both models of the mathematical calculation and finite element analysis. The models of the mathematical calculation and finite element analysis offer general ways to analyse the ejection process. Both gave similar results for ejection force, where FEA gives more details such as stress distribution, deformation pattern and the maximum stress location

6. The possibility of buckling in closure ejection process has been evaluated. The general mathematical algorithm and finite element analysis are used to analyse the buckling problem. FEA gives more details of buckling, such as stress distribution, deformation pattern and the maximum stress location. The buckling analyses show that since the minimum load for ejection is lower than critical buckling load at the same temperature, the possibility of the buckling is very small.

5. FURTHER WORK

Plastics forming is a complex area. This work has highlighted the need for further study in the following areas:

1. THE BEHAVIOUR OF THE MATERIAL IN VERY HIGH SPEED PROCESSING.

For more accurate calculations in closure ejection, the strain rate dependent behaviour of the material could be considered. At very high strain rates, the plastics material behaves more like a linear elastic material but still different to perfect elastic materials such as metals.

2. THE RIGID BODY CONTACT ANALYSIS IN CLOSURE EJECTION.

A full solution of the closure buckling problem is more complicated than allowed by the eigenvalue buckling approach. Confined by the structure of the mould, the deformation of the closure can only be in a certain direction, whereas in the eigenvalue buckling the deformation can be any direction. Rigid body contact analysis would yield a more accurate analysis.

The rigid body method allows the modelling of the interaction between a deformable body (such as the closure) and a rigid body (such as the mould), in the general case when finite sliding and separation (such as the ejection) may occur.

REFERENCE

1. *Kwon T N*, "MOLD COOLING SYSTEM DESIGN USING BOUNDARY ELEMENT METHOD", J Eng. for Industry. Trans. ASME 110, 4 Nov 1988 pp 384-394

2. *Wang K K, Himasekhar K, Chiang H H, Jong W R & Wang V W*, "INTEGRATED CAE OF INJECTION MOLDING USING A THREE-LAYER APPROACH", ANTEC '91, pp 267-273

3. *Davidoff A, Bung H & Chen S C*, "AN INTEGRATED ANALYSIS OF THE INJECTION MOLDED PLASTIC PART", ANTEC '91, pp 274-281

4. *Bernhard M & Hsu C*, "HOW TO USE THE MOLD FILLING AND MOLD COOLING PROGRAMS TO SOLVE MOLD DESIGN AND MOLDING PROBLEMS", ANTEC '87, pp 262-263

5. *Floutier A*, "CAD/CAM SYSTEM FOR THE MOLD INDUSTRY", ANTEC '89, pp 1255-1257

6. *Burton T E*, "INTEGRATED ANALYSIS OF INJECTION MOLDING", ANTEC '90, pp 351-354

7. *Akin D K*, "COMPUTER AIDED DESIGN: DEVELOPING A LIBRARY FOR MOLD DESIGN", ANTEC '86, pp 212-214

8. *Schuder D & Caren S*, "MOLD DESIGN WITH CAD/CAM/CAE", ANTEC '89, pp 1258-1261

9. *Trantina, G G & Ysseldyke, D A*, "AN ENGINEERING DESIGN SYSTEM FOR THERMOPLASTICS", ANTEC '89, pp 635-639

10. *Filz P & Menges G*, "NEW SOFTWARE DEVELOPMENTS FOR PART DESIGN AND PROCESS SIMULATION IN INJECTION MOULDING", ANTEC '88, pp 310-312

11.*Palit K*, "INFLUENCES OF PLASTICS MATERIAL PROPERTIES ON THE CAE PROGRAMS FOR DESIGNING INJECTION MOLDS", ANTEC '87, pp 1493-1495

12.MOLDFLOW MATERIAL MANUAL RELEASE 9.0.1, Published by Moldflow Pty. Ltd, June 1994

13.PLASCAMS VERSION 6.00, Rapra Technology Ltd 1995

14.CAMPUS VERSION 2, CWFG, 19991

15.*Rosen M*, "A FEATURE BASED, PARAMETRIC, CAD MOLD DESIGN PROGRAM DESCRIBED", ANTEC '89, pp 1251-1254

16.*Brydson J A*, PLASTICS MATERIAL, Fourth Edition, Butterworth 1982

17. *Dealy J M*, RHEOMETERS FOR MOLTN PLASTICS, Sponsored by the Society Plastics Engineers, Van Nostrand Reinhold Company, 1982

18. *Clegg D W and collyer A A*, THE STRUCTURE AND PROPERTIES OF POLYMERIC MATERIALS, The institute of materials, 1993

19.*Weissmann D*, "MOLD FILLING SIMULATIONS -- DO THEY PROVIDE THE NEEDED ANSWERS?", ANTEC '91, pp 264-266

20.*Harry D H*, "MOLD FILLING SIMULATION FOR EDUCATIONAL OBJECTIVES", ANTEC '90, pp 1719-1722

21.*Hieber C A, Wang P J & Wang K K*, "INJECTION MOLDING A CENTRE-GATED DISK: MODELLING AND MEASUREMENTS FOR THE FILLING AND POST-FILLING STAGES INCLUDING GAPWISE", ANTEC '91, pp 259-263

22.*Wang V W, Hieber C A & Wang K K*, "MOLD-FILLING SIMULATION IN INJECTION MOLDING OF THREE-DIMENSIONAL THIN PARTS", ANTEC '86, pp 97-102

23.MOLDFLOW USER MANUAL, Release 9.0.1, Moldflow Pty. Ltd July 1994

24. FILLCALC V INTERIM MANUAL, Release 1.05, Rapra Technology Ltd, 1994

25.*Chen S C, Hu S Y & Davidoff A*, "HYBRID METHODS FOR INJECTION COOLING PROCESS SIMULATION AND COOLING SYSTEM ANALYSIS", ANTEC '91, pp 499-503

26.*Chen S C, Wang S M, Chang Y L & Wang C H*, "A STUDY OF COMPUTER AIDED MOLD COOLING SIMULATIONS BASED ON DIFFERENT METHOD", ANTEC '90, pp 359-364

27.*Himasekhar K, Lottey J & Wang K K*, "DESIGN OF A COOLING SYSTEM IN INJECTION MOLDING USE OF A CAD TOOL", ANTEC '90, pp 1103-1106

28.*Himasekhar K, Hieber C A & Wang K K*, "COMPUTER AIDED DESIGN SOFTWARE FOR COOLING SYSTEM IN INJECTION MOLDING", ANTEC '89, pp 352-355

29.*Kwon T H, Shen, S F & Wang K K*, "COMPUTER AIDED COOLING-SYSTEM DESIGN FOR INJECTION MOLDING", ANTEC '86, pp 110-115

30.*Himasekhar K, Lottey J & Wang K K*, "CAE OF MOLD COOLING IN INJECTION MOLDING USING A THREE-DIMENSIONAL NUMERICAL SIMULATION", J of Eng. for Industry, May 1992, Vol. 114, pp 213-221

31.*Pusz A & Gliwice*, "SIMPLIFIED METHOD FOR CALCULATING THE COOLING OF INJECTION MOLD PARTS", German Plastics 79 (1989) 10, pp 116-117

32.*Bernhard M G*, "COMPUTER AIDED MOULD COOLING DESIGN IMPROVES PART QUALITY AND OVERALL PRODUCTIVITY". Composite Materials Technology, Detroit. 24-28 Feb 1986 pp 69-71.

33.*Hsu C*, HOW TO ACHIEVE BALANCED COOLING WITH INTERNAL MANIFOLDING, 13th Annual Structural Foam Conference and Parts Competition, SPI, 1985, pp 111-114

34.*DiScipio W, Wagle A & McCarthy S P*, "VERIFICATION MOULD FOR FLOW, COOLING, SHRINKAGE AND WARPAGE ANALYSIS", ANTEC '90, pp 283-287

35.*Austin C*, "VERIFICATION OF FLOW ANALYSIS SOFTWARE: THEORY AND PRACTISE", ANTEC '90, pp 390-392

36.*Brnhardt E C & Bertacchi G*, "COMPUTER SIMULATION OF MOLD FILLING AND COOLING -- HOW TO TEST AND EVALUATE PROGRAMS", ANTEC '85, pp 158-161

37.*Croft D R and Lilley D G*, HEAT TRANSFER CALCULATIONS USING FINITE DIFFERENCE EQUATIONS, Applied Science Publishers Ltd, 1977

38. *Rogers G F C and Mayhew Y R*, ENGINEERING THERMAODYNAMICS WORK AND HEAT TRANSFER, Longman Group Ltd, 1967

39.*Patterson W I, Kamal M R & Gao F*, "MOLD TEMPERATURE MEASUREMENT AND CONTROL", ANTEC '90, pp 227-232

40.*Kamal, M R, Mutel, A T, Salloum, G & Garcia-Rejon, A*, "HEAT TRANSFER MEASUREMENT AT THE MOLD SURFACE DURING INJECTION MOLDING OF THERMOPLASTIC MELTS", ANTEC '91, pp 483-487

41.*Kefalas C G & Seferis J C*, HEAT TRANSFER ANALYSIS DURING HEATING FOR DYNAMIC MECHANICAL MEASUREMENTS OF POLYMERS AND COMPOSITES, ANTEC '89, pp 1045-1047

42. *Shetterly D M and Huff N T*, MOLD SURFACE TEMPERATURE DURING GLASS CONTAINER FORMING, Journal of Non-crystalline Solids 38 & 39 (1980), pp 867-872

43.*Lobo S & Cohen C*, MEASUREMENT OF THERMAL CONDUCTIVITY OF POLYMER MELTS BY THE LINE SOURCE METHOD, ANTEC '88, pp 609-611

44.*Rietveld J & Budiman,* REAL TIME MEASUREMENT OF TRANSIENT POLYMER MELT TEMPERATURES DURING THE INJECTION MOLDING PROCESS, ANTEC '90, pp 222-226

45.*Gao B. Sweeney P & Campbell G A*, "SIMULTANEOUS SURFACE AND BULK TEMPERATURE MEASUREMENT OF POLYETHYLENE DURING FILM BLOWING", ANTEC '89, pp 35-38

46.*Holman R A,* MOLD TEMPERATURE MEASUREMENT FOR GLASS-PRESSING PROCESS, Application of Radiation Thermometry, ASTM STP 895, 1985, pp 67-73

47.*Heimann W & Mester U,* NON-CONDTACT DETERMINATION OF TEMPERATUREA BY MEASURING THE INFRARED RADIATION EMITTED FROM THE SURFACE OF A TARGET, European Conference on Temperature measurement 1975, pp 300-321

48.*Agerskans J,* THERMAL IMAGING, A TECHNICAL REVIEW, European Conference on Temperature measurement 1975, pp 350-364

49.*Fellows C J & Shaw F,* A LABORATORY INVESTIGATION OF GLASS TO MOULD HEAT TRANSFER DURING PRESSING, Glass Technology Vol. 19 No. 1 February 1978, pp 4-9

50.*Boulton H et al,* THERMAL IMAGE GENERATION AND ANALYSIS, Evaluation Engineering, Jan. 1986, pp 46-51

51. *Danaher H,* THERMOGRAPH - UNDERSTANDING THE EXPANDED ROLE OF THERMAL IMAGERS IN PRODUCTION TESTING, Evaluation Engineering, Dec. 1988, pp 74-76 & 78-79

52.*Wallin B*, ADVANCEMENT IN THERMAL IMAGING, Evaluation Engineering, May 1990, pp 90-93

53.*Walcutt J,* TECHNOLOGY CHOICE IN INFRARED THERMAL IMAGING, Evaluation Engineering, Nov. 1991, pp ,42-47

54.*Tivin P et al,* INFRARED IMAGING ENHANCES MANUFACTURING OPERATIONS, Laser Focus World, Dec. 1992, pp 107-111

55.*Bennett G A et al,* CALIBRATION PROCEDURE DEVELOPMENT FOR IR SURFACE - TEMPERATURE MEASUREMENT, IEEE Transaction on Components, Hybrids, and Manufacturing Technology, Vol. 12, No. 4, 1989, pp 690-695

56. *Schott J R,* IMAGE PROCESSING OF THERMAL INFRARED IMAGES, Photogrammetric Engineering and Remote Sensing, Vol. 55, No. 9, Sept. 1989, pp 1311-1321

57. *Webb P W,* THERMAL IMAGING OF ELECTRONIC DEVICES WITH LOW SURFACE EMISSIVITY, IEEE Proceeding-G, Vol. 138, No. 3, June 1991, pp 390-400

58. *Sobrino J A et al,* A FIELD METHOD FOR MEASURING THE THERMAL INFRARED EMISSIVITY, ISPRS Journal of Photogrammetry and remote Sensing, Vol. 48, No. 3, 1993, pp 24-31

59. *Mcdonald F A et al,* RESOLUTION AND DEFINITION IN THERMAL IMAGING, IEEE Ultrasonics Symposium, 1984, pp 622-628

60. *Cuthbertson G M,* THERMAL IMAGING, GEC Review Vol. 2, No. 1, 1986, pp 21-31

61.*Austin C,* "MOULD COOLING", 43rd annual Conference. Soc. Plastics Engineering Inc. Washington DC. 1985 pp 764-766.

62.*Chen S C & Chung Y C,* "SIMULATIONS OF CYCLIC TRANSIENT MOLD SURFACE TEMPERATURE IN INJECTION MOLD-COOLING PROCESS", INT. CCOMM. HEAT MASS TRANSFER, 1992, Vol 19, pp 559-568

63.*Opolski S W & Kwon T W,* "INJECTION MOLDING COOLING SYSTEM DESIGN", ANTEC '87, pp 264-268

64.*Groth K B,* COMPUTER-AIDED MOULD COOLING DESIGN FOR PLASTIC PARTS, Int. J. of Vehicle Design, SP6, 1986, pp76-79

65.*Bernhardt E C,* COMPUTER AIDED ENGINEERING FOR INJECTION MOLDING, Hanser, 1983

66.*Crawford R J,* PLASTICS ENGINEERING, Pergamon Press, 1983

67.*Allen H G & Bulson P S,* BACKGROUND TO BUCKLING, McGRAW-HILL Book Company (UK) Ltd., 1980

68. *Kokubo K, Nagashima H, Takayanagi M & Mochizuki A,* ANALYSIS OF SHEAR BUCKLING OF CYLINDRICAL SHELLS, JSME International Journal, Series A. Vol. 36, No. 3 1993, pp 256-266

69.*Delpy U,* PLASTICS SNAP JOINTS, CALCULATION PRINCIPLES AND TEST RESULT, Konstruktion 30 (1978) 5 & 8, pp 179-184 307-310

APPENDIXES

A1. SUMMARY OF THE FILLING ANALYSIS OF MF/FLOW

```
**********************************************
*          MULTI-LAMINATE          *
*          FILLING ANALYSIS        *
**********************************************
Restart File
============
Restart File Name          : NONE

Cooling Results
===============
FCLP File Name             : NONE

Model Information
=================
MODEL (master) file name : CAP2-1
   545   nodes, highest no.=  545
   850 elements, highest no.=  850
Maximum aspect ratio of   2.824 at element :   86
Minimum aspect ratio of   1.190 at element :  159
Average aspect ratio of triangular elements :    1.813

Boundary Condition File
=======================
Boundary Condition File Name  : NONE

Material Information
====================
 Local Personal Database RAX files NOT Available
 Project Personal Database RAX files NOT Available
 Local Company Database RAX files NOT Available
STANDARD database accessed is version $V16_0_0
 This supplier/Grade does not have PVT Data
 For PVT using GENERIC DATA - supplier: MOLDFLOW   Grade code: PVT200

Material DATABASE type : MATDB <STANDARD>
SUPPLIER/file name    : NESTE
GRADE code            : NT900
Material MODEL order  : 2
Material description  :
NT900  PP COMP FT 2032              NESTE     VI(260)73  NESTE   JAN90
Conductivity   W/m/degC          0.205000
Specific Heat  J/kg/degC      2600.000000
Density        kg/cu.m         893.000000
Freeze Temp    deg.C           143.000000
```

No Flow Temp deg.C 155.000000

Viscosity

==========

Temperature deg.C	Shear Rate 1/s	Viscosity Pa.s
240.000	1000.000	83.269997
260.000	100.000	244.929993
260.000	1000.000	72.570000
260.000	10000.000	16.150000
280.000	100.000	209.889999
280.000	1000.000	63.990002

Injection Node(s)

==========

Number of injection nodes : 1

Injection node numbers :

329

Molding Conditions

==========

Mold temperature : 50.00 deg.C

Melt temperature : 200.00 deg.C

Injection time : 0.11 sec

Total Volume : 3.55 cu.cm

Flow rate : 32.27 cu.cm/s

Analysis Options

==========

Maximum injection pressure : 500.0 MPa

Maximum Clamp Force : 20000.0 tonne

Nominal Injection Profile :

% Shot Vol	% Nominal Flow Rate
100.000	100.000

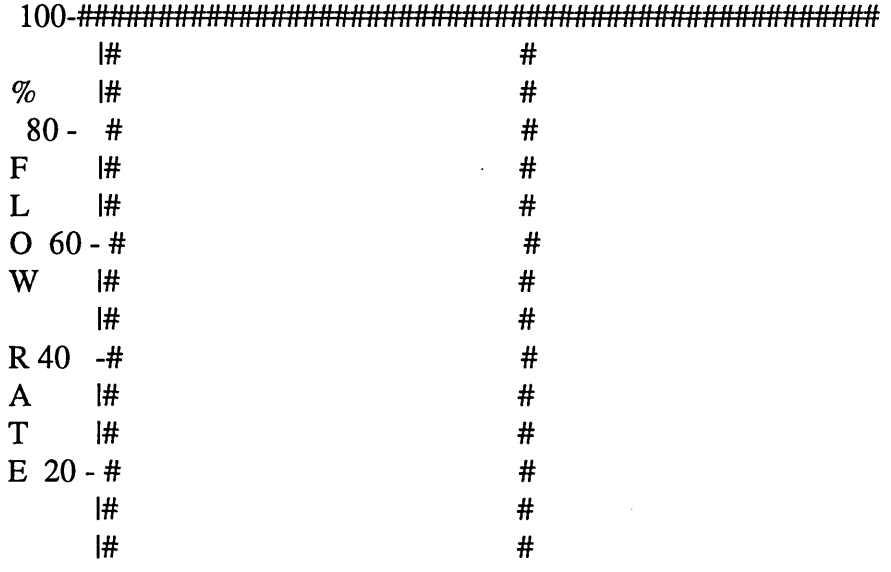

```
 0 ----------|---------|---------|---------|---------|
          20        40        60        80       100
                    % SHOT VOLUME
```

Constant Pressure Mode : Percentage Volume
Const. Pressure Change-over at (%Vol) : 98.0 %
Change-over to Pressure : Automatic
Change-over Pressure Factor : 1.000
Stroke Volume : AUTOMATIC
Mold Conductivity : 41.90 W/m/degC
Mold Density : 7750.00 kg/cu.m
Mold Heat Capacity : 460.5500 J/kg/degC

Output Options
==========
No. intermediate results files : 0
Time Series Step Mode : Constant Time Increments
Number of Time Increments : 20
No. Restarts files : 0
Screen Output Format : Short Format

Numerical Parameters
==========
Iteration Limit : 1000
Iteration Tolerance : 0.0005000
Viscosity Iteration Limit : 10
Viscosity Iteration Tolerance : 0.01000000
Density Iteration Limit : 20
Density Iteration Tolerance : 0.01000000
Nodal Growth Mechanism : Multiple (Time Based)
Laminations in Plastic : 10
Laminations in Mold Wall : 15
Grid Thickness Ratio (M/P) : 8.00

Result File Core Name : CAP2-1C
==========
****
* FILLING PHASE RESULTS SUMMARY *
****
Maximum - Minimum Values
==========
Max Pressure (at Fill) : 14.1477 MPa
Max Pressure (during cycle) : 14.1477 MPa

Max Clamp Force (during cycle) : 1.3872 tonne
Total projected area : 13.4711 sq.cm

Actual injection time : 0.1181 sec

Min Temperature (at Fill) : 200.0000 deg.C
Max Temperature (at Fill) : 200.4494 deg.C

Min Temperature (flow front) : 200.0000 deg.C
Max Temperature (flow front) : 200.4424 deg.C

Max Shear Rate (at Fill) : 19878.5820 1/s
Max Shear Rate (during cycle) : 51702.1055 1/s

Max Shear Stress (at Fill) : 0.3308 MPa
Max Shear Stress (during cycle) : 0.3340 MPa

Max Solidification Time (Tri. Elements): 1.92 sec (Element 86)
Min Solidification Time (Tri. Elements): 0.22 sec (Element 844)

Throughputs
==========

Node	Throughput [cu.cm]
329	3.637

Pressure when Throughput exceeded Part Volume : 14.148 MPa
Pressure when Displaced Ram Volume exceeded Part Volume : 14.148 MPa

Output files produced
=====================
No. Restart File(s) : 1
0.118106 sec CAP2-1C.FR0
No. Intermediate Results File(s) : 0
Nodal Result File : CAP2-1C.FNR
Elemental Result File : CAP2-1C.FER
Summary File : CAP2-1C.FSU
Laminate Result File : CAP2-1C.FLM
Time Series File : CAP2-1C.FTS

Actual Injection Profile
========================

% Shot vol.	% Nom. flow rate
9	91
20	96
31	97
42	98
49	98
64	98
82	98
93	99
97	99
100	100

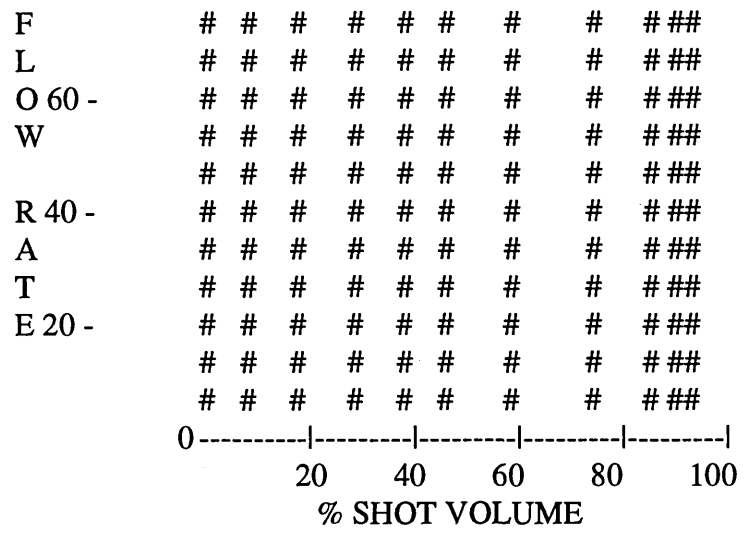

Analysis Display Summary

Time	Volume	Flow rate: Actual	Flow rate: Nominal	Pressure	Clamp force:
sec	%	cu.cm/s	%	MPa	tonne
0.11811	100.00	7.803	100.00	14.15	1.39

* Change to Press. Control at 98.5 % Shot Volume (0.11403 sec)
Pressure = 14.148 MPa

Warning and Error Diagnostics

[FPISLV - 1] VISCOSITY SOLVER ITERATION LIMIT

0.021447 (57.98%)	0.016695 (58.53%)	0.062097 (72.58%)
0.019565 (72.87%)	0.065043 (73.03%)	0.091905 (77.61%)
0.042596 (77.89%)	0.054357 (78.15%)	0.116304 (81.49%)
0.115684 (81.77%)	0.106667 (82.05%)	0.012851 (84.20%)
0.068626 (84.35%)	0.011029 (88.41%)	0.041423 (88.69%)
0.070573 (88.96%)	0.100204 (92.44%)	0.120217 (92.69%)
0.032946 (93.00%)	0.059278 (95.53%)	0.091699 (95.86%)
0.026660 (96.26%)	0.036289 (96.67%)	0.063236 (98.73%)

Execution Times

EXECUTED 03-JUL-95 10:30
COMPLETED 03-JUL-95 10:49

A2. SUMMARY OF THE FILLING ANALYSIS OF FILLCAL V

```
==========================================================F
ILLCALC V Flow Analysis
Version 1.07
Project name : C:\FCV_BO\CAP-3B
==========================================================
TRANSIENT FLOW ANALYSIS
----------------------
Convergence criterion        0.0500000
Under-relaxation factor      0.5000000
Max. iterations per step      80
Critical FVOF               0.9500000
Pressure switchover %         98

Compression moulding simulation
Second order viscosity model
Non-isothermal
==========================================================
        MATERIAL DATA
==========================================================
Thermoplatics material data -NESTE VB 8042B
Group file name - PP

Thermal Properties
~~~~~~~~~~~~~~~~~~
Specific heat      2883.0000000
Density             905.0000000
Diffusivities         0.0750000      0.0750000
HTC               25000.0000000   25000.0000000
No Flow Temp        162.0000000
Freeze temp.        152.0000000

Viscosity Limits
~~~~~~~~~~~~~~~~
Shear rate      min     10.0000000
                max     24000.0000000
Max. temp.              260.0000000

First Order Model
~~~~~~~~~~~~~~~~~
Viscosity factor   44100.0000000
Shear factor          -0.6365000
Temp. factor          -0.0079600

Second Order Model
~~~~~~~~~~~~~~~~~~
LDratio       0.0000000
Tmin        180.0000000
Tmax        260.0000000
```

Corrected	Corrected
600.7999878	0.0000000
132.3000031	0.0000000
28.7000008	0.0000000
400.2999878	0.0000000
92.4000015	0.0000000
289.5000000	0.0000000

==========

INITIALISATION

==========

Initial Newtonian viscosity (Pa.s) 1000.0000000

Fill Time Specified 0.0000000 (s)

Forced override of all mould temps.
Mould temp 50.0000000
Melt temp 200.0000000

No. of elements 1482
No. of nodes 838
Original bandwidth 756
No. of unused nodes 90
Reduced No. of nodes 748
Maximum degree 9
Reduced bandwidth 53
Reduced stiffness matrix requires 32250 double-precision numbers
Total projected area (XY) 0.124E-002 sq. m
Total volume 0.398E-005 cu. m
Estimated weight 0.360E-002 kg
Initial charge volume 0.402E-005 cu. m
Fill factor 1.00839
Cavity will be overfilled
Started at 14:31:06.76

==========

FILLING PHASE

==========

Time (s)	Fill (%)	Pres max (Pa)	Force (T)
0.04028	10	0.312E+005	0.000
0.08231	20	0.180E+006	0.004
0.09580	30	0.111E+007	0.065
0.09997	40	0.135E+007	0.078
0.10423	50	0.287E+007	0.201
0.10884	60	0.442E+007	0.351
0.11099	70	0.504E+007	0.395
0.11320	80	0.725E+007	0.636
0.11531	90	0.963E+007	0.886
0.11668	100	0.119E+008	1.109

Time 0.117 s

Data Item	Minimum Data Value	Element	Lam.	Maximum Data Value	Element	Lam.
Temps. C	58.4703	1436	8	202.3390	112	6

Calculated fill time 0.11668 s
XY Force (fill) 0.109E+005 N 1.10852 Tonnes
XY Force (max) 0.148E+005 N 1.50385 Tonnes
Stopping on time >= 0.0000000
Finished at 14:40:44.58

A3. HEAT TRANSFER CALCULATION PROGRAME IN TURBO C++

```
#include <stdlib.h>
#include <stdio.h>

main ()
{
float Fo1, Fo2, Bi, a1, a2;
float K1, K2, p1, p2, Cp1, Cp2, h;
float t, x;
float T[14];
int i,j,m,count;

K1=19;
p1=7865;
Cp1=460;
K2=0.118;
p2=907;
Cp2=2930;
h=1500;
x=0.00025;

Bi=h*x/K1;
t=0.00595/(1+(1.3258E-5*h));
a1=(K1/p1)/Cp1;
a2=(K2/p2)/Cp2;
Fo1=((a1*t)/x)/x;
Fo2=((a2*t)/x)/x;

fprintf(stdprn, "\n");
fprintf(stdprn, "h= %3.1f \t", h);
```

```
fprintf(stdprn, "t= %0.5f \t", t);
fprintf(stdprn, "Fo1= %3.5f \t", Fo1);
fprintf(stdprn, "Fo2= %3.5f \t", Fo2);
fprintf(stdprn, "Bi= %3.5f ",Bi);
fprintf(stdprn, "\n");

for (i=0; i<14; ++i)
   T[i]=20;


j=0;
count=1;

do{
 fprintf(stdprn, "count= %d\n", count);
 fprintf(stdprn, "%1.3f ", j*0.000);
 T[0]=16;

 T[12]=215;
 T[13]=215;
 T[11]=(T[12]+T[10])/2;

 for (i=0; i<14; i=i+1)
    fprintf(stdprn, "%4.1f ", T[i]);

 fprintf(stdprn, "\n");
 for(j=2; j<1001; j=j+1)
   {
   T[1] =2*Fo1*(T[2]+Bi*T[0]+(1/(2*Fo1)-Bi-1)*T[1]);
   for (i=2; i<11; i=i+1)
        T[i] =Fo1*(T[i-1]+T[i+1]+(1/Fo1-2)*T[i]);

   T[11]=Fo1*(T[10]-T[11])+Fo2*(T[12]-T[11])+T[11];
```

```
    T[12]=Fo2*(T[11]+T[13]+(1/Fo2-2)*T[12]);
    T[13]=Fo2*(2*T[12]+(1/Fo2-2)*T[13]);

        if((j%100)==0)
          {
          fprintf(stdprn, "%1.3f ",j*t);
          for (i=0; i<14; i=i+1)
             fprintf(stdprn, "%4.1f ", T[i]);

          fprintf(stdprn, "\n");
          }
    }
    fprintf(stdprn, "\n");

    for (m=1; m<81; m=m+1)
        {
        T[1] =2*Fo1*(T[2]+Bi*T[0]+(1/(2*Fo1)-Bi-1)*T[1]);
        for (i=2; i<11; i=i+1)
          T[i] =Fo1*(T[i-1]+T[i+1]+(1/Fo1-2)*T[i]);
        T[11]=Fo1*(T[10]-T[11])+T[11];
        }
    fprintf(stdprn, "%1.3f ", 80*t);
    for (i=0; i<12; ++i)
        fprintf(stdprn, "%4.1f ", T[i]);
    fprintf(stdprn, "\n");

    count++;
    fprintf(stdprn, "\n");
  }while(count<=10);
}
```

--

A4. SUMMARY OF THE COOLING ANALYSIS OF ORIGINAL COOLING SYSTEM IN STANDARD CONDITION

FCLP version 1.2.3 Summary of analysis : CAP1C203.CSU
Iteration Results

Target temp : 50

Iteration No :	1	2	3	4
max sur temp:	88.6	87.6	87.7	87.6
T min sur temp:	54.0	50.8	51.2	51.1
O av sur temp:	74.0	72.5	72.7	72.7
P std deviation:	9.0	9.1	9.1	9.1
shrink index:	20.0	20.0	20.0	20.0
max sur temp:	79.5	79.4	79.4	79.4
B min sur temp:	48.6	48.2	48.2	48.2
O av sur temp:	67.8	67.5	67.5	67.5
T std deviation:	8.2	8.5	8.5	8.5
shrink index:	16.1	16.2	16.2	16.2
warpage index:	7.3	6.2	6.3	6.3
% part frozen:	100.0	100.0	100.0	100.0
max freez time:	3.9	3.9	3.9	3.9
cooling time:	5.2	5.2	5.2	5.2
inlet temp B1:	16.0	16.0	16.0	16.0
inlet temp B2:	16.0	16.0	16.0	16.0

Circ.	Flowrate l/min	Reynolds No. range	Metal surface temp range	avrg	Press drop kPa	Temp rise
1	0.25	3181 - 925	57.6 - 29.1	44.8	31.0	0.7
2	0.25	7025 - 7025	19.3 - 19.1	19.2	898.2	0.3
3	0.25	7025 - 7025	19.3 - 19.1	19.2	898.2	0.3
4	0.25	5831 - 5831	20.3 - 19.7	20.0	483.1	0.6
5	0.25	5831 - 5831	20.3 - 19.7	20.0	483.1	0.6
6	0.25	4195 - 4195	20.7 - 20.1	20.4	112.5	0.6
7	0.25	4195 - 4195	20.7 - 20.1	20.4	112.5	0.6
8	0.25	3976 - 1469	26.1 - 18.9	23.6	51.1	0.6
9	0.25	3976 - 1469	25.6 - 18.8	23.4	57.3	0.6
10	0.25	3181 - 925	57.6 - 29.1	44.8	31.0	0.7
11	0.25	3181 - 925	57.6 - 29.1	44.8	31.0	0.7
12	0.25	3181 - 925	57.6 - 29.1	44.8	31.0	0.7
13	0.25	3181 - 925	57.6 - 29.1	44.8	31.0	0.7
14	0.25	3181 - 925	57.6 - 29.1	44.8	31.0	0.7

Process Data

Target mold temp: 50.00 deg.C
Injection time: 0.12 sec

1. MFL Patran Result File (MULTI) : CAP2-1.FSU
2. Model filename (1st part) : CAP2-1
3. Packing time : 0.50 sec
4. Cooling time (constant) : 5.170 sec
5. Clamp open time : 0.50 sec
6. Cooling files name (1st part) : CAP1C2

Circ	inlet point	flowrate	inlet temp	Block	Cond
1	1	0.3	16(const)	2	41.90
2	9	0.3	16(const)	1	41.90
3	18	0.3	16(const)	1	41.90
4	10	0.3	16(const)	1	41.90
5	27	0.3	16(const)	1	41.90
6	11	0.3	16(const)	1	41.90
7	38	0.3	16(const)	1	41.90
8	39	0.3	16(const)	1	41.90
9	57	0.3	16(const)	1	41.90
10	63	0.3	16(const)	2	41.90
11	70	0.3	16(const)	2	41.90
12	77	0.3	16(const)	2	41.90
13	84	0.3	16(const)	2	41.90
14	91	0.3	16(const)	2	41.90

8. Auto flow balancing by pres. drop: off
9. Auto flow balancing by flow rate: off
10. Type of coolant in circuits: water
11. Coolant inlet temps. of blocks
12. Change die metal conductivity of blocks
13. No of plastic laminates (default): 15
14. Type of analysis: Constrained automatic
15. FCLP results file name: CAP1C203
16. Special options: Opaque elements

Total heat lost from plastic to block 1 = 0.4625830E+00 kJ
Total heat lost from plastic to block 2 = 0.4419005E+00 kJ

average element heat split = 47.9% / 52.1%
std deviation = 0.0121

A5. SUMMARY OF THE COOLING ANALYSIS OF DESIGN B

COOLING SYSTEM IN STANDARD CONDITION

FCLP version 1.2.3 Summary of analysis : CAP3-202.CSU
Iteration Results

Target temp :	50		
Iteration No :	1	2	3
max sur temp :	82.8	82.7	82.7
T min sur temp :	31.1	31.1	31.1
O av sur temp :	64.4	64.3	64.3
P std deviation :	11.3	11.3	11.3
shrink index :	19.6	19.5	19.5
max sur temp :	78.0	77.8	77.8
B min sur temp :	46.0	45.9	45.9
O av sur temp :	65.9	65.7	65.7
T std deviation :	11.0	10.9	10.9
shrink index :	18.7	18.5	18.5
warpage index :	2.6	2.5	2.5
% part frozen :	100.0	100.0	100.0
max freez time:	3.8	3.8	3.8
cooling time :	5.2	5.2	5.2
inlet temp B1 :	16.0	16.0	16.0
inlet temp B2 :	16.0	16.0	16.0

Circ.	Flowrate l/min	Reynolds No. range	Metal surface temp range	avrg	Press drop kPa	Temp rise
1	0.19	3607 - 1111	28.0 - 18.8	25.6	59.2	0.9
2	0.19	11020 - 11020	18.3 - 18.0	18.1	17527.5	0.4
3	0.19	11020 - 11020	18.3 - 18.0	18.1	17527.5	0.4
4	0.19	8816 - 8816	18.5 - 18.0	18.2	8320.3	0.6
5	0.19	8816 - 8816	18.5 - 18.0	18.2	8320.3	0.6
6	0.19	6297 - 6297	18.9 - 18.3	18.6	1720.7	0.7
7	0.19	6297 - 6297	18.9 - 18.3	18.6	1720.7	0.7
8	0.19	3607 - 1111	27.5 - 19.0	25.4	65.7	0.9
9	0.19	11020 - 11020	19.3 - 19.1	19.2	13976.9	0.3
10	0.19	11020 - 11020	19.3 - 19.1	19.2	13976.9	0.3
11	0.19	3607 - 596	31.7 - 23.7	24.9	73.1	0.7
12	0.19	3607 - 596	31.7 - 23.7	24.9	73.1	0.7
13	0.19	3607 - 596	31.7 - 23.7	24.9	73.1	0.7
14	0.19	3607 - 596	31.7 - 23.7	24.9	73.1	0.7
15	0.19	3607 - 596	31.7 - 23.7	24.9	73.1	0.7
16	0.19	3607 - 596	31.7 - 23.7	24.9	73.1	0.7
17	0.19	3607 - 596	31.7 - 23.7	24.9	73.1	0.7

18	0.19	3607 - 596	31.7 - 23.7	24.9	73.1	0.7

Process Data

Target mold temp : 50.00 deg.C
Injection time : 0.12 sec

1. MFL Patran Result File (MULTI) : CAP2-1.FSU
2. Model filename (1st part) : CAP2-1
3. Packing time : 0.50 sec
4. Cooling time (constant) : 5.170 sec
5. Clamp open time : 0.50 sec
6. Cooling files name (1st part) : CAP3-2

Circ	inlet point	flowrate	inlet temp	Block	Cond
1	5	0.2	16(const)	1	41.90
2	8	0.2	16(const)	1	41.90
3	22	0.2	16(const)	1	41.90
4	23	0.2	16(const)	1	41.90
5	45	0.2	16(const)	1	41.90
6	46	0.2	16(const)	1	41.90
7	73	0.2	16(const)	1	41.90
8	111	0.2	16(const)	1	41.90
9	112	0.2	16(const)	1	41.90
10	123	0.2	16(const)	1	41.90
11	3	0.2	16(const)	2	41.90
12	129	0.2	16(const)	2	41.90
13	135	0.2	16(const)	2	41.90
14	141	0.2	16(const)	2	41.90
15	147	0.2	16(const)	2	41.90
16	153	0.2	16(const)	2	41.90
17	159	0.2	16(const)	2	41.90
18	165	0.2	16(const)	2	41.90

8. Auto flow balancing by pres. drop: off
9. Auto flow balancing by flow rate : off
10. Type of coolant in circuits : water
11. Coolant inlet temps. of blocks
12. Change die metal conductivity of blocks
13. No of plastic laminates (default) : 15
14. Type of analysis : Constrained automatic
15. FCLP results file name : CAP3-202
16. Special options : Opaque elements

Total heat lost from plastic to block 1 = 0.4582433E+00 kJ
Total heat lost from plastic to block 2 = 0.4742289E+00 kJ

average element heat split = 49.2% / 50.8%
std deviation = 0.0043

A6. SUMMARY OF THE COOLING ANALYSIS OF DESIGN B

COOLING SYSTEM IN STANDARD CONDITION

FCLP version 1.2.3 Summary of analysis : CAP3-102.CSU
Iteration Results

Target temp : 50			
Iteration No :	1	2	3
max sur temp :	82.6	82.5	82.5
T min sur temp :	34.8	34.9	34.9
O av sur temp :	66.2	66.1	66.1
P std deviation :	10.8	10.8	10.8
shrink index :	19.4	19.4	19.4
max sur temp :	78.1	77.8	77.8
B min sur temp :	46.4	46.3	46.3
O av sur temp :	66.3	66.1	66.1
T std deviation :	10.5	10.4	10.4
shrink index :	18.7	18.5	18.5
warpage index :	2.4	2.4	2.4
% part frozen :	100.0	100.0	100.0
max freez time:	3.8	3.8	3.8
cooling time :	5.2	5.2	5.2
inlet temp B1 :	16.0	16.0	16.0
inlet temp B2 :	16.0	16.0	16.0

Circ.	Flowrate l/min	Reynolds No. range	Metal surface temp range	avrg	Press drop kPa	Temp rise
1	0.19	3626 - 1116	28.0 - 18.8	25.6	59.8	0.9
2	0.19	11079 - 11079	18.3 - 18.0	18.1	17713.4	0.4
3	0.19	11079 - 11079	18.3 - 18.0	18.1	17713.4	0.4
4	0.19	8863 - 8863	18.4 - 18.0	18.2	8408.5	0.6
5	0.19	8863 - 8863	18.4 - 18.0	18.2	8408.5	0.6
6	0.19	6331 - 6331	18.9 - 18.3	18.6	1739.0	0.7
7	0.19	6331 - 6331	18.9 - 18.3	18.6	1738.9	0.7
8	0.19	3626 - 1116	27.5 - 19.0	25.4	66.3	0.9
9	0.19	11079 - 11079	19.2 - 19.1	19.1	14125.2	0.3
10	0.19	11079 - 11079	19.2 - 19.1	19.1	14125.2	0.3
11	0.19	599 - 599	27.5 - 23.0	26.3	49.8	0.7
12	0.19	599 - 599	27.5 - 23.0	26.3	49.8	0.7
13	0.19	599 - 599	27.5 - 23.0	26.3	49.8	0.7
14	0.19	599 - 599	27.5 - 23.0	26.3	49.8	0.7
15	0.19	599 - 599	27.5 - 23.0	26.3	49.8	0.7
16	0.19	599 - 599	27.5 - 23.0	26.3	49.8	0.7
17	0.19	599 - 599	27.5 - 23.0	26.3	49.8	0.7
18	0.19	599 - 599	27.5 - 23.0	26.3	49.8	0.7

Process Data

Target mold temp : 50.00 deg.C
Injection time: 0.12 sec

1. MFL Patran Result File (MULTI): CAP2-1.FSU
2. Model filename (1st part) : CAP2-1
3. Packing time : 0.50 sec
4. Cooling time (constant) : 5.170 sec
5. Clamp open time : 0.50 sec
6. Cooling files name (1st part) : CAP3-1

Circ	inlet point	flowrate	inlet temp	Block	Cond
1	5	0.2	16(const)	1	41.90
2	8	0.2	16(const)	1	41.90
3	22	0.2	16(const)	1	41.90
4	23	0.2	16(const)	1	41.90
5	45	0.2	16(const)	1	41.90
6	46	0.2	16(const)	1	41.90
7	73	0.2	16(const)	1	41.90
8	111	0.2	16(const)	1	41.90
9	112	0.2	16(const)	1	41.90
10	123	0.2	16(const)	1	41.90
11	3	0.2	16(const)	2	41.90
12	127	0.2	16(const)	2	41.90
13	131	0.2	16(const)	2	41.90
14	135	0.2	16(const)	2	41.90
15	139	0.2	16(const)	2	41.90
16	143	0.2	16(const)	2	41.90
17	147	0.2	16(const)	2	41.90
18	151	0.2	16(const)	2	41.90

8. Auto flow balancing by pres. drop: off
9. Auto flow balancing by flow rate : off
10. Type of coolant in circuit 1 : water
11. Coolant inlet temps. of blocks
12. Change die metal conductivity of blocks
13. No of plastic laminates (default): 15
14. Type of analysis: Constrained automatic
15. FCLP results file name: CAP3-102
16. Special options: Opaque elements

Total heat lost from plastic to block 1 = 0.4592185E+00 kJ
Total heat lost from plastic to block 2 = 0.4671677E+00 kJ

average element heat split = 49.3% / 50.7%
std deviation = 0.0050

Model: Caplc2

Melt temperature: 200 °C

Master file: Cap2-1a

Temperature °C

Analysis condition	Model	Lowest max.tmp	Highest max.tmp	min inside.tmp	Max inside.tmp	Min outside.tmp	Max outside.tmp
1. MF auto (Red 10,000) at 5.2 sec & 16 C	caplc222	26.608	103.101	16.168	51.272	16.383	46.911
3.MCG standard condition at 1.514 l/min & 5.2 sec & 16 C	caplc216	46.089	106.418	22.005	58.971	16.906	50.656
4. Increase flow rate to max (25%, 40%) at 5.2 sec & 16 C	caplc219	42.303	105.331	20.127	56.514	16.561	50.169
5. Reduce inlet temperature to 10 C at 5.2 sec &1.514 l/min	caplc217	41.356	103.766	16.956	55.052	11.028	45.961
6. Max condition at 25%, 40%, 5.2 sec & 10 C	caplc220	40.974	102.985	15.071	53.499	10.659	45.581
7. Reduce cooling time to 4.5 sec at 1.514 l/min & 16 C	caplc218	50.341	115.775	22.555	63.011	16.992	54.723
8. Reduce cooling time to 4.5 sec at 25%,40% & 10 C	caplc221	45.373	112.692	15.544	57.658	10.722	49.794

Table 3.3.4.1 Cooling analysis on origenal cooling system

Temperature °C

Cooling model	Analysis condition		Lowest max.temp	Highest max.tmp	min inside.temp	Max inside.temp	Min outside.temp	Max outside.temp
Original Cooling Channel (cap1c2)	1. MF auto (Red 10,000) at 5.2 sec & 16 °C	cap1c200	29.051	122.335	16.205	59.057	16.467	53.764
	2. Min cooling time at 16 °C & 100% freeze	cap1c201	40.981	147.297	16.251	69.055	16.386	64.755
	3. MCG standard condition at 1.514 l/min & 5.2 sec & 16 °C	cap1c203	52.736	126.354	23.325	68.418	17.105	58.298
	4. Increase flow rate to max (25%, 40%) at 5.2 sec & 16 °C	cap1c202	48.131	125.037	21.089	65.431	16.684	57.706
	5. Reduce inlet temperature to 10 °C at 5.2 sec &1.514 l/min	cap1c204	48.051	123.773	18.434	64.635	11.247	53.631
	6. Max condition at 25%, 40%, 5.2 sec & 10 °C	cap1c206	47.596	122.833	16.148	62.761	10.799	53.172
	7. Reduce cooling time to 4.5 sec at 1.514 l/min & 16 °C	cap1c215	57.701	137.261	23.964	73.122	17.205	63.021
	8. Reduce cooling time to 4.5 sec at 25%, 40% & 10 °C	cap1c207	52.702	134.081	16.697	67.575	10.872	58.035
			Lowest max.temp	Highest max.tmp	min inside.temp	Max inside.temp	Min outside.temp	Max outside.temp
New design A cap3-2	1. MF auto (Red 10,000) at 5.2 sec & 16 °C	cap3-200	26.818	121.217	16.064	49.159	16.317	53.522
	2. Min cooling time at 16 °C & 100% freeze	cap3-201	39.365	147.322	16.078	57.321	16.394	65.221
	3. MCG standard condition at 1.514 l/min & 5.2 sec & 16 °C	cap3-202	32.941	123.685	21.801	55.811	16.465	59.024
	4. Increase flow rate to max (25%, 40%) at 5.2 sec & 16 °C	cap3-204	32.735	123.171	20.279	54.701	16.357	58.786
	5. Reduce inlet temperature to 10 °C at 5.2 sec &1.514 l/min	cap3-203	27.493	120.888	16.699	51.412	10.499	54.311
	6. Max condition at 25%, 40%, 5.2 sec & 10 °C	cap3-206	27.274	120.325	14.987	50.201	10.381	54.063
	7. Reduce cooling time to 4.5 sec at 1.514 l/min & 16 °C	cap3-208	37.551	134.741	22.298	59.581	16.501	63.849
	8. Reduce cooling time to 4.5 sec at 25%,40% & 10 °C	cap3-207	32.014	131.718	15.459	54.078	10.413	59.037
			Lowest max.temp	Highest max.tmp	min inside.temp	Max inside.temp	Min outside.temp	Max outside.temp
New design B cap3-1	1. MF auto (Red 10,000) at 5.2 sec & 16 °C	cap3-100	27.663	120.507	16.061	42.315	16.316	53.596
	2. Min cooling time at 16 °C & 100% freeze	cap3-101	41.081	147.674	16.074	53.592	16.397	65.724
	3. MCG standard condition at 1.514 l/min & 5.2 sec & 16 °C	cap3-102	36.697	123.417	21.806	51.826	16.463	59.329
	4. Increase flow rate to max (25%, 40%) at 5.2 sec & 16 °C	cap3-103	36.411	122.817	20.168	51.568	16.362	59.098
	5. Reduce inlet temperature to 10 °C at 5.2 sec &1.514 l/min	cap3-104	31.398	120.649	16.704	49.942	10.498	54.628
	6. Max condition at 25%, 40%, 5.2 sec & 10 °C	cap3-105	31.082	119.993	14.886	46.666	10.387	54.387
	7. Reduce cooling time to 4.5 sec at 1.514 l/min & 16 °C	cap3-106	41.484	134.485	22.327	55.679	16.051	64.139
	8. Reduce cooling time to 4.5 sec at 25%,40% & 10 °C	cap3-107	36.011	131.395	15.298	50.622	10.421	59.331

Table 3.3.4.2 The analysis results of three different cooling systems

Table 3.3.4.3 Temperatrue trend of design A in standard flow rate

Temperature °C

Process speed (caps/min)	C-min	C-max	C-thread	S-thread	T-max	T-min	T-av	B-max	B-min	B-av
540	30.878	106.031	93.505	58.014	72.4	29.3	57	68.6	42	58.2
560	31.817	108.407	95.642	59.175	73.9	30.1	58.5	70	43.3	59.6
570	32.317	109.616	96.732	59.766	74.6	30.5	59.2	70.7	44	60.4
580	32.784	110.706	97.719	60.304	75.3	30.9	59.9	71.3	44.7	61.1
590	33.272	111.809	98.719	60.581	75.9	31.3	60.6	71.9	45.4	61.8
600	33.779	112.924	99.733	61.404	76.6	31.7	61.3	72.6	46.1	62.5
610	34.243	113.911	100.633	61.899	77.2	32.1	61.9	73.2	46.7	63.2
620	34.791	115.051	101.673	62.469	77.9	32.5	62.6	73.8	47.4	63.9
630	35.293	116.059	102.598	62.981	78.5	33	63.3	74.4	48	64.6
640	35.812	117.078	103.533	63.495	79.1	33.4	63.9	75	48.7	65.2
650	36.281	117.965	104.351	63.953	79.7	33.8	64.5	75.5	49.3	65.8

Table 3.3.4.4 Temperatrue trend of design B in standard flow rate

Temperature °C

Process speed (caps/min)	C-min	C-max	C-thread	S-thread	T-max	T-min	T-av	B-max	B-min	B-av
540	34.267	105.913	94.001	61.284	72.5	32.7	58.8	68.7	42.4	58.8
560	35.255	108.289	96.116	62.482	73.9	33.5	60.2	70.1	43.7	60
570	35.775	109.498	97.21	63.089	74.4	34	61	70.8	44.5	60.8
580	36.264	110.588	98.2	63.642	75.3	34.4	61.6	71.4	45.1	61.5
590	36.773	111.691	99.204	64.204	76	34.8	62.3	72	45.8	62.2
600	37.3	112.806	100.221	64.77	76.6	35.2	63	72.7	46.5	62.9
610	37.784	113.794	101.125	65.277	77.2	35.6	63.7	73.2	47.1	63.5
620	38.358	114.936	102.173	65.864	77.9	36.1	64.4	73.9	47.8	64.3
630	38.882	115.947	103.102	66.388	78.6	36.6	65.1	74.5	48.4	64.9
640	39.411	116.964	104.038	66.907	79.2	37	65.7	75.1	49.1	65.6
650	39.913	117.859	104.868	67.391	79.7	37.4	66.3	75.6	49.7	66.2

Table 3.3.4.5 Temperatrue trend of design A in increased flow rate

Temperature °C

Process speed (caps/min)	C-min	C-max	C-thread	S-thread	T-max	T-min	T-av	B-max	B-min	B-av
540	30.669	105.482	93.013	57.264	71.5	29.1	56.5	67.6	41.2	57.7
560	31.717	108.159	95.418	58.853	73.5	30	58.3	69.4	43	59.4
570	32.215	109.371	96.511	59.473	74.3	30.4	59	70.1	43.7	60.2
580	32.682	110.462	97.498	60.011	74.9	30.8	59.7	70.7	44.4	60.9
590	33.171	111.566	98.501	60.557	75.6	31.2	60.4	71.4	45	61.6
600	33.676	112.683	99.515	61.111	76.3	31.6	61.1	72	45.7	62.3
610	34.141	113.672	100.416	61.604	76.9	32	61.7	72.6	46.3	62.9
620	34.688	114.813	101.458	62.173	77.6	32.4	62.4	73.2	47.1	63.7
630	35.082	115.547	102.136	62.219	77.6	32.7	62.7	73.8	47.3	64.1
640	35.598	116.569	103.073	62.731	78.2	33.2	63.4	74.4	48	64.8
650	36.363	117.455	103.889	63.182	78.8	33.5	64	75.1	48.5	65.3

Table 3.3.4.6 Temperatrue trend of design B in increased flow rate

Temperature °C

Process speed (caps/min)	C-min	C-max	C-thread	S-thread	T-max	T-min	T-av	B-max	B-min	B-av
540	33.992	105.288	93.405	60.301	71.4	32.4	58.2	67.7	41.6	58.1
560	34.974	107.671	95.554	61.489	72.9	33.3	59.6	69.1	43	59.6
570	35.495	108.885	96.653	62.095	73.6	33.7	60.4	69.8	43.7	60.3
580	35.983	109.979	97.646	62.645	74.2	34.1	61	70.6	44.3	61
590	36.492	111.086	98.653	63.204	74.9	34.5	61.7	71.3	45	61.7
600	37.018	112.205	99.673	63.768	75.6	35	62.4	72	45.7	62.4
610	37.501	113.197	100.581	64.272	76.2	35.4	63.1	72.7	46.3	63
620	38.067	114.341	101.628	64.852	76.8	35.8	63.8	73.5	47	63.8
630	38.588	115.355	102.561	65.371	77.5	36.3	64.4	74.1	47.6	64.4
640	39.122	116.378	103.502	65.892	78.1	36.7	65.1	74.8	48.3	65.1
650	39.631	117.279	104.337	66.379	78.6	37.1	65.7	75.4	48.9	65.7

Figure 1.1[@] The structure of the plastic closure

The photo also shows the different surface conditions in different part of the closure

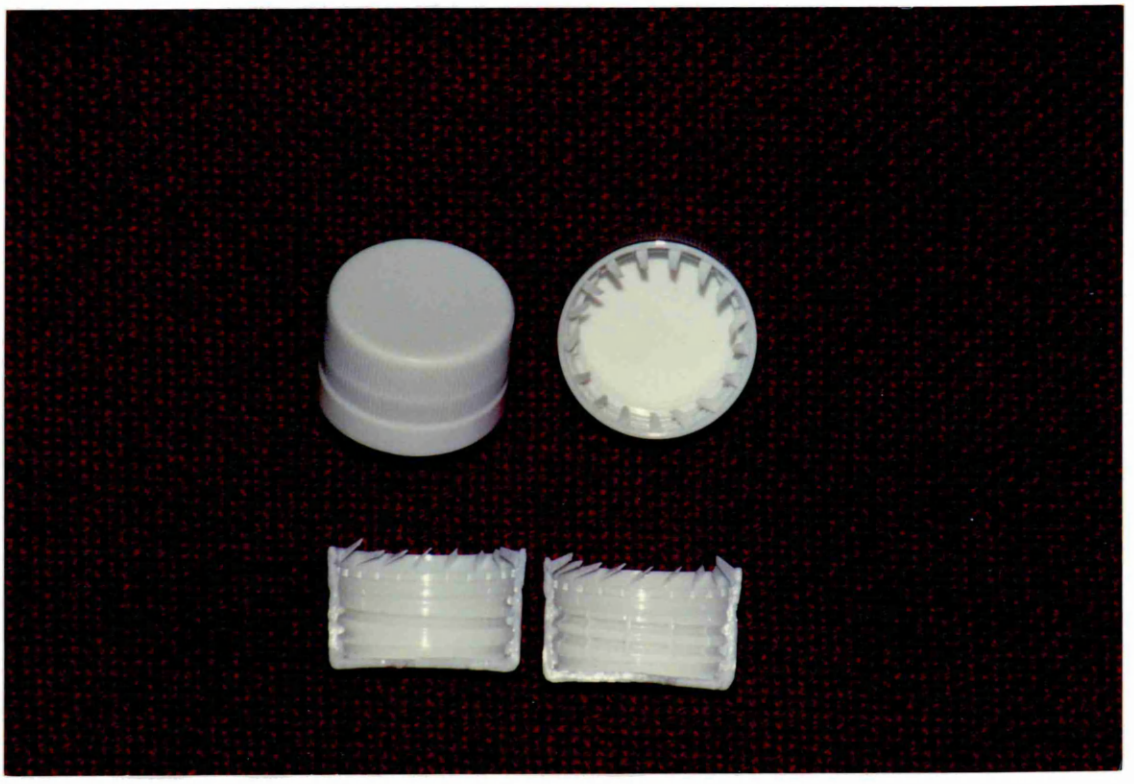

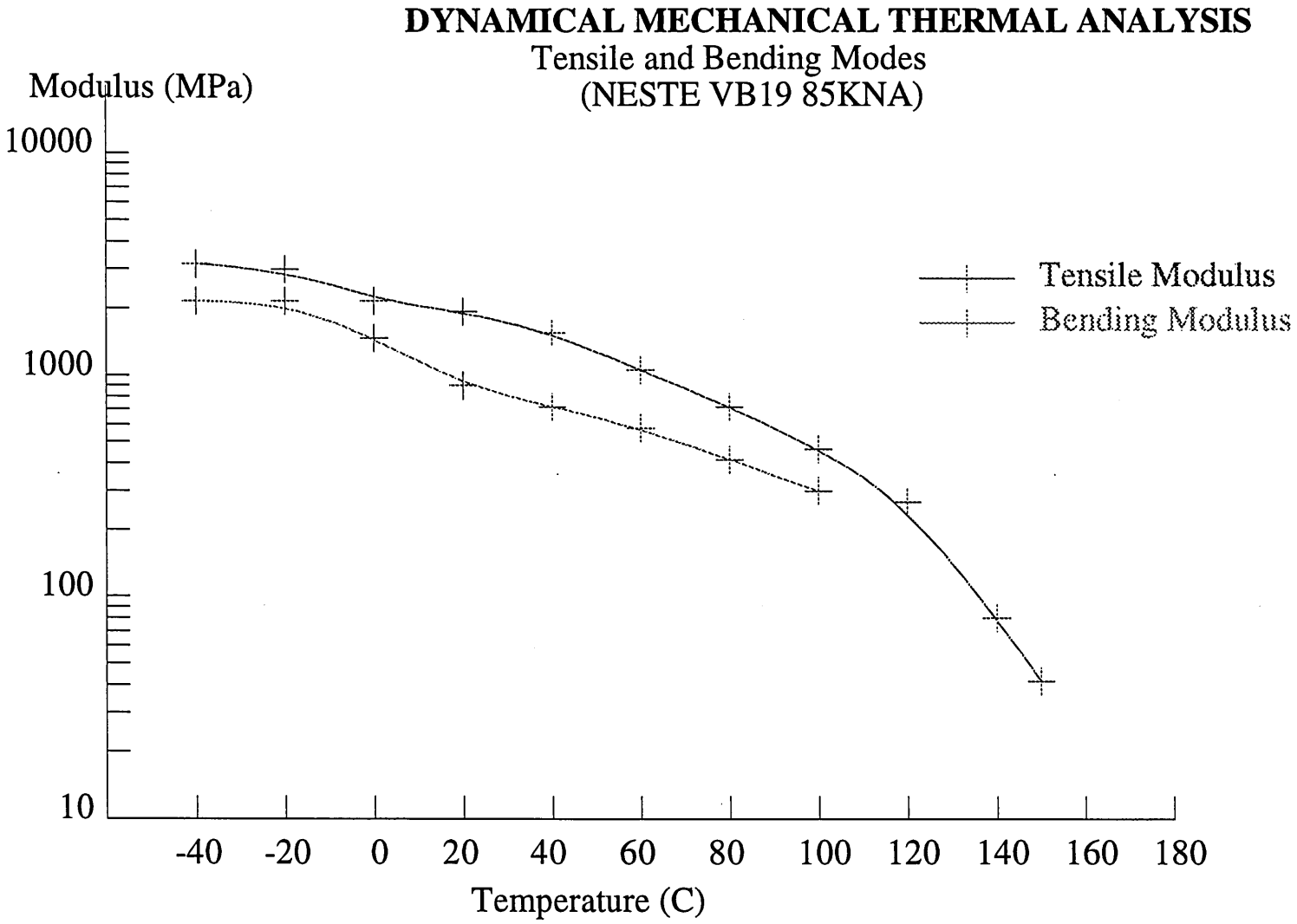

Figure. 3.1.3 The effect of the temperature on modulus of the material

Figure 3.2.1[@] The manufacturing machine for closure forming

* The orange box in the right is the is the pump to inject melt to mould.

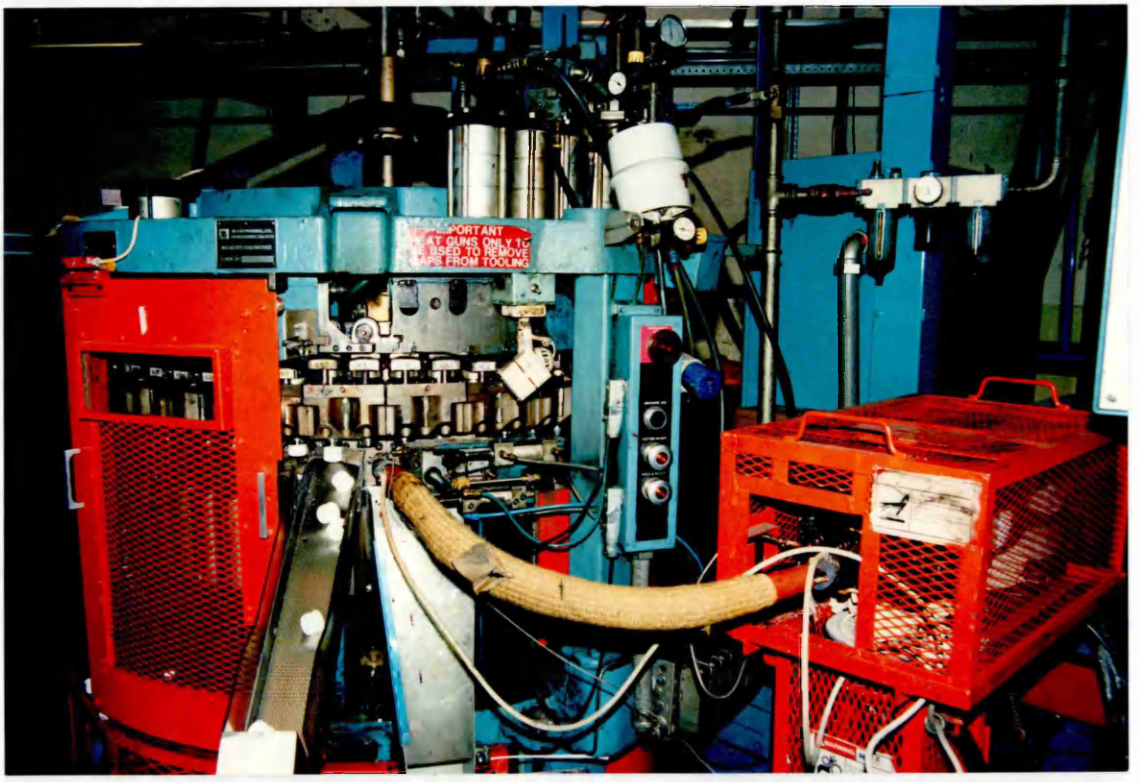

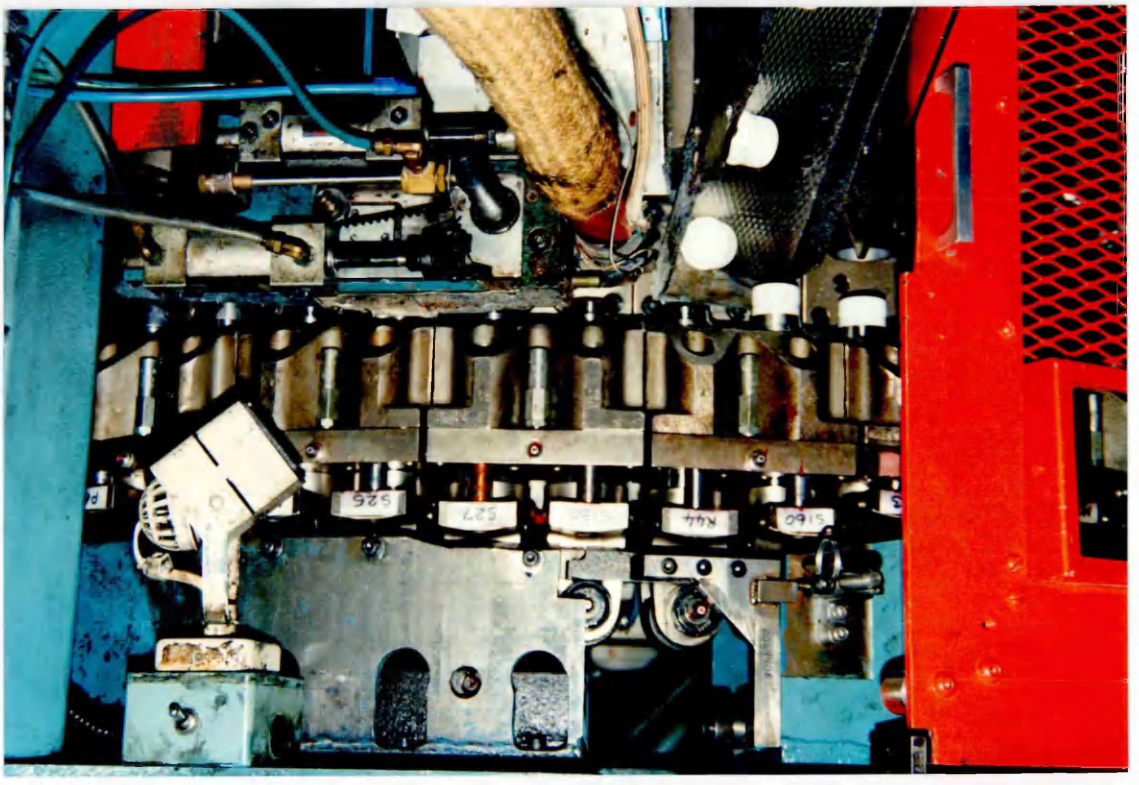

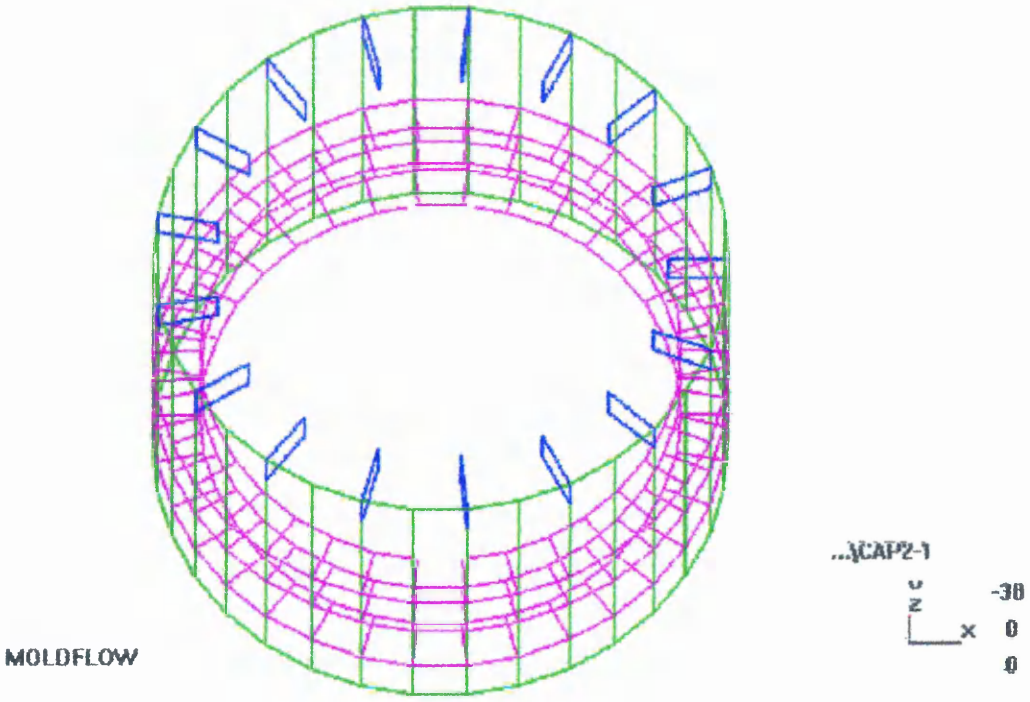

a. 3D model

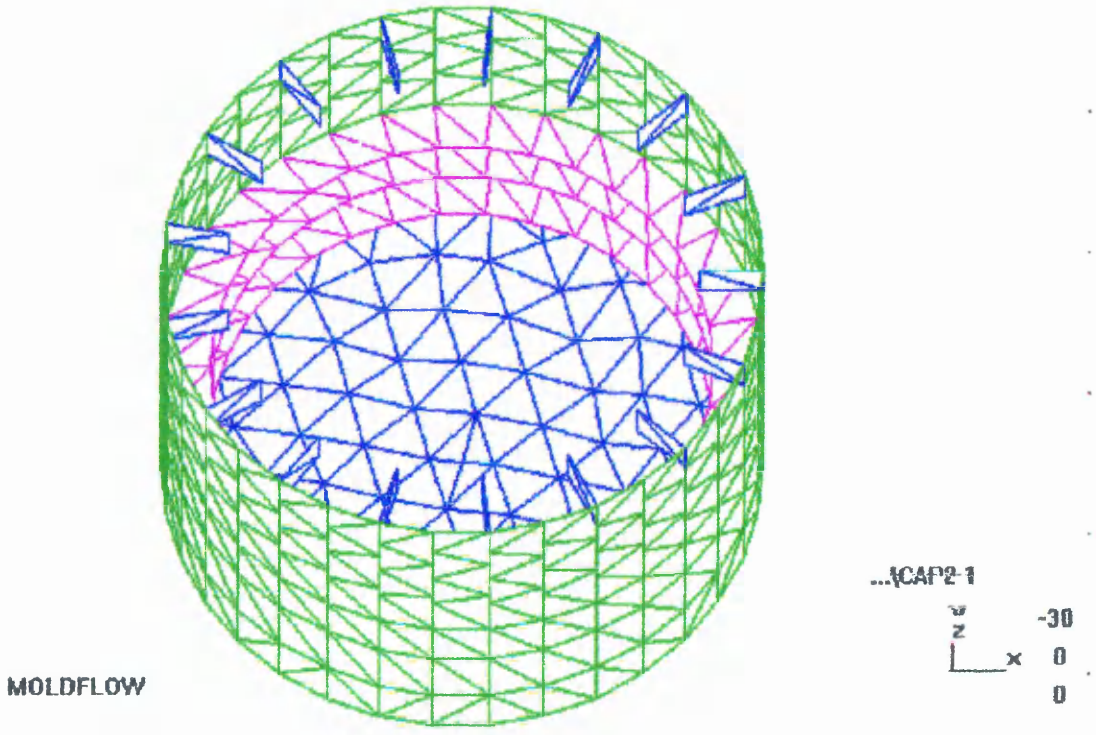

b. Finite element mesh

Figure 3.2.2 Three dimension model and finite element mesh for MF/FLOW filling analysis

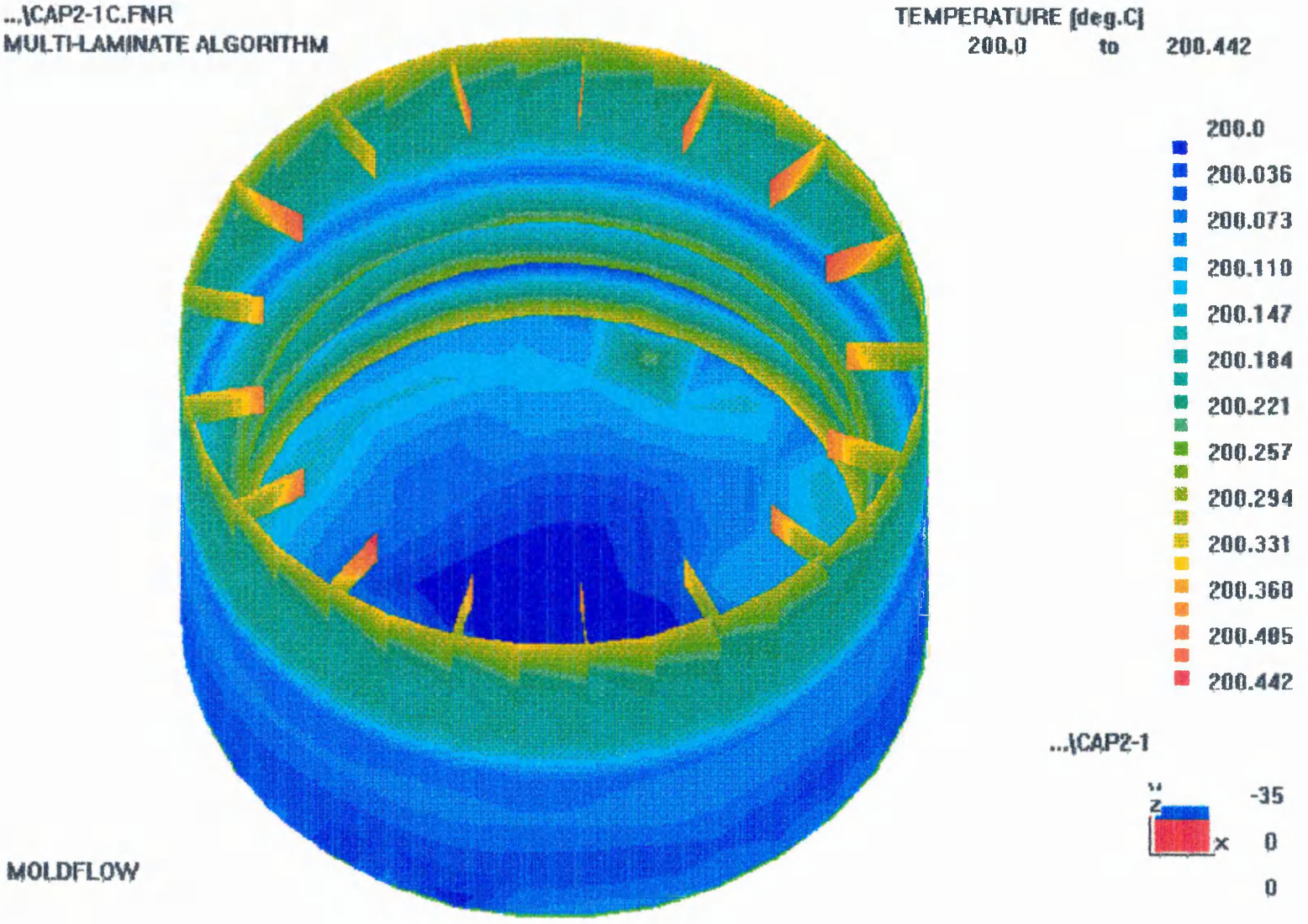

Figure 3.2.4 The temperature distribution of the closure at the end of the filling processing by MF/FLOW (200C melt temperature and 514 caps/min)

Figure 3.2.5[@] Three dimension model and finite element mesh for FILLCALC V[@]

filling analysis

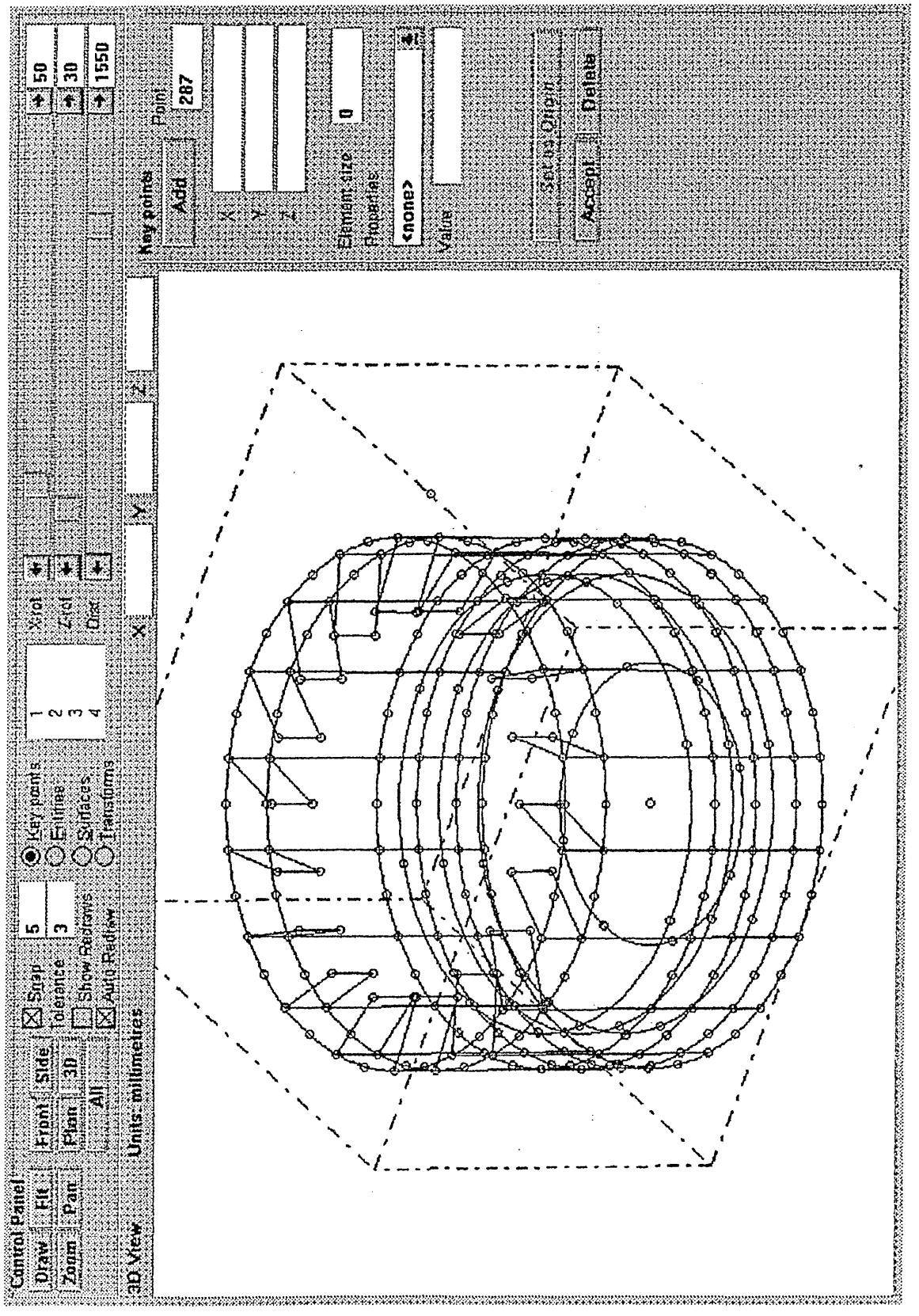

Figure 3.2.6[@] The temperature distribution of the closure at the end of the filling processing by FILLCALC V[@]

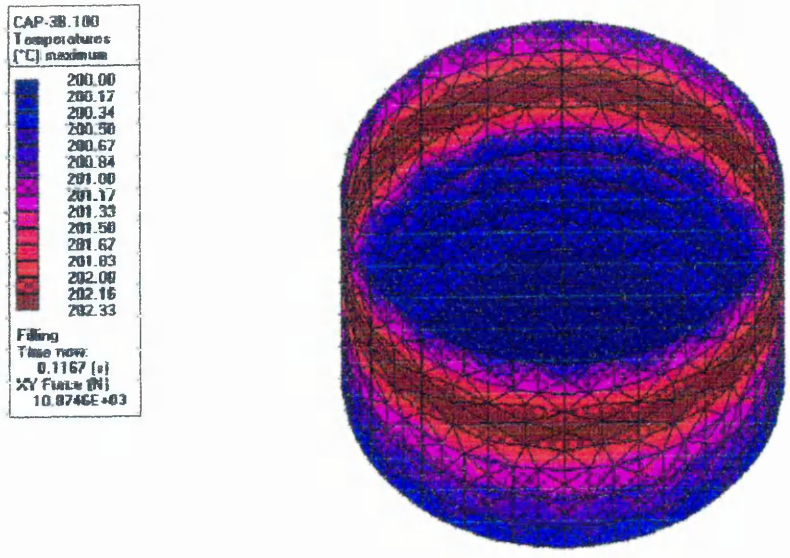

a. Maximum temperature in the cross-section

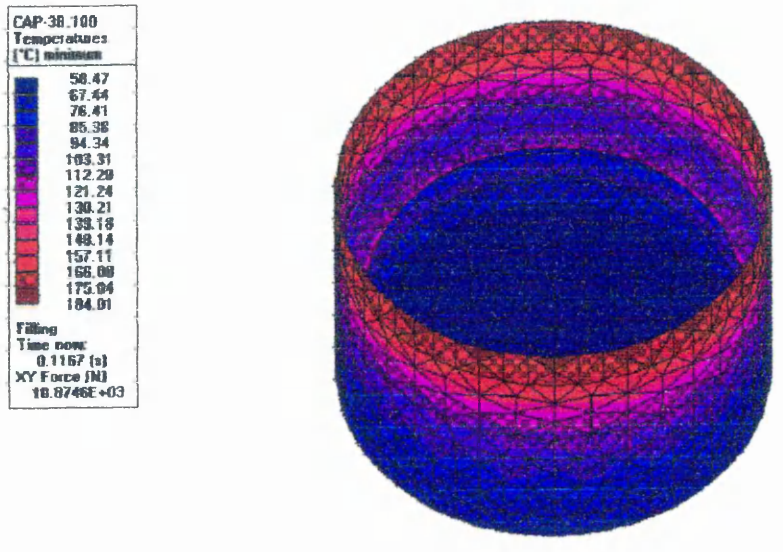

b. Minimum temperature in the cross-section

Figure 3.3.3.1[@] LAND Cyclops TI 35 thermal image system

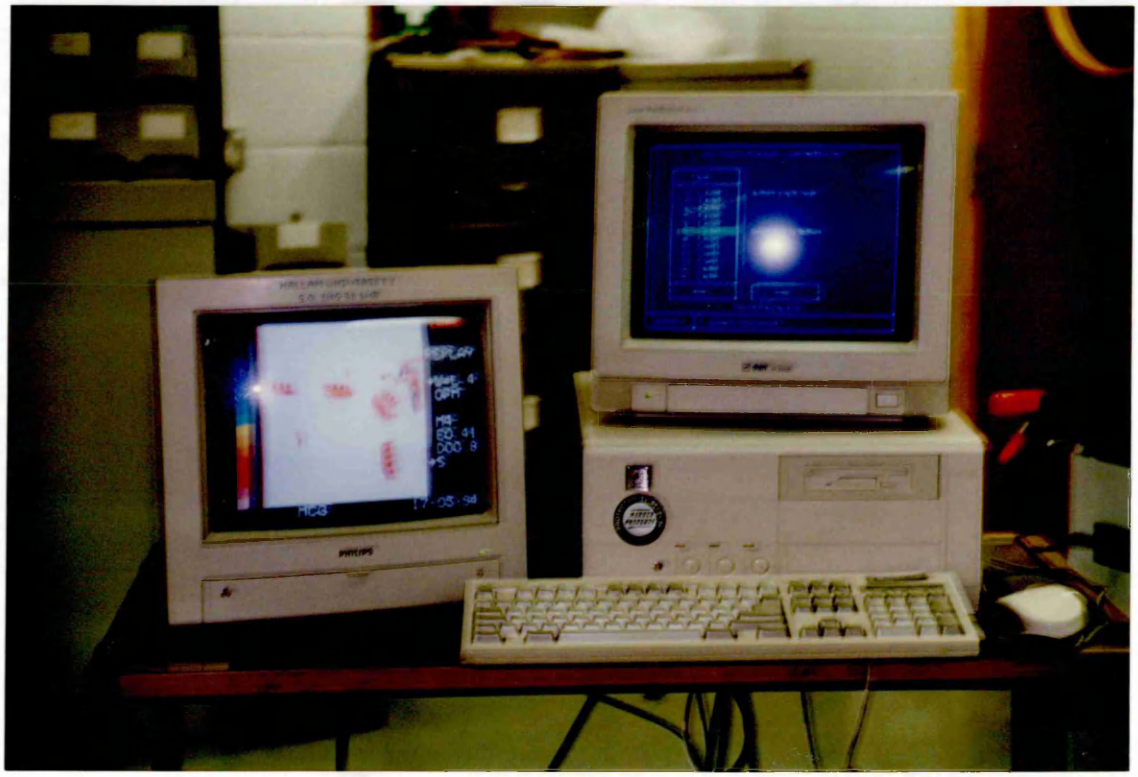

Figure 3.3.3.2[@] The emissivity measurement at 90 °C

Figure 3.3.3.3[@] The temperature profile in the bottom side of the closure measured by thermal image system

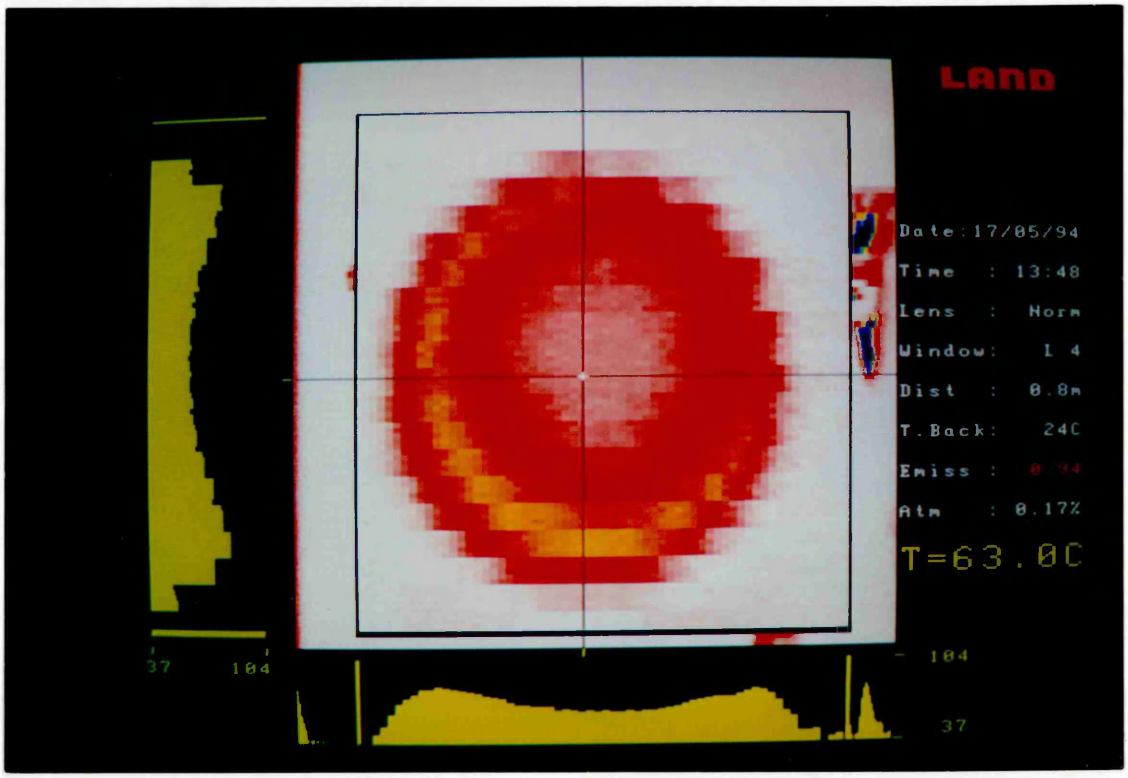

Figure 3.3.3.4[@] The temperature profile in the bottom side of the closure measured by thermal image system

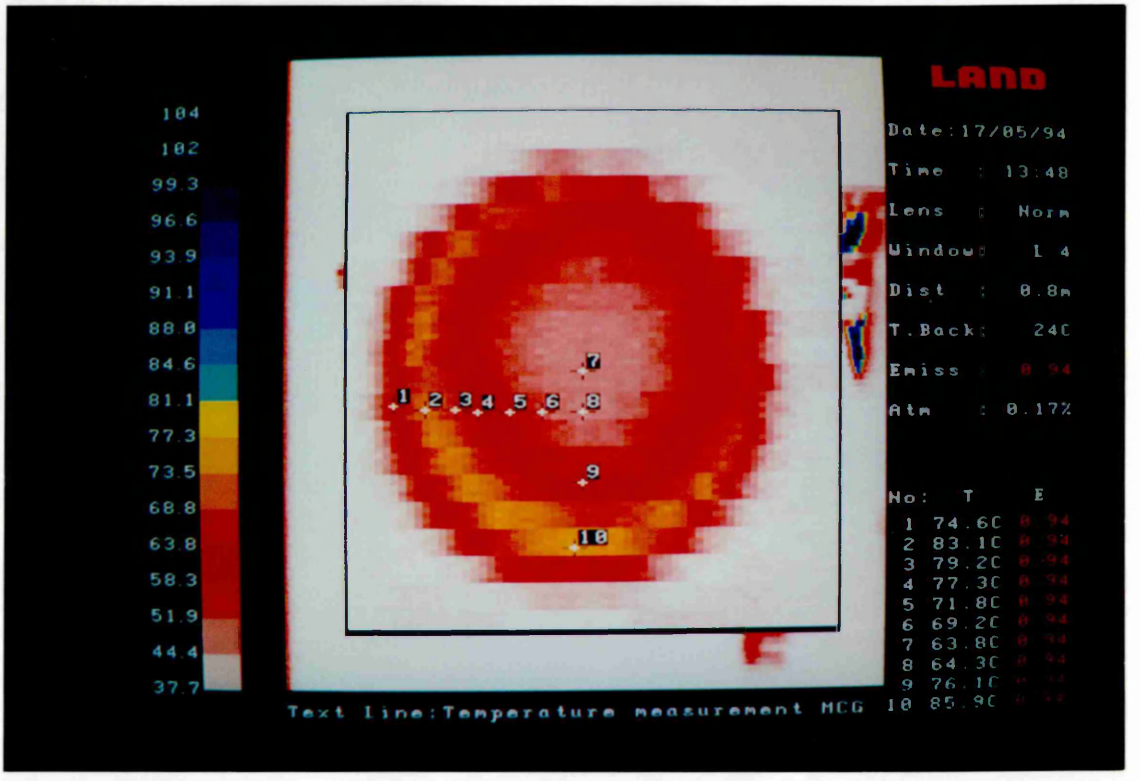

Figure 3.3.3.5[@] The temperature profile in the continuous thread side of the closure measured by thermal image system

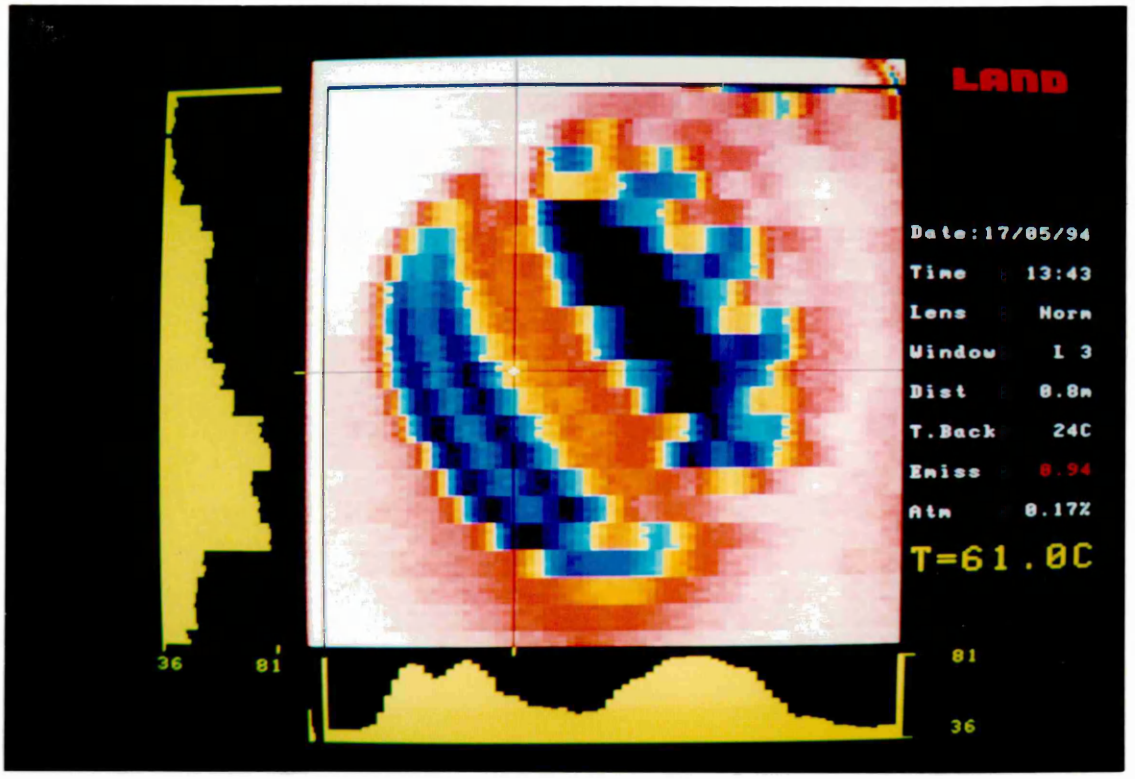

Figure 3.3.3.6[@] The temperature profile in the interrupted thread side of the closure measured by thermal image system

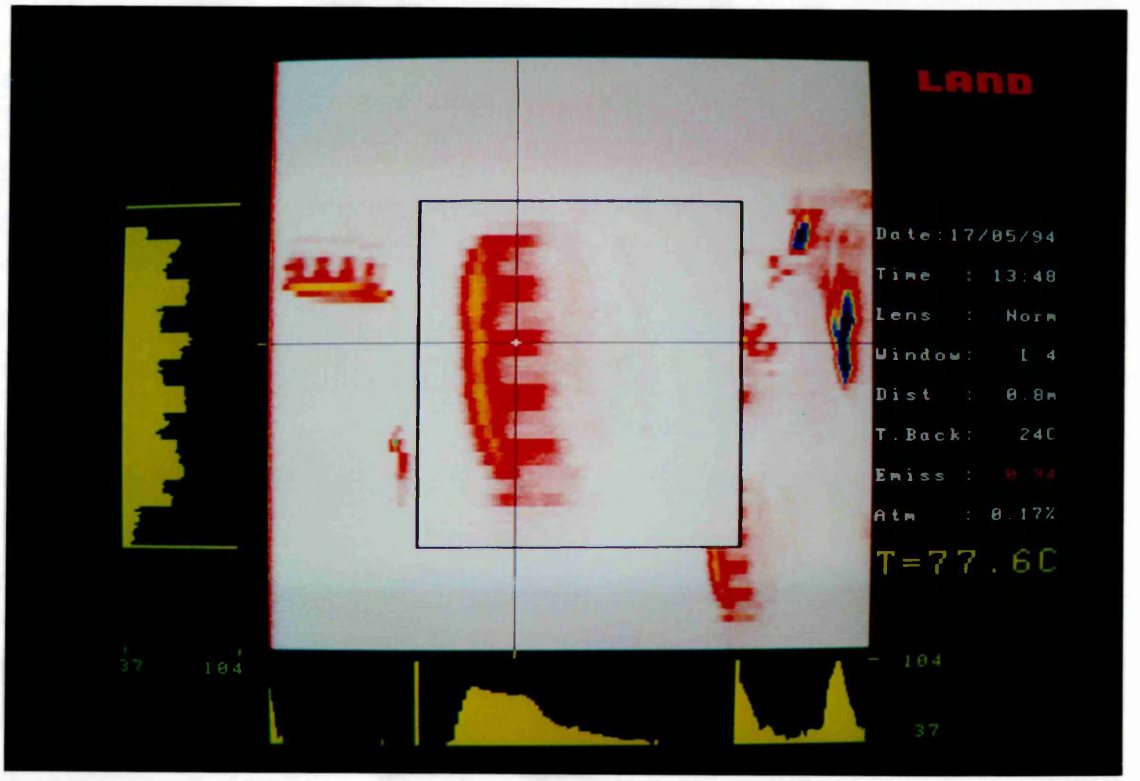

Figure 3.4.2.2[@] Cam mounted strain gauges

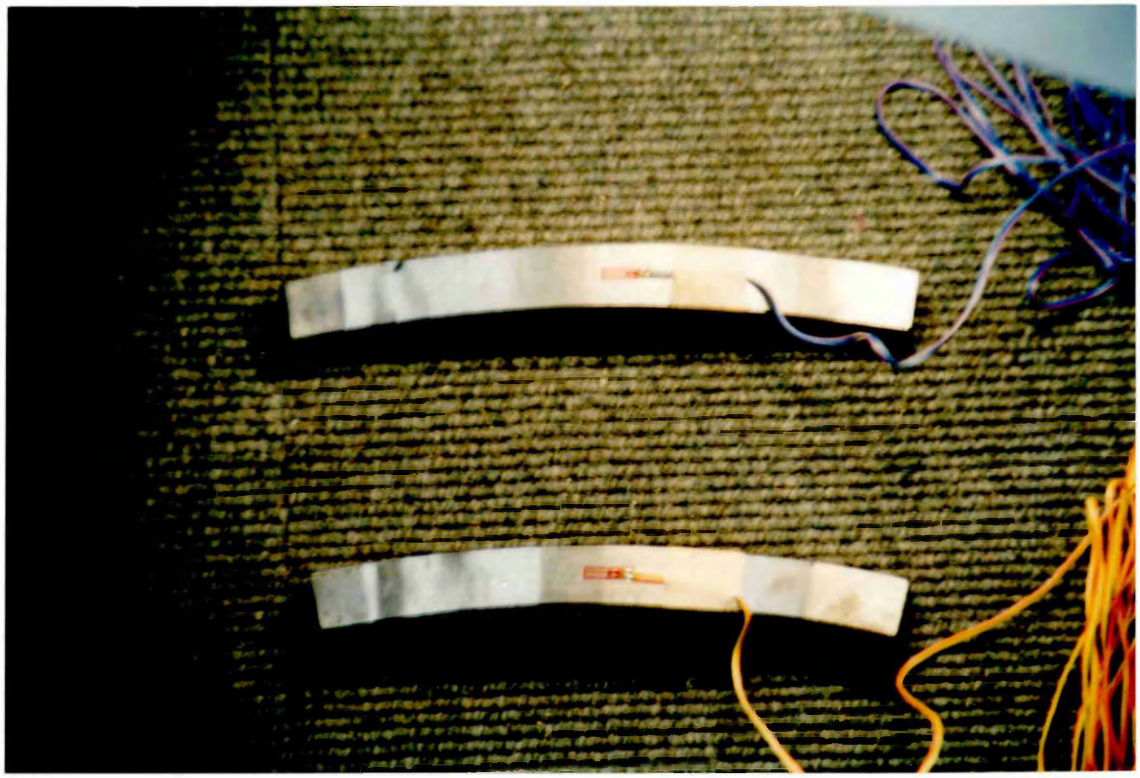

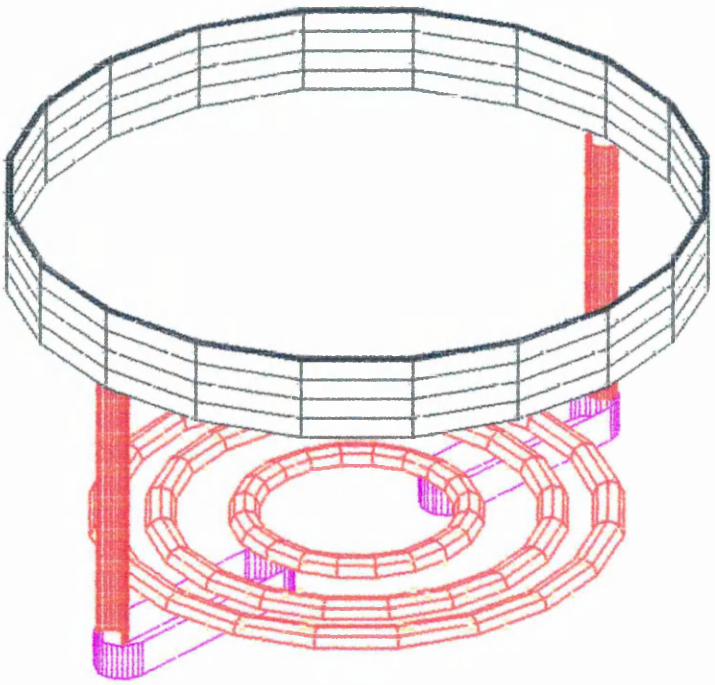

Fig 3.3.4.1 Cooling channels in the cavity of the mould

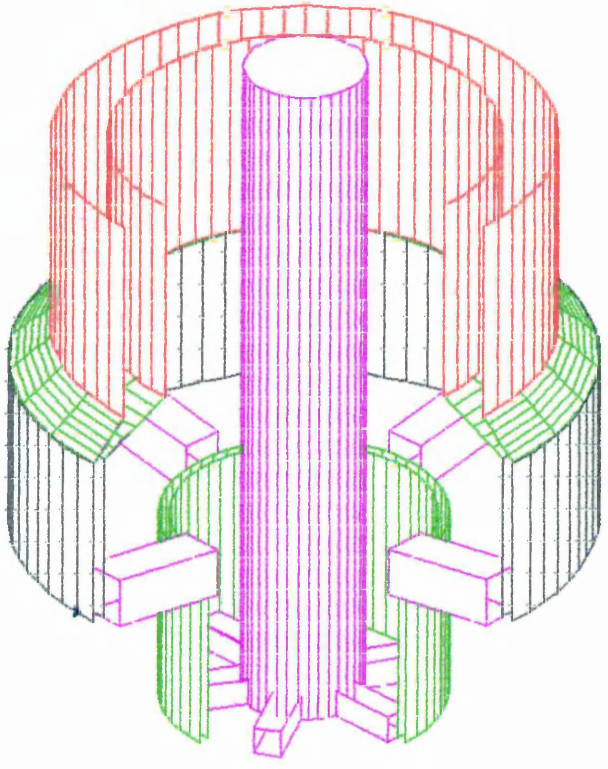

Fig 3.3.4.2 Cooling channel in the pin of the mould

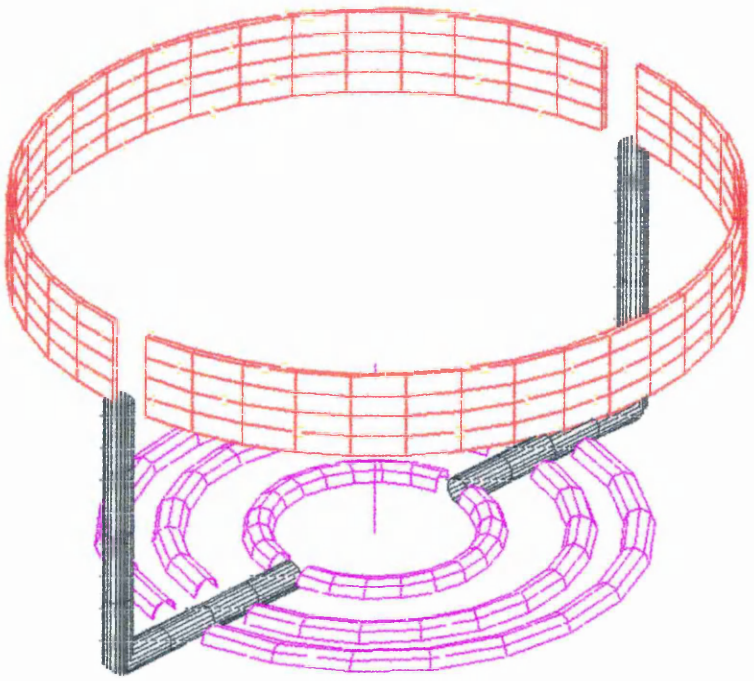

Fig 3.3.4.3 Cooling channel simulation in the cavity of the mould

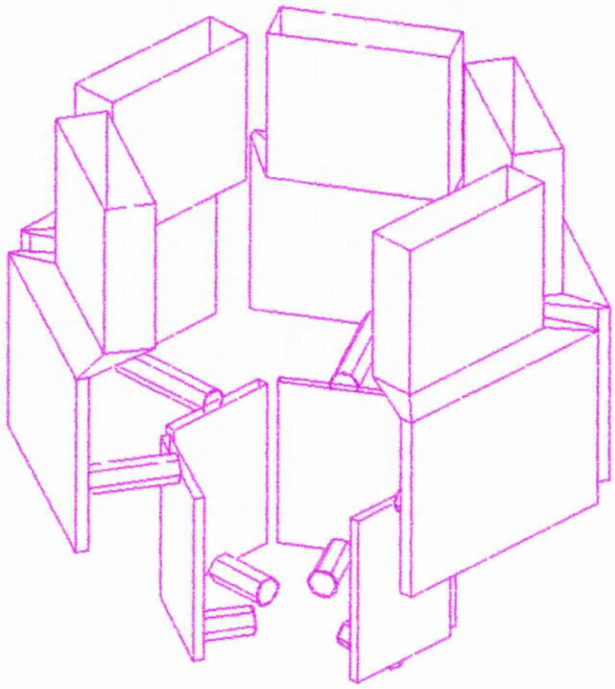

Fig 3.3.4.4 Cooling channel simulation in the pin of the mould

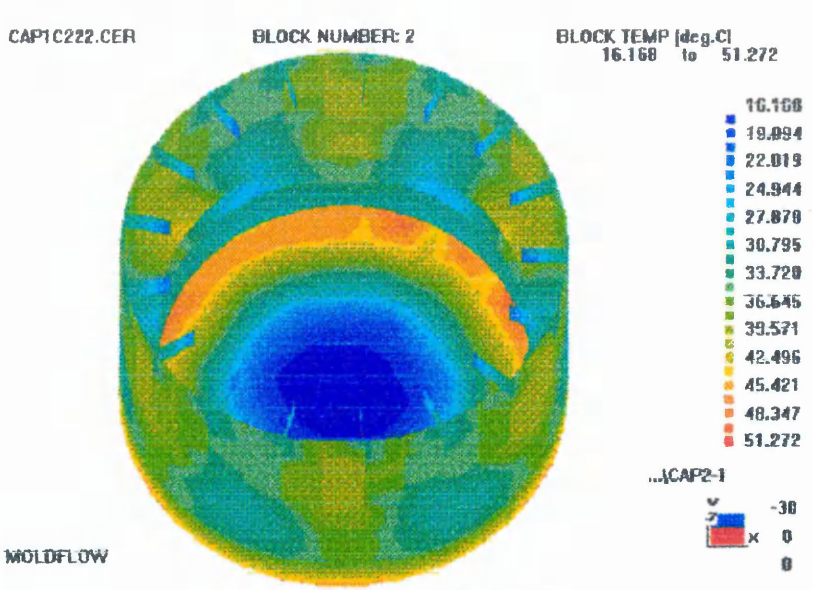

a. Temperature in pin side

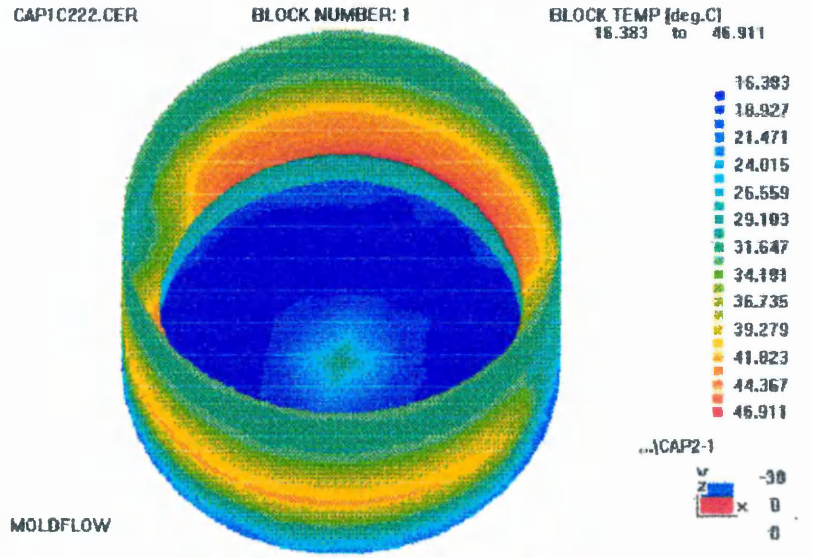

b. Temperature in cavity side

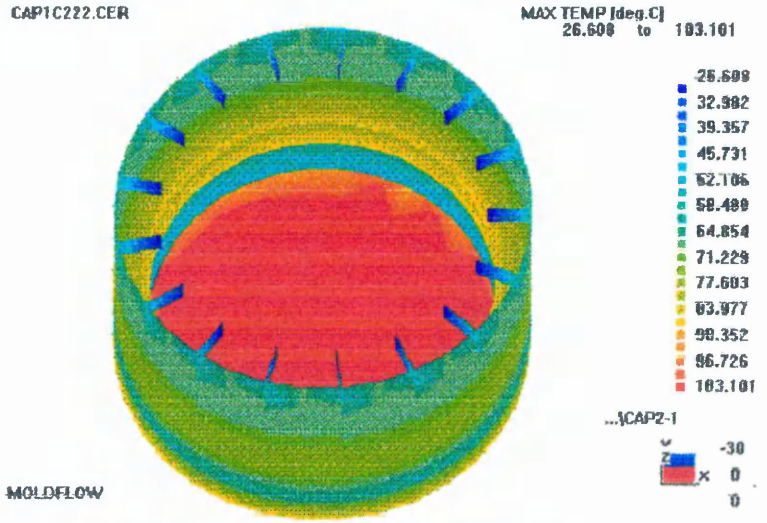

c. Maximum temperature in the middle of cross-section

Figure 3.3.4.5 Analysis in Moldflow suggested flow rate (minimum Re at 10,000)

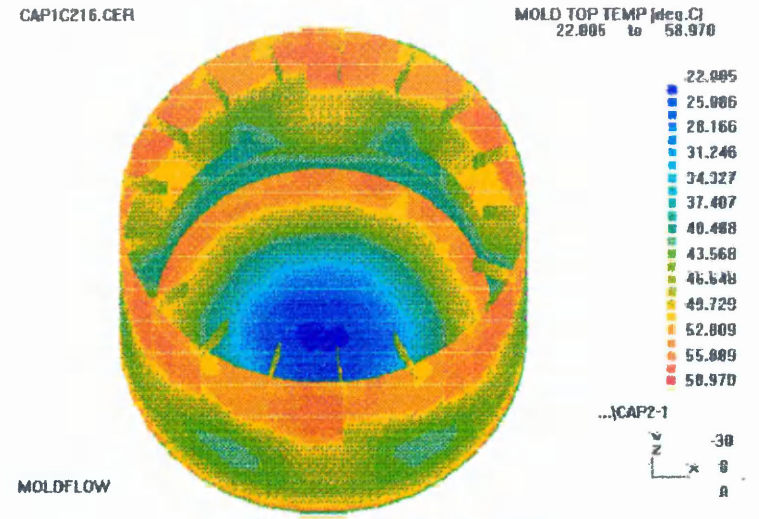

A. Temperature in pin side

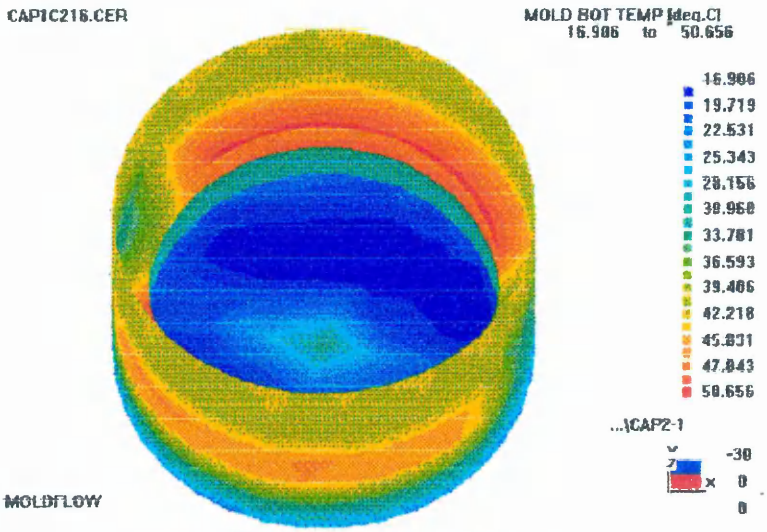

b. Temperatrue in cavity side

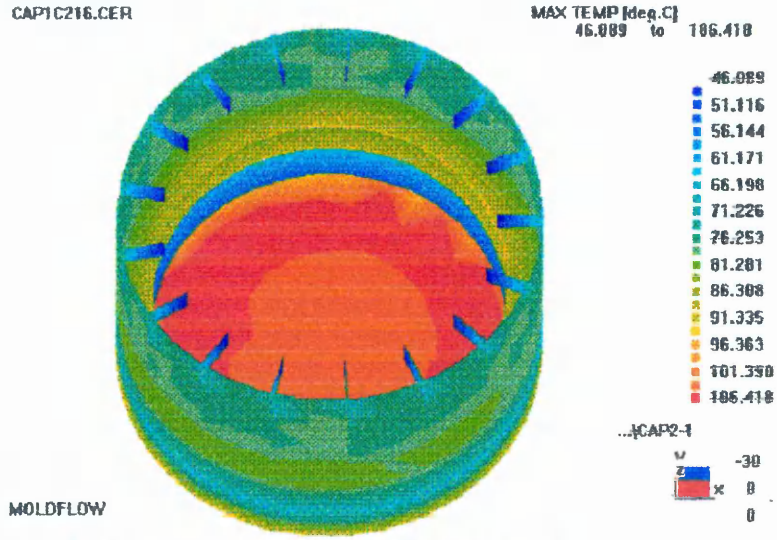

c. Maximum temperature in the middle of cross-section

Figure 3.3.4.6 Analysis in standard machine flow rate (1.26 l/min)

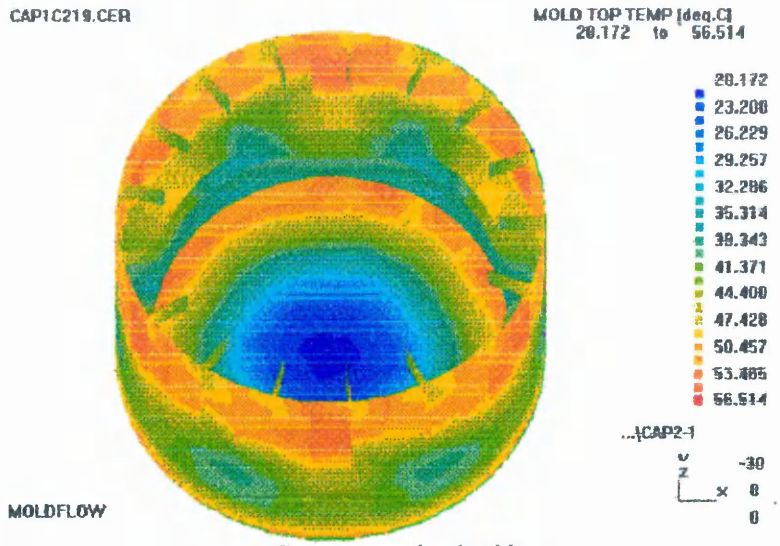

a. Temperature in pin side

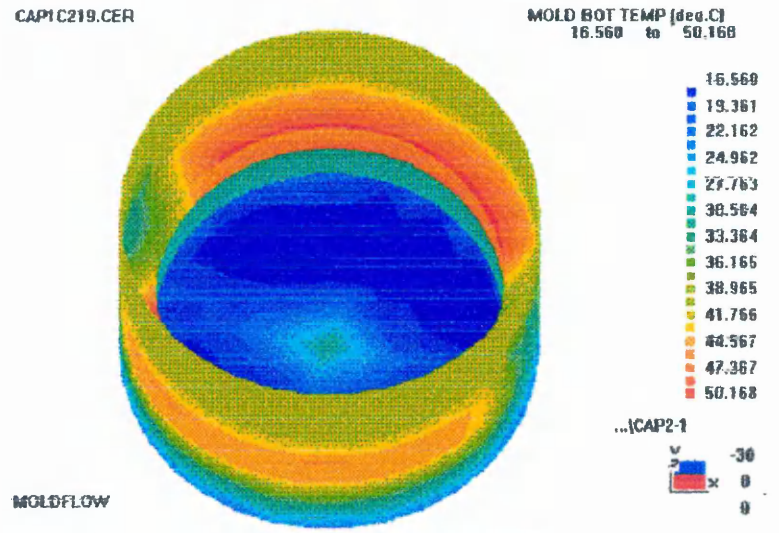

b. Temperature inn cavity side

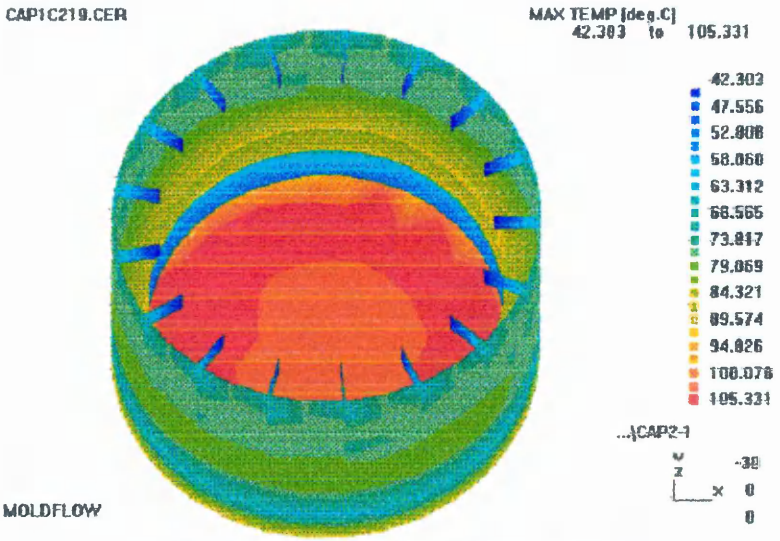

c. Maximum temperature in the cross-section

Figure 3.3.4.7 Analysis in maximum machine flow rate(1.575l/min in pin & 1.764 in cavity)

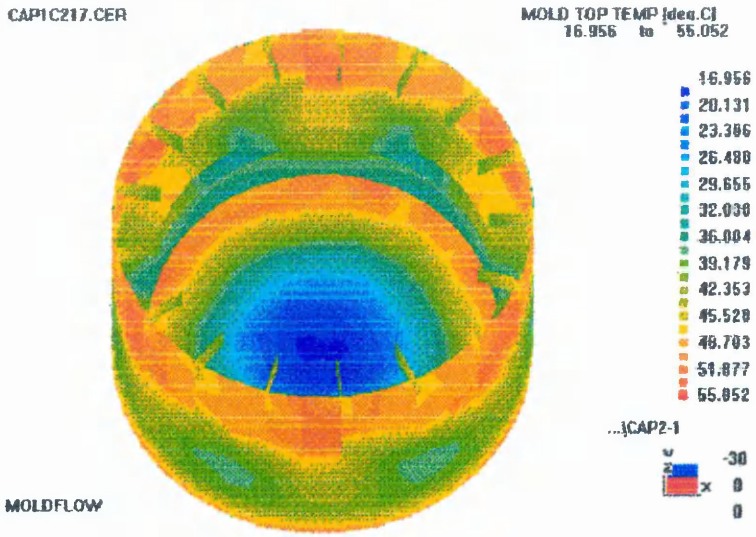

a. Temperature in pin side

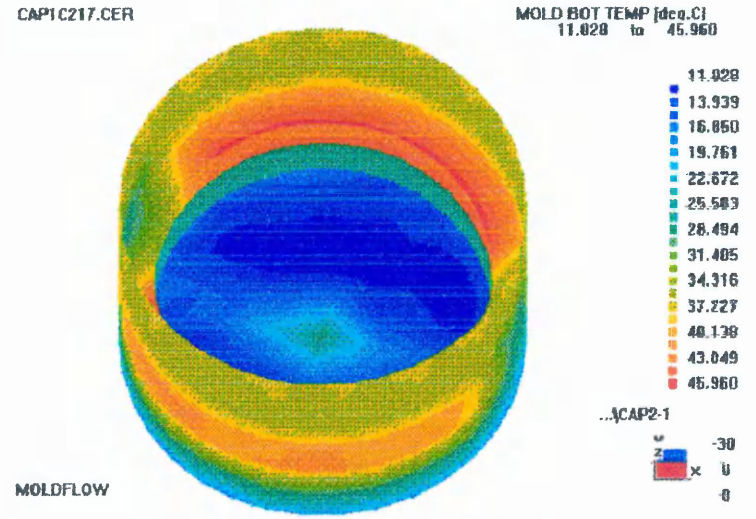

b. temperature in cavity side

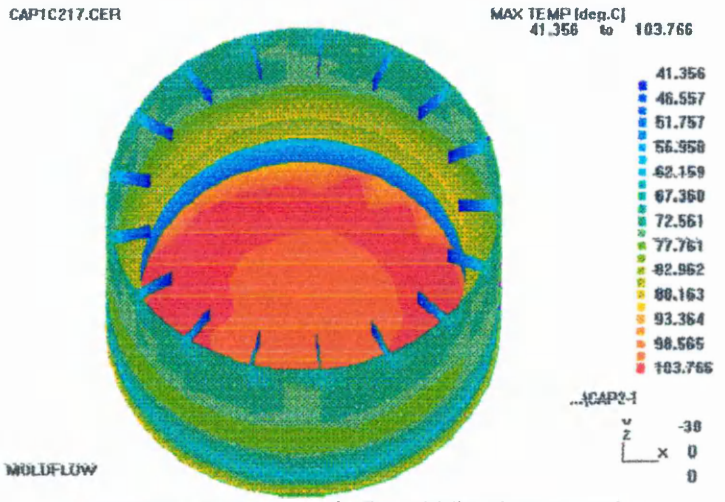

c. Maximum temperature in the middle of cross-section

Figure 3.3.4.8 Analysis in reduced inlet temperature to 10 °C & standard flow rate

(1.26l/min)

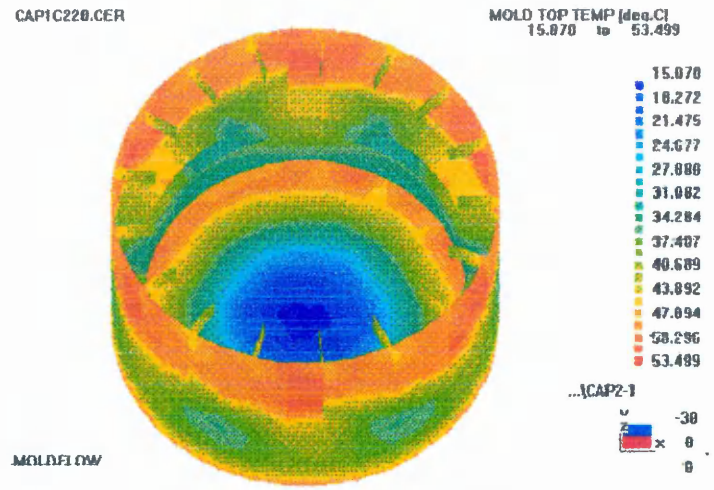

a. Temperature in pin side

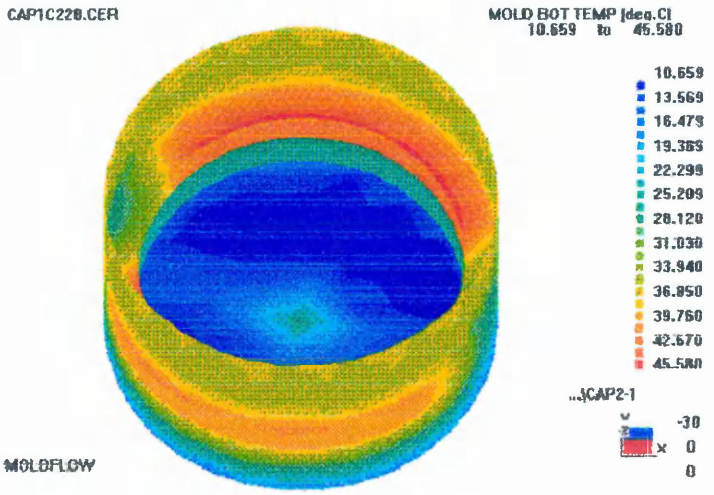

b. Temperature in cavity side

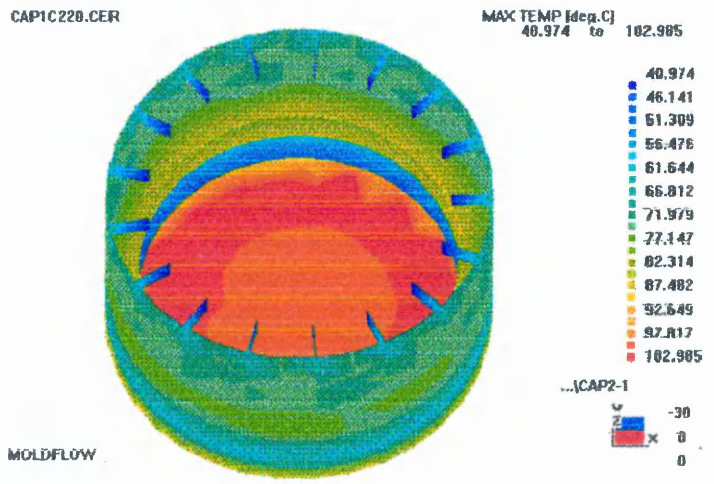

c. Maximum temperature in the middle of cross-section

Figure 3.3.4.9 Analysis in reduced inlet temperature to 10 °C & max. flow rate

(1.57l/min in pin & 1.76 in cavity)

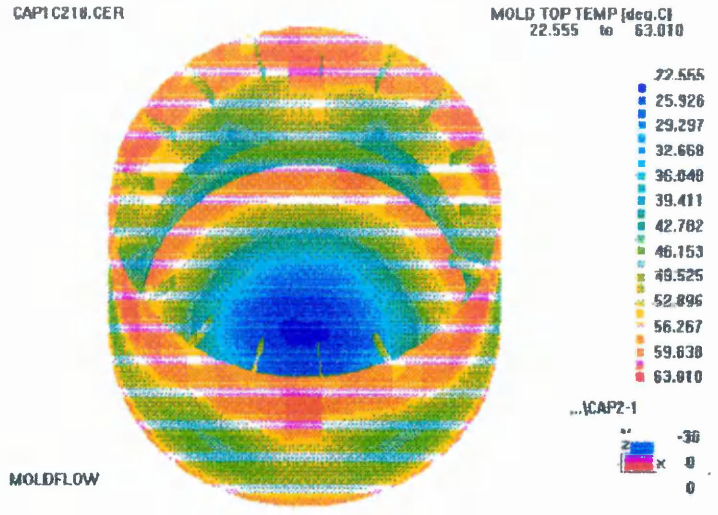

a. Temperature in pin side

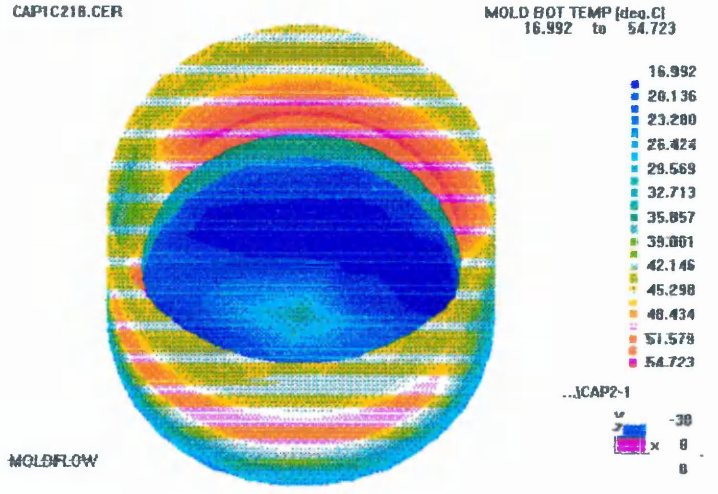

b. Temperature in cavity side

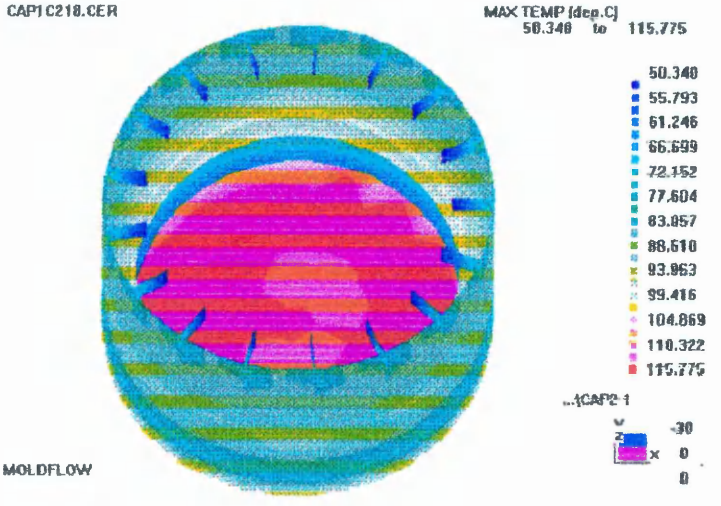

c. Maximum temperature in the middle of cross-section

Figure 3.3.4.10 Analysis in 4.5 sec cooling time and standard flow rate(1.26l/min)

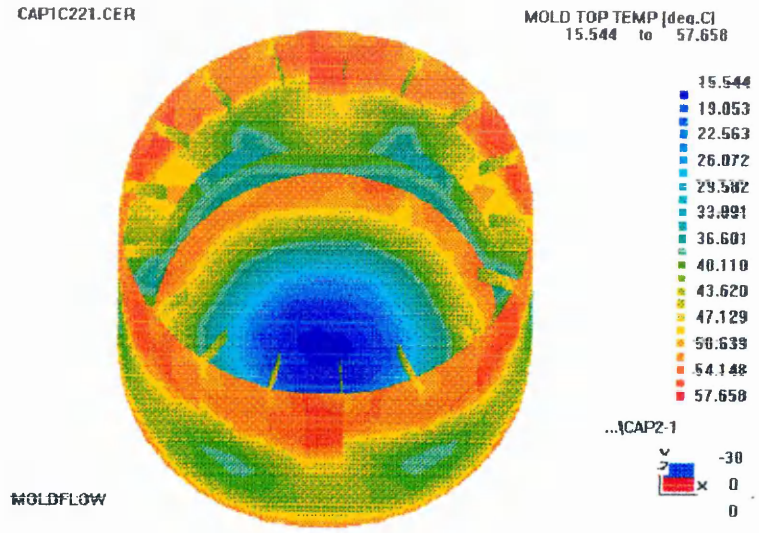

a. Temperature in pin side

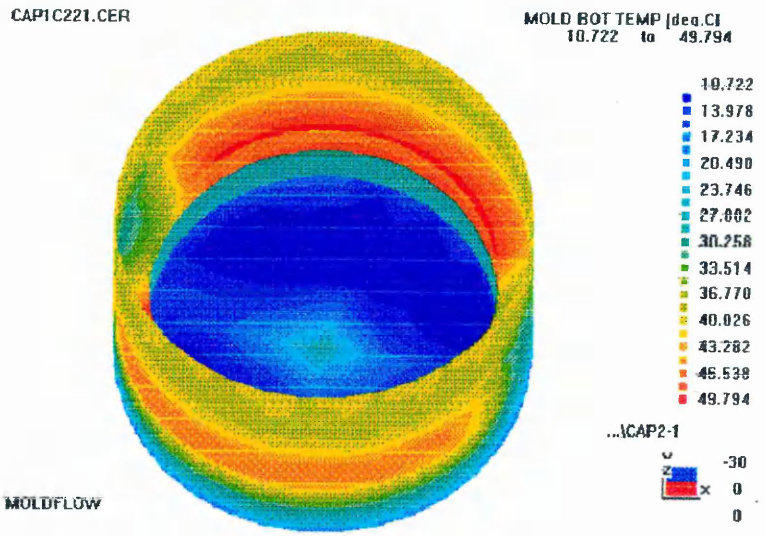

b. Temperature in cavity side

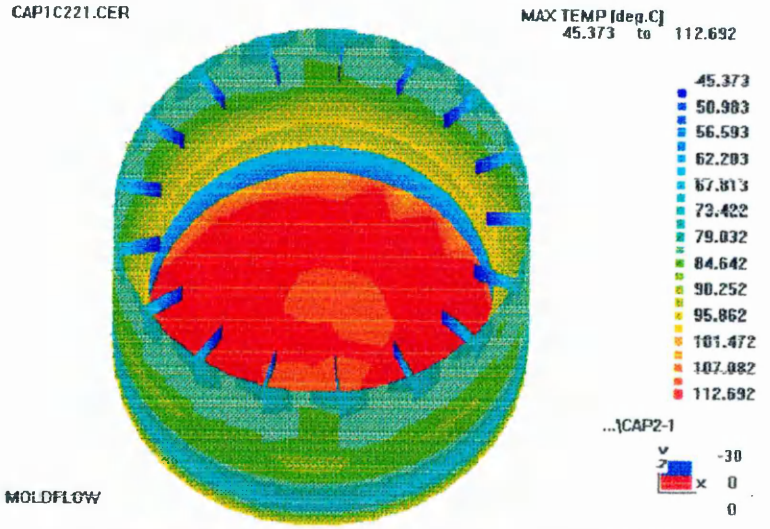

c. Maximum temperature in the middle of cross-section

Fig 3.3.4.11 Analysis in cooling maximum conditions

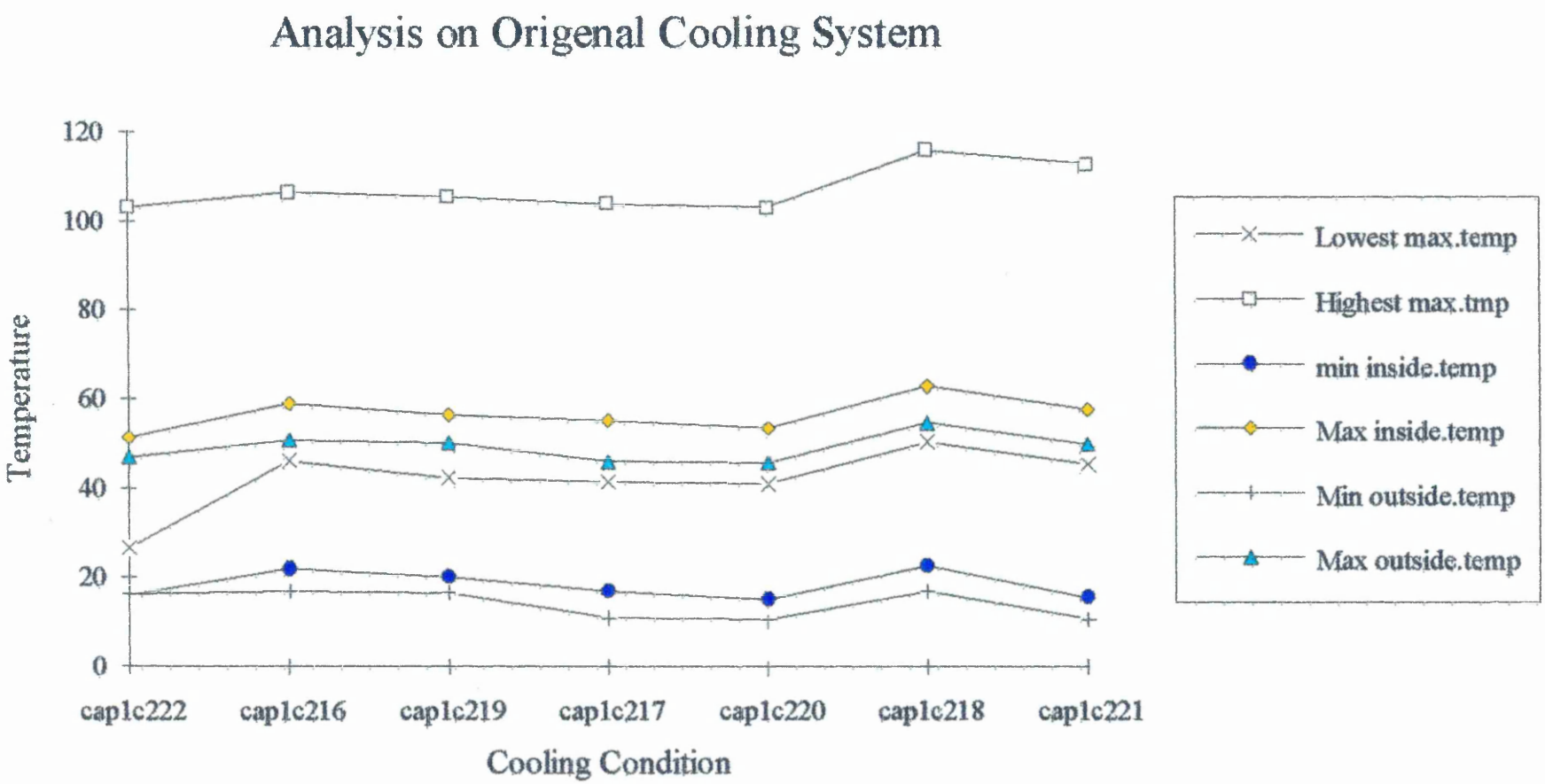

Figure 3.3.4.12 Summary chart for the cooling analysis results

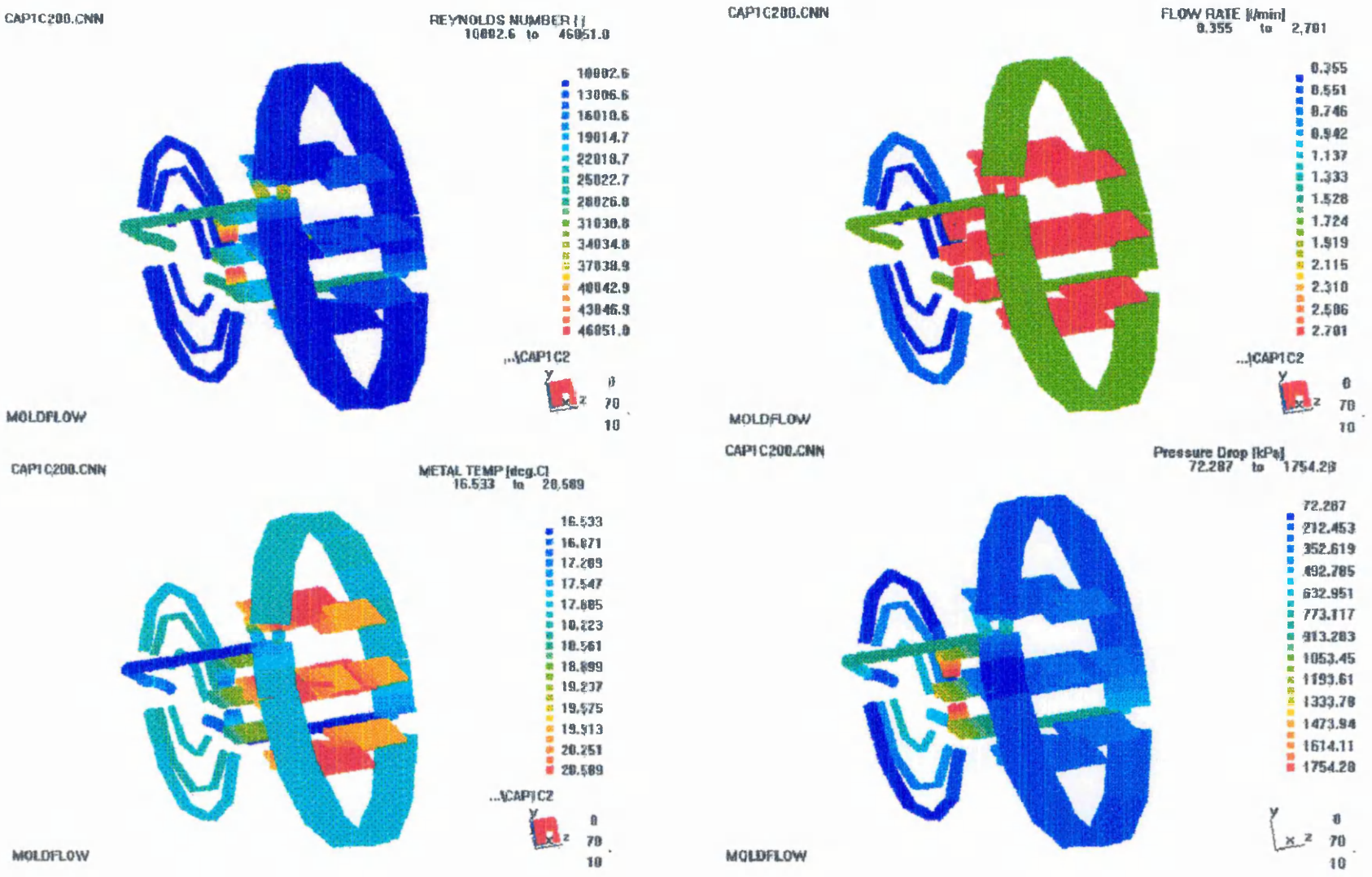

Figure 3.3.4.13 Analysis results for cooling channels at Moldflow assume flow rate

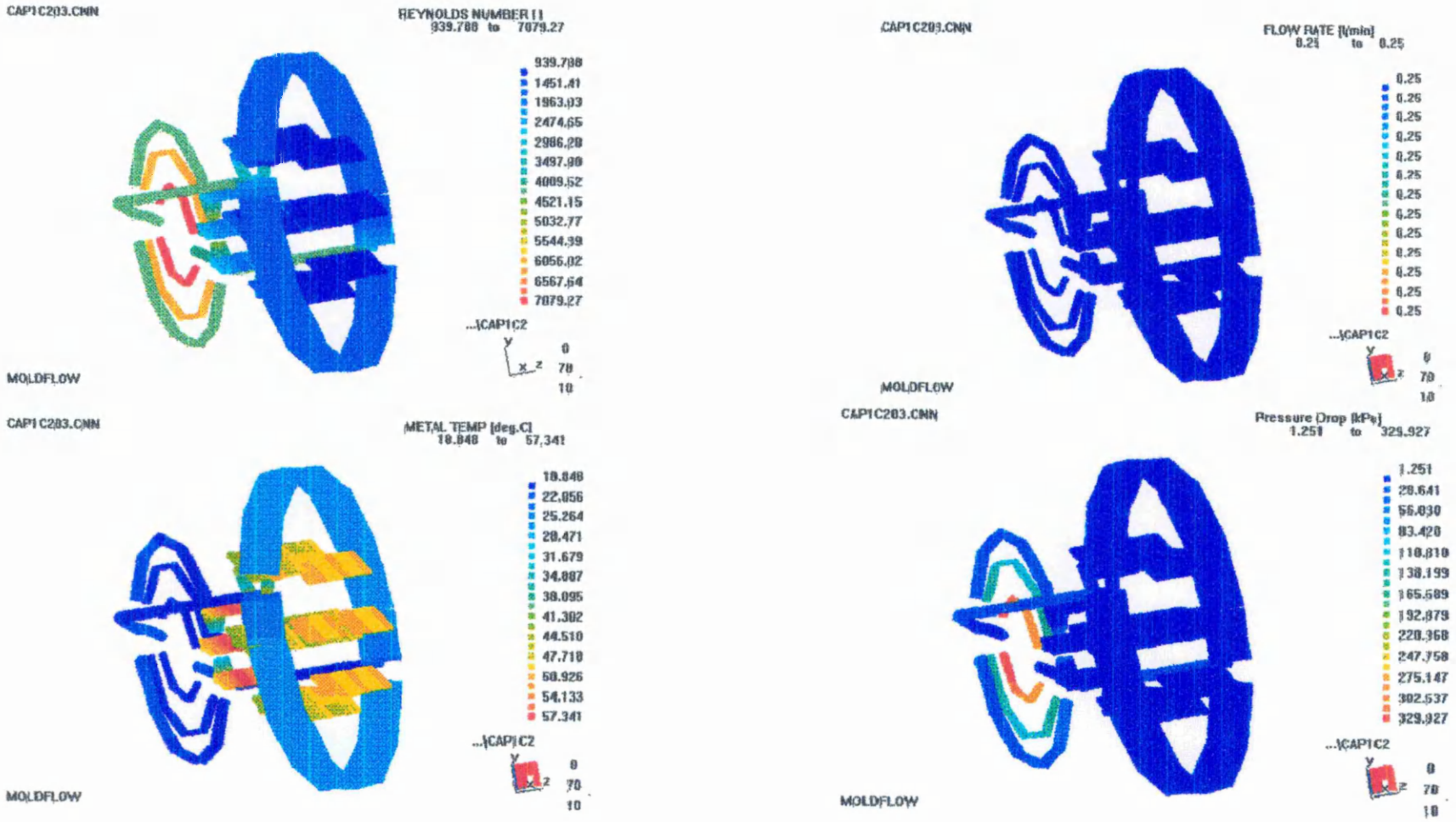

Figure 3.3.4.14 Analysis results for cooling channels at machine standard flow rate

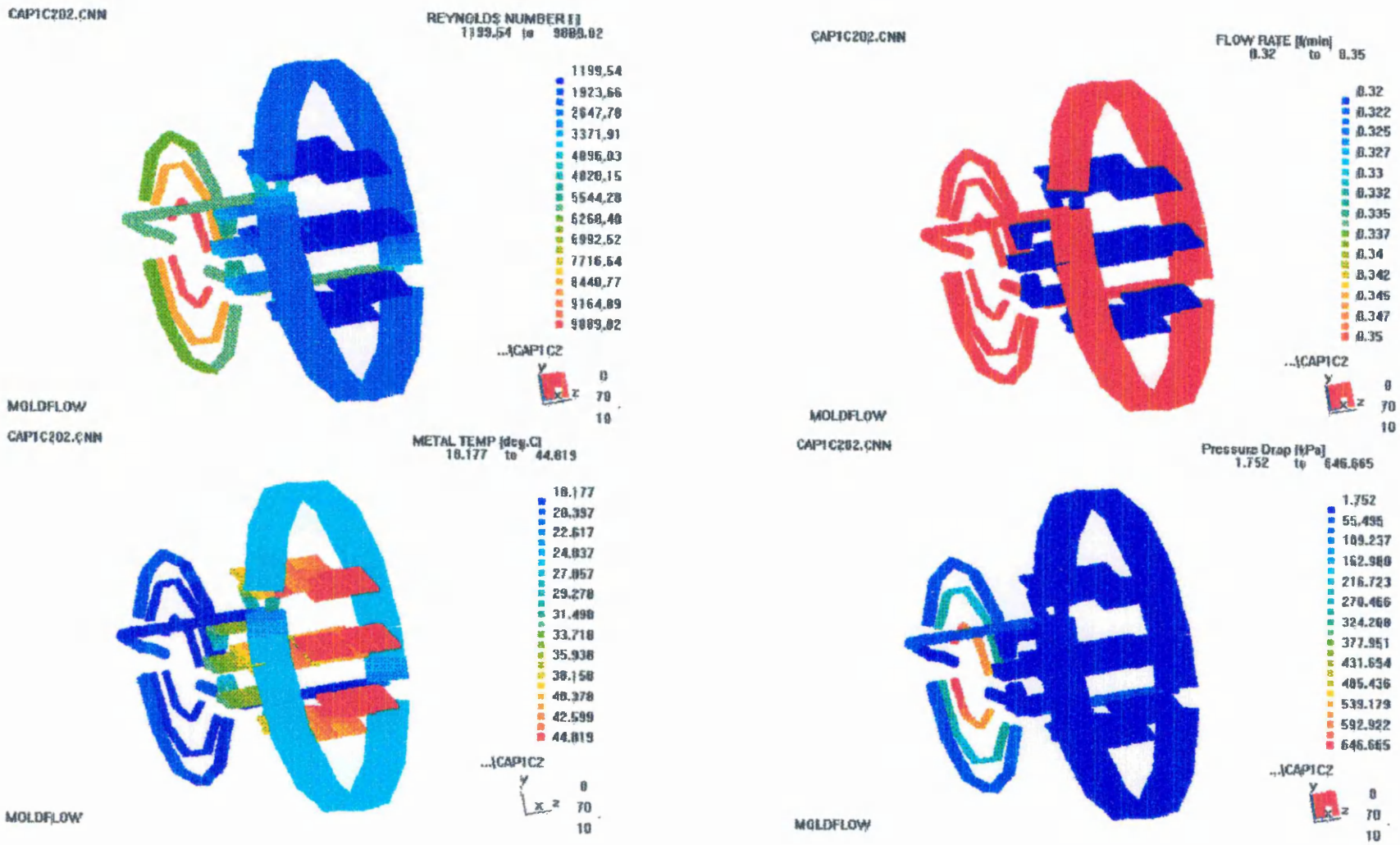

Figure 3.3.4.15 Analysis results for cooling channels at machine maximum flow rate

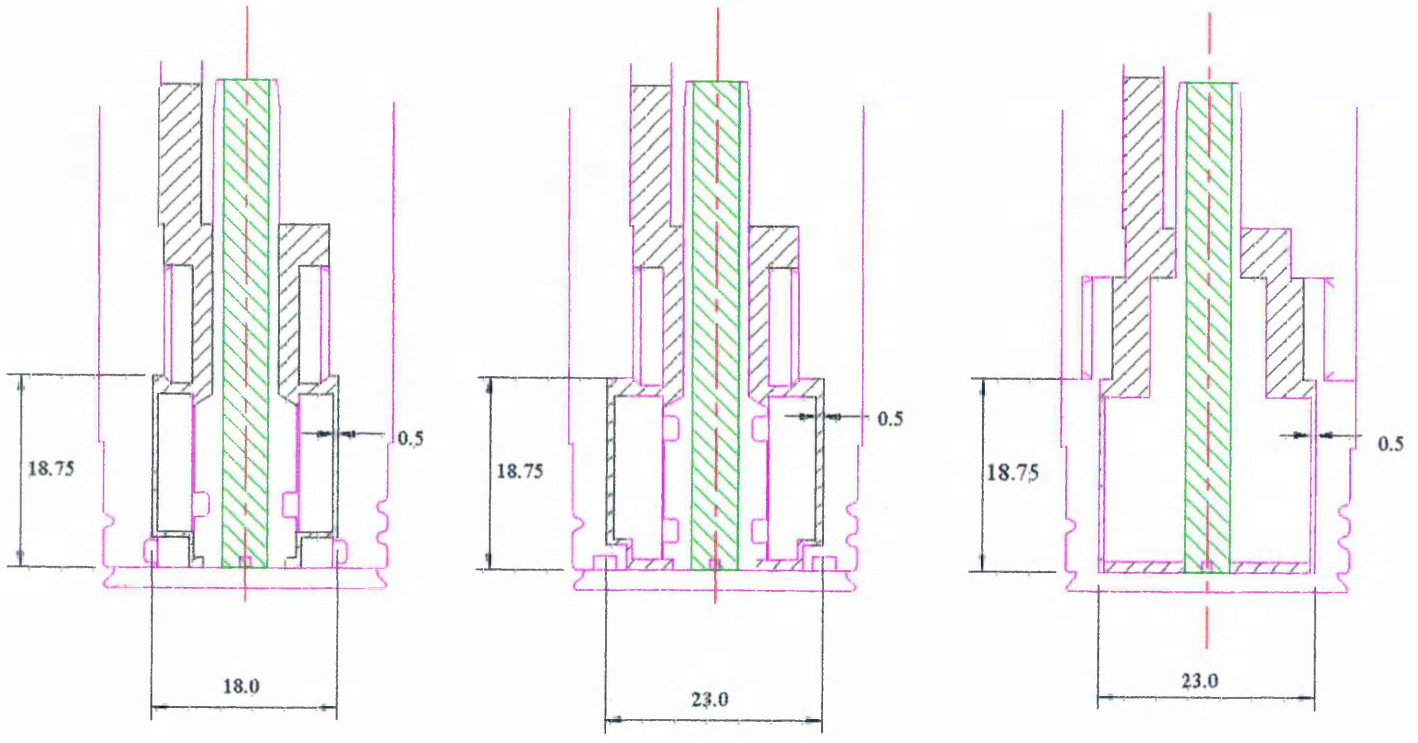

Origenal Cooling Channel in Pin New Design A New Design B

Fig 3.3.4.16 The structure of the pin cooling system for original design, design A and design B

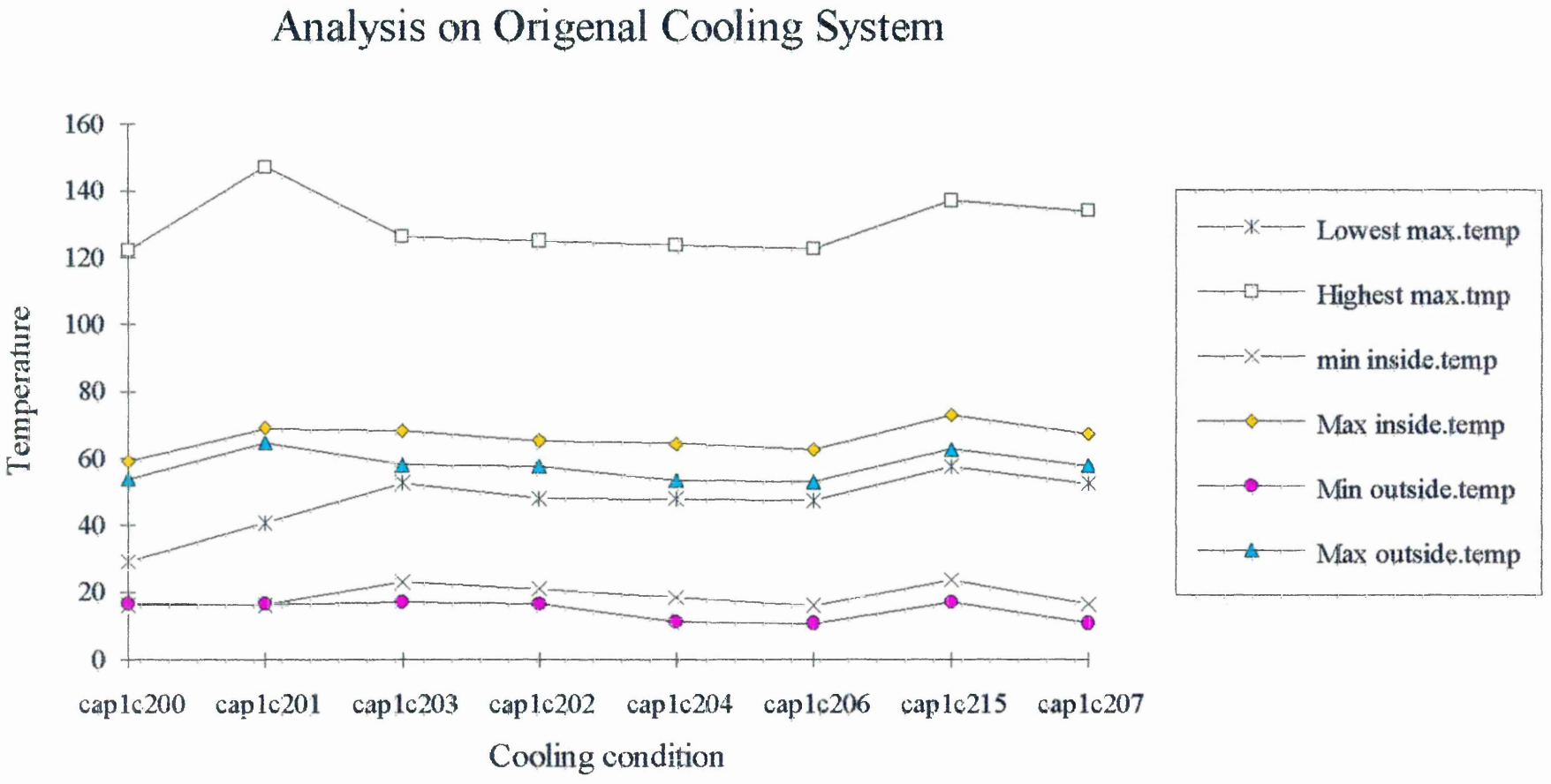

Figure 3.3.4.17 Analysis on original cooling system

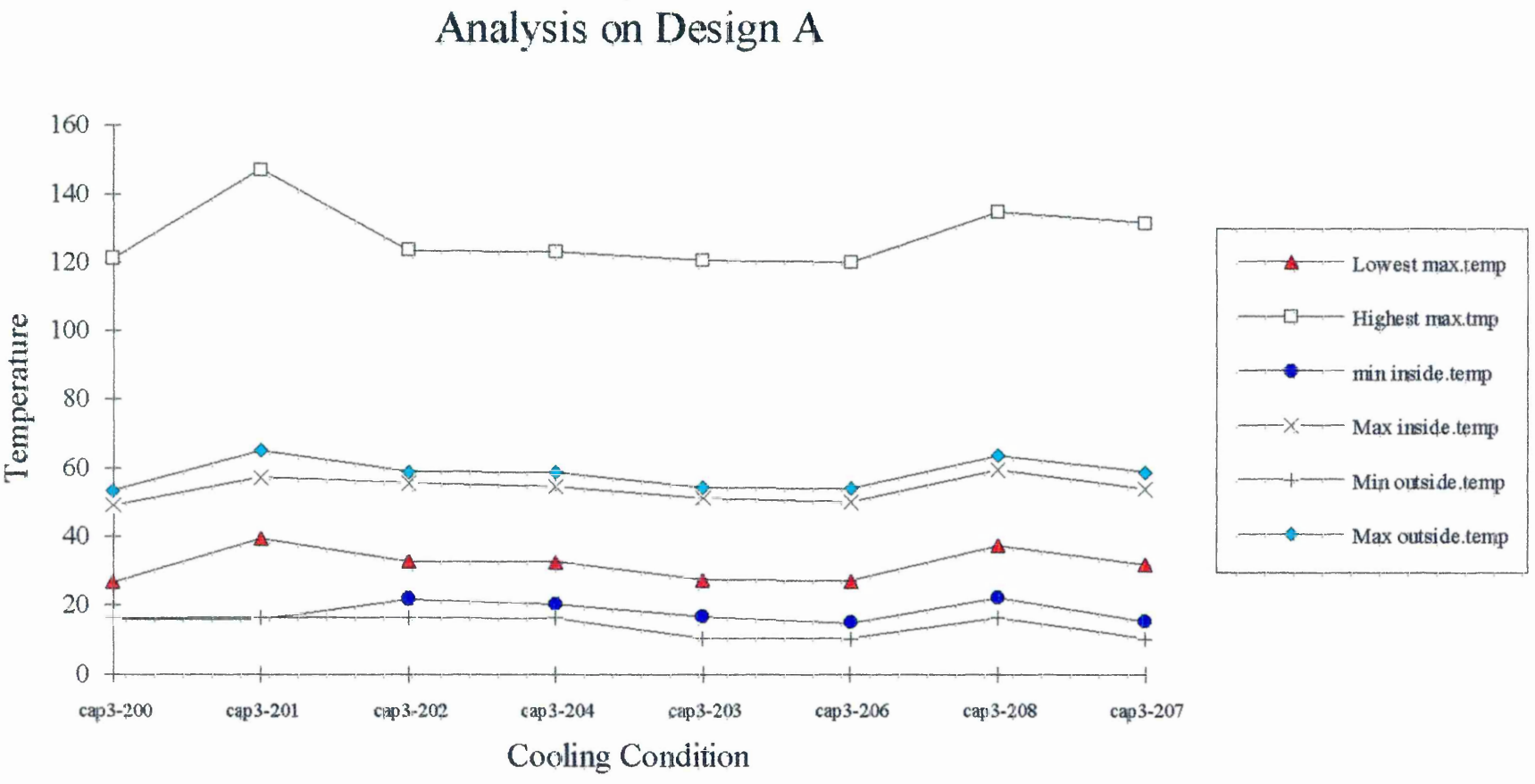

Figure 3.3.4.18 Analysis on new design A cooling system

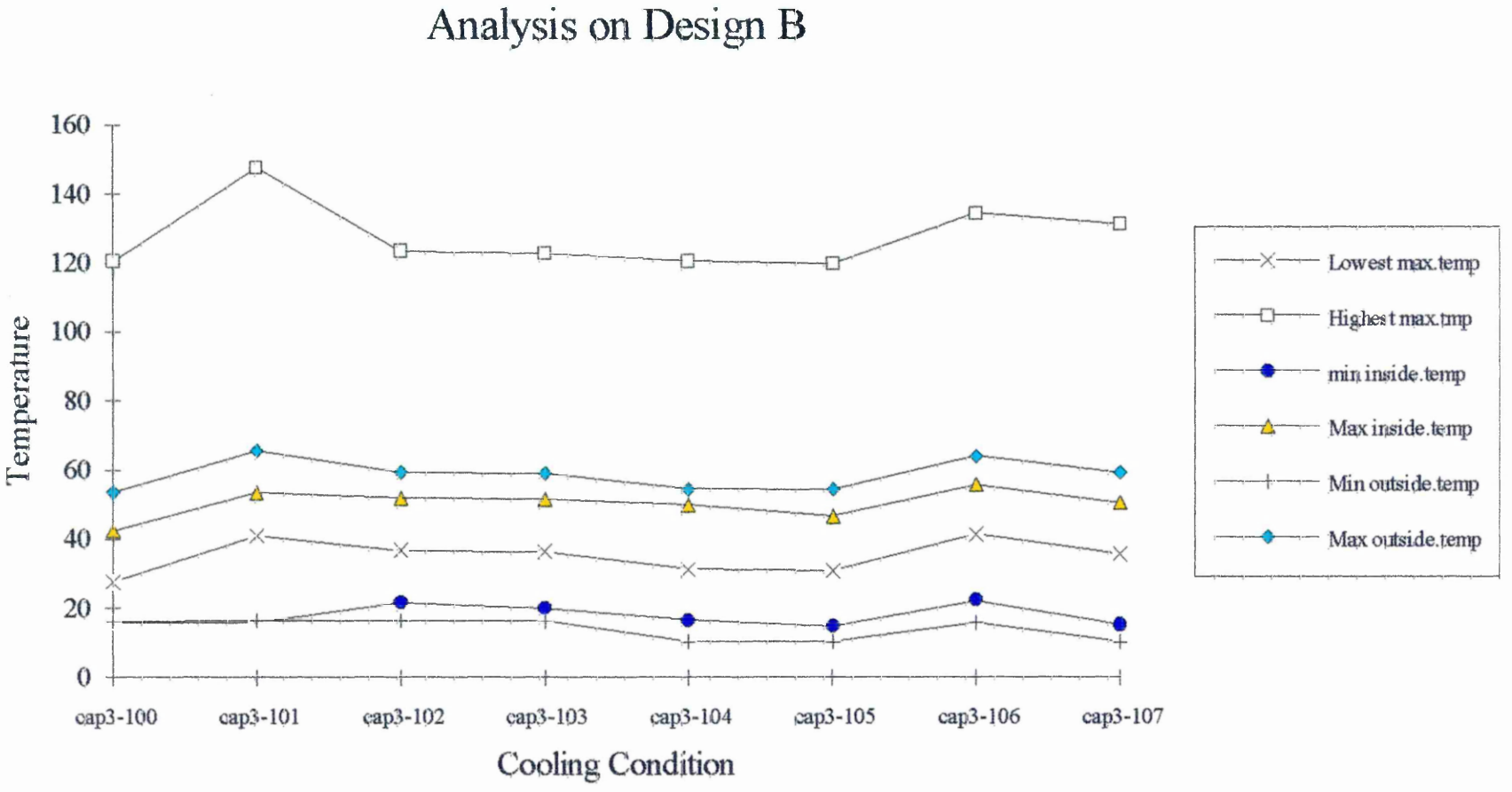

Figure 3.3.4.19 Analysis on new design B cooling system

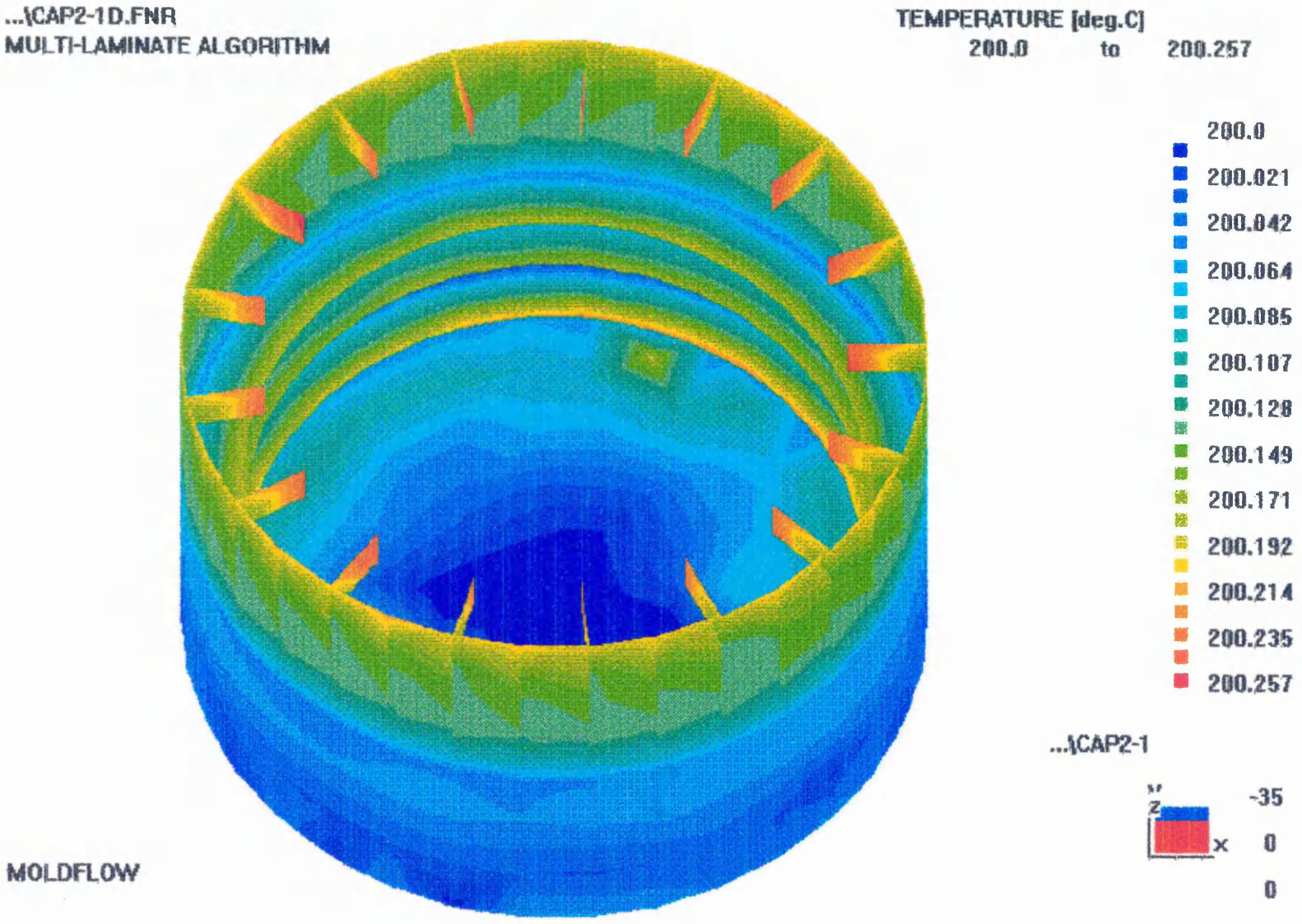

Figure 3.3.4.20 The temperature distribution of the filling analysis (cap2-1d, at 540 caps/min)

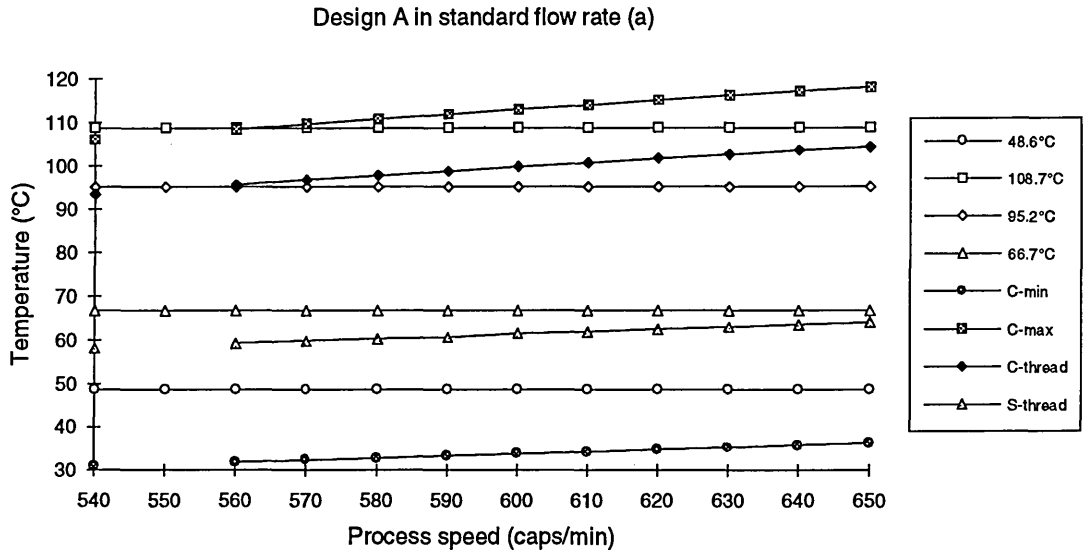

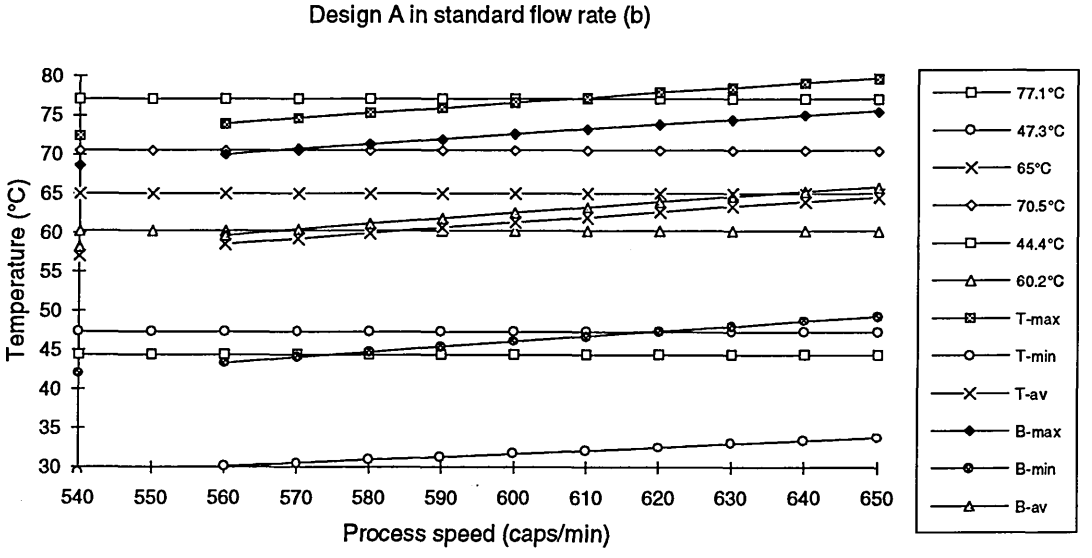

Figure 3.3.4.21 The temperature trend of design A in standard flow rate

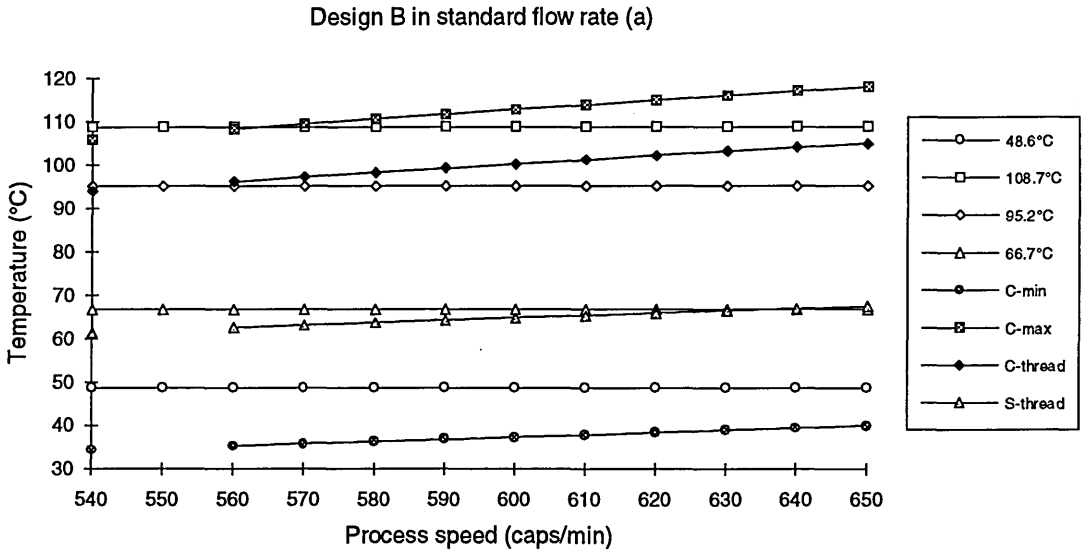

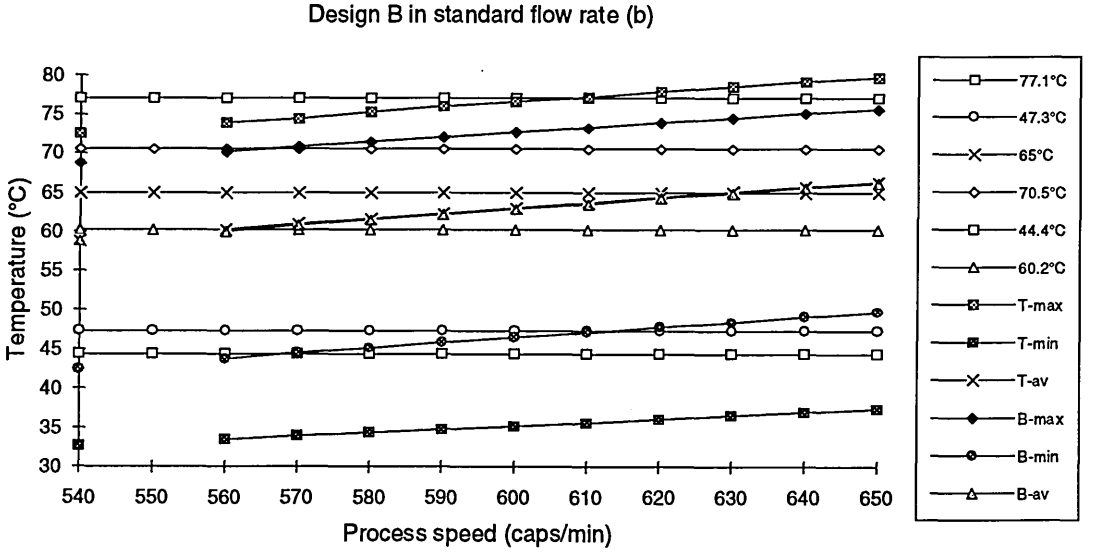

Figure 3.3.4.22 The temperature trend of design B in standard flow rate

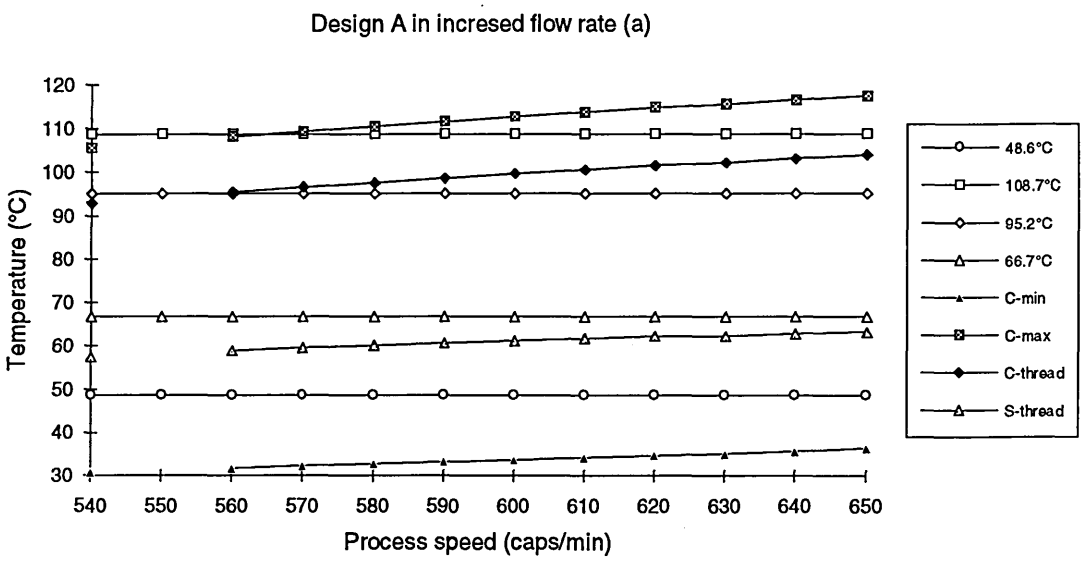

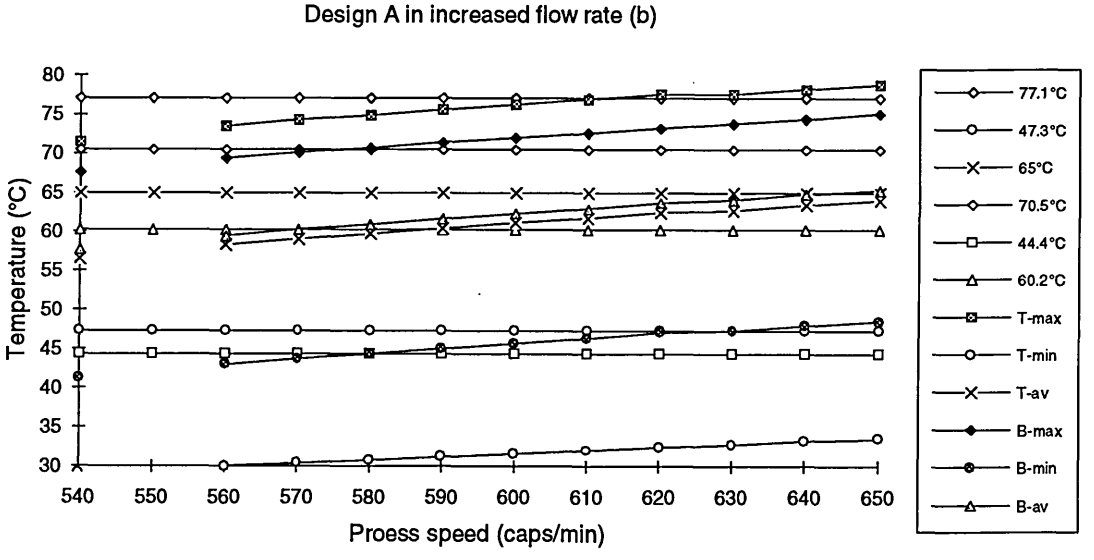

Figure 3.3.4.23 The temperature trend of design A in increased flow rate

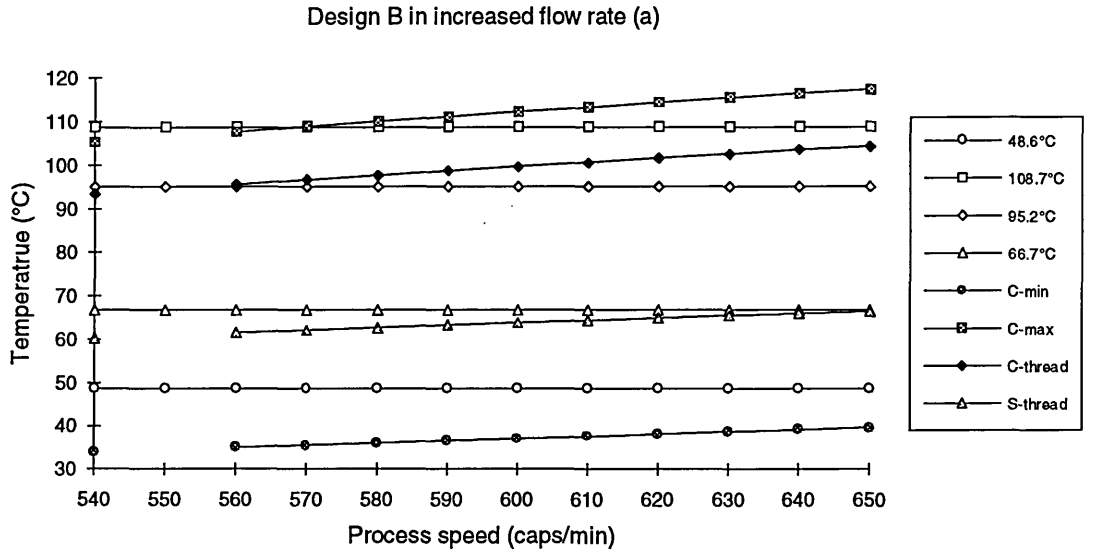

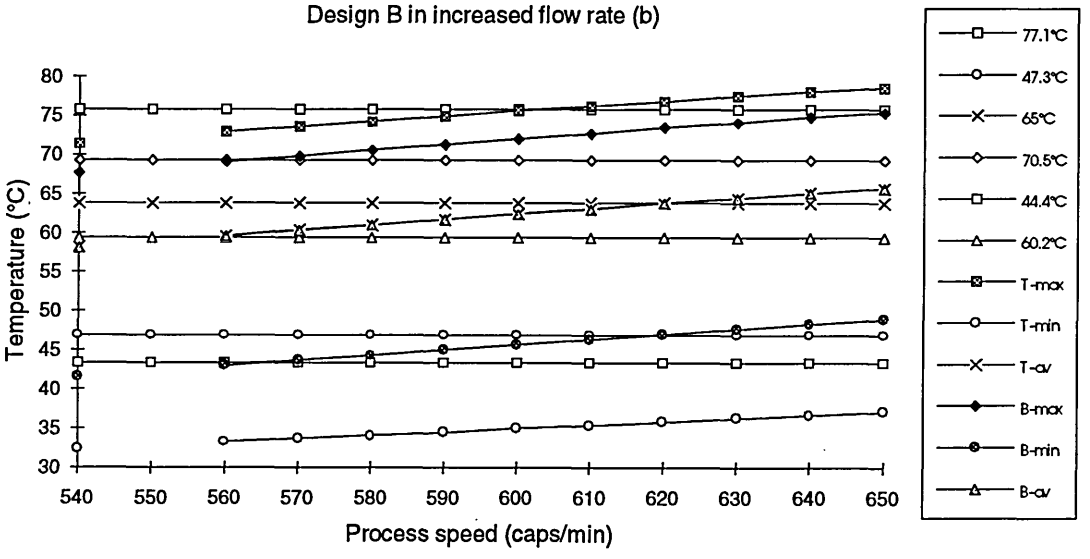

Figure 3.3.4.24 The temperature trend of design B in increased flow rate

Figure 3.4.2.3@ Standard varied loads acted on the top surface of the cam

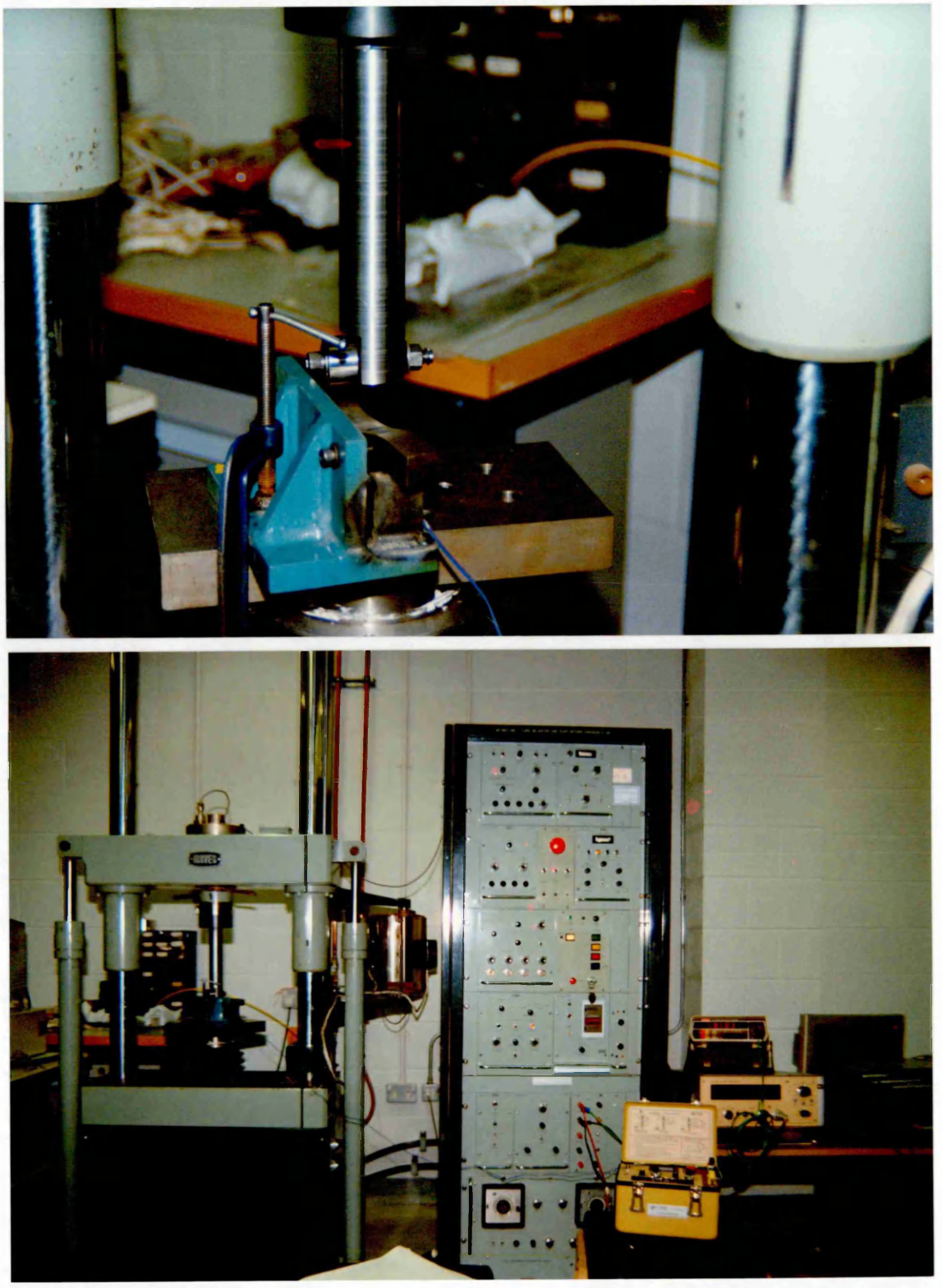

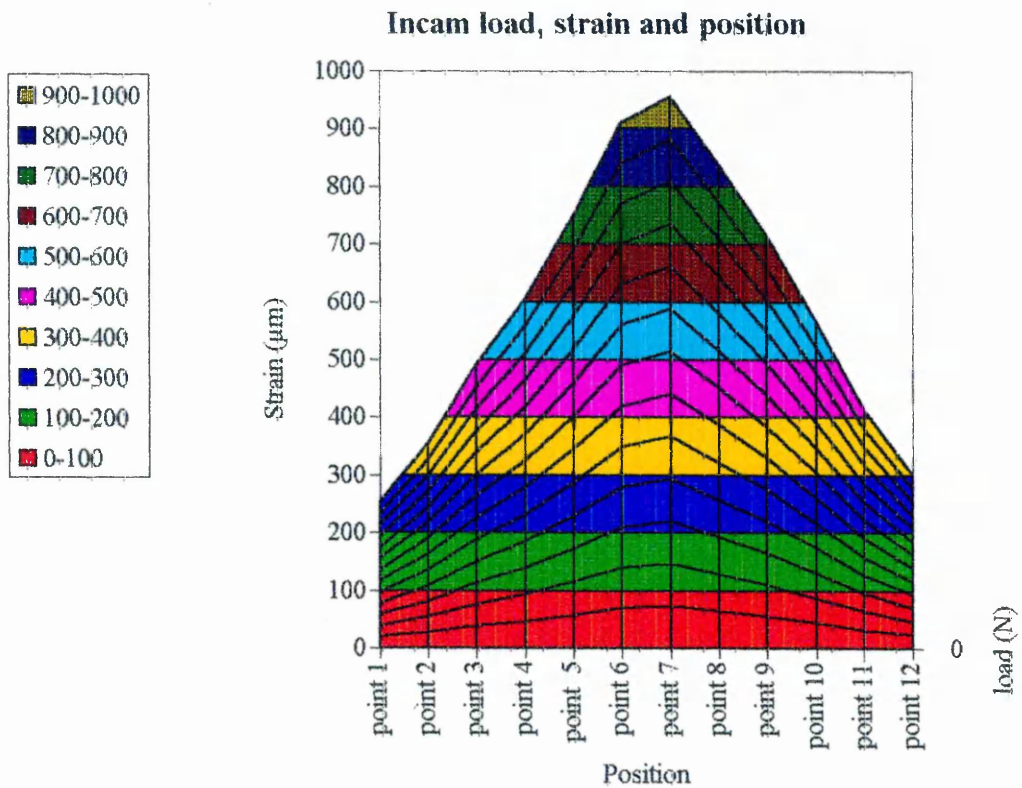

Figure 3.4.2.4 The results of the measurement of relationship between the load, strain and position for inside cam

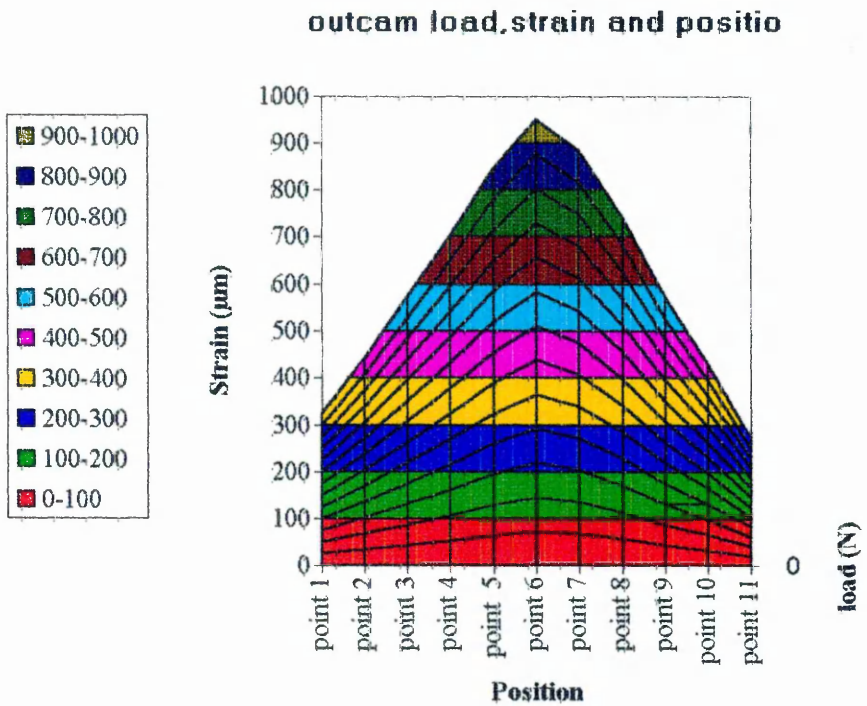

Figure 3.4.2.5 The results of the measurement of relationship between the load, strain and position for outside cam

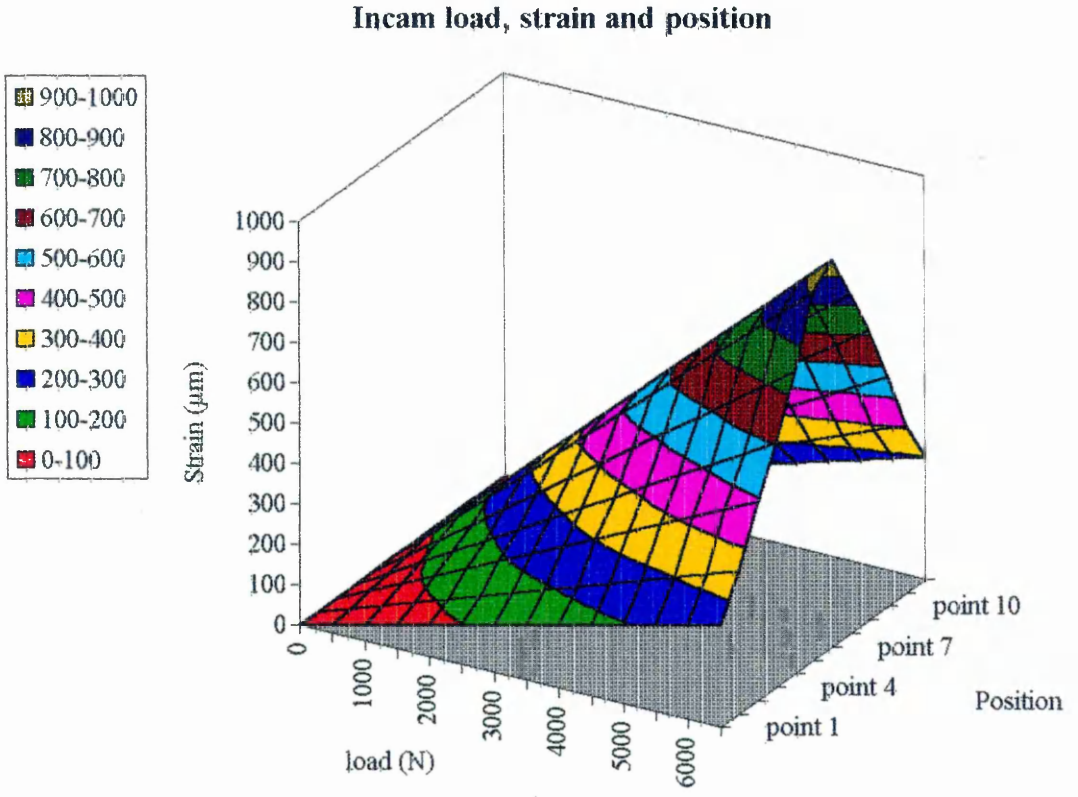

Figure 3.4.2.6 The 3D figure of the measurement of relationship between the load, strain and position for inside cam

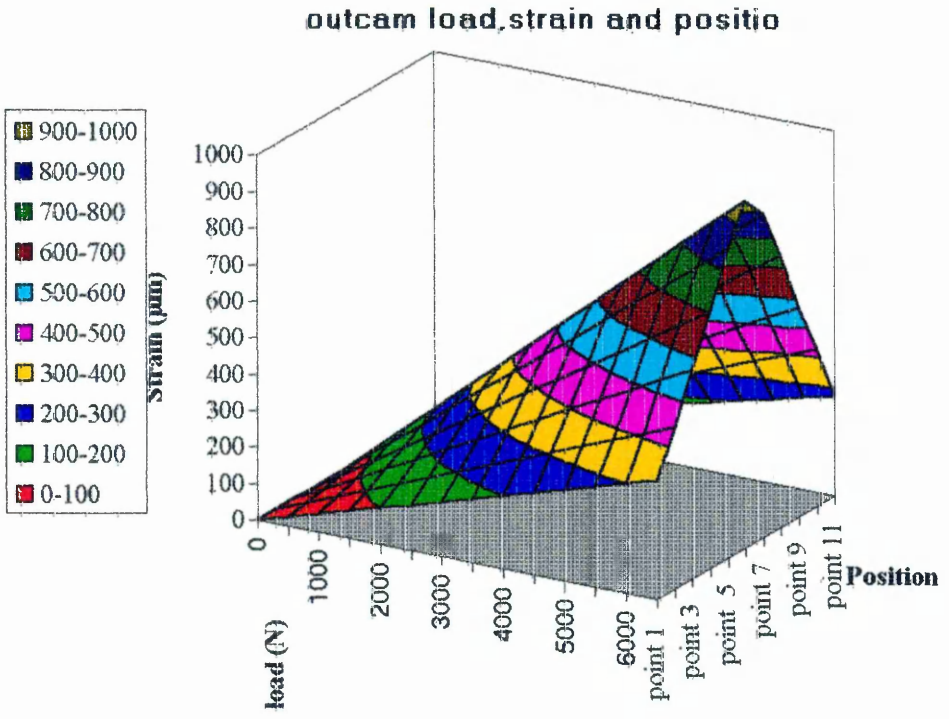

Figure 3.4.2.7 The 3D figure of the measurement of relationship between the load, strain and position for outside cam

Figure 3.4.2.8@ The results of the relationship of strain and time of the cams measured in real machine

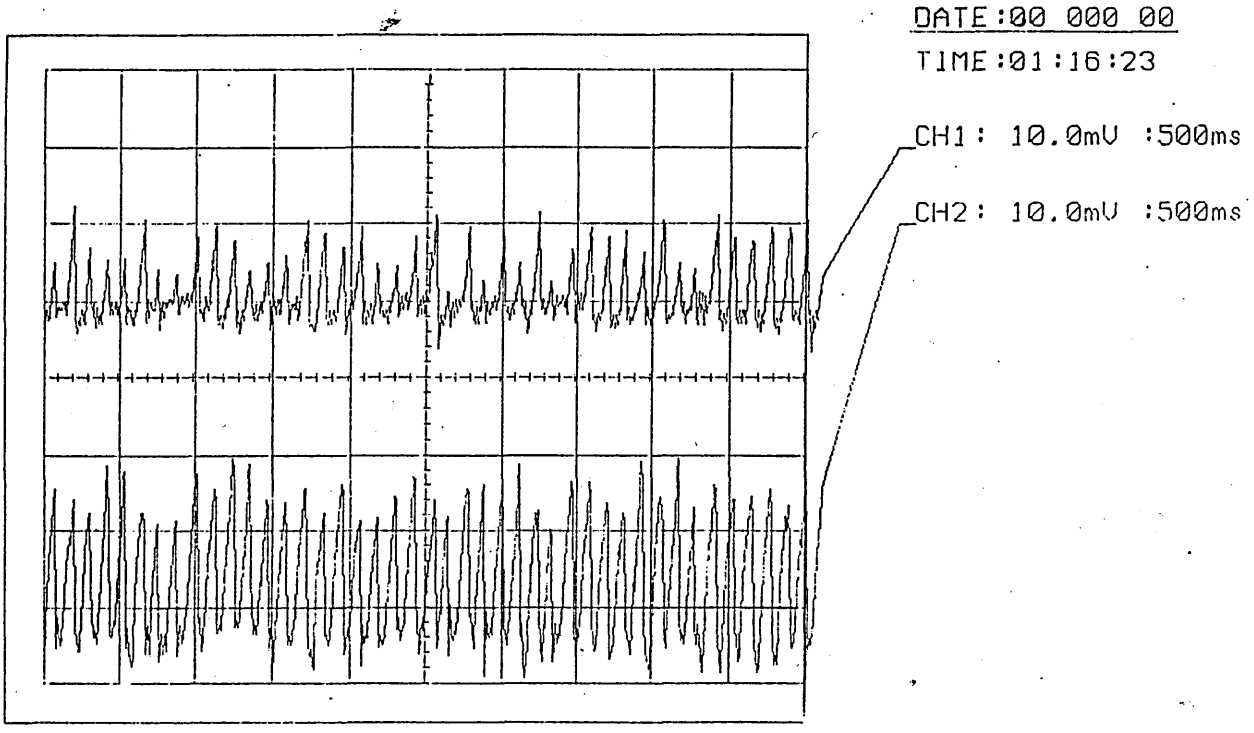

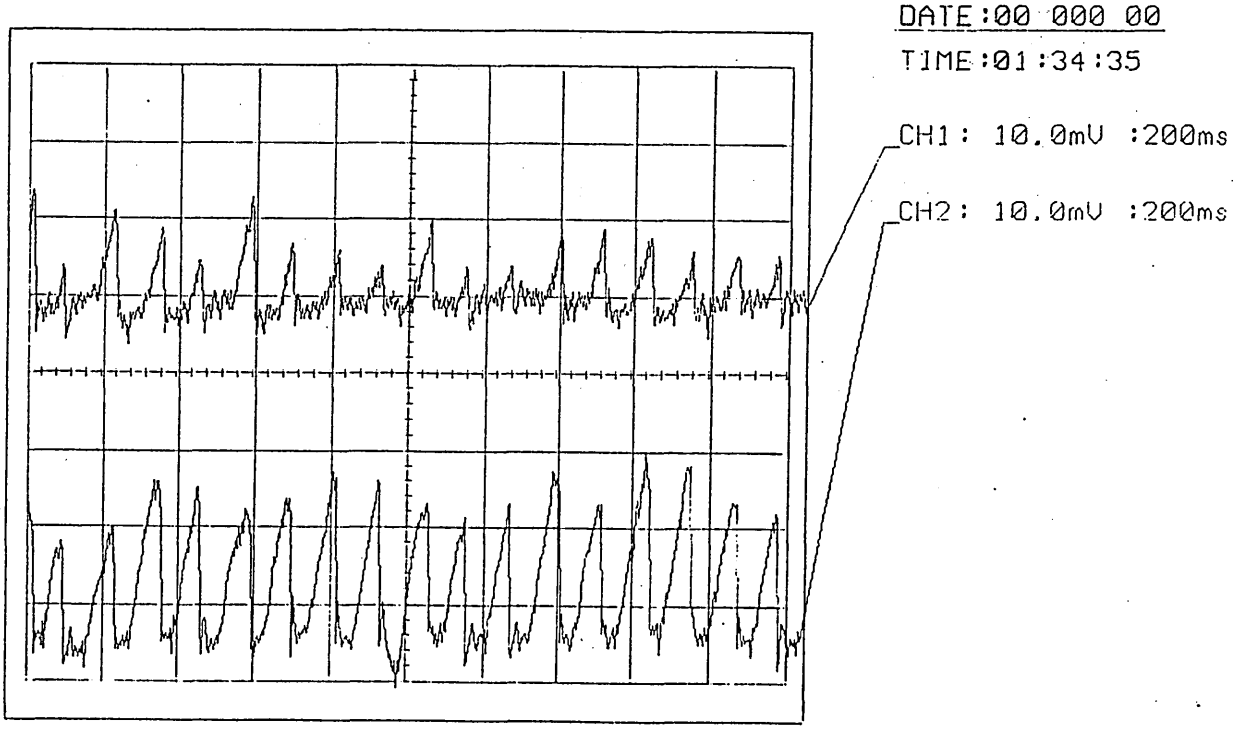

Figure 3.4.2.9@ The results of the relationship of strain and time of the sample cam measured in real machine

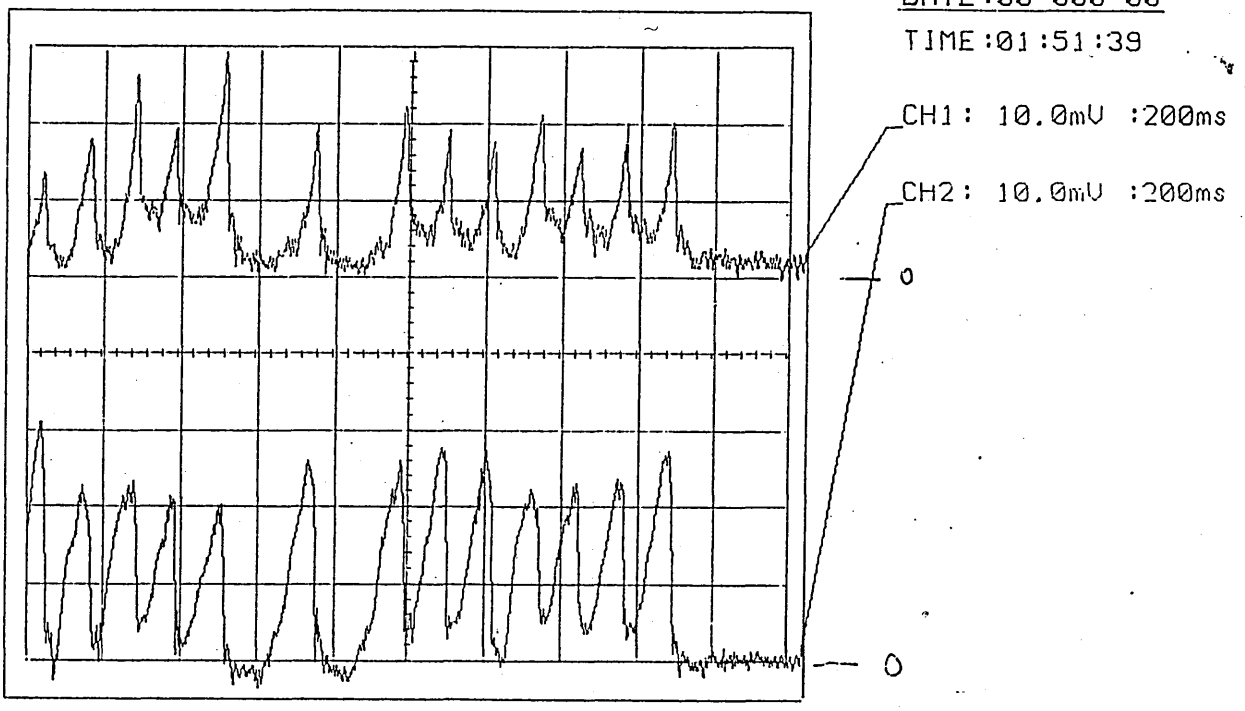

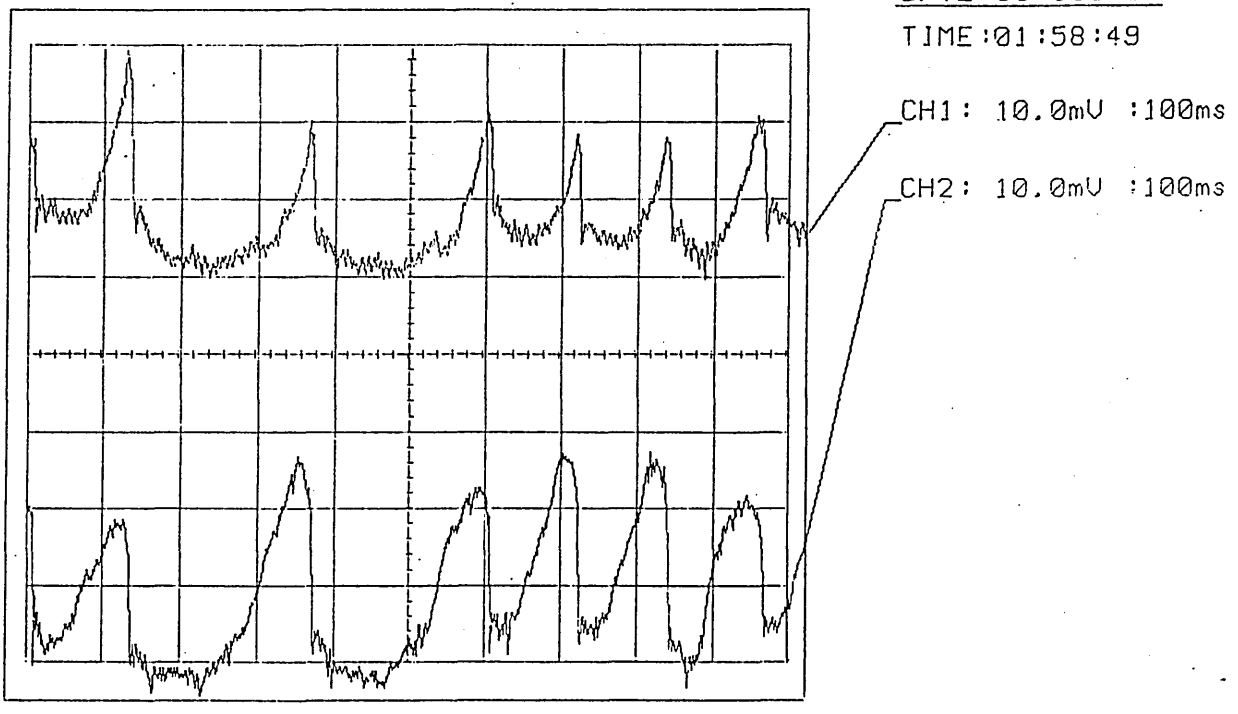

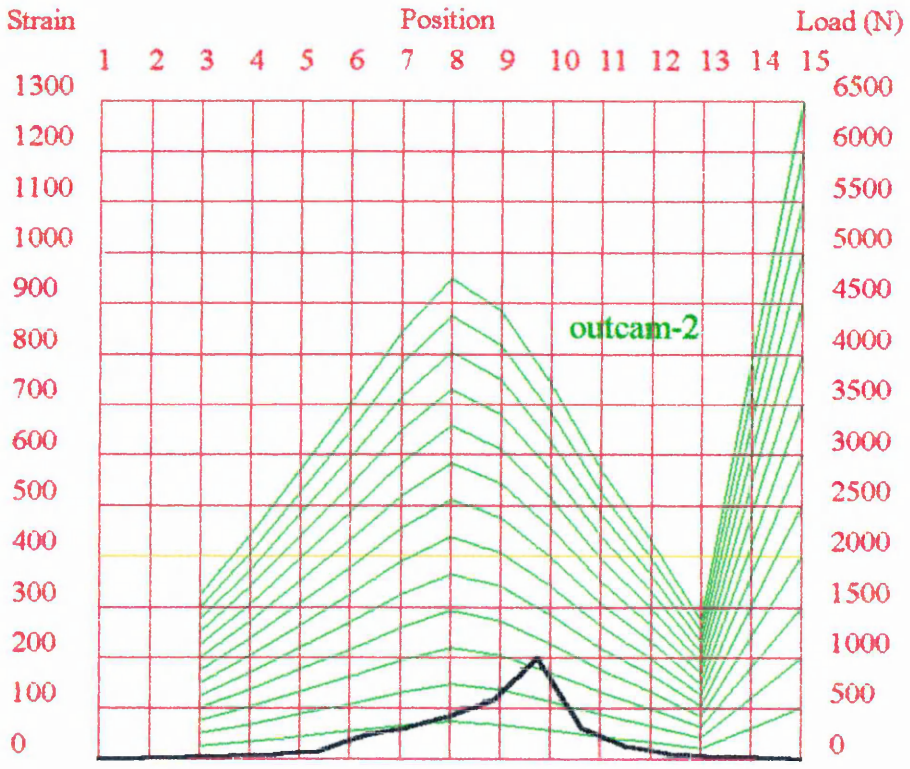

Fig 3.4.2.11 The overlay of the measurement for outer cam

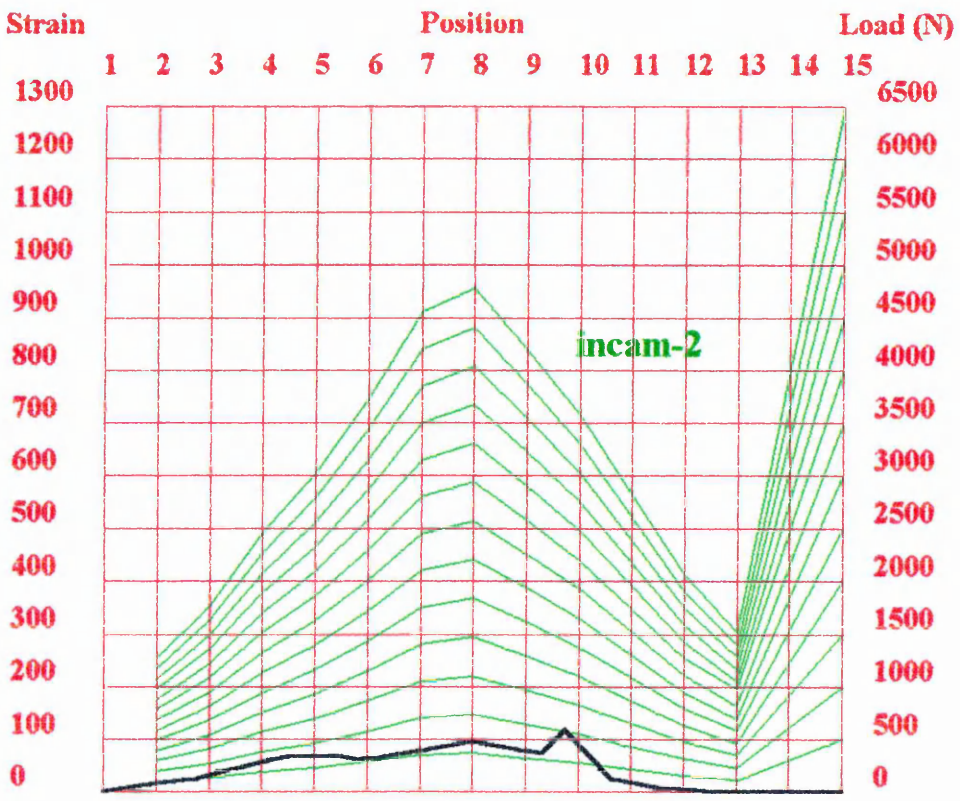

Fig 3.4.2.12 The overlay of the measurement for inner cam

Figure 3.4.3.1@ A Davenport Extrusion Rheometer for the material melt temperature control and injected shear rate control

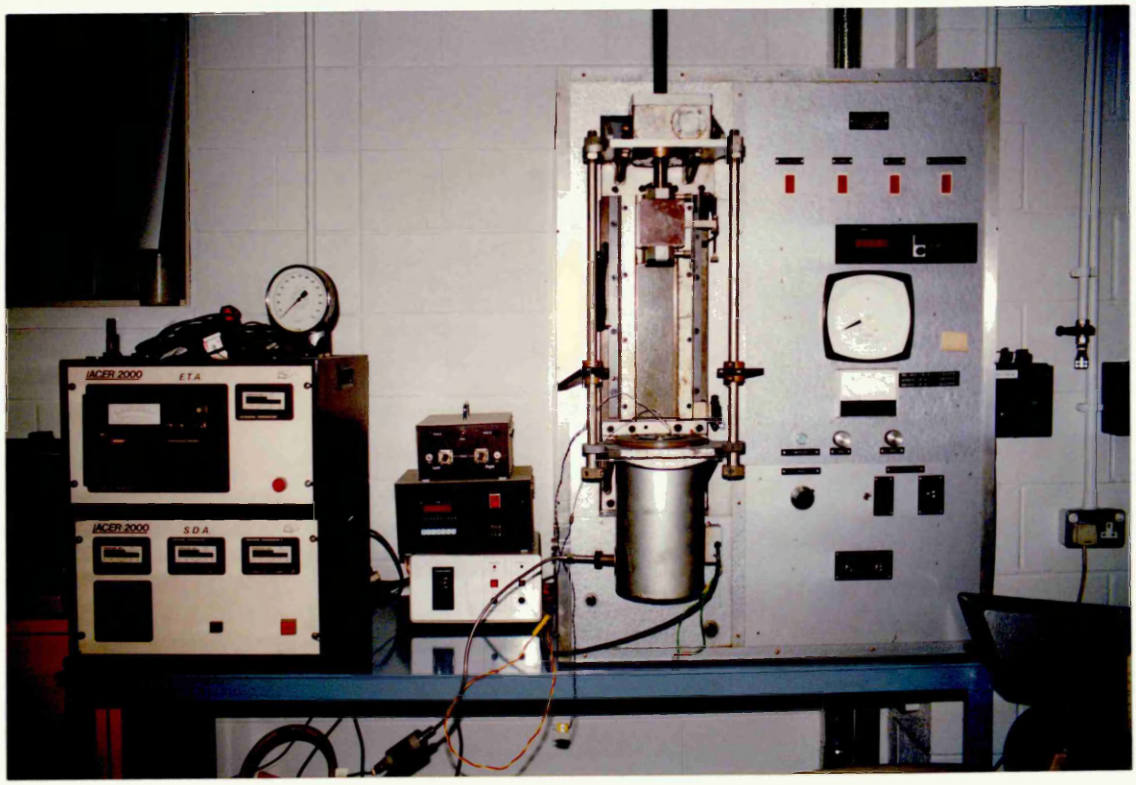

Figure 3.4.3.2@ A compression machine for compressing moulding

Figure 3.4.3.4@ A JJ test machine for the processing of the closure ejection

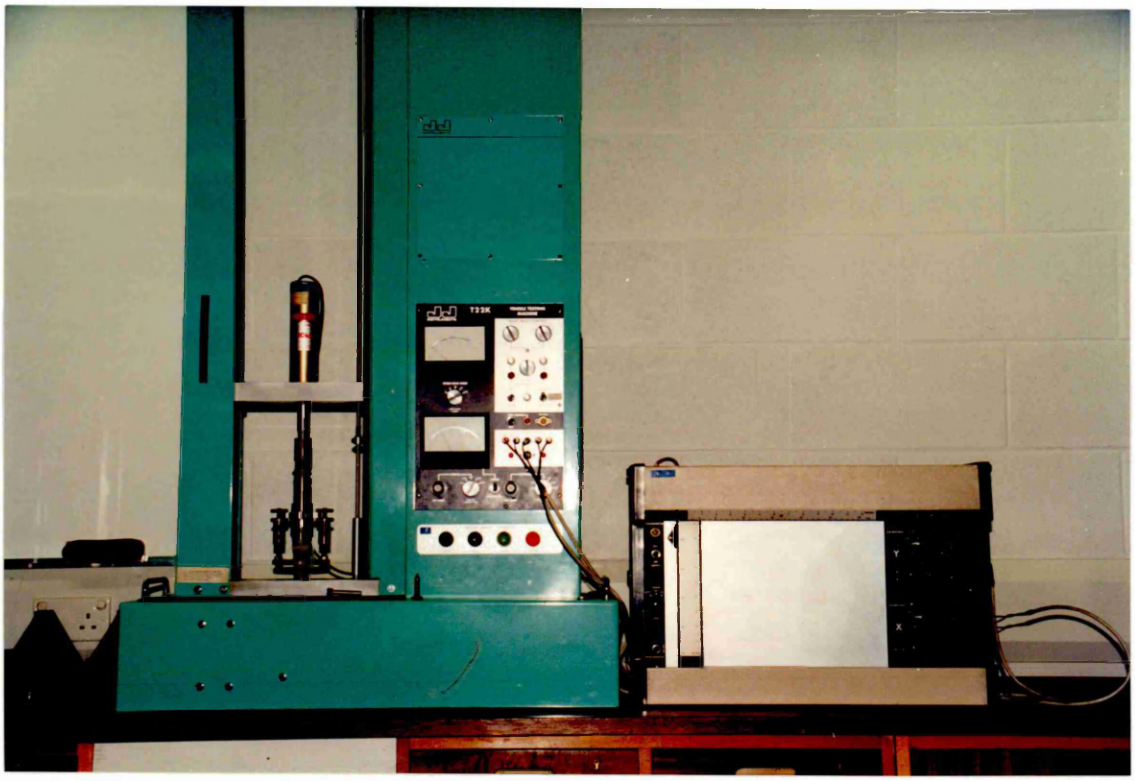

Figure. 3.4.3.5@ One set (set No. 2) of the measuring results plotted by X-Y plotter

Durham University

Date	28 June 94	Loadcell Magnification	
Customer		Extension Magnification	
Job Description		Crosshead Speed	75 mm/min
Sample Number	Group 7	Melt Temperature	240°C
Material	Neste PP	Ejecting Temperature	60°C
Tested By	B WANG		

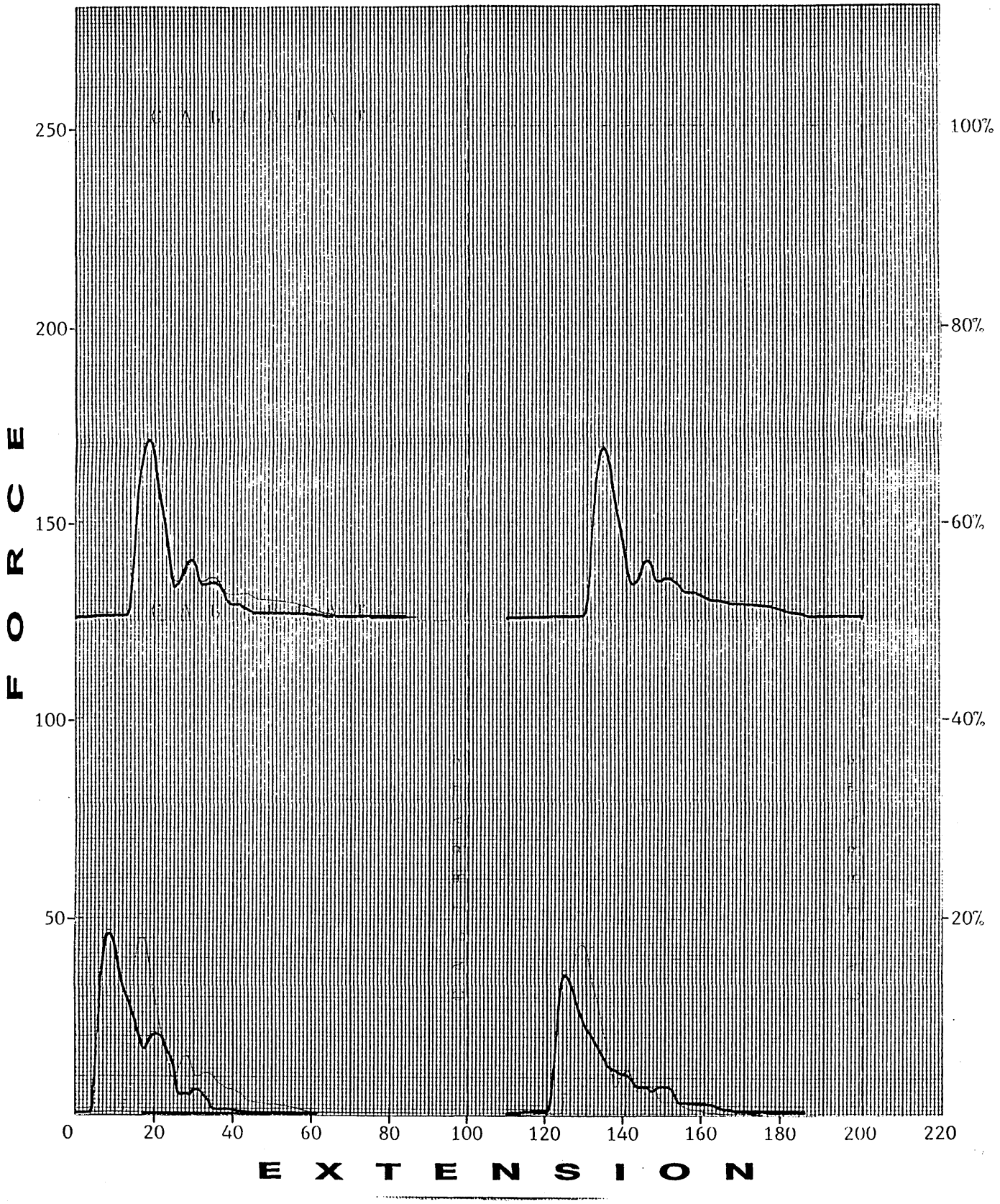

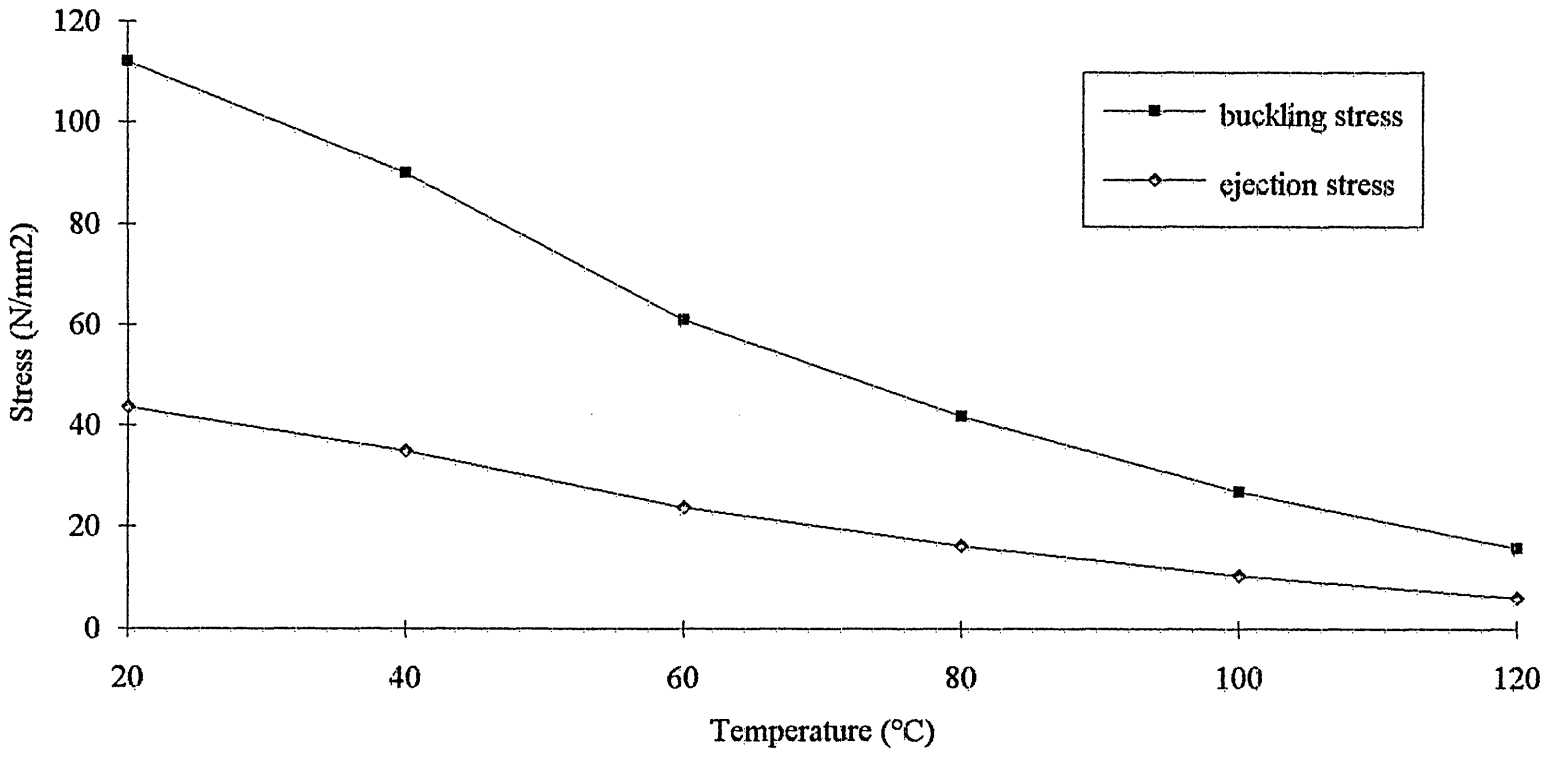

Fig 3.5.1.2 The comparison of the ejection stress and critical buckling stress with temperature

Figure 3.5.2.1[@] The model for the closure ejection analysis and eigenvalue buckling analysis

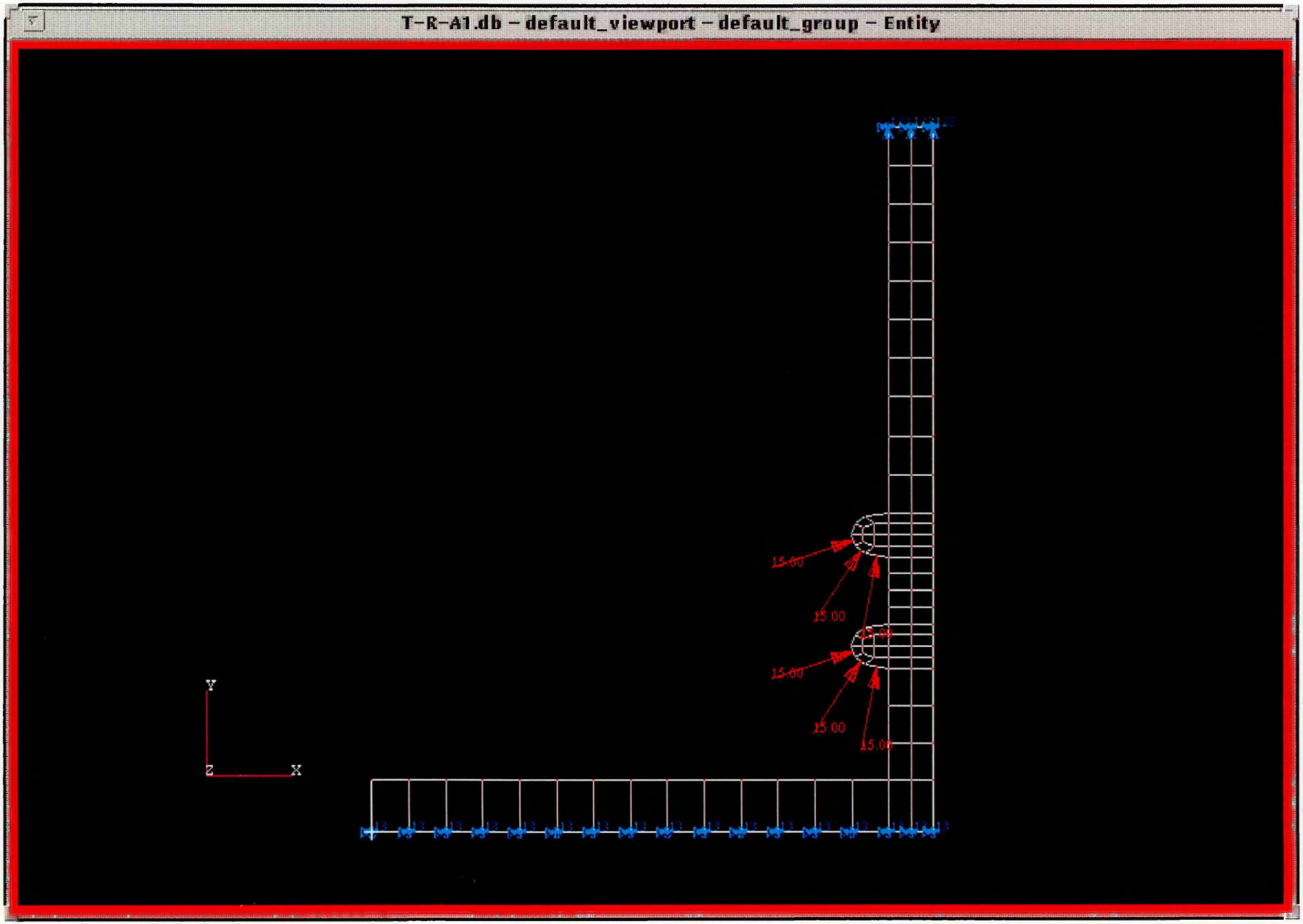
T-R-A1.db - default_viewport - default_group - Entity
15.00
15.00
15.00
15.00
15.00
Y
Z
X

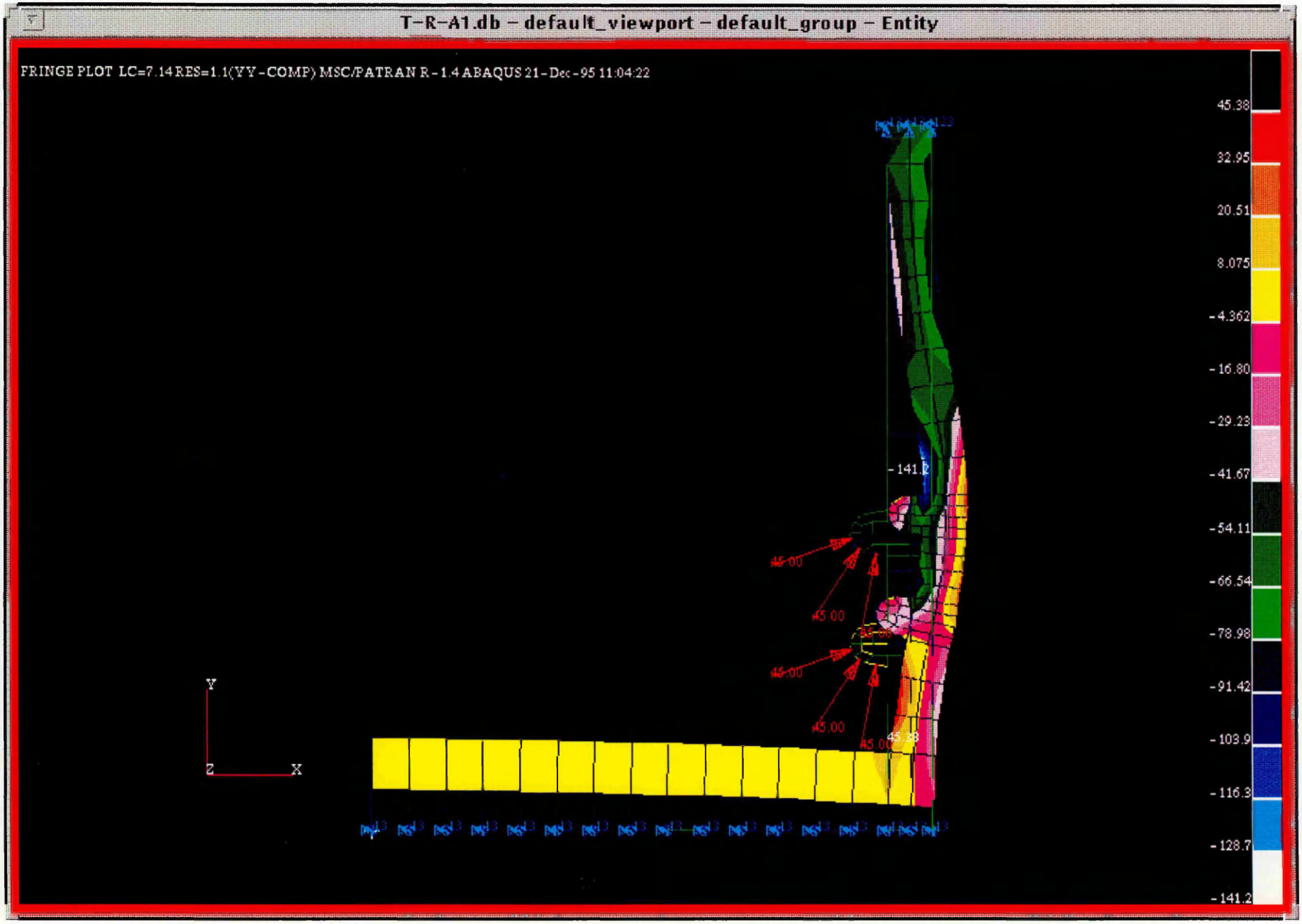
T-R-A1.db - default_viewport - default_group - Entity
FRINGE PLOT LC=7.14 RES=1.1(YY-COMP) MSC/PATRAN R-1.4 ABAQUS 21-Dec-95 11:04:22
45.38
32.95
20.51
8.075
-4.362
-16.80
-29.23
-41.67
-54.11
-66.54
-78.98
-91.42
-103.9
-116.3
-128.7
-141.2
-141.2
45.00
45.00
45.00
45.00
45.00
45.38
Y
Z
X

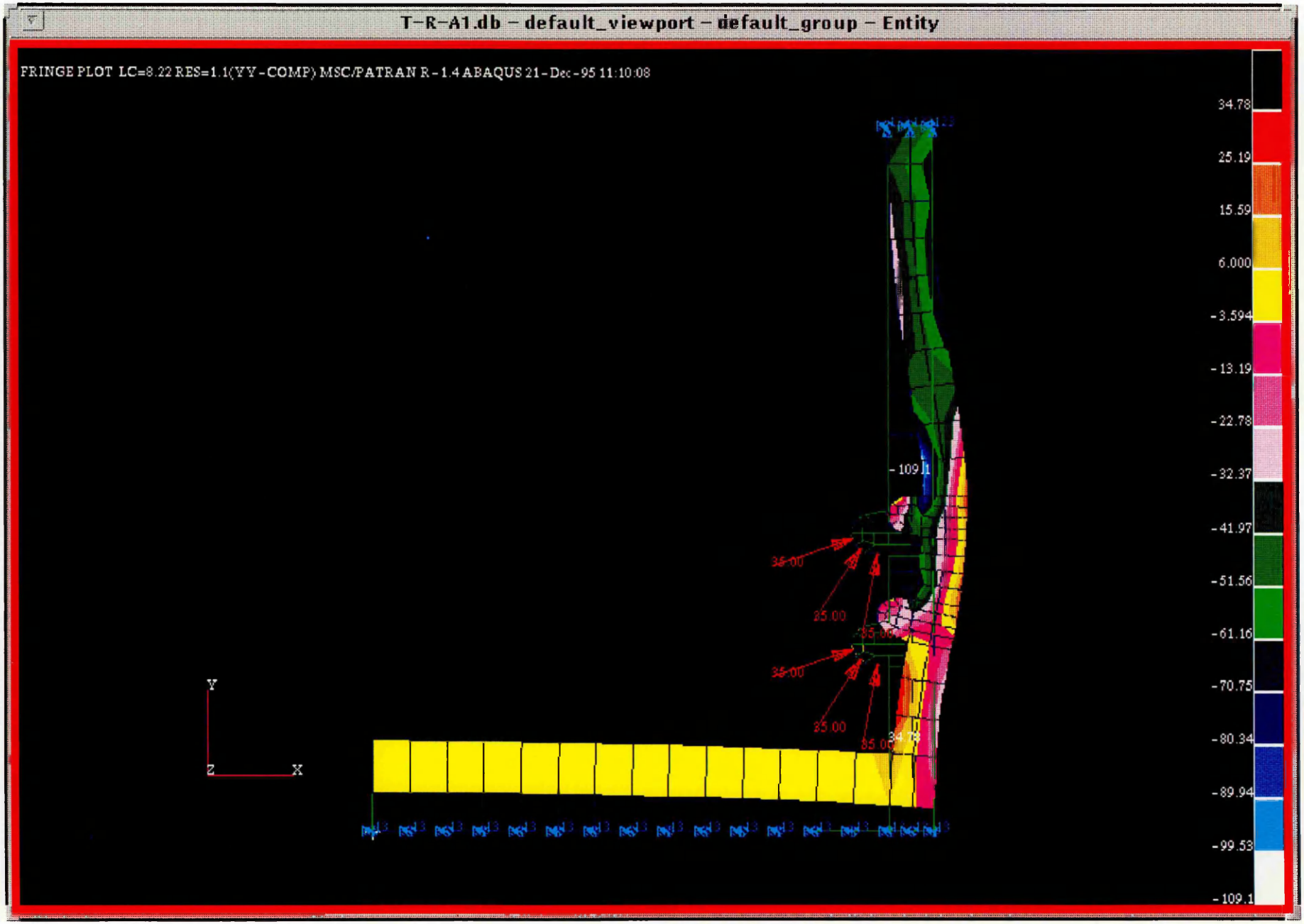
T-R-A1.db - default_viewport - default_group - Entity
FRINGE PLOT LC=8.22 RES=1.1(YY-COMP) MSC/PATRAN R-1.4 ABAQUS 21-Dec-95 11:10:08
34.78
25.19
15.59
6.000
-3.594
-13.19
-22.78
-32.37
-41.97
-51.56
-61.16
-70.75
-80.34
-89.94
-99.53
-109.1
-109.1
35.00
35.00
35.00
35.00
34.78
Y
Z
X

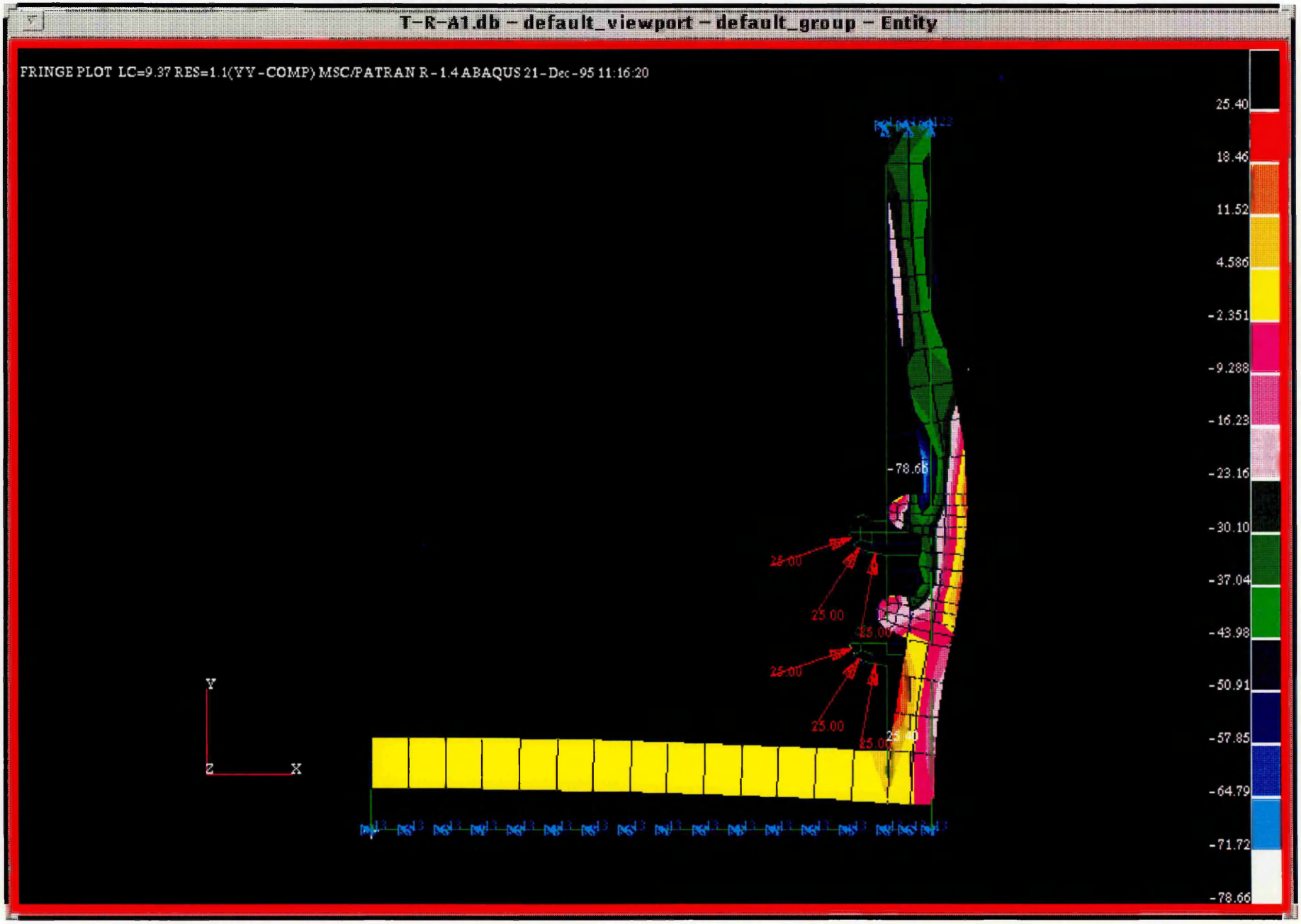
T-R-A1.db - default_viewport - default_group - Entity
FRINGE PLOT LC=9.37 RES=1.1(YY-COMP) MSC/PATRAN R-1.4 ABAQUS 21-Dec-95 11:16:20
25.40
18.46
11.52
4.586
-2.351
-9.288
-16.23
-23.16
-30.10
-37.04
-43.98
-50.91
-57.85
-64.79
-71.72
-78.66
-78.66
25.00
25.00
25.00
25.00
25.00
25.00
Y
Z
X

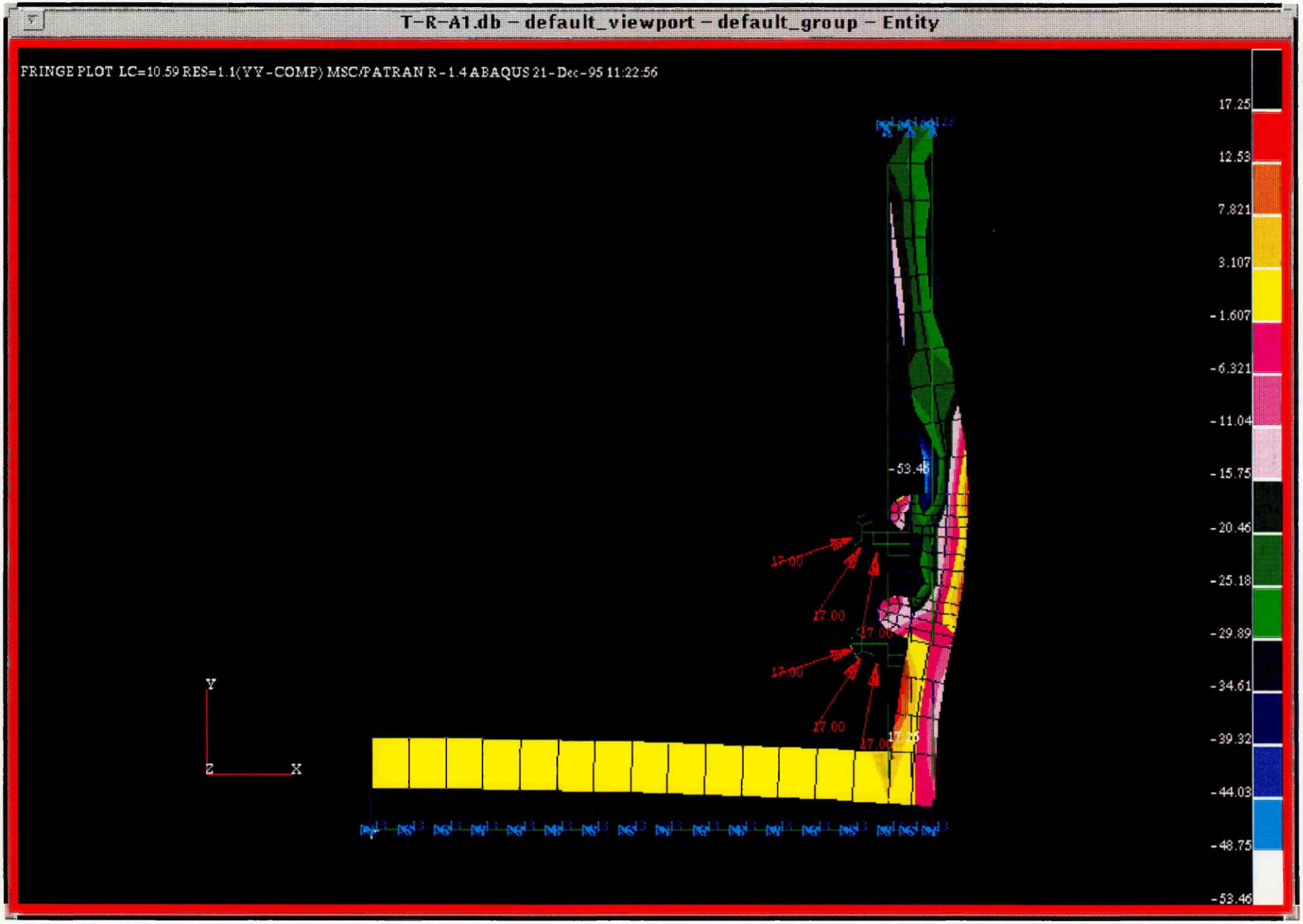
T-R-A1.db - default_viewport - default_group - Entity
FRINGE PLOT LC=10.59 RES=1.1(YY-COMP) MSC/PATRAN R-1.4 ABAQUS 21-Dec-95 11:22:56
17.25
12.53
7.821
3.107
-1.607
-6.321
-11.04
-15.75
-20.46
-25.18
-29.89
-34.61
-39.32
-44.03
-48.75
-53.46
-53.46
17.00
17.00
17.00
17.00
17.00
17.00
Y
Z
X

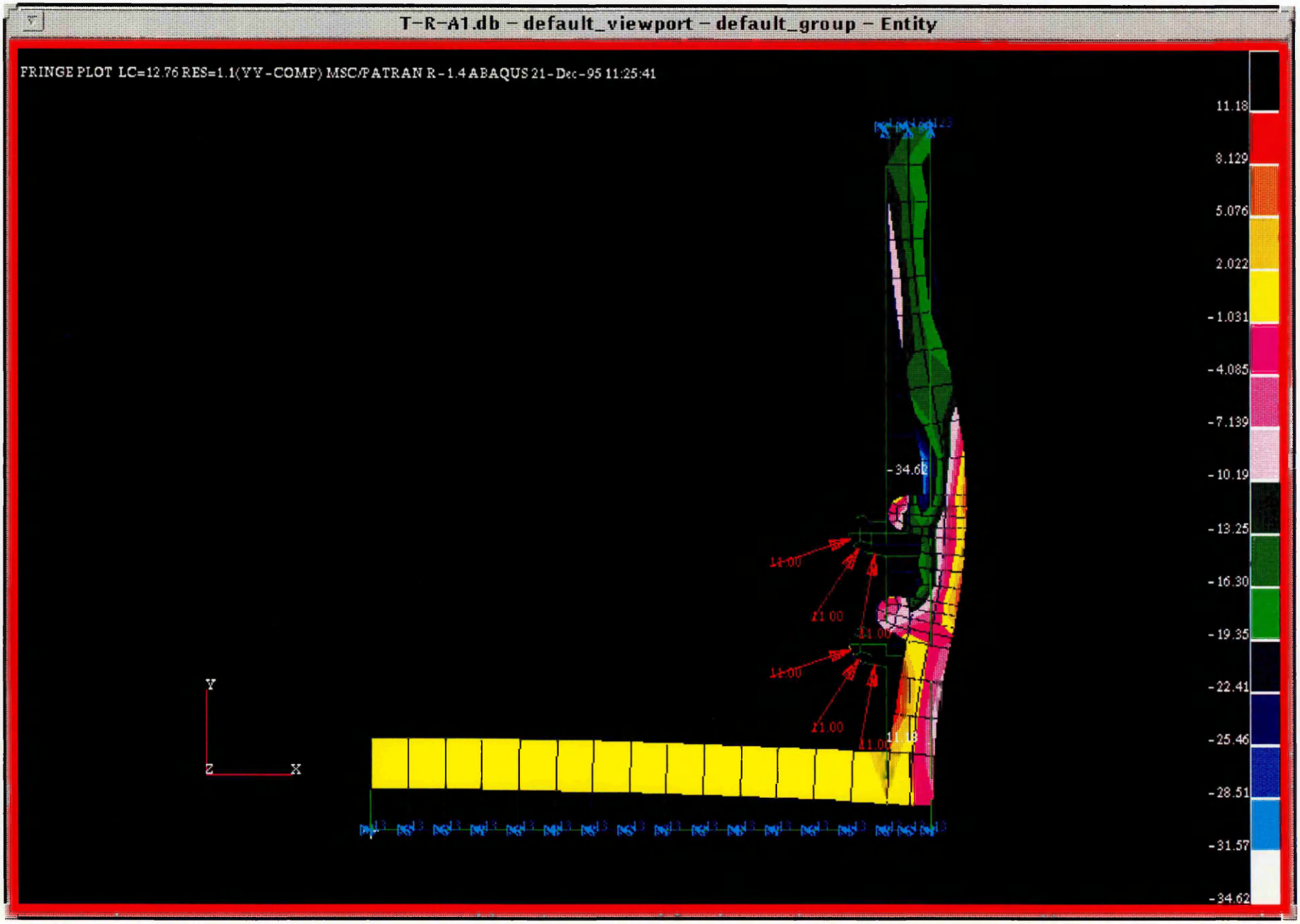
T-R-A1.db - default_viewport - default_group - Entity
FRINGE PLOT LC=12.76 RES=1.1(YY-COMP) MSC/PATRAN R-1.4 ABAQUS 21-Dec-95 11:25:41
11.18
8.129
5.076
2.022
-1.031
-4.085
-7.139
-10.19
-13.25
-16.30
-19.35
-22.41
-25.46
-28.51
-31.57
-34.62
-34.62
11.00
11.00
11.00
11.00
11.00
11.00
11.18
Y
Z
X

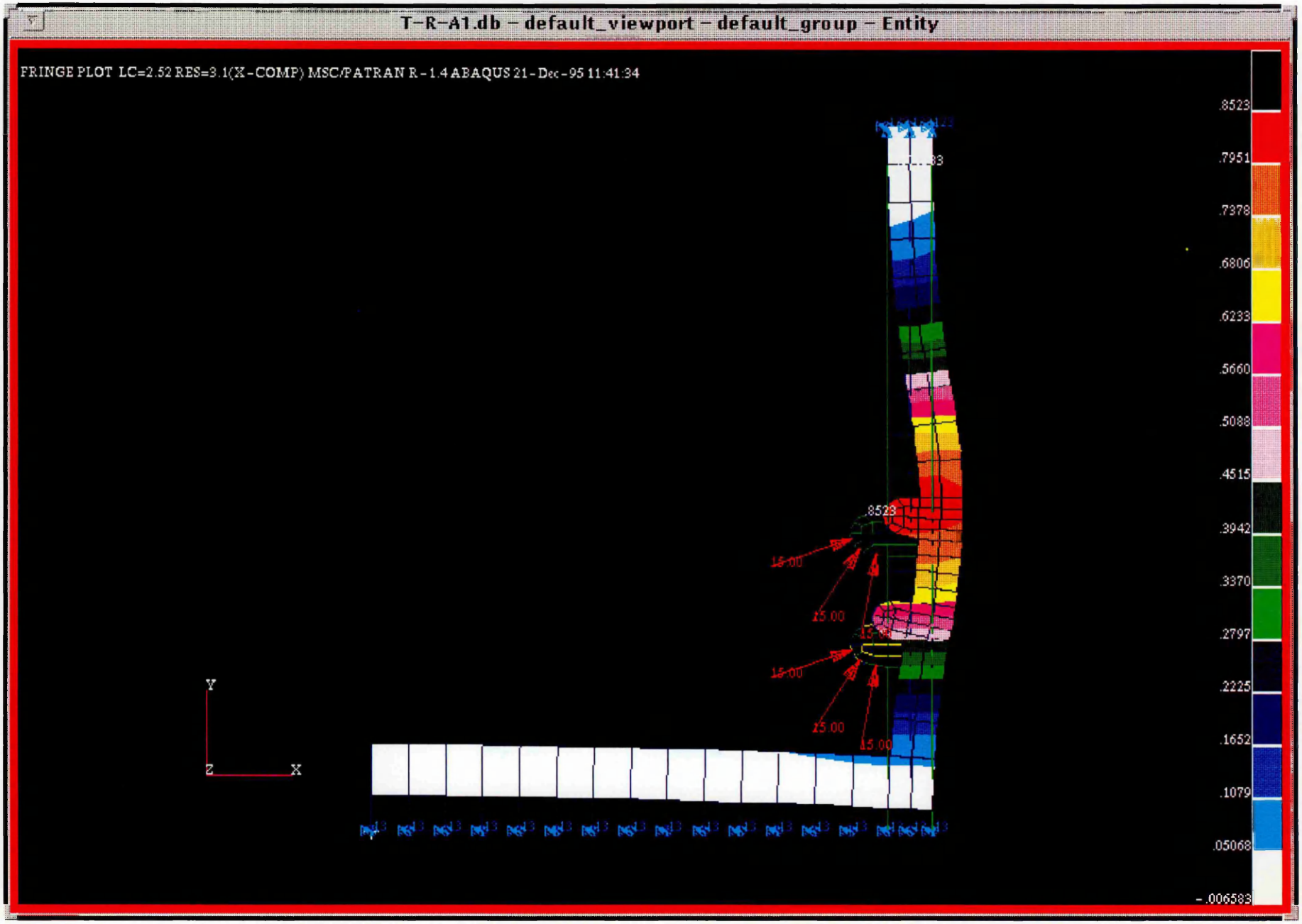
T-R-A1.db - default_viewport - default_group - Entity
FRINGE PLOT LC=2.52 RES=3.1(X-COMP) MSC/PATRAN R-1.4 ABAQUS 21-Dec-95 11:41:34
.8523
.7951
.7378
.6806
.6233
.5660
.5088
.4515
.3942
.3370
.2797
.2225
.1652
.1079
.05068
-.006583
15.00
15.00
15.00
15.00
15.00
Y
Z
X

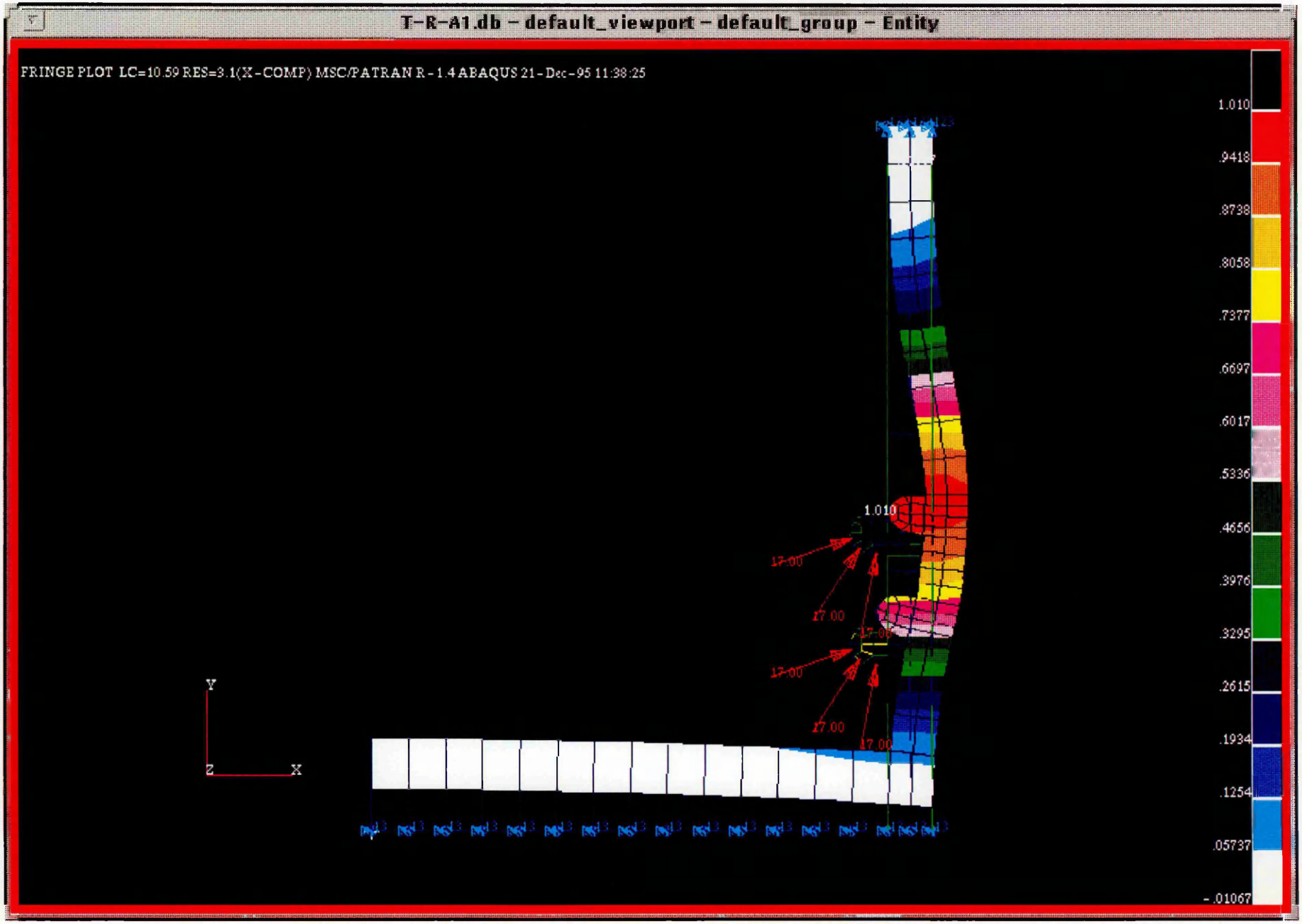
T-R-A1.db - default_viewport - default_group - Entity
FRINGE PLOT LC=10.59 RES=3.1(X-COMP) MSC/PATRAN R-1.4 ABAQUS 21-Dec-95 11:38:25
1.010
.9418
.8738
.8058
.7377
.6697
.6017
.5336
.4656
.3976
.3295
.2615
.1934
.1254
.05737
-.01067
1.010
17.00
17.00
17.00
17.00
17.00
17.00
Y
Z
X

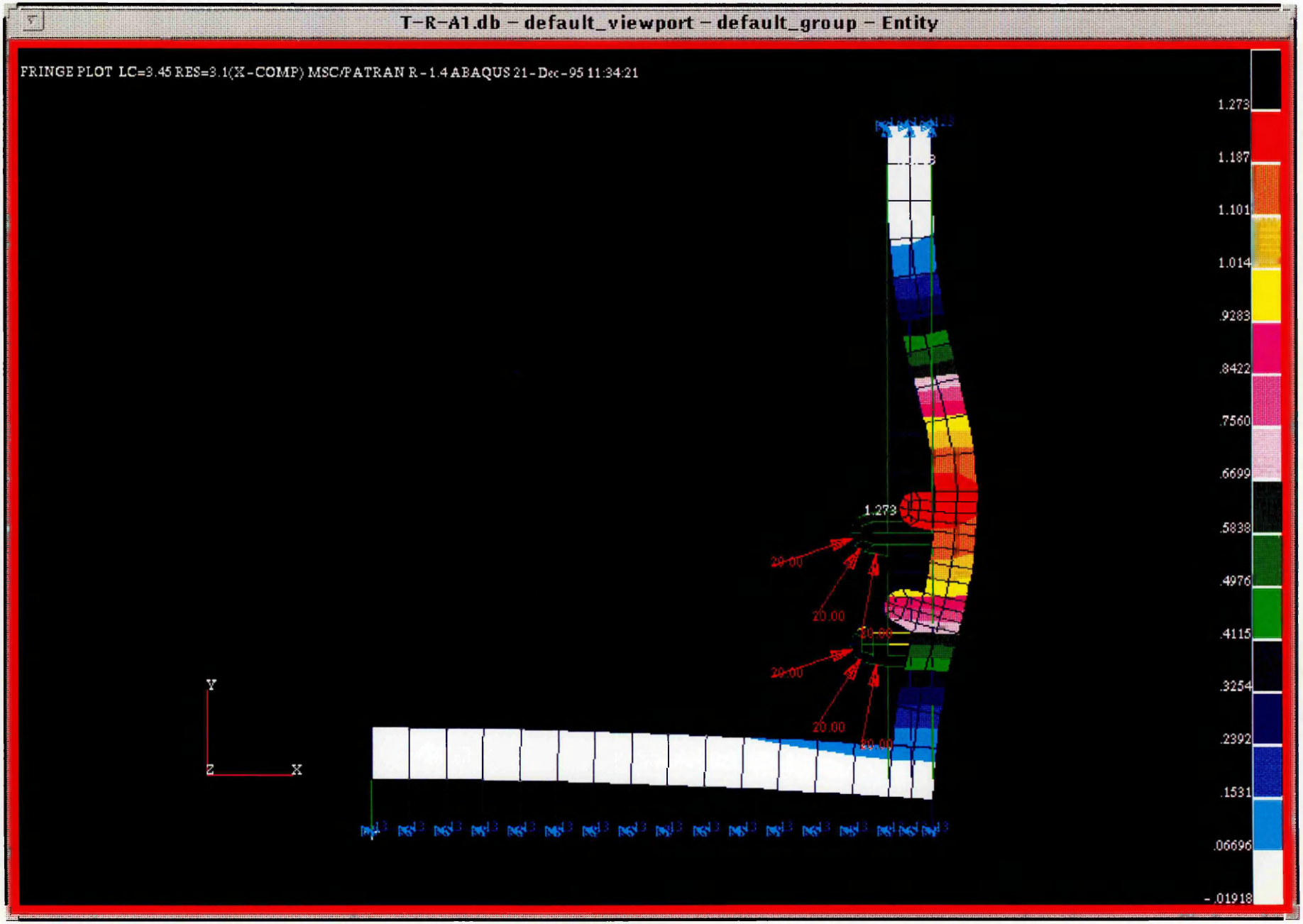
T-R-A1.db - default_viewport - default_group - Entity
FRINGE PLOT LC=3.45 RES=3.1(X-COMP) MSC/PATRAN R-1.4 ABAQUS 21-Dec-95 11:34:21
1.273
1.187
1.101
1.014
.9283
.8422
.7560
.6699
.5838
.4976
.4115
.3254
.2392
.1531
.06696
-.01918
1.273
20.00
20.00
20.00
20.00
20.00
20.00
Y
Z
X

Figure 3.5.3.1[@] The buckling deformation pattern under critical buckling stress

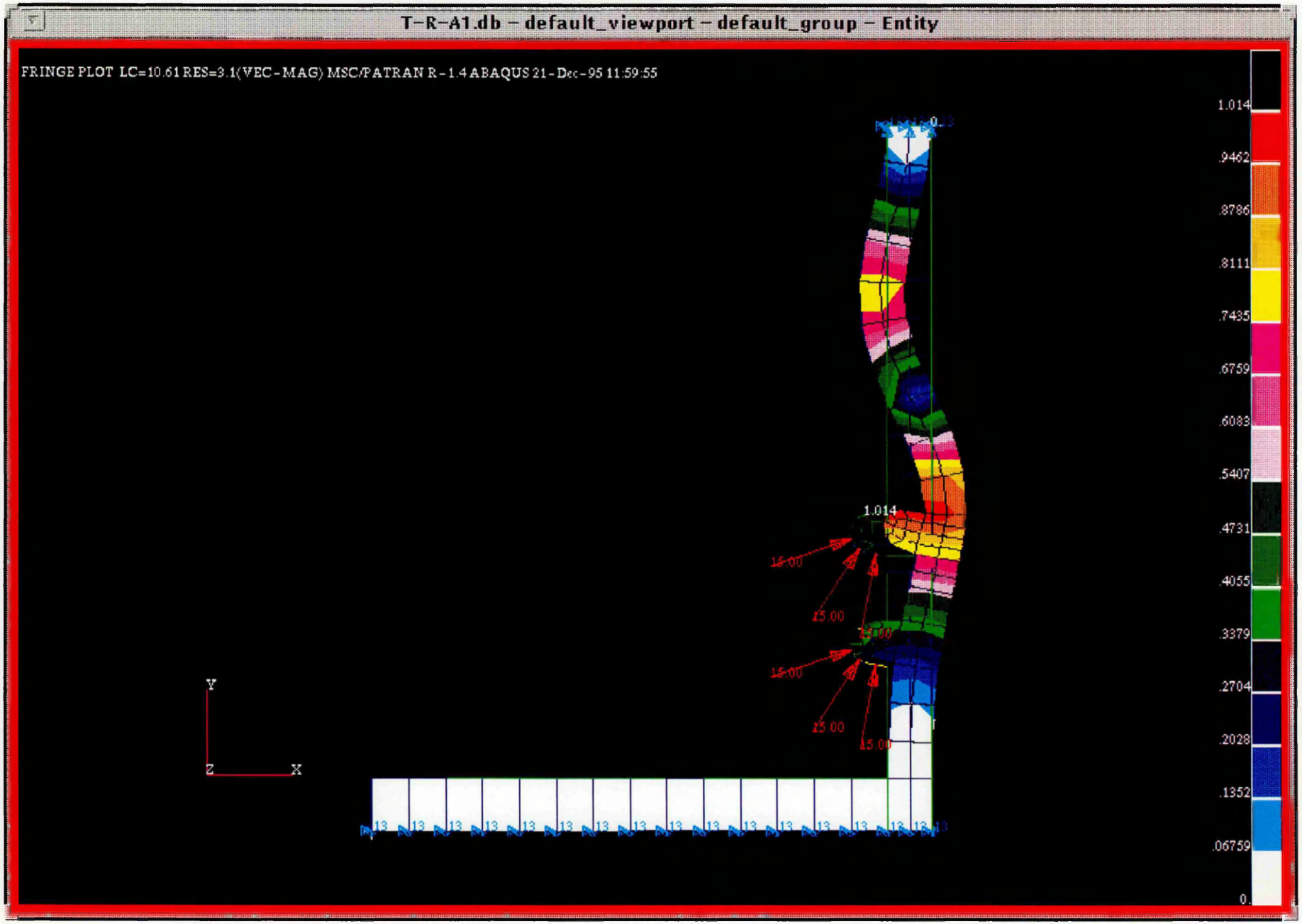
T-R-A1.db – default_viewport – default_group – Entity
FRINGE PLOT LC=10.61 RES=3.1(VEC-MAG) MSC/PATRAN R-1.4 ABAQUS 21-Dec-95 11:59:55
1.014
.9462
.8786
.8111
.7435
.6759
.6083
.5407
.4731
.4055
.3379
.2704
.2028
.1352
.06759
0.
1.014
15.00
15.00
15.00
15.00
15.00
Y
Z
X

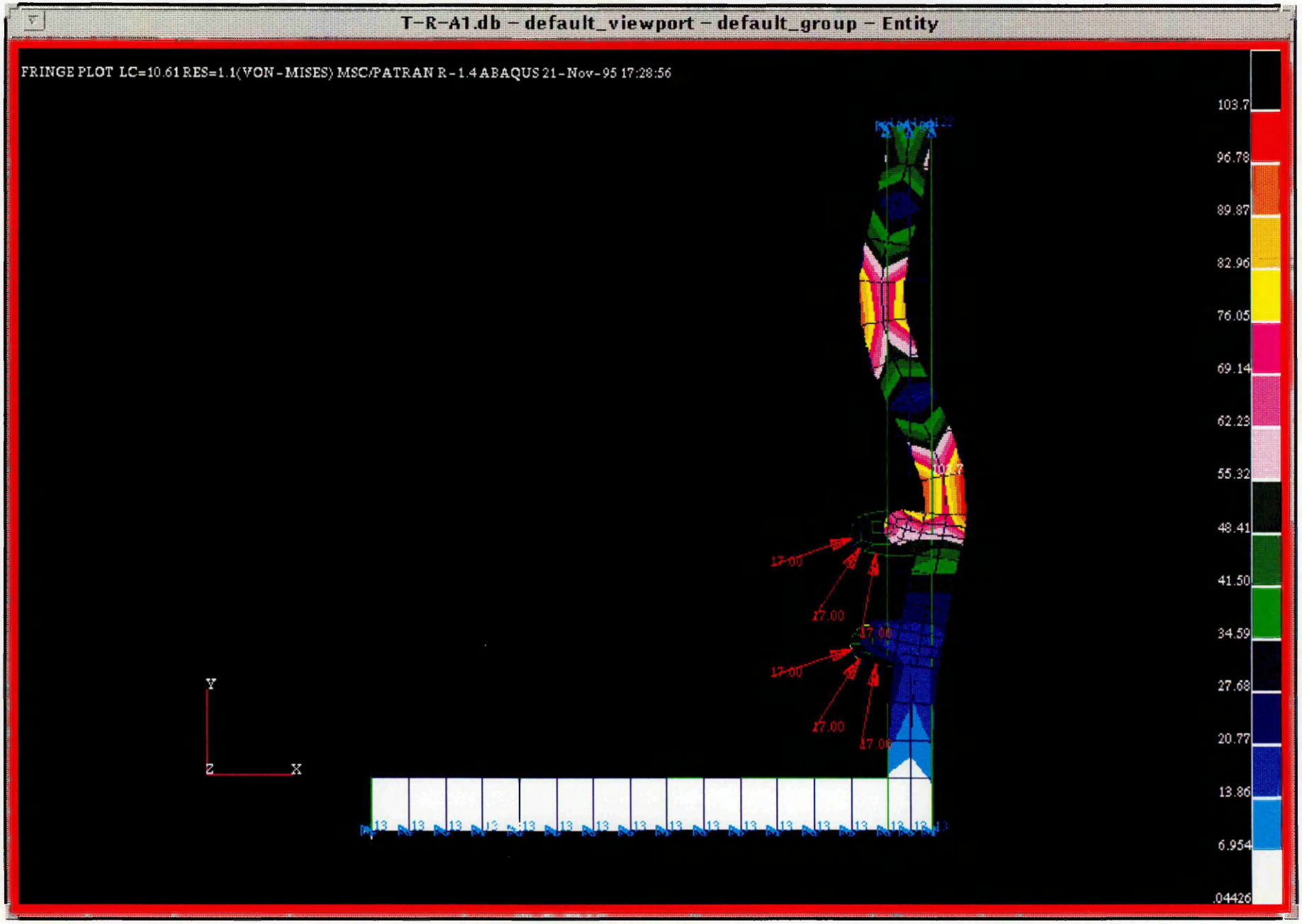
T-R-A1.db - default_viewport - default_group - Entity
FRINGE PLOT LC=10.61 RES=1.1(VON-MISES) MSC/PATRAN R-1.4 ABAQUS 21-Nov-95 17:28:56
103.7
96.78
89.87
82.96
76.05
69.14
62.23
55.32
48.41
41.50
34.59
27.68
20.77
13.86
6.954
.04426
17.00
17.00
17.00
17.00
17.00
17.00
Y
Z
X

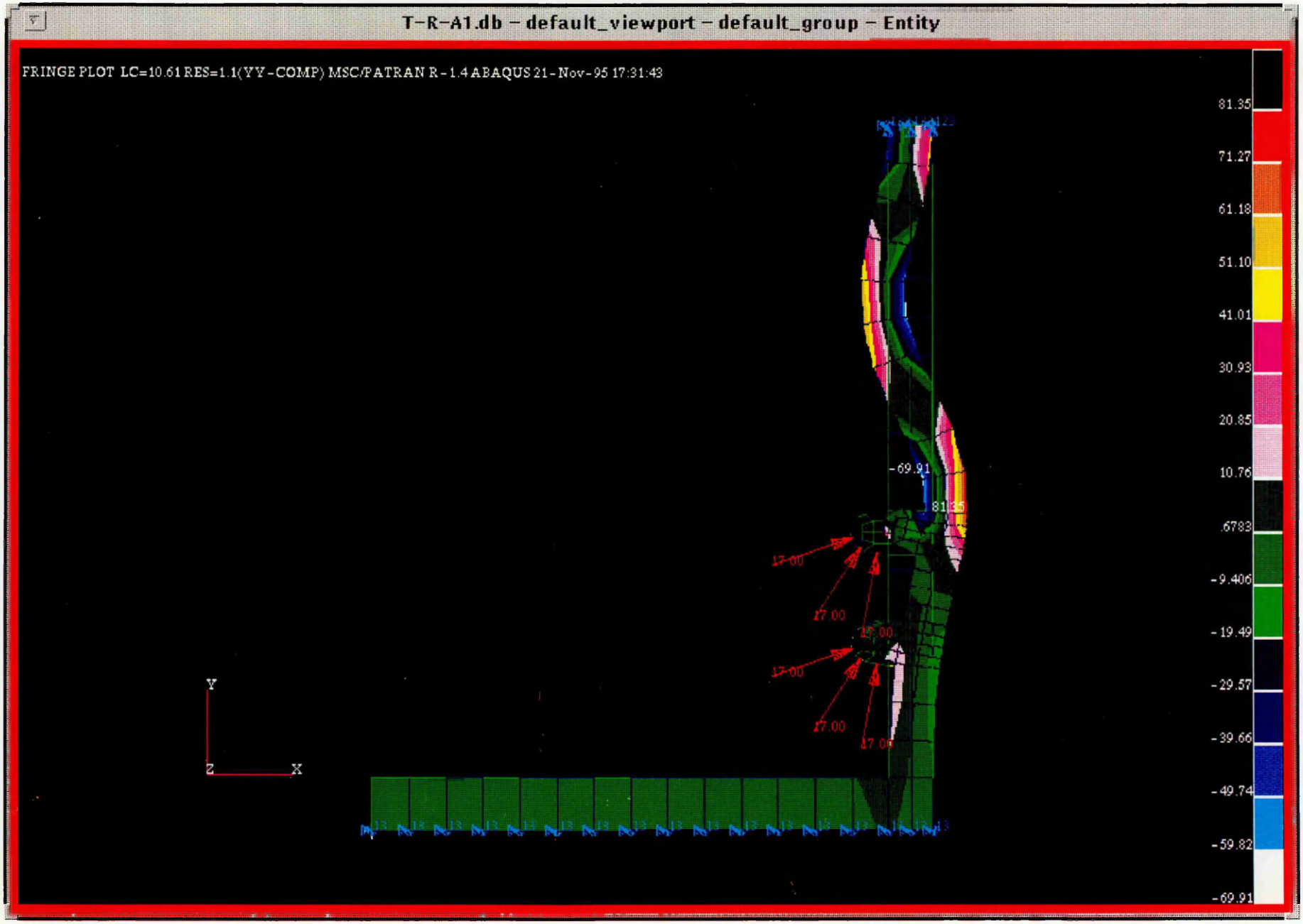
T-R-A1.db – default_viewport – default_group – Entity
FRINGE PLOT LC=10.61 RES=1.1(YY-COMP) MSC/PATRAN R-1.4 ABAQUS 21-Nov-95 17:31:43
81.35
71.27
61.18
51.10
41.01
30.93
20.85
10.76
.6783
-9.406
-19.49
-29.57
-39.66
-49.74
-59.82
-69.91
-69.91
17.00
17.00
17.00
17.00
17.00
17.00
Y
Z
X